

Unravelling the contribution of small non-coding RNAs to Huntington's disease pathogenesis

Anna Guisado Corcoll

ADVERTIMENT. La consulta d'aquesta tesi queda condicionada a l'acceptació de les següents condicions d'ús: La difusió d'aquesta tesi per mitjà del servei TDX (www.tdx.cat) i a través del Dipòsit Digital de la UB (diposit.ub.edu) ha estat autoritzada pels titulars dels drets de propietat intel·lectual únicament per a usos privats emmarcats en activitats d'investigació i docència. No s'autoritza la seva reproducció amb finalitats de lucre ni la seva difusió i posada a disposició des d'un lloc aliè al servei TDX ni al Dipòsit Digital de la UB. No s'autoritza la presentació del seu contingut en una finestra o marc aliè a TDX o al Dipòsit Digital de la UB (framing). Aquesta reserva de drets afecta tant al resum de presentació de la tesi com als seus continguts. En la utilització o cita de parts de la tesi és obligat indicar el nom de la persona autora.

ADVERTENCIA. La consulta de esta tesis queda condicionada a la aceptación de las siguientes condiciones de uso: La difusión de esta tesis por medio del servicio TDR (www.tdx.cat) y a través del Repositorio Digital de la UB (diposit.ub.edu) ha sido autorizada por los titulares de los derechos de propiedad intelectual únicamente para usos privados enmarcados en actividades de investigación y docencia. No se autoriza su reproducción con finalidades de lucro ni su difusión y puesta a disposición desde un sitio ajeno al servicio TDR o al Repositorio Digital de la UB. No se autoriza la presentación de su contenido en una ventana o marco ajeno a TDR o al Repositorio Digital de la UB (framing). Esta reserva de derechos afecta tanto al resumen de presentación de la tesis como a sus contenidos. En la utilización o cita de partes de la tesis es obligado indicar el nombre de la persona autora.

WARNING. On having consulted this thesis you're accepting the following use conditions: Spreading this thesis by the TDX (**www.tdx.cat**) service and by the UB Digital Repository (**diposit.ub.edu**) has been authorized by the titular of the intellectual property rights only for private uses placed in investigation and teaching activities. Reproduction with lucrative aims is not authorized nor its spreading and availability from a site foreign to the TDX service or to the UB Digital Repository. Introducing its content in a window or frame foreign to the TDX service or to the UB Digital Repository is not authorized (framing). Those rights affect to the presentation summary of the thesis as well as to its contents. In the using or citation of parts of the thesis it's obliged to indicate the name of the author.



Unravelling the contribution of small non-coding RNAs to Huntington's disease pathogenesis

Degree of doctor by the University of Barcelona

Dissertation submitted by:

Anna Guisado Corcoll

This work was performed at the Department of Biomedicine in the Faculty of Medicine and Health Sciences of the University of Barcelona under the supervision of Dr. Esther Pérez Navarro and Dr. Eulàlia Martí Puig

Anna Guisado Corcoll

Esther Pérez Navarro

Eulàlia Martí Puig

Programa de Doctorat en Biomedicina per la Universitat de Barcelona

RESUM

ANTECEDENTS I OBJECTIUS

La malaltia de Huntington (MH) és una malaltia neurodegenerativa d'herència autosòmica dominant causada per una expansió anormal en el nombre de triplets CAG localitzats a l'exó 1 del gen de la huntingtina (HTT), donant lloc a una porció expandida de glutamines (polyQ) en una regió pròxima a l'extrem amino terminal de la proteïna HTT (The Huntington's Disease Collaborative Research Group, 1993). Aquesta expansió contribueix a la formació d'una proteïna aberrant i mal plegada que s'ha associat amb l'agregació i la toxicitat (Labbadia & Morimoto, 2013), els quals són mecanismes que s'han implicat en múltiples desordres neurològics. A més, tot i que aquesta mutació es troba de forma ubiqua a totes les cèl·lules del cos, s'ha descrit una vulnerabilitat selectiva per part de les neurones espinoses de mida mitjana (MSNs) localitzades al nucli estriat, format pel caudat i el putamen en els humans (Vonsattel et al., 1985). Aquestes MSNs estriatals es poden classificar en dos tipus en funció dels receptors que expressen i de les àrees cerebrals a les que projecten (Gerfen et al., 1990), formant la via directa i la via indirecta dels ganglis basals. El correcte equilibri de senyalització entre aquestes vies és el que permet el control voluntari dels moviments de manera que l'atròfia estriatal, preferentment de la via indirecta a l'inici, durant la progressió de la malaltia comporta una alteració en els circuits donant lloc a la simptomatologia motora característica de la MH (Albin et al., 1989).

Fins a data d'avui, la major part de la recerca sobre els mecanismes moleculars implicats en la fisiopatologia de la MH s'ha centrat en les alteracions causades per la proteïna mutada (Zuccato et al., 2010). Tot i això, en els últims anys, s'ha observat que la toxicitat generada per la proteïna mutada coexisteix amb mecanismes patogènics mediats per RNA, els quals es poden subdividir en aquells associats a I'RNA expandit amb repeticions CAG i aquells relacionats amb altres RNAs no codificants. Per una banda, s'ha observat que l'RNA amb expansió de triplets CAG pot exercir la seva toxicitat a través de múltiples mecanismes (Heinz et al., 2021; Malik et al., 2021; Martí, 2016). Entre ells, trobem la formació de RNAs de mida curta (21 nt) amb repeticions CAG (sCAG) a través de Dicer, els nivells dels quals són dependents de la llargada de l'expansió de triplets (Bañez-Coronel et al., 2012). Aquestes espècies tenen capacitat de silenciament gènic de manera que s'han associat a alteracions transcriptòmiques i poden afectar la viabilitat neuronal per se (Bañez-Coronel et al., 2012). A més, el nostre grup també ha descrit que els seus efectes es poden revertir parcialment amb l'ús d'un oligonucleòtid anti-sentit modificat, dirigit a les repeticions CAG (LNA-CTG), produint una recuperació de la funció motora i dels nivells de múltiples marcadors estriatals en un model murí de la MH (Rué et al., 2016).

Per altra banda, en els últims anys també s'han descrit diferents mecanismes de toxicitat a través d'RNA implicant múltiples biotipus d'RNAs no codificants de mida

curta (sRNA, <200 nt), com per exemple els microRNAs (miRNA), els RNAs ribosomals (rRNA) o els RNAs de transferència (tRNA), els quals també s'han associat de forma clara amb la regulació de l'expressió gènica, entre moltes altres funcions (Cech & Steitz, 2014). En paral·lel, s'ha observat que en el context de la MH existeix una important desregulació transcriptòmica en diferents regions cerebrals (Martí et al., 2010), apuntant a un possible paper dels sRNA en la fisiopatologia de la MH. A més, tot i que la funció canònica descrita dels tRNA es basa en permetre la síntesi de proteïnes al ribosoma descodificant la informació a nivell de mRNA, també s'han descrit implicacions dels tRNA en altres processos biològics com la senyalització i la supervivència cel·lular, l'apoptosi, el metabolisme dels aminoàcids o, fins i tot, en programes de resposta a estrès (Raina & Ibba, 2014). Concretament, moltes d'aquestes funcions s'han atribuït a fragments derivats d'aquests tRNA (tsRNA), alguns dels quals són components constitutius de totes les cèl·lules, mentre que d'altres només es produeixen en situacions d'estrès cel·lular (Anderson & Ivanov, 2014) i s'han relacionat amb diferents situacions patològiques com ara càncers, infeccions i diferents paradigmes de neurodegeneració (R. Magee & Rigoutsos, 2020).

Basant-nos en la informació bibliogràfica exposada, la nostra hipòtesi és que els mecanismes patogènics causats per RNA, i específicament sRNA, estan molt més implicats del que es pensava en la MH i que el seu estudi esdevé d'alta importància tant per entendre les bases fisiopatològiques de la MH com per desenvolupar noves teràpies. Per tant, el principal objectiu d'aquest projecte va ser identificar noves espècies de sRNA implicades en els mecanismes patogènics de la MH i determinar la seva contribució a les alteracions característiques d'aquesta patologia.

RESULTATS I DISCUSSIÓ

Dins el marc del primer objectiu, es va dur a terme un estudi *in vivo* de la potencial capacitat neurotòxica dels sRNA obtinguts del cervell de pacients de la MH. En primer lloc, es va caracteritzar la distribució cel·lular i subcel·lular dels sRNA quan s'injectaven al nucli estriat en ratolins control (WT). Així, es va observar que els sRNA injectats es trobaven en MSNs i en cèl·lules microglials, mentre que els oligodendròcits, els astròcits i les interneurones estriatals no presentaven sRNA en les condicions estudiades. A més, els sRNA tot i trobar-se preferentment en el nucli de les cèl·lules indicades, també es podien detectar en el citoplasma, fet que és consistent amb els mecanismes en els quals s'han vist implicats (Quan et al., 2017; Qureshi & Mehler, 2012; Salta & De Strooper, 2012).

Tot seguit, per tal de demostrar que els sRNA derivats del putamen de pacients de la MH (HD-sRNA-PT) contribueixen a la patogènesi es van injectar dues vegades per setmana durant dues setmanes al nucli estriat de ratolins WT. Així, es va veure que la injecció intraestriatal de HD-sRNA-PT, en absència de la proteïna mutada i els

seus derivats, induïa alteracions motores en aquests ratolins. Tot seguit, es va avaluar mitjançant següenciació si aquesta disfunció motora estava acompanyada de canvis transcriptòmics en el nucli estriat dels animals injectats. Aquest anàlisi va mostrar una important desregulació transcripcional en els animals injectats amb HD-sRNA-PT en comparació amb els respectius controls. És important remarcar que les alteracions detectades eren anàlogues a les que s'han descrit tant en pacients com en models murins de la MH (Durrenberger et al., 2015; Hodges et al., 2006; Langfelder et al., 2016). Molts dels transcrits que presentaven una davallada en la seva expressió estaven relacionats amb la funció neuronal, mentre que els que s'expressaven de forma més elevada s'associaven a una activació del sistema immune. En paral·lel, també es va analitzar si hi havia alteracions específiques de tipus cel·lular i es va observar que la majoria de transcrits disminuïts corresponien a gens de la subpoblació de MSNs de la via indirecta, que és la més afectada en la MH (Bergonzoni et al., 2021; Richfield et al., 1995; Rikani et al., 2014), mentre que la majoria dels que presentaven una major expressió estaven enriquits en gens microglials indicant microgliosis, un procés que també s'ha descrit en el putamen dels pacients de la MH (Pavese et al., 2006; Tai et al., 2007). També es va validar la baixada en l'expressió de transcrits neuronals, clàssicament descrits com a alterats en la MH (Fourie et al., 2014; Saavedra et al., 2011; van Dellen et al., 2000), així com en els nivells de proteïna, juntament amb una reducció significativa del nombre de MSNs i un augment de cèl·lules expressant caspasa-3 fragmentada, com a marcador de mort cel·lular. En paral·lel, també es va confirmar la resposta pro-inflamatòria causada pels HD-sRNA-PT a través de l'anàlisi de múltiples gens relacionats amb la resposta immune, com Il1b o Tnf. En resum, aquests resultats van aportar la primera evidència de toxicitat in vivo generada per HD-sRNA-PT i el desenvolupament posterior d'un fenotip similar al descrit en la MH.

A més, també es va estudiar si la inflamació era prèvia o posterior a la neurotoxicitat observada. Per investigar-ho, es van fer injeccions agudes de HD-sRNA-PT i es van avaluar marcadors inflamatoris i neuronals 24 h després. Així, es va observar una activació pro-inflamatòria que no anava acompanyada per canvis a nivell neuronal, suggerint que la inflamació precedeix a la neurodegeneració causada pels HD-sRNA-PT. Cal destacar que estudis similars també han mostrat que existeix una activació microglial per exposició a determinats sRNA (Coleman et al., 2017; Lehmann et al., 2012; Pawar et al., 2020), però que aquesta no és essencial per desencadenar la neurotoxicitat causada pels sRNA (Lehmann et al., 2012). Per tant, el conjunt d'evidències suggereixen que la resposta immune inicial causada pels sRNA podria ser potenciadora de la posterior neurodegeneració però no la principal causa.

RESUM

Un cop definits els efectes causats per la barreja de HD-sRNA-PT, ens vam plantejar si la producció d'espècies de sRNA és específica de regions cerebrals vulnerables, com és el cas del putamen, o aquestes es generen de forma anàloga en altres regions menys afectades. Per adreçar-ho, vam injectar sRNA tant de pacients de la MH com d'individus no afectats, obtinguts del còrtex, com a regió afectada, i del cerebel, com a àrea cerebral menys alterada en la MH, tant histològicament com a nivell transcriptòmic (Hodges et al., 2006; Rosas et al., 2003). Es va observar que els sRNA produïts en el cervell de la MH, independentment de la regió, pertorbaven el comportament motor. En canvi, no es van poder detectar canvis en marcadors neuronals ni inflamatoris quan aquests sRNA provenien del còrtex i del cerebel, suggerint que les propietats bioquímiques intrínseques dels sRNA derivats de les àrees més afectades són les responsables de l'efecte patogènic. Tot i això, no es va poder descartar el fet que també existeixi una vulnerabilitat selectiva d'algunes zones cerebrals davant certes espècies de sRNA.

Tot seguit, es va analitzar la contribució de les espècies d'sCAG en els efectes derivats de la injecció intraestriatal dels HD-sRNA-PT, basant-nos en estudis previs que demostren la seva capacitat neurotòxica (Bañez-Coronel et al., 2012; Lawlor et al., 2011; Z. Yu et al., 2011). Per tal de determinar la seva potencial participació, es van seguir dues estratègies complementaries: la primera basada en el bloqueig de les espècies sCAG dins de la barreja de HD-sRNA-PT gràcies a l'LNA-CTG, el qual ja havia demostrat efecte en estudis anteriors (Rué et al., 2016), i la segona basada en la injecció d'espècies sCAG sintètiques pures. Ambdues estratègies van confirmar la implicació d'aquestes espècies en la patogènesi de la MH tant a nivell de comportament motor com en quant a la neuropatologia, consistentment amb el que havíem observat anteriorment (Bañez-Coronel et al., 2012; Rué et al., 2016). Per tant, aquests resultats van accentuar la rellevància dels efectes perjudicials mediats per l'expansió de trinucleòtids a nivell de RNA, no només en la MH, sinó també en altres malalties causades per expansió de trinucleòtids (Krol et al., 2007; Nalavade et al., 2013). Tot i això, els sCAG no permetien explicar tots els efectes tòxics observats i per tant, era necessari caracteritzar de forma exhaustiva la barreja de HD-sRNA-PT per tal d'identificar altres espècies de sRNA implicades en la neurotoxicitat i la desregulació transcripcional observades.

Passant al segon objectiu i amb la finalitat d'identificar noves espècies de sRNA candidates a ser les responsables dels efectes observats, es va seqüenciar la barreja de HD-sRNA-PT en paral·lel amb sRNA obtinguts del putamen d'individus no afectats. D'aquesta manera es va validar l'alteració de certs miRNA, ja descrits com a desregulats en el putamen de la MH (Hoss et al., 2014). A més, es va veure que les espècies de sRNA més abundants en HD-sRNA-PT eren els tsRNA, mentre que en la situació control els més expressats corresponien a miRNA. L'anàlisi exhaustiu

dels tsRNA va mostrar que hi havia una sobreproducció de fragments derivats de l'extrem 5' dels tRNA (5'halves i 5'tRF) i alguns dels més sobre-representats derivaven dels tRNA de glicina, valina i alanina. De fet, aquests resultats van en línia amb estudis que relacionen certs tsRNA amb situacions d'estrès oxidatiu i neurodegeneració (Anderson & Ivanov, 2014; Blanco et al., 2014; Hanada et al., 2013). Per tal d'anar un pas més enllà i demostrar el seu potencial neurotòxic, es van tractar cultius primaris estriatals sans amb aquestes espècies i es va observar que un tRF d'alanina era capaç de comprometre la viabilitat d'aquestes neurones. Aguests resultats ens van permetre confirmar que hi ha altres espècies, a part dels sCAG, dins de la barreja de HD-sRNA-PT que poden ser tòxiques per a les neurones estriatals. Tot i això, també caldria comprovar la capacitat neurotòxica d'aquests tRFs in vivo i valorar si el seu bloqueig podria ser considerat com una nova diana terapèutica per la MH. Paral·lelament, també es va estudiar el transcriptoma de sRNA del còrtex i del cerebel de pacients de la MH, els quals també van mostrar una desregulació en espècies de tsRNA però molt més moderada en comparació als canvis observats en el putamen, fet que ens va suggerir que es produeix una fragmentació selectiva i/o una estabilitat diferencial dependent de regió en la MH.

Finalment, vam passar al tercer objectiu basat en l'estudi de la contribució de factors rellevants implicats en la biogènesi dels sRNA en el cervell de la MH. Concretament, vam començar avaluant els nivells de diferents endonucleases descrites com a encarregades de la fragmentació de tRNA (R. Magee & Rigoutsos, 2020) però no vam detectar canvis significatius en el cervell dels pacients de la MH. Tot i això, aquests enzims no són els únics implicats en la biogènesi de tsRNA sinó que les modificacions post-transcripcionals hi tenen un paper molt important i, consequentment, també els enzims encarregats de la seva incorporació o eliminació (Chujo & Tomizawa, 2021; Pereira et al., 2018). De fet, s'ha demostrat que aquestes modificacions permeten expandir el lèxic de l'RNA i s'han vist involucrades en molts processos biològics, com la diferenciació cel·lular, la resposta a estrès, funcions neuronals... (Batista et al., 2014; Chan et al., 2010; Lence et al., 2016). NSun2 és una RNA metiltransferasa capaç de metilar algunes citosines dels tRNA contribuint a la seva estabilitat (Motorin & Helm, 2010). És important destacar que la seva manca s'ha relacionat tant amb un increment de la fragmentació dels tRNA diana (Blanco et al., 2014; Tuorto et al., 2012) com amb alteracions en l'aprenentatge i la memòria en models de Drosophila i de ratolí (Abbasi-Moheb et al., 2012; Blaze et al., 2021; George et al., 2022). A més, mutacions en NSun2 s'han descrit com a causa de discapacitat intel·lectual en humans (Khan et al., 2012; Martinez et al., 2012). Tenint en compte aquestes evidències, vam avaluar NSun2 en el context de la MH i vam observar una reducció dels seus nivells proteics tant en el putamen dels pacients com al nucli estriat de dos models de ratolí de la MH des d'etapes pre-simptomàtiques i de forma

específica de regió, coincidint amb l'àrea cerebral més afectada en els pacients (Vonsattel et al., 1985). Tot i això, caldrien més estudis per saber si aquesta reducció es produeix en un moment concret de la progressió de la MH en humans. En línia amb aquests resultats, també vam detectar un increment en la fragmentació de dianes específiques de NSun2 descrites a la bibliografia (Khoddami & Cairns, 2013) en el putamen de pacients de la MH.

Fins al moment, molts dels resultats obtinguts apuntaven cap a una implicació dels tsRNA en els mecanismes patogènics de la MH. Malgrat això, els estudis de següenciació de sRNA tradicionals han demostrat algunes limitacions a l'hora de detectar aquestes espècies degut a la presència de configuracions alternatives dels extrems de les sequències que impedeixen la correcta lligació dels adaptadors però també a l'elevada quantitat de modificacions epitranscriptòmiques presents que impossibiliten una retro-transcripció completa (H. Shi et al., 2021; E. L. Van Dijk et al., 2014). Per poder solucionar aquestes limitacions i conèixer amb detall el transcriptoma de sRNA associats a la MH, vam utilitzar una estratègia semblant a la de PANDORAseq (J. Shi et al., 2021), basada en el pre-tractament dels sRNA abans de la sequenciació amb la quinasa T4PNK juntament amb diferents desmetilases (D), per tal d'incrementar el nombre de següències compatibles amb el mètode de preparació de llibreries i obtenir una informació més completa del transcriptoma de mida petita. A més, la sequenciació la vam dur a terme amb la fracció de sRNA de mida inferior als 50 nt (ssRNA) ja que ens interessava centrar-nos en aquells sRNA que s'han descrit com a responsables de alteracions transcriptòmiques (miRNA, tsRNA...) i alhora assegurar-nos que estàvem eliminant els tRNA madurs que poden ser una font d'artefactes degut a la seva fragmentació durant el protocol. La següenciació va demostrar que el tractament amb els dos enzims millorava de forma clara la detecció específica dels tsRNA, alhora que també va permetre expandir la diversitat de subtipus detectats. Consegüentment, vam decidir aplicar aquesta estratègia a les mostres de ssRNA obtingudes del putamen i, en paral·lel, vam dur a terme un estudi a través de LC-MS de les modificacions epitranscriptòmiques presents en els tRNA precursors dels mateixos individus. D'aquesta manera vam poder correlacionar alteracions en la biogènesi de certs tsRNA amb canvis en els nivells de modificacions presents en els tRNA precursors en el context de la MH, ja que es tracta d'un mecanisme que s'ha associat àmpliament amb múltiples patologies (Lyons et al., 2018). A més, el fet de dur a terme una següenciació de les mateixes mostres pre-tractades amb T4PNK i amb T4PNK+D ens va permetre obtenir un resultat indirecte del nivell de metilació general que presenten els diferents ssRNA en funció de si provenen de pacients de la MH o d'individus no afectats. Concretament, vam poder associar l'increment de tsRNA derivats del tRNA d'alanina en el putamen de pacients de la MH amb una baixada en els nivells de metilació m¹I, la qual és específica per aquests tRNA,

contribuint a la seva desestabilització. Per últim, també vam descriure una sèrie de tsRNA significativament sobreexpressats en el putamen dels pacients de la MH i que postulem com a candidats per estar contribuint als mecanismes patogènics de la mateixa.

CONCLUSIONS

En resum, els resultats d'aquesta tesi reforcen la idea de que els sRNA generats en el putamen de pacients de a MH estan jugant un paper important en la patogènesis, contribuint tant a la neurotoxicitat com a la desregulació transcriptòmica en aquesta malaltia. A més, aquest estudi aporta nous recursos i obre noves vies d'investigació basades en (1) la identificació d'espècies de tsRNA produïdes en el decurs de la malaltia i associades a la severitat de la mateixa, (2) la comprensió dels mecanismes que regulen la seva biogènesi així com el paper que té la HTT mutada en la seva producció i (3) l'estudi dels mecanismes moleculars associats a la seva activitat neurotòxica i pro-inflamatòria subjacents a la MH. Conseqüentment, aquestes troballes porten a pensar que els sRNA generats en el context de la MH, especialment els tsRNA, han de ser considerats en els futurs abordatges terapèutics per tal d'assegurar el seu èxit.

acp³U 3-(3-amino-3-carboxypropyl)uridine

aCSF Artificial cerebrospinal fluid

AD Alzheimer's disease

ADAT Adenosine deaminase

Ago Argonaute

ALS Amyotrophic lateral sclerosis

ANG Angiogenin

AP Anteroposterior

ASO Antisense oligonucleotide

BAC Bacterial artificial chromosome

BDNF Brain-derived neurotrophic factor

BSA Bovine serum albumin

CAG Cytosine-adenine-guanine

CB Cerebellum

CC Corpus callosum

cDNA Complementary DNA

ChAT Choline acetyltransferase

circRNA Circular RNA

CTL Control

CTX Cortex

Cy3 Cyanine 3

D Dihydrouridine

DAB 3'-diaminobenzidine

DAPI 4',6-diamino-2-phenylindole

DARPP32 Dopamine- and cAMP-regulated phosphoprotein of 32kDa

DE Differentially expressed

DEG Differentially expressed gene

DIV Days in vitro

DM1 Myotonic dystrophy type 1

DMEM Dulbecco's modified Eagle's medium

DNA Deoxyribonucleic acid

DRD1 Dopamine receptor D1

DRD2 Dopamine receptor D2

dsRNA Double stranded RNA

dSTR Dorsal striatum

DV Dorsoventral

EDTA Ethylenediaminetetraacetic acid

ENK Enkephalin

5-formylcytosine

FBS Fetal bovine serum

FC Fold change

FDA US Food and Drug Administration

FXS Fragile X syndrome

GABA Gamma-aminobutyric acid

GO Gene ontology

GPe External globus pallidus

GPi Internal globus pallidus

H₂**O**₂ Hydrogen peroxide

HD Huntington's disease

Hdh Huntington's disease homolog

HRP Horseradish peroxidase

HTLV-1 Human T-cell leukemia virus type 1

HTT Huntingtin human gene

Htt Huntingtin mouse gene

HTT Huntingtin human protein

Htt Huntingtin mouse protein

I Inosine

INF Interferon

iPSC Induced pluripotent stem cells

ISG Interferon-stimulated gene

IT15 Interest transcript 15

KI Knock-in

LC-MS/MS Liquid chromatography – tandem mass spectrometry

LNA Locked nucleic acid

IncRNA Long non-coding RNA

LV Lateral ventricle

m¹A 1-methyladenosine

m¹G 1-methylguanosine

m¹l 1-methylinosine

m³C 3-methylcytosine

m⁵C 5-methylcytosine

m⁵**U** 5-methyluridine

m⁶**A** 6-methyladenosine

MBNL1 Muscleblind-like splicing regulator 1

mHTT Mutant huntingtin human gene

mHtt Mutant huntingtin mouse gene

mHTT Mutant huntingtin human protein

mHtt Mutant huntingtin mouse protein

miRNA Micro RNA

ML Mediolateral

mRNA Messenger RNA

MS Multiple sclerosis

MSN Medium spiny neuron

ncRNA Non-coding RNA

NHS Normal horse serum

NMDA N-methyl-D-aspartate

NPY Neuropeptide Y

nt Nucleotides

OH- Hydroxyl group

P- Phosphate group

PAGE Polyacrylamide gel electrophoresis

PARV Parvalbumin

PB Phosphate buffer

PBS Phosphate-buffered saline

PCH Pontocerebellar hypoplasia

PD Parkinson's disease

PHLPP1 PH domain and leucine rich repeat protein phosphatase 1

PMD Post-mortem delay

PMSF Phenylmethanesulfonylfluoride

PolyQ Polyglutamine

PSD95 Post-synaptic density protein of 95kDa

PT Putamen

Q Queuosine

RAN Repeat associated non-ATG-initiated

RBP RNA-binding protein

RIN RNA integrity number

RISC RNA-induced silencing complex

RNA Ribonucleic acid

rpm Rotations per minute

RQ Relative quantification

rRNA Ribosomal RNA

RSV Respiratory syncytial virus

RT Room temperature / Reverse transcription

RT-qPCR Quantitative reverse transcription polymerase chain reaction

SCA Spinocerebellar ataxia

sCAG Small CAG repeated RNA

SCB Scrambled

scRNA Small conditional RNA

SDS Sodium dodecyl sulphate

SEM Standard error of the mean

siRNA Short interfering RNA

snoRNA Small nucleolar RNA

SNpc Substantia nigra *pars compacta*

SNpr Substantia nigra *pars reticulata*

snRNA Small nuclear RNA

sRNA Small RNA (<200 nucleotides)

ssRNA Small RNA (17 to 50 nucleotides)

STEP Striatal-enriched protein tyrosine phosphatase

T4PNK T4 polynucleotide kinase

TBS-T Tris-buffered saline-Tween 20

tiRNA tRNA-derived stress induced RNAs

TLR Toll-like receptor

TNR Trinucleotide repeats

TOG Terminal oligoguanine motif

TRED TNR expanded diseases

tRF tRNA-derived fragments

tRNA Transfer RNA

tsRNA tRNA-derived small RNAs

UTR Untranslated region

Veh Vehicle

VS Vonsattel grade

WB Western blot

WT Wild type

Y Pseudouridine

YAC Yeast artificial chromosome

TABLE OF CONTENTS

INTRODUCTION	2
1. Huntington's disease	3
1.1 Huntingtin gene and protein	4
1.2 Epidemiology	5
1.3 Clinical features	6
1.4 HD treatment	8
1.5 Neuropathology and circuitry in HD	8
1.6 HD models	12
1.7 HD neuropathogenic mechanisms	16
2. RNA-mediated toxicity and its implications in disease	19
2.1 Expanded CAG RNA toxicity	20
2.2 Non-coding RNA toxicity	27
AIMS	41
METHODS	45
1. Human <i>post-mortem</i> samples	47
2. Mouse models	48
2.1 R6/1 mouse model	49
2.2 Hdh ^{Q7/Q111} mouse model	49
3. Cell cultures	49
3.1 Primary neuronal cultures	49
3.2 Striatal cell lines	50
3.3 Cell viability assay	50
4. Molecular biology techniques	51
4.1 Total RNA isolation	51
4.2 sRNA purification	51
4.3 Isolation of specific-sized RNAs	51
4.4 RNA quality control and quantification	51
4.5 sRNA labelling	52
4.6 ssRNA enzymatic pre-treatments	52
4.7 Quantitative reverse transcription PCR (RT-qPCR)	53

	4.8 RNA polyadenylation and PCR amplification of sCAG and HTT exon 1	55
	4.9 RNA mass spectrometry (LC-MS/MS)	56
	4.10 Total protein extraction	57
	4.11 Protein quantification	57
	4.12 Western Blot (WB) analysis	57
5.	Morphological analysis	59
	5.1 Tissue preparation	59
	5.2 Nissl staining	59
	5.3 Immunohistochemistry	59
	5.4 Bright field image acquisition and analysis	60
	5.5 Immunohistofluorescence	60
	5.6 Confocal image acquisition and analysis	62
6.	In vivo approaches	62
	6.1 Intrastriatal cannula implantation	62
	6.2 Preparation of sRNA pools for <i>in vivo</i> injections	63
	6.3 Intrastriatal infusion	64
	6.4 Intrastriatal injection	65
	6.5 Behavioral analysis	65
7.	Sequencing approaches	66
	7.1 sRNA-sequencing of human and mice samples	66
	7.2 RNA sequencing of mice samples	67
	7.3 PANDORA-sequencing of human samples	67
8.	Bioinformatic analysis	67
	8.1 Quality control and adapter trimming	67
	8.2 Alignment of reads and data analysis	68
	8.3 Downstream analysis of sequencing data	69
9.	Statistical analysis	69
RESU	JLTS	71
	Study of the potential neurotoxic role of sRNA derived from HD patients'	73
	1.1 Distribution of sRNA after their injection in the striatum of WT mice	73

1.2 Intrastriatal injection of HD-sRNA-PT alters motor function in WT mice. 78
1.3 HD-sRNA-PT induce selective gene expression alterations in WT mice striatum concordant with an HD-associated transcriptional signature 80
1.4 HD-sRNA-PT induces specific neuronal degeneration in WT mice striatum 84
1.5 HD-sRNA-PT induces striatal inflammation in WT mice
1.6 HD-sRNA from different brain regions differentially affect motor function but do not recapitulate HD molecular abnormalities in WT mice striatum 89
1.7 sCAG are partial contributors to the detrimental effects of HD-sRNA-PT93
2. Characterization of the sRNA transcriptome in different areas of HD brains and potential roles in HD pathogenesis
2.1 Different areas of the HD brain present dysregulated sRNA signatures, with an overproduction of tsRNA
2.2 Specific tsRNA species which are overproduced in HD putamen display neurotoxic effects
3. Study of the contribution of key players involved in tsRNA biogenesis in HD pathogenesis
3.1 The RNA methyltransferase NSun2 is altered in HD patients and several HD models
3.2 Overcoming RNA modifications expands the repertoire of detected tsRNA
3.3 Epitranscriptomic tRNA modifications regulate specific tsRNA biogenesis ir
DISCUSSION
1. Involvement of HD-sRNA-PT in HD neuropathology 140
2. Identification of HD-sRNA-PT neurotoxic species
3. Importance of sRNA biogenesis in HD putamen
4. Limitations of the study
5. Potential and future perspectives
CONCLUSIONS
REFERENCES
ANNEX 215

INTRODUCTION

Neurodegenerative diseases have a major impact on the lives of people who suffer them, resulting in a progressive decline in their physical, cognitive and social abilities. Although the aetiopathologies of these neurodegenerative disorders commonly involve complex spatial-temporal interactions between internal genetic factors and external environmental stimuli, the case of Huntington's disease (HD) is an example of a monogenic neurological disorder whose investigation should be more straightforward as a single genetic factor drives disease progression. However, there are no cures that can halt or, at least, delay this devastating deterioration. Therefore, there is an actual need to unravel the pathological processes underlying HD to efficiently treat patients.

For many years most research in HD has focused on the pathogenic effects of the resultant mutated protein products. Conversely, the mutated RNA has traditionally been seen as a mere intermediary to transfer DNA information into protein codification (Brenner et al., 1961). However, growing evidence indicates that aberrantly expanded RNA and its derivatives actively participate in HD pathophysiology, although the individual contribution of protein versus RNA toxicity remains uncertain. In this thesis, we have focused on deeply characterizing the small non-coding RNA transcriptome in HD to identify RNA species that are enriched in the most affected brain areas and potentially contribute to the pathogenic mechanisms.

1. Huntington's disease

HD is a neurodegenerative disorder characterized by multiple motor manifestations, cognitive disturbances, and psychiatric symptoms. Although before the 16th century this condition was known as "St Vitus's dance", it was not until 1872 that it was first described by George Huntington (Wexler, 2013). In the paper "On chorea" published in the *Medical and Surgical Reporter* of Philadelphia, he reported an exhaustive description of the motor, cognitive and psychiatric symptoms observed together with the hereditary nature of the disease and the progressive affectation of the patients starting in the adult life (Huntington, 2003). The disease was then termed as "hereditary chorea" due to the characteristic movements observed in the patients and afterwards the name was changed to HD to encompass all the manifestations of the disease.

However, the discovery of the mutated gene responsible for HD was not reported until many years later. In 1983, it was described that the gene related to HD resided on chromosome 4 (Gusella et al., 1983), specifically on the short arm of this chromosome (4p16.3) and finally in 1993, the *IT15* gene (interest transcript 15) was identified as the defective gene in HD presenting a coding sequence with an expanded trinucleotide repeat in the affected individuals (The Huntington's Disease Collaborative Research Group, 1993). The *IT15* gene is nowadays commonly known

INTRODUCTION

as huntingtin (*HTT*) gene in humans and its murine homologous is the *Hdh* gene which is located in the chromosome 5 (Grosson et al., 1994; Nasir et al., 1994).

1.1 Huntingtin gene and protein

In HD, there is an abnormal expansion of the number of cytosine-adenine-guanine (CAG) repeats within the exon 1 of the *HTT* gene, leading to an expanded RNA that encodes for a polyglutamine (polyQ) track in the HTT protein (The Huntington's Disease Collaborative Research Group, 1993). *HTT* gene spans around 180 kb, consists of 67 exons and although it is well-conserved among vertebrates, it presents a poor homology with invertebrates (Gissi et al., 2006; Tartari et al., 2008).

HD is a monogenic disorder presenting an autosomal dominant inheritance. In non-affected individuals, the alleles of this gene present repeat lengths with 10 to 35 CAGs (Kremer et al., 1994). In contrast, individuals with a stretch of more than 36 CAG repeats will develop HD, although different penetrances have been described depending on the length of the expansion. Alleles presenting 36 to 39 CAG repeats have been correlated with a reduced penetrance, while HD is exhibited at full penetrance in subjects presenting more than 40 trinucleotide repeats (Walker, 2007). Due to these variable rates of penetrance, CAG repeat length appears as causal in individuals presenting 40 or more CAG repeats while it is necessary but not sufficient to define HD in individuals with 36-39 CAG repeats and needs to be complemented with additional measures to confirm a biological diagnosis (Tabrizi, Schobel, et al., 2022). Moreover, above the threshold of 50 glutamine encoding repeats, a juvenile manifestation of HD emerges as it develops in early life in an aggressive form (Gordon, 2003; Figure 1).

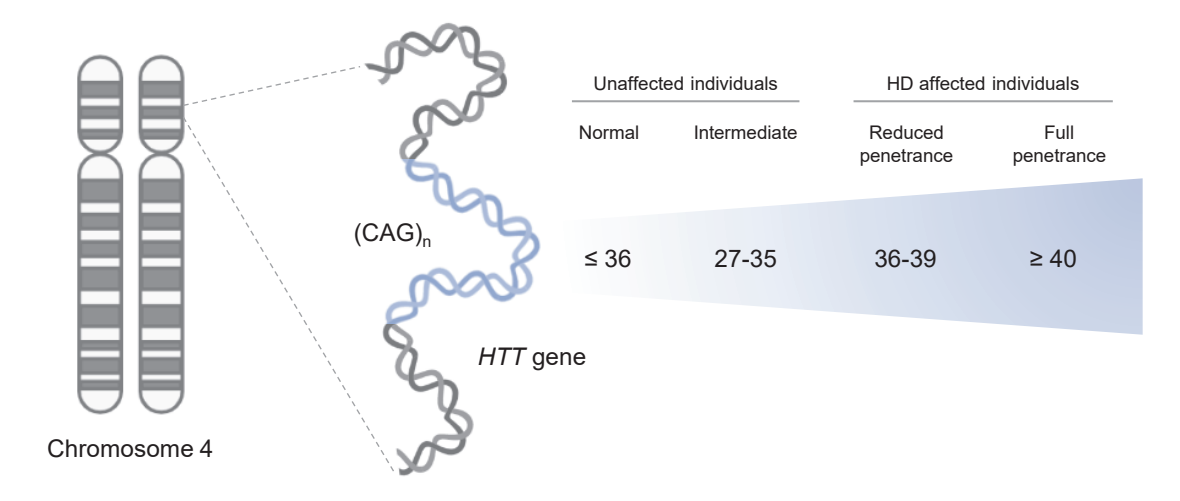


Figure 1. Cytogenetic localization of human *HTT* gene and differential affectation depending on CAG repeat length. *HTT* gene is located within the short arm of the chromosome 4 (4p16.3) and presents a polymorphic CAG stretch in the exon 1. CAG expansion length is associated with HD clinical manifestations resulting in a classification of individuals between unaffected (normal and intermediate alleles) and affected patients with reduced or full penetrance.

It is worth mentioning that a meiotic CAG instability is common, especially during spermatogenesis, and could explain earlier onsets and more severe manifestations of HD in successive generations, with the more striking cases occurring in paternal transmissions (Duyao et al., 1993; Telenius et al., 1994).

Although inter-individual clinical expression and age of onset are substantially variable among affected individuals, the most common age of clinical onset is around 40 years old (Novak & Tabrizi, 2010). As it has been mentioned, longer CAG expansions have been correlated with earlier onsets, with juvenile cases defined by an onset before the age of 21 years old (Ross & Tabrizi, 2011; J. G. van Dijk et al., 1986). Conversely, CAG repeat length has little impact on the rate of progression (Rosenblatt et al., 2006). Finally, HD is uniformly fatal, with a life expectancy after symptoms appearance of 10 to 20 years (Ross et al., 2014).

HTT protein in the wild-type (WT) form is composed by 3144 amino acids with a total molecular weight of 348 kDa. Its expression is ubiquitous both throughout the different tissues and different cell types with variable levels among them, displaying the highest levels in brain and testis. Concerning the brain, HTT is mainly expressed in the striatum, neocortex, hippocampus and cerebellum. HTT present a widespread subcellular distribution, as it can be found in the nucleus but also in the cytoplasm as well as associated with multiple organelles (Borrell-Pagès et al., 2006; Trottier et al., 1995). Consistently, HTT has been reported to be involved in multiple cellular processes including vesicle trafficking and endocytosis, cell division and morphology, autophagy, cell survival and even regulation of transcription (reviewed in Saudou & Humbert, 2016). In fact, its expression is critical for embryonic development and a knock-out of *Htt* in mice leads to lethality before birth (Duyao et al., 1995).

In contrast, the expansion of the CAG stretch within the *HTT* gene gives rise to a mutated HTT protein (mHTT) which has been reported to display a toxic gain-of-function (Bates et al., 2015; Saudou & Humbert, 2016; Tabrizi et al., 2020). mHTT misfolds abnormally due to the aberrant polyglutamine tract giving rise to soluble monomers which combine generating oligomers that act as seeds forming large inclusions and aggregates, found both in the nucleus and the cytoplasm (Cooper et al., 1998; Davies et al., 1998). Whether mHTT aggregates are a protective mechanism or pathogenic is still under debate.

1.2 Epidemiology

There are important differences in HD prevalence depending on the geographic localization, with estimates of more than 10-fold variations between regions (Rawlins et al., 2016). While in Western populations between 10.6 and 13.7 individuals per 100.000 is affected by HD, a lower prevalence is observed in Japan,

Taiwan and Hong Kong with 1-7 cases per million (McColgan & Tabrizi, 2018). In fact, it has been reported that populations from Europe, North America and Australia present the highest prevalence rates in comparison to Asian populations (Pringsheim et al., 2012; Warby et al., 2011). In contrast, the Maracaibo Lake in Venezuela has been reported as the region with the highest incidence worldwide with 700 affected individuals per 100.000. Remarkably, HD chromosomes reported in the United States, Canada, South Africa, Australia, the Caribbean, the Indian Subcontinent and Venezuela can be genealogically linked to European ancestors (Warby et al., 2011).

1.3 Clinical features

HD patients present a broad range of clinical features including progressive motor decline, cognitive disturbances and psychiatric symptoms (Figure 2). Although chorea usually appears early in the disease progression, substantial cognitive and behavioral alterations may manifest years before the onset of motor symptoms (Ross & Tabrizi, 2011).

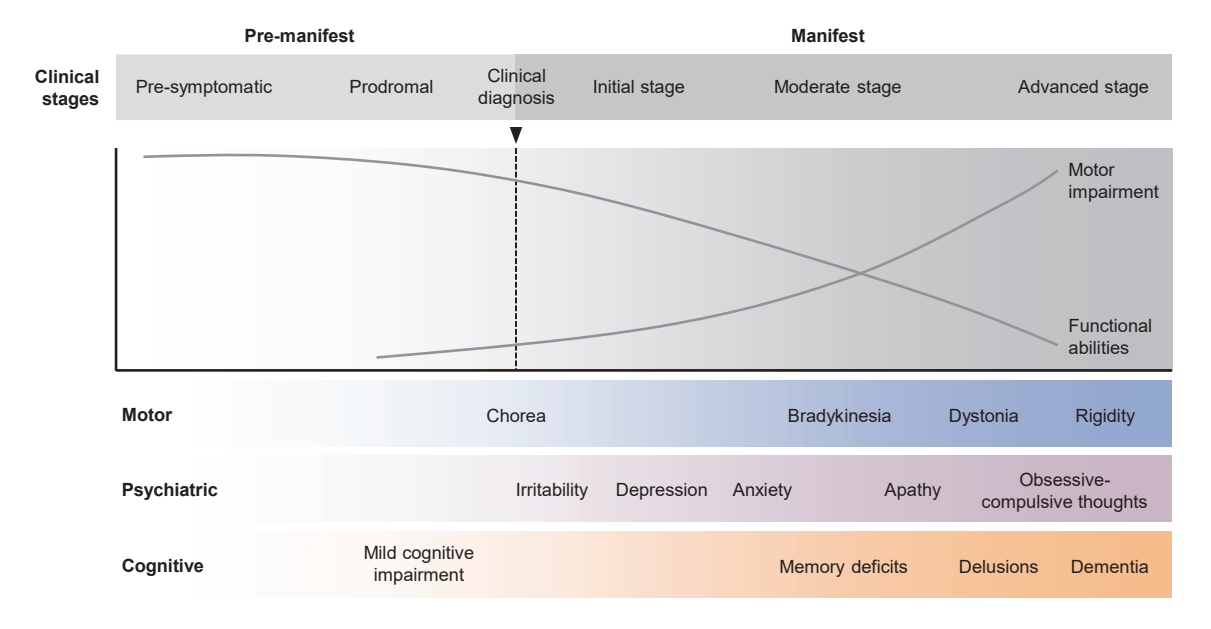


Figure 2. HD clinical progression. Schematic representation of the evolution of motor, psychiatric and cognitive symptoms along the different stages of the disease. HD patients suffer a progressive decline in their functional abilities from pre-symptomatic to advanced stages.

In recent years, the HD Integrated Staging System (HD-ISS) has been developed for the classification of HD progression centered on the combination of biological, clinical and functional evaluations (Tabrizi, Schobel, et al., 2022). However, the course of HD has been classically divided into two different stages, namely premanifest and manifest. Along the pre-manifest period, HTT mutation carriers are not clinically distinct from non-affected subjects (referred to as pre-symptomatic) and it can extend up to 10-15 years before the clinical onset. Following this phase

and also within the pre-manifest period, these individuals enter into the prodromal stage in which subtle alterations appear in terms of motor, cognitive and behavioral signs (Ross et al., 2014). Formal clinical diagnosis of HD is based on characteristic motor symptoms, especially chorea, together with genetic testing and/or family history.

Regarding the motor dysfunction observed in HD, it encompasses two different components. While the first category is based on involuntary movements as chorea or oculomotor dysfunction, the second includes defective voluntary movements leading to incoordination (impaired limb coordination and hand function), dystonia, rigidity and bradykinesia (Young et al., 1986). In fact, although choreiform movements are the most prominent symptoms during early stages, the hypokinetic symptoms become more pronounced as the disease progresses being the most functionally disabling (Novak & Tabrizi, 2010). In the case of juvenile HD, patients rarely present chorea but a more prominent bradykinesia at the onset (Rosenblatt et al., 2006; J. G. van Dijk et al., 1986).

Alterations in cognitive performance initiate years before patients' diagnosis leading to a gradual decline that may be as distressing and disabling as the motor impairments. mHTT-carriers commonly present difficulties in tasks requiring strategy shifting in the pre-manifest stages (A. K. Ho et al., 2003) together with disrupted verbal fluency, alterations in procedural learning, emotion recognition, planning and explicit motor learning, among others, as the disease progresses (reviewed in Giralt et al., 2012; Ross et al., 2014). At late disease stages, sub-cortical dementia emerges resulting in a worsen in several cognitive skills (reviewed in Puigdellívol et al., 2016).

Considering the neuropsychiatric signs, depressive symptoms and irritability have been widely reported in HD patients along the early stages of the disease (Berrios et al., 2002; Paulsen et al., 2005; Ross et al., 2014) in addition to the affective disorder which is an important trait present in the prodromal stage (Julien et al., 2007; Paulsen et al., 2001). Apathy is gradual and frequently disabling, especially in advanced stages (van Duijn et al., 2014). Dysphoria, agitation, anxiety, obsessive-compulsiveness and psychoticism are also commonly observed symptoms among HD patients (Duff et al., 2007). Finally, prevalence of suicide is higher in HD patients compared to general population, with depression and impulsivity as risk factors (Novak & Tabrizi, 2010; van Duijn et al., 2014).

Importantly, alterations non-related to the brain have also been described in HD patients due to the fact that the mutated protein is also expressed in the peripheral tissues. Non-neurological abnormalities include sleep disturbances, metabolic and immune alterations, muscle atrophy, osteoporosis and weight loss (van der Burg et

al., 2009). The most frequent causes of death observed in affected individuals are pneumonia and cardiovascular diseases (Sørensen & Fenger, 1992), occurring between 15 to 20 years after onset (Ross & Tabrizi, 2011).

1.4 HD treatment

Currently, there is no effective treatment which can cure, prevent, or slow HD. Therefore, the clinical care of HD patients is focused on the symptomatic management via multidisciplinary interventions, combining pharmacological and non-pharmacological strategies. Tetrabenazine and deutetrabenazine are the only approved drugs by the US Food and Drug Administration (FDA) for treating chorea (Bates et al., 2015; A. Kim et al., 2021). Both treatments aim to modulate hyperkinesia, however undesirable side effects are not negligible. Treatment of cognitive and psychiatric symptoms is based on cognitive behavior therapy in addition to antipsychotics and selective serotonin uptake inhibitors (Ross & Tabrizi, 2011).

1.5 Neuropathology and circuitry in HD

HD neuropathology is mainly characterized by a prominent and progressive atrophy of the striatum, comprising the caudate and putamen brain areas in humans (Figure 3A; Vonsattel et al., 1985). Notably, there is a correlation between caudate degeneration and the chorea observed in the affected subjects (Vonsattel & DiFiglia, 1998). In fact, although mHTT is ubiquitously expressed in all tissues, there is a preferential degeneration of the GABAergic medium-sized spiny neurons (MSNs) representing the main neuronal population in the striatum. In contrast, striatal interneurons are moderately spared (Ferrante et al., 1987; Rikani et al., 2014; Zuccato et al., 2010).

Considering striatal atrophy as a major hallmark in HD, Jean Paul Vonsattel in 1985 stablished a grading system to evaluate the neuropathological changes within HD brains based on macroscopic and microscopic morphological analyses (Vonsattel et al., 1985). Five grades of ascending severity (from 0 to 4) were defined depending on the neuropathological abnormalities observed. Brains classified as Vonsattel grade 0 are almost indistinguishable from non-affected brains, although patients present clinical symptoms and a 30-40% of neuronal loss can be observed in the caudate. Vonsattel grade 1 (VS1) is determined by the emergence of a moderate astrogliosis that becomes more severe in the following grades. Grades 2 and 3 (VS2-3) comprise brains with a prominent striatal degeneration together with an enlargement of lateral ventricles, while grade 4 (VS4) include the more severe cases of striatal atrophy displaying up to 95% of neuronal loss (Figure 3B; Vonsattel, 2008; Vonsattel et al., 1985).

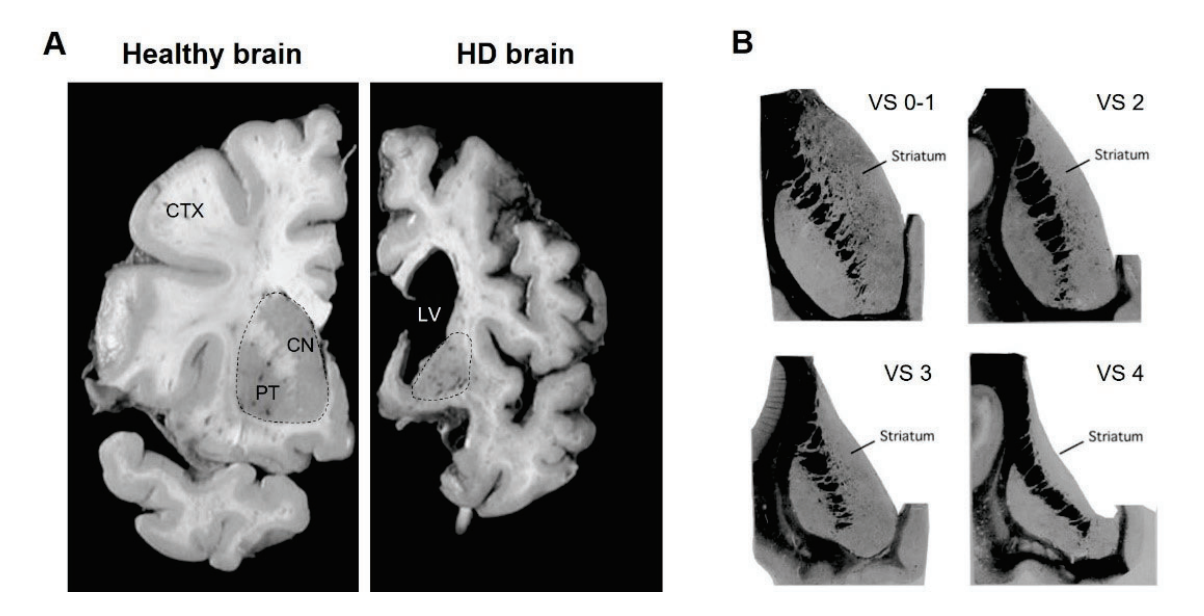


Figure 3. Neuropathological hallmarks in HD brain. (A) HD patients undergo a progressive neurodegeneration with a striatal atrophy (formed by the caudate and the putamen in humans) as the major hallmark. In parallel, an enlargement of the lateral ventricles and a shrinkage of the cortex are also observed. CTX: cortex, CN: caudate nucleus, PT: putamen, LV: lateral ventricle. (B) Illustrations showing striatal neurodegeneration and the corresponding Vonsattel grade (VS) from 0 to 4. Adapted from Reiner et al., 2011.

However, *post-mortem* HD brains present a smaller size than non-affected brains in advanced stages of the disease, evidencing neuropathological alterations in non-striatal regions in a variable severity and becoming widespread with disease progression (Novak & Tabrizi, 2010; Vonsattel & DiFiglia, 1998). Layers III, V and VI of the cerebral cortex present a pronounced degeneration in advanced stages of the disease. In addition, globus pallidus, thalamus, subthalamic nucleus, substantia nigra, white matter, cerebellum and hippocampus have been also described as affected brain regions (Vonsattel & DiFiglia, 1998). Confirming the neuropathological findings, substantial volume reductions of almost all brain areas have been observed in MRI studies (Rosas et al., 2003).

As a consequence of the selective degeneration of MSNs in the striatum, encompassing for the 90-95 % of the neuronal population of this area (Gerfen, 1988), a dysregulation of the basal ganglia circuitry arises in the context of HD pathology. Basal ganglia comprise a group of interconnected subcortical nuclei including the globus pallidus, the subthalamic nucleus, the substantia nigra and the striatum (comprising the caudate and the putamen) with a complex interconnectivity among the different areas (Albin et al., 1989; Gerfen, 1988). In turn, globus pallidus is subdivided into the external and the internal globus pallidus (GPe and GPi) and also the substantia nigra presents two differentiated segments, the substantia nigra pars compacta (SNpc) and the substantia nigra pars reticulata (SNpr). The integration of excitatory inputs from the cortex and the thalamus

through basal ganglia and their proper output allow an optimal control of voluntary movement, however affectations in individual nuclei lead to global circuitry impairments (Gerfen et al., 1990).

The striatum comprises different neuronal subtypes classified as projection neurons and interneurons (Ferrante et al., 1987). MSNs are GABAergic projection neurons that can be divided into two subtypes depending on the expression of different dopamine family receptors, the neuropeptide content, and their projection into other brain regions. The first type of MSNs mainly express the dopamine receptor D1 (DRD1) and the muscarinic receptor M4 and can be identified by the expression of substance P and dynorphin. Conversely, the second type of MSNs are characterized by the expression of the dopamine receptor D2 (DRD2) and the enkephalin (ENK) neuropeptide (reviwed in Bergonzoni et al., 2021). Although the main neuronal population in the striatum is constituted by MSNs (Gerfen, 1988), a small percentage of the total striatal population is formed by striatal GABAergic and cholinergic interneurons (Tepper & Bolam, 2004). Two different groups of GABAergic interneurons are generally recognized: the first subtype expresses neuropeptide Y (NPY), somatostatin and nitric oxide synthase while the other one is characterized by the expression of parvalbumin (PARV) and calretinin (Kawaguchi et al., 1995; Tepper et al., 2010). Regarding the cholinergic interneurons, they are recognized by the expression of choline acetyltransferase (ChAT) (Bolam et al., 1984; Kimura et al., 1980).

Focusing on basal ganglia connectivity, extrinsic excitatory inputs to the striatum mainly arise from the cortex (glutamatergic) and to a lesser extent from the thalamus (glutamatergic) and the SNpc (dopaminergic). The excitatory inputs are mostly integrated and processed by striatal MSNs that send inhibitory outputs (GABAergic) through two different pathways. While MSNs expressing DRD1 (D1-MSNs) form the direct pathway connecting the striatum with the GPi and with the SNpr, MSNs presenting DRD2 (D2-MSNs) send outputs to the GPe that, in turn, project to the GPi via the subthalamic nucleus (STN). Classically, it has been described that these two pathways have opposite effects, with an activation of movement through the direct pathway and an inhibition via the indirect pathway (see Healthy brain in Figure 4; Albin et al., 1989).

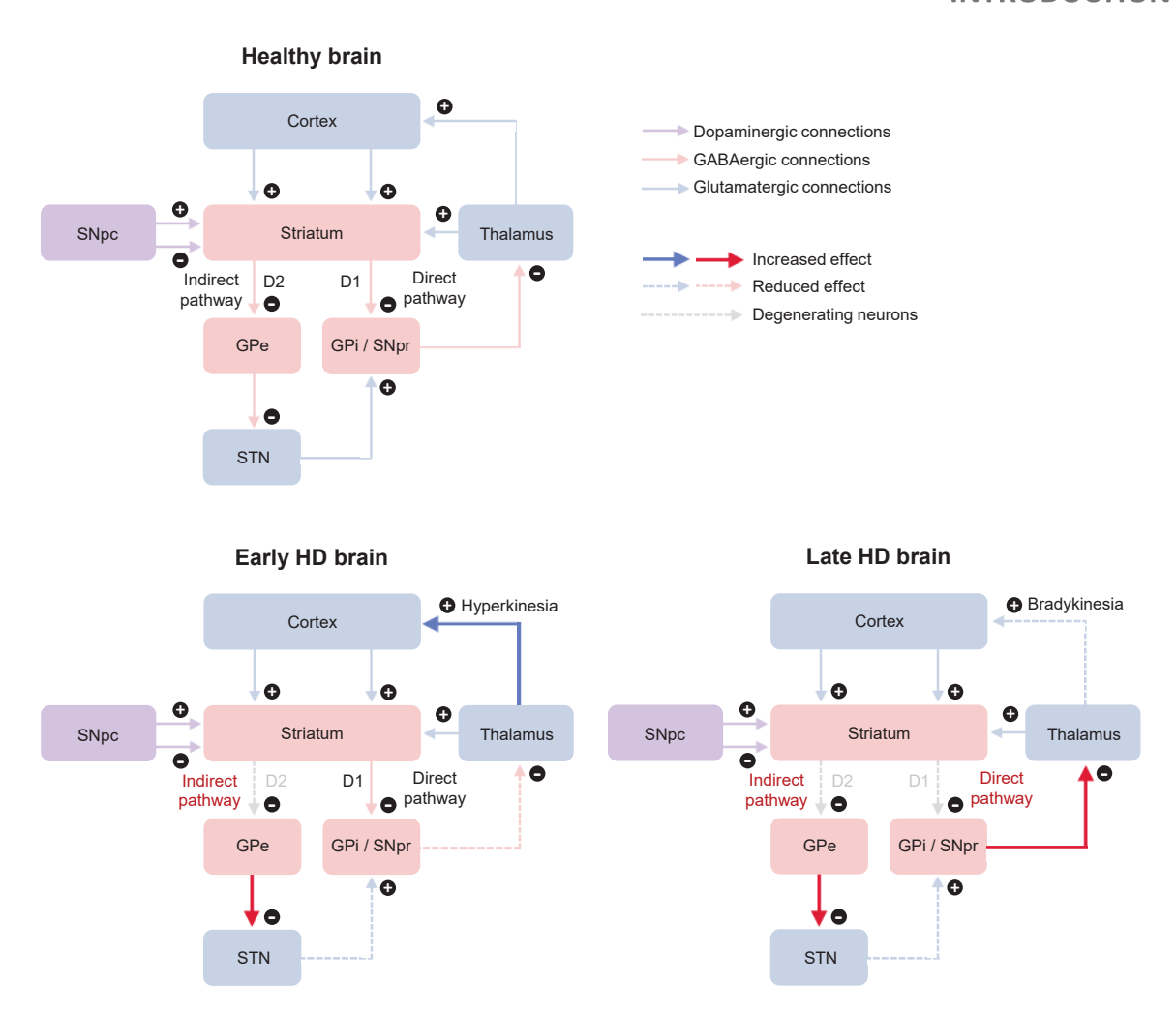


Figure 4. Basal ganglia circuitry and its alterations during HD progression. Simplified representation of basal ganglia circuitry in a healthy brain and in early and late stages of HD. An increase or a decrease in the activity of specific connections is indicated with darker or discontinued arrows, respectively. Grey discontinued arrows indicate a neuronal loss. GPe: external globus pallidus, GPi: internal globus pallidus, SNpc: substantia nigra *pars compacta*, SNpr: substantia nigra *pars reticulata*, STN: subthalamic nucleus.

In the context of HD, it is well established that there is a sequential degeneration of MSNs with a selectively early loss of D2-MSNs and a subsequent affectation of D1-MSNs throughout disease progression (Reiner et al., 1988; Richfield et al., 1995; Rikani et al., 2014; Sapp et al., 1995). Hence, the initial disinhibition of the GPe due to the lack of striatal D2-MSNs leads to an overactivation of the cortex that explain the choreiform movements described in the early stages of HD (see Early HD brain in Figure 4; Hendreen & Folstein, 1995). Nevertheless, during advanced stages of the disease, D1-MSNs also undergo degeneration triggering a considerable inhibition of the thalamus and consequently of the cortex that can explain the hypokinesia and rigidity observed in the patients (see Late HD brain in Figure 4; Bergonzoni et al., 2021; Y. P. Deng et al., 2004).

Apart from the progressive neuronal atrophy, it has been described that a gradual astrogliosis becomes more prominent along disease progression (Vonsattel et al., 1985). In line with this observation, a role of astrocytes has been proposed since alterations in these cells contribute to exacerbate neuronal excitotoxicity (Estrada-Sánchez & Rebec, 2012). In addition, reactive astrocytes and microglia have been identified in human HD brains and might participate in the pathogenesis through the perpetration of inflammation (Sapp et al., 2001; Vonsattel et al., 1985).

1.6 HD models

In order to unravel the molecular basis of HD, *post-mortem* human samples constitute an important source of information. However, since the study of many aspects of disease symptomatology and progression are limited in these samples, HD models represent a valuable tool in the research on both the neuropathology and preclinical validation of therapeutic strategies. Currently, there are many different HD paradigms including *in vitro* and *in vivo* models.

Regarding the *in vitro* models, the most commonly used cell lines for initial assessments are PC-12 cells (Song et al., 2002) and the striatal cell line STHdh^{Q111/Q111} (Trettel et al., 2000), in addition to other valuable *in vitro* options such as primary neuronal cell cultures and induced pluripotent stem cells (iPSC). An important advantage of these models is their potential to be genetically modified making them a good option for the dissection of the mechanisms underlying the disease.

A broad variety of invertebrate species have been used, comprising flies (*Drosophila Melanogaster*; Jackson et al., 1998; Marsh et al., 2003), worms (*Caenorhabditis elegans*; Brignull et al., 2006; Faber et al., 1999) and zebrafish (*Danio rerio*; Karlovich et al., 1998; Schiffer et al., 2007), since they are especially useful for genetic manipulation apart from their short generation times, high reproductive rates, and limited life spans, defining perfect models for high-throughput drug screenings. Notably, relevant hallmarks of HD are observed in these models such as progressive motor dysfunction and neuronal degeneration in the case of the fruit fly HD model (reviewed in Zuccato et al., 2010). Larger mammals have also been used for HD investigation, including sheep (Jacobsen et al., 2010), minipigs (Baxa et al., 2013) and non-human primates (S. H. Yang et al., 2008). These models are preferred for preclinical trials due to their suitability for safety, tolerability, and efficacy tests in longitudinal studies. However, the murine models represent the most popular HD animal models, being widely used to study the behavioral and molecular alterations related to HD pathogenesis (Table 1).

Table 1. Genetically modified HD mouse models. The table contains a description of the characteristics of the most frequently used genetic murine HD models including their behavioral and neuropathological hallmarks. Mice ages are expressed in weeks (w) or months (m).

Hdh ^{Q7/Q111} (KI)	BACHD	YAC128	N171-82Q	R6/2	R6/1	Mouse
Full-length mouse htt gene expressing an expanded CAG stretch	Full-length human HTT gene expressed in a bacterial artificial chromosome	Full-length human HTT gene expressed in a yeast artificial chromosome	N-terminal fragment of human <i>HTT</i> gene	N-terminal fragment of human <i>HTT</i> gene (3 copies)	N-terminal fragment of human <i>HTT</i> gene (1 copy)	Transgene
Mouse <i>Hdh</i> promoter	Human <i>HTT</i> promoter	Human <i>HTT</i> promoter	Mouse prion protein promoter	Human <i>HTT</i> promoter	Human <i>HTT</i> promoter	Promoter
111 CAG	97 CAA-CAG	128 CAG	82 CAG	144 CAG	116 CAG	PolyQ expansion
6m	12m	18m	16w	4w	9w	Aggregates
2m	2m	2m	14w	4w	12w	Cognitive deficits
8 3	2m	6m	12w	5-6w	14-16w	Motor
Not altered	Not altered	Not altered	20-24w	13-16w	32-40w	Life span
Neurodegeneration	Degenerating neurons	Striatal neuronal loss	Apoptotic neurons	Not detected	Not detected	Neuronal death
Loss	Increase	Increase	Loss	Loss	Loss	Body weight

1.6.1 Genetic mouse models

Prior to the discovery of the mutation leading to HD, murine models were induced by striatal lesion using different compounds, namely quinolinic acid as an N-methyl-D-aspartate (NMDA) agonist leading to MSNs death (Beal et al., 1991) and 3-nitropropionic acid as a mitochondrial toxin that inhibited the complex II of the mitochondrial respiratory chain (Borlongan et al., 1995). An important limitation of these models was the inability to replicate disease progression due to the acute origin of the striatal lesions. Moreover, extra-striatal and peripheral neuropathology was also lacking in these animals, highlighting an insufficient recapitulation of HD-linked pathogenic mechanisms. Therefore, genetic mouse models appeared as the most suitable model to provide deeper comprehension of the disease. Multiple techniques have been employed for the development of HD mouse models, generating transgenic mice (N-terminal and full-length) and *knock-in* (KI) animals. These models differ depending on the mHtt origin, the promoter driving its expression and the length of the polyglutamine expansion, leading to different temporal patterns of disease progression and severities.

1.6.1.1 N-terminal transgenic mouse models

The N-terminal transgenic mouse was the first genetic model generated and it was named R6 (Mangiarini et al., 1996). This model presents a genomic fragment of the 5' region of the *mHTT* human gene, including the 5'UTR with the human promoter and the exon 1 containing the expanded CAG stretch, inserted in a random position within the mouse genome. Original R6 models were divided into R6/1 and R6/2 depending on the number of CAG repetitions present within exon 1 of the *HTT* gene, with 116 and 144 repeats, respectively. The number of transgene copies is also different among models, with a single copy in the R6/1 while up to 3 copies are found in R6/2 mice. Consequently, phenotypic expression appears to be more pronounced when the gene dosage is higher, resulting in a reduction of their lifespan.

Both animal models recapitulate multiple HD-related symptoms such as stereotypic movements, resting tremor and epileptic seizures as well as classical HD neuropathological hallmarks including increased brain atrophy, reduced striatal volume and general weight loss (Mangiarini et al., 1996). Neuronal nuclear mHtt inclusions and decreased striatal dopamine D1 and D2 receptors have also been described in these models, resembling human neuropathological events (reviewed in Zuccato et al., 2010). Although a reduction in multiple synaptic markers in different brain regions have been described (Anglada-Huguet et al., 2014; Cummings et al., 2006; Nithianantharajah et al., 2008), the absence of neuronal death represents an important limitation of this model (Ferrante, 2009; Naver et al., 2003).

Therefore, R6 models display an early onset of the disease with an accelerated disease progression giving rise to an aggressive phenotype in a short period of time, defining a useful mouse line for testing therapeutic strategies and investigating HD pathogenic mechanisms. In contrast, these features make this model less suitable for the study of pre-symptomatic stages of the disease.

A similar mouse model is the N171-82Q transgenic mice expressing a truncated N-terminal fragment of the mHTT protein formed by 171 amino acids, including a polyglutamine stretch containing 82Q (G. Schilling et al., 1999). Moreover, the promoter of the transgene is a mouse prion protein leading to a specific expression in neurons. However, the behavioral and pathological alterations observed in these animals resemble the phenotypes described for the R6 models, despite for the presence of some apoptotic neurons in the striatum and cortex (Z. X. Yu et al., 2003).

1.6.1.2 Full-length transgenic mouse models

Full-length mouse models present the entire *mHtt* gene randomly inserted in the genome or gene-targeted into the *Htt* gene murine locus (*Hdh* locus), resulting in YAC and BAC models or KI models, respectively. In both cases, overexpression of full-length *mHtt* leads to a milder phenotype than the one observed in N-terminal models, resulting in similar lifespans between animal models and the non-affected littermates. Hence, these mouse models are especially useful for studies of the entire Htt protein and for the investigation of early symptomatic stages of the disease due to the slow development of the phenotype. However, cost and time requirements need to be considered when using these models.

YAC and BACHD models present the full-length human genomic *mHTT* gene together with all regulatory elements. They were developed either by using artificial chromosome vectors from yeast (YAC; Hodgson et al., 1999) or bacteria (BAC; Gray et al., 2008) allowing the expression of large DNA sequences. Although multiple CAG expansion lengths were used to generate different YAC lines, YAC72 and YAC128 (expressing 72 and 128 CAG repeats, respectively) are the only ones presenting a clear HD phenotype. In turn, BACHD animals contain 97 CAA-CAG mixed repeats within the full-length *mHtt* gene. Notably, these models show a correct expression of the mHtt within tissues and along disease progression, exhibiting progressive cognitive and motor deficits. An important advantage of these models is the presence of selective neuronal death (Slow et al., 2003). However, some caveats were also detected, as the number of mHtt aggregates is lower than in other models and restricted to certain brain areas and they display weight gain (Gray et al., 2008; van Raamsdonk et al., 2007).

1.6.1.3 Knock-in (KI) mouse models

In contrast to the abovementioned models, KI mice are characterized by a targeted insertion of CAG repeats in the murine *Htt* gene and, therefore, the mutation is found in the appropriate genomic locus and under the correct promoter with an homozygous or heterozygous genotype (White et al., 1997). Multiple KI lines have been generated expressing different CAG stretch lengths, namely 92, 111, 140 and 175 repeats (Menalled, 2005; Menalled et al., 2012). In turn, whereas transgenic mouse models (N-terminal and full-length) express the inserted transgene together with the two copies present in the endogenous mouse genome, KI mice present a correct gene dosage. Therefore, this model is considered the most faithful as the appropriate genetic context and dosage provides accurate temporal and spatial expressions of the mutant protein. Consequently, KI mice present a subtle phenotype with a mild progression of the disease reproducing precisely human pathology and providing an optimal tool for the study of initial pathological events.

1.7 HD neuropathogenic mechanisms

Despite the fact that precise mechanisms underlying selective neuronal vulnerability in the striatum remain poorly understood, multiple neuropathogenic mechanisms have been described as potential contributors. Among them, mHTT has been associated with a loss of brain-derived neurotrophic factor (BDNF), excitotoxicity, misfolding and aggregation, autophagy disruption, mitochondrial dysfunction, alterations in transcriptional activity and inflammation (reviewed in Bates et al., 2015; Labbadia & Morimoto, 2013; Zuccato et al., 2010; Figure 5).

Glutamatergic excitotoxicity promoting MSNs dysfunction is a major pathogenic mechanism described in HD. The main alterations underlying excitotoxicity include an excessive glutamate release from cortical afferents into the striatal MSNs together with a low uptake of glutamate by glial cells leading to an aberrant activation of the NMDA receptors (Estrada-Sánchez et al., 2009; Fan & Raymond, 2007). The excitotoxic hypothesis in HD is reinforced by the fact that multiple HD models have been produced by the injection of quinolinic acid and kainic acid, two agents that cause cell death through this mechanism (Beal et al., 1991). In parallel, mitochondrial dysfunction has also been proposed as a critical contributor to HD pathology, as it has been described that there is an accumulation of fragmented mitochondria resulting in alterations in energy metabolism and in Ca²⁺ homeostasis (Cherubini et al., 2020; Reddy & Shirendeb, 2012).

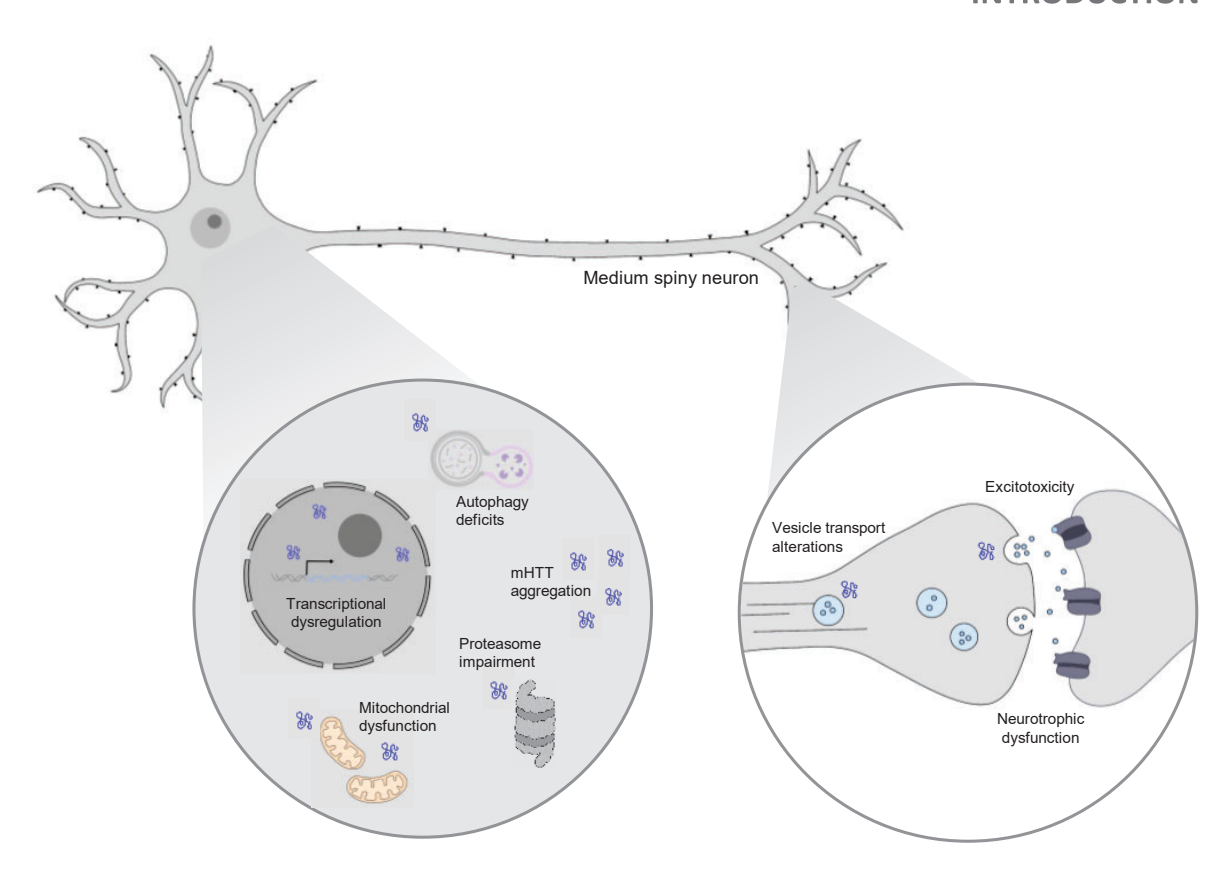


Figure 5. Alterations in cellular mechanisms induced by mHTT protein. Schematic illustration showing the main cellular mechanisms impaired by the presence of mHTT protein in neuronal cells, including transcriptional dysregulation, autophagy deficits, proteasome impairment, mitochondrial dysfunction, vesicle transport alterations, excitotoxicity, neurotrophic dysfunction as well as mHTT aggregation.

Multiple roles of mHtt aggregates have been described including nuclear inclusions as responsible for transcription factor sequestering and cytoplasmic aggregates impairing different functions such as axonal transport (Gunawardena et al., 2003; W. C. M. Lee et al., 2004). This increase in protein aggregation is accompanied by altered degradation, since both autophagy and ubiquitin-proteasome pathways are impaired (S. H. Park et al., 2013; Rué et al., 2013). Furthermore, a large number of studies have reported transcriptional alterations in HD caused by the direct interaction of mHTT protein with the transcriptional machinery or even with the DNA and changes in histone modifications (Kumar et al., 2014), but also through many other mechanisms related to the mHTT RNA, as it will be explained in next sections. Moreover, it is worth noting that many intracellular pathways altered in HD participate in the regulation of protein synthesis (Osterweil et al., 2010; X. Wang & Proud, 2006; Wiseman et al., 2013), which in turn has been found to be aberrantly increased in HD (Creus-Muncunill et al., 2019) and also associated with neuronal toxicity in multiple neurodegenerative disorders (Baleriola et al., 2014; I. Martin et al., 2014; Santini et al., 2013; A. Sharma et al., 2010; Topol et al., 2015).

Finally, increasing evidence points to an important role of neuroinflammation in HD pathogenesis (Crotti & Glass, 2015; Valadão et al., 2020). In fact, activated microglia is present in the putamen of pre-symptomatic HD patients (Tai et al., 2007) with an increased activation correlating with HD severity (Pavese et al., 2006) and also in the brain of different HD mouse models (Franciosi et al., 2012; Simmons et al., 2007).

In conclusion, mHTT is able to trigger several pathogenic mechanisms compromising neuronal homeostasis and function, further contributing to the selective loss of striatal MSNs. However, in recent years RNA-mediated mechanisms that are linked to cellular dysfunction in HD have also attracted attention.

2. RNA-mediated toxicity and its implications in disease

Short tandem repeats are common motifs found in the human genome with stretches of 2 to 12 bp repeating sequences of DNA located both in coding and non-coding regions. These tracts of repeats present a variable length and upon a threshold, they have been associated with pathogenic mechanisms (Krzyzosiak et al., 2012). Amyotrophic lateral sclerosis (ALS) and C9orf72 frontotemporal dementia are different examples of these disorders. For instance, trinucleotide repeats (TNR) are a type of short tandem repeats and disorders that present an abnormal TNR expansion within a translated or an untranslated region (UTR) of the causative gene are classified as TNR expanded diseases (TREDs), including spinocerebellar ataxias (SCA), myotonic dystrophy type 1 (DM1), fragile X syndrome (FXS), among others. HD is considered a TRED as it presents an expanded CAG stretch located within an exon resulting in the production of a polyglutamine tract in the translated protein. Therefore, HD is also classified as a polyglutamine disorder (reviewed in Martí, 2016).

In TREDs, whenever the expanded TNR is found in a non-coding region of the gene, it has been suggested that the pathogenic mechanisms must be associated to the expanded RNA as the resulting protein is not affected. This finding gives rise to the term "RNA toxicity" which describes the direct ability of the expanded RNA transcript to induce pathogenesis. Hence, the study of polyglutamine disorders becomes more challenging as there is a coexistence of protein and RNA detrimental effects (reviwed in Martí, 2016).

In recent years, there has been emerging evidence indicating that RNA toxicity can be exerted by multiple classes of RNA, both coding and non-coding RNAs, that eventually contribute to pathogenesis. Although the most well-studied human genome sequences are the protein-coding ones, the functional relevance of the non-protein-coding genome is becoming evident. In fact, there is a plethora of non-coding RNAs (ncRNAs) that are being recently described as important contributors to the development of many different human disorders (Aznaourova et al., 2020; Bhatti et al., 2021; Esteller, 2011; Mercer et al., 2009).

ncRNAs can be broadly categorized on the basis of transcript size as long ncRNAs presenting more than 200 nt (IncRNA) and short/small ncRNAs comprising RNAs which range from 18 to 200 nt (sncRNA or sRNA)(Kapranov et al., 2007). Moreover, sRNA are further classified into several different biotypes including microRNAs (miRNA), transfer RNAs (tRNA), ribosomal RNAs (rRNA), small nuclear RNAs (snRNA), small nucleolar RNAs (snoRNA), small conditional RNAs (scRNA), circular RNAs (circRNA), among others (Dozmorov et al., 2013). Although some ncRNAs, such as tRNA or rRNA, are highly and ubiquitously expressed playing essential roles in cell homeostasis, miRNA are an example of ncRNA with high sensibility that

present a tight regulation and cell-specific expression patterns with important functions in modulating transcriptional and post-transcriptional gene expression depending on the cell requirements. Notably, the highest diversity of ncRNA has been described in the brain (Quan et al., 2017; Qureshi & Mehler, 2012), where these species are particularly important for the finetuning and regulation of neuronal networks (Salta & De Strooper, 2012).

Here, we will focus on two major mechanisms of RNA toxicity, one involving expanded CAG repeat-containing RNAs and the other related to different classes of small ncRNAs.

2.1 Expanded CAG RNA toxicity

Multiples lines of evidence demonstrate that expanded CAG repeats exert toxicity at the RNA level, including cell dysfunction and degeneration associated with expanded untranslated transcripts containing expanded CAG repeats in multiple *in vivo* models.

Studies in *Drosophila melanogaster* provided the first proof of neurodegeneration linked to both expanded stretches of translated and untranslated CAG repeats. In addition, neurotoxic consequences were less pronounced when the CAG repeated track was interrupted with CAA trinucleotides (L. B. Li et al., 2008). This finding was also observed in human neuronal cells showing milder cell viability defects when expressing CAA rather than CAG expansions (Bañez-Coronel et al., 2012). The detrimental effect of untranslated CAG expansions was also confirmed in Caenorhabditis elegans, where the CAG repeats were inserted into the 3'UTR of a specific protein leading to an increased phenotypic severity in a length-dependent manner. Upon a certain number of CAG repeats, transgenic nematodes presented a decreased motility together with reduced life span, reaching lethality during embryogenesis in the most expanded CAG tracks (L. C. Wang et al., 2011). Experiments in mouse models further support a role of RNA toxicity in inducing disease phenotypes, as in the case of a transgenic expression of expanded CAG repeats within mice muscles causing severe histological alterations and behavioral abnormalities (Hsu et al., 2011). Another evidence reinforcing this hypothesis was found using a specific LNA complementary to CAG repeats that reversed motor deficits in R6/2 mice without inhibiting either mHtt protein levels nor mHtt mRNA expression and stability, pointing to a selective deleterious activity of the expanded CAG RNA (Rué et al., 2016).

Regarding the described mechanisms by which expanded CAG RNA can exert its toxicity in CAG repeat expansion disorders, there are essentially four interrelated categories: (1) RNA gain of function through small CAG repeated RNA (sCAG) production, (2) sequestering of RNA-binding proteins (RBPs), (3) protein gain-of-

function due to altered RNA processing and (4) RAN translation of toxic peptides (Heinz et al., 2021; Malik et al., 2021; Martí, 2016). The coexistence of these toxic mechanisms and even its synergy, together with the protein-related alterations, gives rise to the striking complexity of HD pathogenesis (Figure 6).

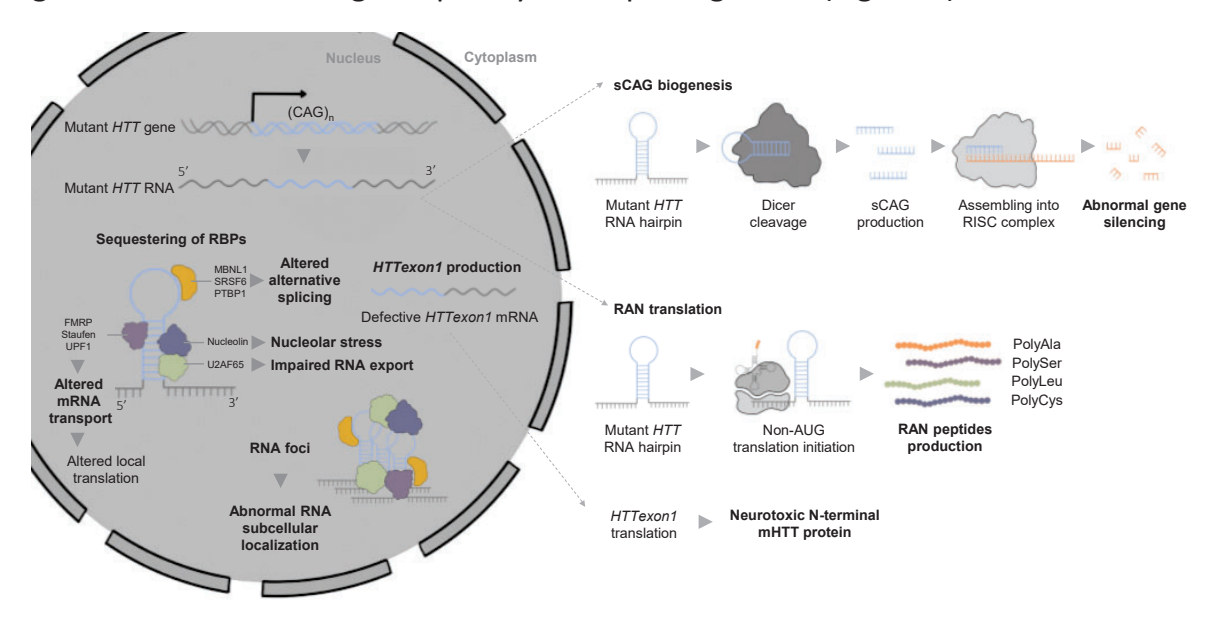


Figure 6. Pathogenic molecular mechanisms of CAG repeat expansion. Schematic of the expanded CAG RNA deleterious effects, including the sequestering of RBPs and their multiple detrimental consequences, *HTTexon1* generation resulting in the production of a neurotoxic N-terminal mHTT protein, RNA foci formation, sCAG biogenesis and RAN translation.

2.1.1 sCAG production

CNG trinucleotide repeats, where N can be any nucleotide (A, C, G or U), are commonly found along the human genome (Kozlowski et al., 2010). These sequences present multiple secondary structures with semi-stable hairpins being the most commonly observed (Sobczak et al., 2003). In the case of the *mHTT* gene, the expanded CAG region folds into a hairpin structure with a stem formed by repetitive pairs of G-C and C-G nucleotides followed by A-A mismatches and a terminal loop (de Mezer et al., 2011; Sobczak et al., 2003). Increasing CAG repeat lengths have been associated with longer hairpins with higher stability (Nalavade et al., 2013; Sobczak & Krzyzosiak, 2004).

Hairpin-like structures constituted by the CAG repeat expanded RNAs resemble double stranded RNAs (dsRNAs) and therefore, act as an appropriate substrate for Dicer, a type III endonuclease implicated in miRNA biogenesis (Krol et al., 2007). The Dicer enzyme is involved in the generation of dsRNA products (20-25 nt) that assemble into the RNA-induced silencing complex (RISC) to select one of the strands to specifically bind to complementary RNA target sequences, leading to the downregulation of the target RNA sequences via mRNA degradation and/or

translational repression (Nalavade et al., 2013; Wilson & Doudna, 2013). Hence, CAG expanded RNA in HD represents a source of uninterrupted CAG-repeated sequences with 21 nt in length known as sCAG. The generation of sCAG is CAG-repeat length dependent and its biogenesis has been reported in HD cell models as well as in fibroblasts and in different brain areas of HD patients, correlating with the CAG repeat length (Bañez-Coronel et al., 2012; Krol et al., 2007). Furthermore, sCAG display a direct neurotoxic activity that is dependent on the RISC complex and also participate in the dysregulation of genes containing CTG repeats through the RNA interference pathway (Bañez-Coronel et al., 2012). Finally, several studies in *Drosophila melanogaster* models have also demonstrated the neurotoxic potential of 21-nt triplet repeat-derived RNAs. Hence, co-expression of long CAG and CUG stretches leads to neurodegeneration in a Dicer-2 dependent manner (Lawlor et al., 2011; Z. Yu et al., 2011).

For all these reasons, sCAG biogenesis represents a pathogenic mechanism in HD that must be considered. However, further investigation is required to unravel whether the adverse effects of sCAG only rely on the silencing effect or also contribute to perturbations in gene expression networks via other mechanisms.

2.1.2 Sequestering of RBPs

RBPs are critical regulators of all aspects of RNA biology, including transcription, alternative splicing, transport, localization, stability, and translation and decay of RNAs (Gebauer et al., 2020). More than 50% of the described RBPs are expressed in the brain with important functions in the maintenance of cell homeostasis (Bryant & Yazdani, 2016). Therefore, it is not surprising that functional perturbations of RBPs underly the origin of multiple neurological and neurodegenerative disorders, including TREDs. In fact, sequestering of RBPs by expanded CAG repeat RNAs has been linked to alterations in multiple pathways including nucleolar stress, inhibition of nuclear export, alterations in RNA transport and abnormal activation of the RNA interference pathway, among others (Galka-Marciniak et al., 2012; Martí, 2016).

Nucleolar stress

Nucleolar stress is a process that has been linked to apoptosis and, in turn, to neurodegeneration in multiple paradigms (Kalita et al., 2008; Rieker et al., 2011). It can be induced by perturbations in different steps of ribosome biogenesis, including rRNA transcription, rRNA maturation, and ribosome assembly (Tsoi & Chan, 2014). All these processes are regulated by nucleolin, a protein located in the nucleolus that binds to an upstream control element of the rRNA promoter, preventing a CpG hypermethylation of this DNA region. However, it has been reported that expanded CAG repeats sequester nucleolin, resulting in a reduced interaction with the rRNA

promoter, enabling its hypermethylation and leading to hindered rRNA expression, nucleolar stress and finally, apoptosis via p53 (Tsoi et al., 2012; Tsoi & Chan, 2013).

Altered nuclear export

U2 small nuclear ribonucleoprotein auxiliary factor 65 (U2AF65) is a protein involved in the processes of alternative splicing and nuclear export of RNAs (Blanchette et al., 2004; J. W. Park et al., 2004), which presents a high specific binding affinity to expanded CAG RNAs, but not other trinucleotide repeats. In physiological conditions, U2AF65 plays a role as an adaptor that links the RNA export receptor NXF1 with the RNA substrate in each case (Blanchette et al., 2004). However, RNA export pathway through U2AF65/NXF1 is compromised in HD due to a progressive reduction of U2AF65 expression along the disease, resulting in a decline in nuclear export and, in turn, in an accumulation of expanded CAG RNA in the nucleus causing RNA toxicity (Sun et al., 2015; Tsoi et al., 2011).

Altered RNA transport

Important roles of RBPs within the cytoplasm have also been described, including the modulation of mRNA stability (Masuda et al., 2012) and as mediators of RNA transport by shuttling RNAs into different cell compartments for their proper functions (Farina et al., 2003; Taliaferro et al., 2016; E. T. Wang et al., 2012). An important phenomenon giving rise to CAG repeat expansion RNA toxicity is the aberrant RNA granulation linked to the sequestration of RBPs, resulting in an impairment in RNA transport dynamics and, in turn, a defective localization of RNAs (Konieczny et al., 2018; Malik et al., 2021).

Local mRNA translation is essential for the maintenance of synaptic strength and neuronal circuits (Holt et al., 2019; Kapur et al., 2017). Therefore, impairments in mRNA transport into the synapses result in fatal consequences (Fernandopulle et al., 2021; Thelen & Kye, 2020). Neuronal RNA granules are responsible for the transport of mRNAs from the nucleus to the neurites associated with several ribosomal proteins and other RBPs, such as fragile X mental retardation protein (FMRP), Staufen, UPF1, among others (Burguete et al., 2015; Nabariya et al., 2022). However, upon CAG expanded RNA trapping of these RBPs, there is a breakdown of the transport machinery compromising axonal transport and synaptic excitability that may lead to neuronal excitotoxicity (Heinz et al., 2021; Savas et al., 2010).

Alterations in alternative splicing

In multiple pathological contexts, expanded RNAs containing the repeats accumulate within cells constituting higher order assemblies commonly referred to as RNA foci. Although these repeat RNA foci represent a hallmark in multiple TREDs, they can differ in size, shape, abundance and composition depending on the

disorder. RNA foci are predominantly retained in the nucleus, but cytoplasmic foci have also been reported (Wojciechowska & Krzyzosiak, 2011).

It is important to note that RNA foci are not only constituted by repeat RNAs. In fact, multiple RBPs presenting specific structures and/or sequence motifs are attracted by expanded repeat RNAs into the foci. Hence, this recruitment can be toxic whenever it leads to a depletion of the RBPs from the nucleoplasm and/or cytoplasm, resulting in cell dysfunction (Malik et al., 2021).

One example is found in DM1 in which CUG foci colocalize with multiple RBPs of the muscleblind-like splicing regulator 1 (MBNL1) family (Miller et al., 2000). As MBNL1 function is the regulation through activation or inhibition of the alternative splicing of target mRNAs modulating specific isoforms expression, this sequestration leads to the transcriptome-wide dysregulation of alternative splicing described in this disease (Ho et al., 2004; Wang et al., 2012). RNA foci co-localizing with MBNL1 and the associated alternative splicing defects have also been reported in the nucleus of fibroblasts from patients with HD and SCA3 and in human cell lines expressing a CAG repeat expansion (Mykowska et al., 2011). In addition, an aberrant splicing of the MBNL1 target Clcn1 potassium channel has been linked to the skeletal muscle hyperexcitability described in the R6/2 HD mouse model (Waters et al., 2013).

Similarly to MBNL1, serine/arginine-rich protein SRSF6 is another RNA-binding splicing factor that can be aberrantly captured by the CAG-containing expanded RNA. This binding leads to SRSF6 loss of function and subsequently to alterations in alternative splicing, in this case specifically affecting the *HTT* gene (Gipson et al., 2013; Sathasivam et al., 2013).

Regarding HD human brain, several mis-spliced transcripts were detected with the splicing factor PTBP1 playing an important role in this dysregulation (L. Lin et al., 2016). In addition, further characterization of all the RPBs sequestered by the CAG expanded RNA confirmed that several defectively bound proteins are functionally related to splicing (Schilling et al., 2019), reinforcing the spliceopathy as a major RNA-mediated toxicity mechanism.

2.1.3 HTTexon1 production

As it has just been mentioned, the sequestration of multiple factors linked to alternative splicing not only has an impact on several transcripts but also affects the CAG-repeat expanded RNA itself. In particular, it has been described that multiple alternatively spliced and polyadenylated mRNA isoforms are generated from the *HTT* gene, all of them resulting in the translation of the canonical HTT protein (B. Lin et al., 1993; Romo et al., 2017; Romo et al., 2018). However, expanded CAG repeats disrupt the proper RNA splicing leading to the production of

a short polyadenylated transcript containing the expanded CAG stretch and termed *HTTexon1* (Neueder et al., 2017). This defective mRNA can be actively translated into the highly neurotoxic exon1 mHTT protein (Gipson et al., 2013; Sathasivam et al., 2013). It has also been reported that *HTTexon1* mRNA production takes places in a CAG repeat length dependent fashion (Neueder et al., 2018; Sathasivam et al., 2013). Furthermore, there is a correlation between *HTTexon1* transcript levels and the onset of behavioral alterations and the striatal distribution of HTT aggregates (Franich et al., 2019). In conclusion, accumulating evidence supports the idea of *HTTexon1* mRNA as another key player in HD pathogenesis.

2.1.4 RAN translation

The repeat associated non-ATG-initiated (RAN) translation represents another layer of complexity in the study of the molecular mechanisms underlying repeat expansion disorders. RAN translation of repetitive elements is an alternative mechanism of translation that bypasses the need for the canonical AUG start codon and occurs across expanded repeats forming hairpins in a repeat-length dependent manner and across multiple reading frames (Cox & Cooper, 2016; Zu et al., 2011). In fact, while CAG and CUG repeat RNA support RAN translation, it is not the case for CAA repeats, suggesting that the formation of a secondary structure of the repeat RNA is required (Zu et al., 2011). RAN translation initiation uses canonical translation machinery resembling non-AUG upstream open reading frame (uORF) translation initiation. However, expanded repeats impede a proper ribosomal scanning, increasing the dwell time of the initiation complex at near-cognate codons resulting in a decreased start codon fidelity. Additionally, RAN translation can also initiate in a cap-independent manner through an internal ribosome entry site (IRES)-like mechanism (reviewed in Malik et al., 2021).

Hence, it results in the formation of different homopolymeric proteins from the trinucleotide expansions, including those located in non-coding regions (Zu et al., 2011). Moreover, from the same gene locus, bidirectional transcription can occur leading to the formation of sense and antisense mRNAs that can be translated from any base since AUG start codon is not required. It has been described that four RAN proteins (polyAla, polySer, polyLeu and polyCys) are translated and accumulated in several brain regions of HD human brains (Bañez-Coronel et al., 2015). However, further experiments are required to unravel the contribution of RAN translated products in the pathogenic mechanisms of HD and its correlation with disease progression, since divergent observations have been reported (S. Yang et al., 2020).

2.1.5 Therapeutic strategies targeting expanded CAG

Although significant research efforts have been focused on the development of therapeutic strategies for HD, currently no effective treatment has been proved to prevent, halt the progression or, at least, delay the onset of this disorder. In fact,

supportive care represents the routinely medical management nowadays. Within this scenario, preclinical studies have been centered in RNA-targeting strategies as promising therapeutic approaches involving the blockage, inhibition or even removal of the *mHtt* allele in several HD models using short interfering RNAs (siRNA; DiFiglia et al., 2007; Harper et al., 2005; Stanek et al., 2014), modified antisense oligonucleotides (ASOs; Carroll et al., 2011; Gagnon et al., 2010; Kordasiewicz et al., 2012; Rué et al., 2016; Skotte et al., 2014; Sun et al., 2014), zincfinger proteins (Garriga-Canut et al., 2012; Zeitler et al., 2019) and CRISPR-Cas9-based strategies (Dabrowska et al., 2018; Heman-Ackah et al., 2016; Monteys et al., 2017; S. Yang et al., 2017).

In all cases, the aim is to reduce mHTT production to potentially prevent its adverse consequences. When using siRNA or miRNA as therapeutic agents, there is a degradation of *HTT* mRNA by the RNA interference pathway in the cytoplasm. Conversely, ASOs can directly induce degradation of the target transcript in the nucleus through ribonuclease RNAse H (reviewed in Bates et al., 2015; Tabrizi et al., 2019). It is important to note that allele selectivity represents a challenge in HD therapeutics as an impairment in the physiological function of the WT HTT leads to potential side effects. Therefore, HTT-lowering therapies are classified between allele selective, when only *mHTT* is targeted, and non-allele selective, finding a reduction in both WT and *mHTT* transcripts (reviewed in Tabrizi, Estevez-Fraga, et al., 2022). Allele-selective therapies can in turn be divided into those targeting single nucleotide polymorphisms in linkage to the mutated allele (Skotte et al., 2014) or directly targeting the CAG expanded track selectively inhibiting *mHTT* expression due to their potential capacity to discriminate between normal and *mHTT* transcripts (Gagnon et al., 2010; Rué et al., 2016; Sun et al., 2014).

Tominersen is an example of a non-selective ASO targeting exon 36 of human *HTT* mRNA developed by Ionis/Roche and used until a phase III clinical trial (GENERATION-HD1). ASOs directed against single nucleotide polymorphisms unique to the mHTT transcript have also been tested in phase I/II clinical trials (Wave Life Sciences, PRECISION-HD2). Unfortunately, any of them has proven meaningful clinical efficacy pointing to the necessity of alternative designs, including improved targeting of mHTT allele and/or optimized clinical trials targeting mHTT-carrier individuals before clinical motor diagnosis. Besides, approaches that additionally target alternative toxic species implicated in HD pathogenesis, such as *HTTexon1*, should be further considered. However, ongoing improvements in the delivery and distribution of agents, novel biomarkers as well as better knowledge of HD pathogenic mechanisms are encouraging for the development of impactful therapies in HD (reviewed in Tabrizi, Estevez-Fraga, et al., 2022).

2.2 Non-coding RNA toxicity

Intriguingly, although the vast majority of the human genome is transcribed, only a small percentage of these RNAs are going to be translated into protein, giving rise to a huge number of transcripts known as ncRNA. Despite not having the ability to translate into proteins, ncRNA present a widespread distribution along cells regulating a remarkable variety of crucial biological functions (Cech & Steitz, 2014). Due to the emergence of ncRNA as pivotal players in multiple fundamental physiological processes, their dysregulation has also been increasingly implicated in different pathological conditions including cancers as well as neurological, cardiovascular and developmental disorders (Esteller, 2011; Salta & De Strooper, 2012) and thus, many therapeutic strategies counteracting these perturbations have started raising interest. Here, we will focus on two different subtypes of ncRNAs, namely miRNA and tRNA-derived small RNAs (tsRNA), for their putative roles in multiple pathological mechanisms. However, it is noteworthy that other ncRNA species, such as lncRNAs (reviewed in Dong & Cong, 2021; Esteller, 2011; Statello et al., 2020), snoRNAs (reviewed in Z. Huang et al., 2022; Stepanov et al., 2015), circRNAs (reviewed in D'anca et al., 2022; Tang et al., 2021) and even retrotransposons (Ochoa et al., 2023), are also emerging as novel contributors to pathology.

2.2.1 miRNA

Mature miRNA are molecules of 20-24 nt in length that were first identified in 1993 in *Caenorhabditis elegans* (R. Lee et al., 1993) and now represent the most extensively studied sRNA biotype. During miRNA biogenesis, long double-stranded primary miRNA transcripts are processed in the nucleus by Drosha/DGCR8 complex resulting in precursor miRNA. These are exported into the cytoplasm by Exportin 5, where Dicer cleaves them generating mature double-stranded miRNA. Then, strands are separated and the so-called guide strand associates with Ago proteins to form the RISC complex that finally leads to gene translation repression via mRNA degradation, translational inhibition or a combination of both (Figure 7).

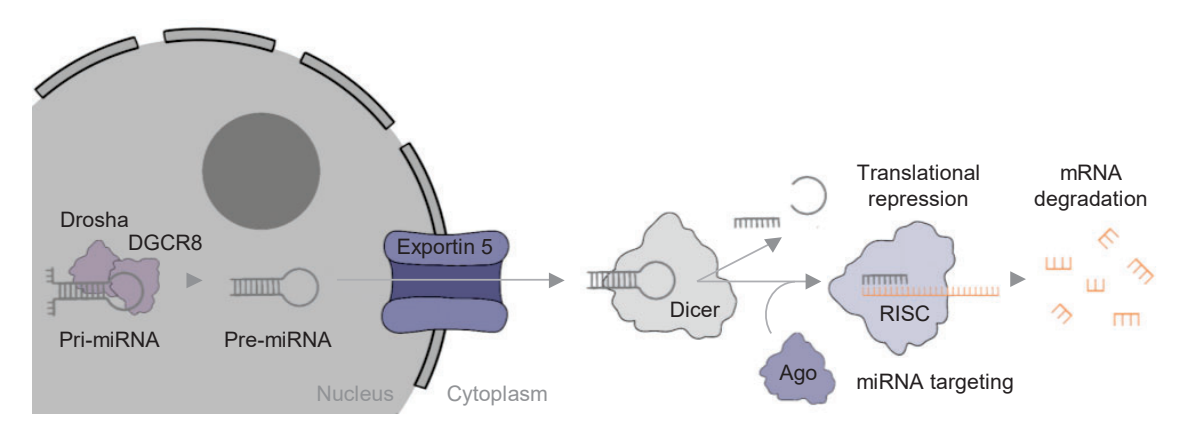


Figure 7. miRNA biogenesis pathway. miRNA genes are transcribed producing large primary transcripts termed pri-miRNA, which are cleaved by the Drosha/DGCR8 microprocessor

complex to form a pre-miRNA. Following transportation to the cytoplasm by Exportin 5, pre-miRNA is processed by Dicer generating a 20-24 nt miRNA duplex. One of the strands associates with Ago into the RISC complex to mediate gene silencing via translational repression or mRNA degradation, depending on the complementarity between the miRNA and the mRNA target transcript.

As a consequence, miRNA are considered fine-tuners of gene expression which is important for the homeostasis of all types of cells. However, a proper miRNA biogenesis and function appears to be indispensable for CNS development and adult brain function (Chmielarz et al., 2017; Hébert et al., 2010; Rajman & Schratt, 2017), and any disruption in their biogenesis pathway could result in fatal consequences. In fact, models showing a loss of function of Dicer first evidenced a major role of miRNA in neuronal survival (A. Schaefer et al., 2007; Shin et al., 2009; Tao et al., 2011). Additionally, alterations in miRNA biogenesis machinery have been described in multiple neurodegenerative conditions, such as DM1 (Rau et al., 2011), FXS (Sellier et al., 2013), ataxia (A. Schaefer et al., 2007), multiple sclerosis (MS; Shin et al., 2009), Parkinson's disease (PD; J. Kim et al., 2007), Alzheimer's disease (AD; Hébert et al., 2010), among others. In the case of HD, miRNA perturbations have been reported in multiple HD mouse models at different stages of the disease, simultaneously to alterations in Dicer, Drosha and Exportin mRNA levels (Bridget & Peplow, 2021; Jin et al., 2012; Langfelder et al., 2018; S. T. Lee et al., 2011; Olmo et al., 2021). Accordingly, a strong miRNA expression dysregulation has also been observed in the most affected areas of human HD brains (Martí et al., 2010).

Regarding HD pathogenesis, dysregulation of miRNA expression can be caused by multiple mechanisms, including alterations in the activity of transcription factors or disease-related genes and/or perturbations in miRNA biogenesis or stability (Martí et al., 2010; Packer et al., 2008). In fact, it has been observed that mutant protein is able to interact with Ago2. Hence, the sequestration of this member of the RISC complex in mHTT aggregates could explain the abnormal miRNA activity and expression levels detected in this disorder (Pircs et al., 2018; Savas et al., 2008).

Moreover, unconventional functions of miRNA have also been described to contribute to neurotoxicity, as in the case of let-7. It has been found that this miRNA is able to be secreted and extracellularly activate the Toll-like receptor (TLR) TLR7 signaling in microglial cells and macrophages, but also in neurons, leading to neurodegeneration (Coleman et al., 2017; Lehmann et al., 2012) and pointing to a role of miRNA in mediating damage in the CNS via TLR activation of neuronal cell death.

2.2.2 tsRNA

tRNA present a ubiquitous distribution and represent between 4 to 10 % of all RNAs present in a cell. tRNA are a class of ncRNA composed of 73-90 nt generating L-shaped tertiary structures. Besides, tRNA adopt cloverleaf secondary structures composed by a D-loop, an anticodon loop, a T-loop, a variable loop and an amino acid acceptor stem (Figure 8). In general terms, tRNA can be classified considering the isoacceptor (tRNA that carry the same amino acid but present different anticodons) or the isodecoder (tRNA that present the same amino acid charged and the same anticodon but differ in other parts of the tRNA sequence) (reviewed in S. Li et al., 2018).

The canonical function of tRNA is the transport of amino acids into the ribosome, linking the genetic code to protein synthesis. Hence, tRNA were classically considered adaptor molecules in translation with a static contribution to gene expression (Banerjee et al., 2010). However, multiple studies in recent years have revealed that tRNA have also non-canonical functions as they represent a source of tsRNA, which are not merely products of random degradation (Schimmel, 2017). In contrast, tsRNA are produced in highly regulated processes giving rise to different small ncRNAs with prominent regulatory functions in pathophysiologic conditions (reviewed in Blaze & Akbarian, 2022; Liu et al., 2021).

2.2.2.1 Classification and biogenesis

tsRNA are biologically active RNAs generally divided into two different types depending on their length and the cleavage site of the precursor tRNA, resulting in tRNA halves or tRNA-derived fragments (tRFs). Besides, their mapping on the parental tRNA sequence defines distinct subcategories (reviewed in Shen et al., 2018).

tRNA halves are sRNA sequences of 31 to 40 nt in length that are generated by a specific cleavage within the anticodon loop of mature tRNA. While 5'halves sequences start from the 5'-end of the mature tRNA and end in the anticodon loop, 3'halves start from the anticodon loop and extend until the 3'-end of the precursor tRNA (Figure 8). Moreover, since tRNA halves are frequently produced under stress conditions, they are also known as tRNA-derived stress induced RNAs (tiRNA) (reviewed in Shen et al., 2018).

tRFs are formed by sequences of 14 to 30 nt and their most common classification mainly include five different categories: (1) 5'tRFs, which are generated from a cleavage in the D-loop of mature tRNA with a length ranging from 15 to 25 nt, (2) 3'tRFs, which are generated from a cleavage in the T-loop of mature tRNA presenting slightly shorter sequences with 13 to 22 nt in length and (3) itRFs, which are entirely contained within the internal region of the mature tRNA, including the

anticodon loop and fragments of the D- and T-loops but excluding the 5'- and 3'ends (Figure 8). The remaining categories are related to tRFs generated from
premature tRNA: (4) 5'U-tRFs which comprise the 5'-leader sequence and (5) 3'UtRFs, also known as tRF-1, which include the 3'-trailer sequence (reviewed in
Krishna et al., 2021; S. Li et al., 2018; Liu et al., 2021; Shen et al., 2018).

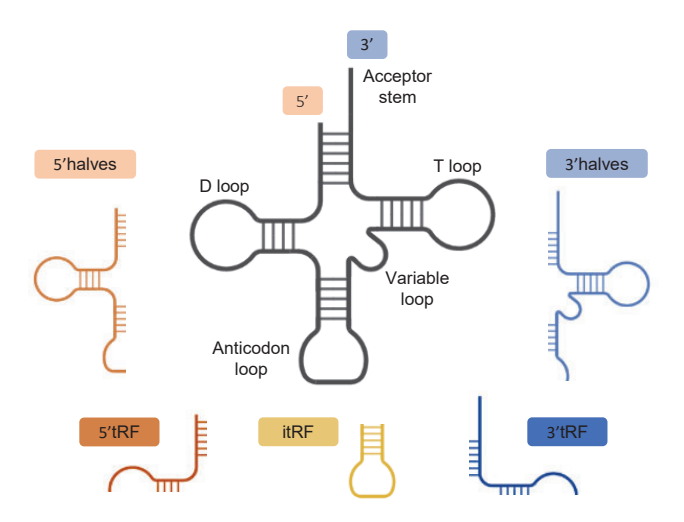


Figure 8. Classification of tsRNA. 5'halves and 3'halves are produced by a cleavage within the anticodon loop. Cleaved fragments derived from the 5'-end to the anticodon loop are considered 5'tRFs while the ones obtained from the 3'-end to the anticodon loop are termed 3'tRFs.

It is worth noting that tRNA halves and tRFs biogenesis comprises complex and highly regulated processes involving multiple enzymes. It has been widely reported that tRNA halves are mainly generated by angiogenin (ANG) and their production is triggered by stress conditions such as hypoxia, heat and cold shocks, amino acid deficiency, phosphate starvation, UV radiation, viral infections and oxidative stress (reviewed in S. Li et al., 2018). However, tRNA halves production has also been described under physiological conditions (reviewed in Liu et al., 2021).

Multiple endonucleases have been involved in tsRNA production, including ANG, Dicer, RNase T2 and RNase Z/ELAC2. ANG is a homolog of the pancreatic ribonuclease A, which is inhibited in homeostatic conditions by its interaction with the Ribonuclease/Angiogenin Inhibitor 1 (RNH1). In contrast, under stress conditions, ANG is no longer retained and targets tRNA for cleavage. Although Dicer has been traditionally linked to miRNA biogenesis, D- and T-loops of mature tRNA represent cleavage target sites for Dicer generating 5'tRFs and 3'tRFs, respectively. Multiple RNAse T2 family members have been linked not only to tRNA halves production through the cleavage in the anticodon loop but also to tRF generation. Additionally, RNAse Z/ELAC2 is involved in the cleavage of a 3'-sequence during the tRNA maturation process, generating 3'U-tRFs that include the unique uridine tail typically present at the 3'-end of premature tRNA (reviewed in R. Magee &

Rigoutsos, 2020). Finally, exposures to double-stranded RNAs, DNA damage or viruses can activate the interferon-stimulated nucleases RNase L, SLFN11, and SLFN13 resulting in a specific cleavage of a limited subset of tRNA (Donovan et al., 2017; M. Li et al., 2018; J. Y. Yang et al., 2018).

2.2.2.2 Mechanisms of action

The considerable heterogeneity in tsRNA subtypes in the different conditions evidences the implication of these sRNA species in several molecular mechanisms to accomplish multiple biological processes.

Post-transcriptional regulation of gene expression

tRFs play a role in the post-transcriptional regulation of gene expression through multiple mechanisms involving a direct mechanism acting like miRNA or the indirect interaction with multiple RBPs associated with the control of gene expression.

Due to sequence similarities with miRNA, tRFs generated by Dicer can perform miRNA-like functions regulating mRNA stability. In particular, tRFs are able to competitively associate with Argonaute (Ago) proteins and enter the RNA interference pathway suppressing the expression of target genes (Haussecker et al., 2010; Yeung et al., 2009). In fact, this process has been proposed as a regulatory mechanism in the primate hippocampus where there is an overexpression of 5'tRFs (Jehn et al., 2020).

As abovementioned, tRFs can also bind with several RBPs for the modulation of gene expression. An important example was found in the tRF-induced downregulation of oncogenes expression via YBX1, inhibiting cancer metastasis. YBX1 is an RBP responsible for mRNA stabilization prior translation. However, under stress conditions, there is an overproduction of specific tRFs that displace the 3'UTR of oncogene mRNAs from binding to YBX1 by direct competition. This results in a reduced stability of oncogenic transcripts leading to an arrest of tumor progression (Goodarzi et al., 2015).

Additionally, other proteins have been implicated in tRF-mediated mRNA stability, such as the long form of the RNAse Z. This endonuclease is able to interact with either miRNA or tRFs for a direct cleavage of mRNAs containing their target sequences, in turn modulating their expression (Elbarbary, et al., 2009a; Elbarbary, et al., 2009b).

Inhibition of translation initiation

The role of tsRNA in translation regulation was first reported in stress-induced conditions (Yamasaki et al., 2009), where it was described that there is also an important production of tRNA halves. Some of the resulting tRNA halves contain terminal oligoguanine motifs (TOG) at their 5'-ends, which have been specially

observed in those derived from tRNA^{Ala} and tRNA^{Cys}. These TOG motifs confer translational repression capacities by promoting the assembly of TOG-containing tsRNA to form tetrameric G-quadruplex structures (G4-tsRNA) (Lyons et al., 2017). G4-tsRNA have the ability to associate with YBX1 and displace eIF4G/eIF4A from binding to the m⁷G cap of mRNA sequences, thus preventing ribosomal recognition and finally inhibiting mRNA translation initiation (Ivanov et al., 2011). However, translational arrest is not limited to tsRNA^{Ala} and tsRNA^{Cys}, but many other 5'halves and 5'tRFs presenting a GG dinucleotide or a pseudouridinilation modification in their sequences also displayed crucial roles in translation repression (Guzzi et al., 2018; Sobala & Hutvagner, 2013).

Regulation of ribosome biogenesis

Apart from the role of tsRNA as regulators of translation initiation machinery, tsRNA have also been implicated in the regulation of ribosome biogenesis. Ribosomes consist in the assembly of four rRNAs with several ribosomal proteins. Notably, multiple studies have also described direct interactions of tsRNA with ribosomes (reviewed in Krishna et al., 2021). In fact, a study performed in *Haloferax volcanii* showed that under stress conditions, the binding of a 5'tRF from tRNA^{Val} to the 16S rRNA impairs the association of mRNAs with the ribosomes, resulting in a reduction in protein synthesis (Gebetsberger et al., 2017).

Another mechanism has been described in mammalian cells where a 3'tRF derived from tRNA^{Leu} is able to target the 3'UTR of the mRNA of two different ribosomal proteins, RPS28 and RPS15. These bindings alter the secondary structures of RPS28 and RPS15 mRNAs enhancing their translation and as a consequence, increasing the abundance of these ribosomal proteins (H. K. Kim et al., 2017, 2019).

Role as a guide RNA regulating RNA reverse transcription

During reverse transcription of viral RNAs, tsRNA can be employed as guide RNAs. It has been described that a specific 3'tRF (referred as tRF-3019) found in host cells is able to associate to the primer-binding sites of human T-cell leukemia virus type 1 (HTLV-1) RNA. This binding triggers reverse transcription of the viral RNA and thereby enhances viral self-synthesis (Ruggero et al., 2014). Likewise, the respiratory syncytial virus (RSV) takes advantage of tsRNA from the host cell to promote infection efficiency. In particular, RSV infection induces a stress response in host cells that activates ANG for the production of tsRNA which, in turn, act as primers for the replication of the viral RNA (J. Deng et al., 2015; Q. Wang et al., 2013; Zhou et al., 2017).

Roles in the immune response

Extensive characterizations of the levels of ncRNA in the circulatory system have highlighted the increase of tRFs in acute inflammation (Dhahbi et al., 2013; Y. Zhang

et al., 2014), suggesting tRF key roles during immune responses. In physiological conditions, human activated T-cells selectively export specific 5'tRFs and itRFs through extracellular vesicles, which are different from the tRFs present in EVs secreted by resting T-cells, suggesting that tRFs are involved in the regulation of T-cell activation (Chiou et al., 2018). In parallel, tRFs were also shown to participate in pathological immune responses. A differential expression of several tsRNA has been reported in systemic lupus erythematosus, an autoimmune disease (Xu et al., 2020). Certain tRFs were highly expressed by T-cells and positively correlated with disease-related detrimental consequences (Geng et al., 2021).

Furthermore, tsRNA direct activation of immune responses have also been described. For instance, specific motif found in a tRNA^{Ala}-derived tRF is recognized by TLRs activating lymphocyte T immune responses (Z. Wang et al., 2006). Besides, infection-induced 5'halves secreted by human monocyte-derived macrophages activate endosomal TLR7 (Pawar et al., 2020). Therefore, there is increasing evidence pointing tsRNA as immune signaling molecules.

Regulation of apoptosis

In oxidative stress conditions, cytochrome C is released from mitochondria triggering the apoptotic cascade. However, tsRNA produced by ANG can bind cytochrome C inhibiting apoptosome formation and caspase 9 activity, enhancing cell survival (Saikia et al., 2014).

2.2.2.3 Role of tsRNA in disease

Alterations in tsRNA levels have been described in several human disorders including neurodegenerative, neurodevelopmental and neuropsychiatric diseases, cancer, inherited metabolic disorders or even during infections. Although further research is needed to determine how these sRNA species are contributing to disease pathogenesis, tsRNA also provide new perspectives for the investigation and development of both novel biomarkers and therapeutic strategies.

Neurodegenerative and neurodevelopmental disorders

In recent years, multiple neurological disorders have been associated to mutations in genes related to tRNA metabolism and tsRNA biogenesis, providing a basis that links neurodegeneration with alterations in tRNA processing and fragmentation.

Several mutations and sequence variants in *ANG* gene have been identified in ALS (Greenway et al., 2006; Padhi et al., 2013), PD (Bradshaw et al., 2017; van Es et al., 2011) and AD patients (Gagliardi et al., 2019). Most of the mutations result in a reduction in ANG ribonucleolytic activity and/or impairments in nuclear translocation hindering its proper functionality (Greenway et al., 2004). Considering that the biogenesis of many tsRNA is ANG-dependent, it is plausible to hypothesize that certain tsRNA could be involved in the pathogenesis of these disorders.

Notably, dysregulations in tsRNA expressions have been described in animal models of neurodegenerative disorders (S. Zhang et al., 2019) and in human samples of PD and AD patients (R. Magee et al., 2019; Wu et al., 2021). In fact, a small set of tRFs in sufficient to distinguish PD patients from non-affected individuals (R. Magee et al., 2019).

Apart from mutations in *ANG* gene itself, it has also been implicated in tsRNA excessive cleavage and accumulation due to defects in other tRNA modification enzymes. Mutations in the cytosine-5 RNA methyltransferases *NSun2* and *Dnmt2* genes have been reported causing intellectual disability and Dubowitz-like syndrome (Abbasi-Moheb et al., 2012; Blanco et al., 2014; Khan et al., 2012; Martinez et al., 2012; M. Schaefer et al., 2010). In the absence of these enzymes, there is an increased ANG-mediated tRNA cleavage that leads to an accumulation of 5'tRFs which trigger a cellular stress response and eventually apoptosis of cortical, hippocampal and striatal neurons, pointing to a potential implication of tsRNA in neuronal death (Blanco et al., 2014).

Another example of the link between altered tRNA metabolism and neurological consequences was found in patients presenting pontocerebellar hypoplasia (PCH), a heterogeneous group of inherited neurodegenerative diseases affecting the development of multiple brain regions. Among other mutations, PCH has been associated to mutations in the *CLP1* gene, which encodes for an RNA kinase responsible for tRNA splicing (Hanada et al., 2013; Karaca et al., 2014; Schaffer et al., 2014). On the cellular level, a loss of CLP1 leads to an accumulation of tsRNA derived from immature pre-tRNA^{Tyr} that sensitize cells to p53-mediated apoptosis (Hanada et al., 2013).

Cancer

A deficiency in blood supply resulting in hypoxic stress is a characteristic hallmark of tumor cells due to its excessive proliferation. Given the fact that tsRNA production is tightly related to stress responses, it is not surprising a strong tsRNA dysregulation in a wide variety of cancers. In fact, the relationship between tsRNA and cancer was one of the earliest investigated (Speer et al., 1979). These initial findings have been reinforced by several subsequent studies showing tRFs in serum and urine of cancer patients (R. G. Magee et al., 2018; Yeri et al., 2017; Y. Zhang et al., 2014), which evidence the potential of tsRNA as biomarkers for tumor diagnosis. Particularly, circulating levels of specific tsRNA highly correlate with the clinical and pathological features observed in breast cancer patients (Dhahbi et al., 2014).

Due to the abundance of studies describing tsRNA dysregulation in cancer, a database of tsRNA associated to different tumors was created (tRF2Cancer; Zheng et al., 2016). Interestingly, almost all types of cancer show increased levels of ANG,

potentially explaining the associated overproduction of tsRNA in such conditions (S. Li & Hu, 2012; Sheng & Xu, 2016). However, tsRNA functions and targets in each malignancy remain to be fully characterized. tsRNA usually act as tumor suppressors as in the case of a 3'tRF derived from tRNA^{Leu} in colorectal cancers that inhibits tumor growth and metastasis (B. Huang et al., 2017) or in the case of the abovementioned set of tRFs that suppress tumor progression via YBX1 displacement from multiple oncogenes, eventually reducing their stability (Goodarzi et al., 2015). Conversely, carcinogenic roles of tsRNA have also been reported, e.g. a 3'tRF from tRNA^{Leu} being important for tumor survival (Shao et al., 2017).In summary, multiple investigations have described a close association between tsRNA and tumor onset, progression and drug resistance (reviewed in Liu et al., 2021), displaying potential to be important therapeutic targets.

Metabolic disorders

Multiple studies have implicated tsRNA with paternal transgenerational inheritance of metabolic disorders, associating diet to tsRNA levels in sperm and thereby, dysregulating the metabolism of the offspring (Q. Chen et al., 2016; U. Sharma et al., 2016). Moreover, maternal high fat diets have also been linked to addictive-like behaviors and obesogenic phenotypes in their offspring (Sarker et al., 2019). Adipogenesis in human bone marrow mesenchymal cells is another process that has been described to be modulated by a specific tsRNA, namely tsRNA-06018. This tsRNA targets the 3'UTR of Stanniocalcin 2 via the ERK1/2 signaling pathway eventually regulating adipogenic differentiation (T. Wang et al., 2020).

Infectious diseases

Although the biological roles of tsRNA in infectious disorders are still not completely defined, tsRNA biogenesis has been observed under multiple infection agents, including bacteria as *Escherichia coli* (Tomita et al., 2000), fungus as *Aspergillus fumigatus* (Jöchl et al., 2008), protozoas as *Giardia lamblia* (Y. Li et al., 2008), nematodes as *Ascaris* (J. Wang et al., 2011), parasites as *Trypanosoma cruzi* (Garcia-Silva et al., 2010) and different viruses (J. Deng et al., 2015; Q. Wang et al., 2013; Zhou et al., 2017). In all cases, there is a tsRNA upregulation with potential roles as virulence factors, drug targets or biomarkers (Garcia-Silva et al., 2013).

2.2.2.4 Role of epitranscriptomics in tRNA metabolism

In recent years, a huge variety of reversible RNA modifications are being described in all known coding and non-coding RNA species within mammalian cells (Frye et al., 2016) composing the recently named epitranscriptome field which adds a novel regulatory layer in post-transcriptional gene expression (Saletore et al., 2012).

More than 150 chemical modifications have been described in RNAs actively regulating their biogenesis, maintaining proper structures and contributing to

develop crucial biological functions. tRNA are the RNAs showing the highest prevalence of post-transcriptional modifications within cells, with an average of 13 different modifications per molecule in eukaryotes (Schimmel, 2017). Additionally, the exact nucleotide position for each of these modifications differs between tRNA molecules, thereby increasing the complexity of epitranscriptomic studies. Currently, 43 different tRNA epitranscriptomic modifications have been described encompassing for multiple functions including tRNA stability and folding, ribosomal interactions and wobble base pairing, among others (Chujo & Tomizawa, 2021; Motorin & Helm, 2010; Pereira et al., 2018).

Far from being irreversible, tRNA modifications are highly dynamic adjusting to environmental stimuli. However, a loss of specific modifications leads to increased sensitivity to stress conditions (Begley et al., 2007; Blanco et al., 2014; M. Schaefer et al., 2010) and consistently, mutations in enzymes linked to tRNA epitranscriptomic modifications have been reported in multiple human diseases, categorized as RNA modopathies, with neurodevelopmental and neurodegenerative disorders being prominently represented (Boccaletto et al., 2022; Chujo & Tomizawa, 2021).

Regulation of tsRNA biogenesis by methylations

Methylations are one of the most frequent post-transcriptional modifications in tRNA and other ncRNAs, thus expanding the complexity already engendered by isoacceptors and isodecoders (Schimmel, 2017). So far, the most abundant tRNA methylation is cytosine-5 methylation (m⁵C), which can be exerted by four different RNA methyltransferases in mammals, commonly referred to as writers (Figure 9; Motorin et al., 2010). It is worth noting that some of these enzymes selectively methylate a subset of tRNA while others install methylations in many different RNA species.

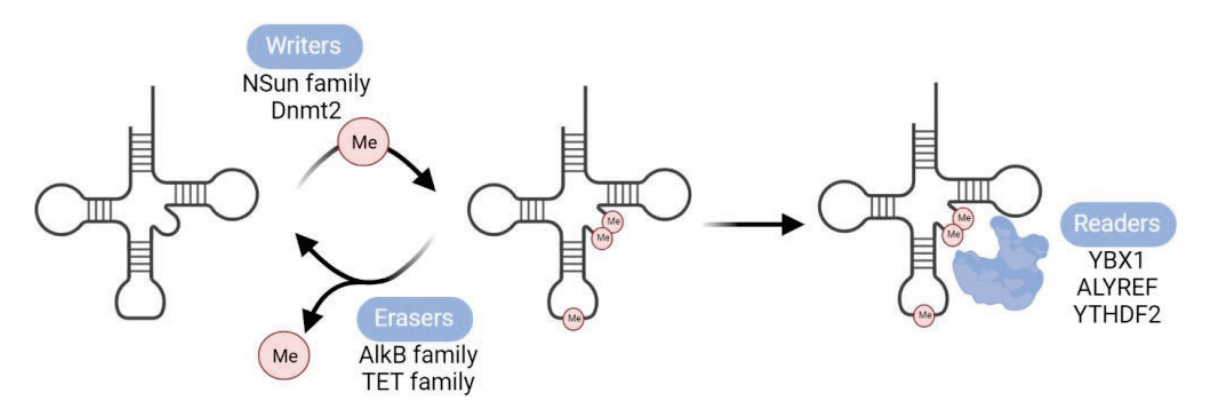


Figure 9. tRNA methylation dynamics. Schematic of the main enzymes involved in the dynamic methylation (writers) and demethylation (erasers) of tRNA species. Multiple RBPs, such as YBX1, ALYREF or YTHDF2, act as readers of these m⁵C methylations.

Regarding the NSun family, NSun3 exclusively methylates the mitochondrial tRNA^{Met} at the position 34 found in the wobble base (Haag et al., 2016; van Haute et al., 2016), NSun6 specifically targets the cytosine 72 in the tRNA^{Cys} and tRNA^{Thr} (Haag et al., 2015; Long et al., 2016) and NSun2 is able to mediate the m⁵C of multiple cytosines (positions 40 and 48-50) located within the anticodon and variable loops of the tRNA (Blanco et al., 2014; Tuorto et al., 2012). Finally, Dnmt2, also known as TRDMT1, is responsible for catalyzing a methylation at a single cytosine located in the position 38 within the anticodon loop of tRNA^{Asp}, tRNA^{Gly} and tRNA^{Val} (Goll et al., 2006; M. Schaefer et al., 2010). This methyltransferase is critical for the establishment of the methylation profile found in mouse sperm tRFs and eventually for the paternal intergenerational transmission (Y. Zhang et al., 2018).

Notably, neurological impairments have been linked to a loss of function of NSun3 (Paramasivam et al., 2020; van Haute et al., 2016) and NSun2 (Abbasi-Moheb et al., 2012; Khan et al., 2012; Komara et al., 2015; Martinez et al., 2012). At the molecular level, a loss of NSun2 leads to tRNA hypomethylation, which are less stable and present a higher affinity for ANG. Consequently, 5'tRFs accumulate within cells resulting in excessive cell death and, thus, a reduced brain size that has been associated with behavioral impairment involving short-term memory and locomotion (Abbasi-Moheb et al., 2012; Blanco et al., 2014) as well as deficits in hippocampal long-term potentiation (George et al., 2022). Moreover, a proper control of tRNA m⁵C methylation is also crucial for cortical brain function and behavior during adult stages (Blaze et al., 2021).

A loss of function of other RNA methyltransferases has also been associated with multiple disorders either impacting the brain or other tissues. Loss-of-function mutations affecting the TRMT10A enzyme have been described as a monogenic cause of microcephaly and early onset diabetes (Cosentino et al., 2018). Guanosine hypomethylation (m^1G) of tRNA in pancreatic β -cells induce an aberrant 5'halve and 5'tRF production resulting in cell apoptosis. An analogous overproduction of 5'tsRNA, especially derived from tRNA^{Gly} and tRNA^{Gly}, has also been observed after the knockdown of the methyltransferase TRMT2A, which catalyzes the uridine-5 methylation (m^5U) at position 54 of multiple cytosolic tRNA (Pereira et al., 2021).

Although many studies have focused on methylation writer enzymes due to their important task in preventing tRNA cleavage, the role of demethylases that erase these epitranscriptomic marks from tRNA is not despicable (Figure 9). Multiple demethylases from the AlkB family have been recently involved in tRNA epitranscriptomic modifications as well as in other RNA species. Particularly, ALKBH3-associated removal of adenosine-1 (m¹A) and cytosine-3 (m³C) methylations from cytoplasmic tRNA leads to an increased biogenesis of 5'tsRNA in

an ANG-dependent fashion, which eventually facilitates ribosomal assembly, enhances translation and inhibits apoptosis (Z. Chen et al., 2019). In conclusion, a precise balance between tRNA methylation and demethylation is essential for a proper processing of tRNA into tRFs.

Regulation of tsRNA biogenesis by RNA editing mechanisms

Although RNA editing mechanisms have not been classically included in the term tRNA epitranscriptomics, these post-transcriptional modifications are equally essential for determining tRNA secondary structures, a proper 3D folding and their interactions with other molecules. Queuosine (Q) is a hypermodified nucleoside that substitutes guanosine and is found in the wobble anticodon of four specific tRNA isoacceptors, including tRNA^{His}, tRNA^{Tyr}, tRNA^{Asn} and tRNA^{Asp}. For instance, this conversion from guanosine to Q increases the resistance of tRNA to stress-induced ANG cleavage (Donovan et al., 2017; X. Wang et al., 2018). Besides, it has been widely demonstrated that Q plays an important role in the fine-tuning of translational fidelity in many different species (Müller et al., 2019; Tuorto et al., 2018; Zaborske et al., 2014).

Pseudouridine (Y) represents the most abundant modification in tRNA species and has a high prevalence in many other RNAs (Spenkuch et al., 2014). It is mainly catalyzed by the pseudouridine synthase PUS7 which is critical for the generation of Y-containing tsRNA that target the translation initiation complex. Mechanistically, 5'tsRNA presenting a Y modification at the position 8 are able to sequester PABPC, a key protein for the initiation of cap-dependent translation, from the eIF4G/A complex, consequently repressing translation (Guzzi et al., 2018). Moreover, mutations in different pseudouridine synthases have been associated with microcephaly and intellectual disability (de Brouwer et al., 2018; Nøstvik et al., 2021; Shaheen et al., 2016).

Another RNA editing mechanism is based on the deamination of adenosine to the non-canonical nucleoside inosine (I), a process regulated by adenosine deaminases (ADAT). Although this modified nucleoside can be methylated like the traditional ones, 1-methylinosine (m¹I) has only been described in the position 37 of the tRNA^{Ala} in eukaryotes (Grosjean et al., 1996). Consistently with the other modifications found at the wobble anticodon position, I is essential for a proper regulation of base pairing and translation (Torres, Piñeyro, et al., 2014) and eventually, alterations in their processing have been linked to intellectual disability, microcephaly and behavioral alterations (Alazami et al., 2013; El-Hattab et al., 2016; Ramos et al., 2019).

- 1. To investigate the potential neurotoxic role of sRNA derived from HD patients' brains in vivo
 - 1.1. To characterize the distribution of sRNA after its injection in the striatum of WT mice
 - 1.2. To explore the behavioral, transcriptional and biochemical consequences of the injection of brain-derived HD-sRNA into the striatum of WT mice
 - 1.3. To analyze the contribution of sCAG species within the effects exerted by brain-derived HD-sRNA injection into the striatum of WT mice
- 2. To characterize the sRNA transcriptome in the brain of HD patients and identify neurotoxic candidates
 - 2.1. To identify potential dysregulated sRNA species in different areas of HD brains
 - 2.2. To evaluate potential neurotoxic effects induced by specific sRNA
- 3. To explore the contribution of relevant players in sRNA biogenesis into HD pathogenesis
 - 3.1. To study the temporal and spatial expression of enzymes involved in sRNA cleavage in HD brains
 - 3.2. To analyze sRNA epitranscriptomic modifications in human HD putamen

1. Human *post-mortem* samples

For this thesis, frozen samples of putamen, frontal cortex, hippocampus and cerebellum from HD patients and non-affected individuals were provided by the Neurological Tissue Bank of the Biobank-Hospital Clínic-Institut d'Investigacions Biomèdiques August Pi i Sunyer (IDIBAPS; Barcelona, Catalonia, Spain) following the guidelines and approval of the local ethic committee (Hospital Clínic Barcelona's Clinical Research Ethics Committee; HCB/2015/0088). Sex, age, pathological diagnosis, Vonsattel stage, CAG repeat length and post-mortem delay (PMD) information are detailed in Table 2. Informed consent was provided by all subjects included in this study.

Human post-mortem samples

Huma	n post	-morte	m samples			
ID	Sex	Age	Pathological	Vonsattel	CAG repeat	PMD
			diagnosis	stage	length	(hh:mm)
810	F	81	Control	-	<25	23:30
1468	M	64	Control	-	<25	10:00
1491	M	83	Control	-	<25	13:00
1541	F	56	Control	-	<25	14:00
1557	M	86	Control	-	<25	7:25
1570	F	86	Control	-	<25	4:00
1679	F	90	Control	-	<25	12:20
1694	M	58	Control	-	<25	5:00
1697	M	78	Control	-	<25	6:00
1733	M	76	Control	-	<25	11:30
1752	F	88	Control	-	<25	24:00
1755	F	77	Control	-	<25	4:30
1818	M	78	Control	-	<25	5:00
1858	F	83	Control	-	<25	7:30
1870	F	97	Control	-	<25	7:20
1888	F	93	Control	-	<25	5:30
1905	M	59	Control	-	<25	6:50
1937	F	83	Control	-	<25	7:33
1949	М	86	Control	-	<25	7:25
2055	M	94	Control	-	<25	15:45
518	F	65	Huntington's disease	3	42	15:15
539	M	68	Huntington's disease	3	44	4:00

643	F	72	Huntington's disease	3	42	17:00
801	M	59	Huntington's disease	4	44	5:30
909	M	60	Huntington's disease	4	43	13:30
1120	M	55	Huntington's disease	3	48	15:00
1193	M	55	Huntington's disease	3-4	-	7:00
1294	M	53	Huntington's disease	3	45 ± 2	7:00
1334	M	73	Huntington's disease	1	40 ± 2	7:00
1438	M	85	Huntington's disease	3	40	5:30
1630	M	76	Huntington's disease	2	38	6:00
1638	M	72	Huntington's disease	2	41	13:10
1758	M	68	Huntington's disease	2-3	42 ± 2	6:10
1844	F	69	Huntington's disease	2	42	15:30
1874	M	56	Huntington's disease	3	43	4:30
1875	M	84	Huntington's disease	2-3	39	8:00
1933	F	86	Huntington's disease	2	40	12:20
1973	F	65	Huntington's disease	3	-	6:30
1980	F	69	Huntington's disease	3	-	12:30
1981	M	66	Huntington's disease	3	43	6:30
2060	F	54	Huntington's disease	2-3	-	7:30
2199	M	62	Huntington's disease	-	-	14:30
2203	M	66	Huntington's disease	-	-	16:42
2250	F	65	Huntington's disease	-	-	6:15
2267	М	33	Huntington's disease	-	-	6:08

Table 2. Details of human post-mortem brain samples used in this thesis. For each subject, information about sex, age, pathological diagnosis, Vonsattel stage, CAG repeat length and post-mortem delay (PMD) is provided. The CAG repeat length includes the longest allelic CAG repeat in the *HTT* gene for each subject.

2. Mouse models

All procedures were performed in compliance with the ethical guidelines of the NIH Guide for the Care and Use of Laboratory Animals and approved by the local animal care committee of the University of Barcelona and the Generalitat de Catalunya, in accordance with the European (2010/63/UE) and Spanish (RD53/2013) regulations for the care and use of laboratory animals. All mice were housed in the Animal Facility of the Faculty of Medicine and Health Sciences, University of Barcelona, Casanova Campus.

All mice were housed with *ad libitum* access to water and food in a colony room maintained under controlled conditions of temperature (19-22 °C), humidity (40-60 %) and a standard light/dark cycle (12:12 h). Mice were housed together in numerical birth order in groups of mixed genotypes, except for specific experiments in which individualization was required. Mice weight was controlled throughout all the experiments.

Mice genotyping was performed by conventional PCR using primers to expand the exon 1 of the *Htt* gene, followed by the visualization of the PCR product in an agarose gel. Samples from both male and female mice were used for molecular characterization experiments while only male animals were used for *in vivo* experimental procedures.

2.1 R6/1 mouse model

For this thesis, one of the main HD animal models used is the R6/1 transgenic mouse model. Original R6/1 mice were purchased from The Jackson Laboratory (Bar Harbor, ME, USA). Heterozygous R6/1 mice express the human N-terminal exon 1 of the *HTT* gene with 115 CAG repeats, which encode for a polyglutamine stretch located in the N-terminal region of the mutant protein (Mangiarini et al., 1996). R6/1 colony breeding was managed by mating WT females to R6/1 males, obtaining an offspring of age-matched heterozygous WT and R6/1 littermates. Mice were maintained in a B6CBA genetic background.

2.2 Hdh^{Q7/Q111} mouse model

Hdh^{Q7/Q111} KI mouse model was originally obtained from Dr M. MacDonald's lab (Lloret et al., 2006) and maintained in a C57BL/6 genetic background. KI mice express a targeted insertion of expanded CAG repeats in the mouse *Htt* gene extending the resulting polyQ stretch up to 111 glutamines (Menalled, 2005; White et al., 1997). An offspring of WT and KI age-matched littermates were obtained crossing WT male mice (Hdh^{Q7/Q7}) to heterozygous Hdh^{Q7/Q111} female mice.

3. Cell cultures

3.1 Primary neuronal cultures

Brains from WT mouse at day 17.5 of embryonic development (E17.5) were obtained and placed in Neurobasal medium (Gibco; 21103-049). Striata were dissected and gently mechanically dissociated with a fire-polished glass Pasteur pipette. Neurons were cultured in 96-well plates, pre-coated with 0.1 mg/ml poly-D-lysine (Sigma; P0899). Cultures were maintained in sterile conditions at 37 °C in a humidified atmosphere containing 5 % CO_2 in Neurobasal medium supplemented with 2 % B27 (Gibco; 17504-044) and 1 % Glutamax (Gibco; 35050-038) until 7 days in vitro (DIV).

3.2 Striatal cell lines

Conditionally immortalized WT (STHdh $^{Q7/Q7}$) and mutant (STHdh $^{Q111/Q111}$) striatal neuronal progenitor cell lines are derived from the KI transgenic mouse models (Hdh $^{Q7/Q7}$ and Hdh $^{Q111/Q111}$) expressing endogenous levels of normal and mutant Htt with 7 and 111 glutamines, respectively (Cattaneo & Conti, 1998; Trettel et al., 2000). Cells were cultured in Dulbecco's modified Eagle's medium with high glucose (DMEM; Gibco; 41966-029) supplemented with inactivated 10 % Fetal Bovine Serum (FBS; Biological Industries; 04-007-1A), 1 % penicillin-streptomycin (Biological Industries; 03-031-1B), 2 mM L-glutamine (Biological Industries; 03-020-1B), 1 mM sodium pyruvate (Thermo Fisher Scientific; 11360039) and 400 µg/ml geneticin (G418; Gibco; 11811-023). Cells were maintained in sterile conditions at 33 °C in a humidified atmosphere containing 5 % CO₂.

3.3 Cell viability assay

To determine cell viability, CellTiter 96° AQueous One Solution Cell Proliferation Assay (MTS) (Promega; G3580) was used. Primary striatal cultures at 7 DIV were treated with different concentrations of synthetic RNA oligonucleotides that mimic 5'tRFs and incubated for 1 h. Then, MTS solution was added to the media and absorbance was measured at 490 nm every 15 min for 3 h. Absorbance at 490 nm is directly proportional to the number of living cells in the culture. Each treatment was performed in duplicates in three independent primary cultures. All synthetic RNA oligonucleotides were purchased from Eurogentec (Liège, Belgium) and present a 5' modification with a phosphate group (-P). Oligonucleotide sequences are provided in Table 3. Hydrogen peroxide (Sigma; H1009; 200 μ M) was used as positive control.

Oligonucleotides

01180110101		
tRF isotype	Strand	Sequence (5'-3')
5'tRF-Ala	Sense	P-GGGGGUGUAGCUCAGUGGUAGAGCGCGUGC
5'tRF-Ala	Antisense	P-GCACGCGCUCUACCACUGAGCUACACCCCC
5'tRF-Gly	Sense	P-GCGCCGCUGGUGUAGUGGUAUCAUGCAAGAU
5'tRF-Gly	Antisense	P-AUCUUGCAUGAUACCACUACACCAGCGGCGC
5'tRF-Val	Sense	P-GGUUCCAUAGUGUAGUGGUUAUCACGUCUGCUUU
5'tRF-Val	Antisense	P-AAAGCAGACGUGAUAACCACUACACUAUGGAACC

Table 3. Synthetic RNA oligonucleotide sequences mimicking 5'tRFs. Both sense and antisense versions of each oligonucleotide were used.

4. Molecular biology techniques

4.1 Total RNA isolation

Both human and mouse dissected brain areas were immediately placed in QIAzol solution (QIAGEN; 79306), followed by RNA extraction with the miRNeasy mini kit (QIAGEN; 217004). Briefly, tissue was homogenized using a hand-held polytron and incubated at room temperature (RT) for 5 min. Chloroform (200 μ l) was added to each sample, mixed, incubated for 3 min (RT) and centrifuged for 15 min at 12000 g (4 °C). The aqueous phase was combined with an equal volume of ethanol 100 %. This mixture was loaded into a column and cleaned. Total RNA was eluted in nuclease-free water.

4.2 sRNA purification

Small RNA (sRNA) fractions were purified from total RNA with the RNA Clean & Concentrator-5 kit (Zymo Research; R1015) according to the manufacturer's instructions. This kit allowed a selective recovery of both highly concentrated large RNAs (>200 nt) and sRNA (17-200 nt) from the same sample.

4.3 Isolation of specific-sized RNAs

For the sRNA fractionation, sRNA samples (<200 nt) were mixed with an RNA loading dye (1:4) and incubated at 95 °C for 5 min. The mixture was loaded into 15 % urea polyacrylamide gel and run in a 0.5x TBE buffer at 120V for 45 min. Using UV shadowing with a fluor-coated TLC plate, a band containing mostly 50-70 nt sRNA (mostly full length tRNA) and a band containing sRNA of 17-50 nt (referred to as ssRNA) were excised based on small RNA ladders. Then, gel bands were incubated with nuclease-free water for 3 h with shaking at 1100 rpm (RT) for a passive elution of the RNA fractions. Then, samples were incubated with 0.1 volumes of 4M sodium chloride, 2 volumes of isopropanol and 1.5 μ l of glycogen overnight at -80 °C. After precipitation, samples were centrifuged for 30 min at 16000 g (4 °C), supernatant was removed, pellet was cleaned with ethanol 85 % and RNA was resuspended in nuclease-free water.

4.4 RNA quality control and quantification

Determination of total RNA integrity was assessed with TapeStation 4200 (Agilent Technologies). All experiments included in this thesis were performed with total RNA samples presenting an RNA integrity number (RIN) of 5 or above. RNA quantification was performed using NanoDrop One Spectrophotometer (Thermo Fisher Scientific) and Bioanalyzer 2100 (Agilent Technologies). Detection and visualization of RNA sizes were monitored through Bioanalyzer 2100 (Agilent Technologies).

4.5 sRNA labelling

Purified sRNA fractions (<200 nt) were labelled using the Label IT siRNA tracker intracellular localization kit Cy3 (Mirus; MIR7212) according to the manufacturer's instructions. A total of 8-10 ng of sRNA was incubated at 37 °C for 1 h with 10 μ l of 10x Labelling buffer A, 10 μ l of Label IT siRNA tracker reagent and nuclease-free water (up to 100 μ l of final volume). Subsequently, sRNA was precipitated through incubation with 0.1 volumes of sodium chloride 5M and 2.5 volumes of ice-cold ethanol 100 % at -80 °C for 30 min and then centrifuged for 30 min at 16000 g (4 °C). Once pelleted, Cy3-labelled sRNA was cleaned with ethanol 70 %, resuspended in Dilution buffer and stored protected from light for further use.

4.6 ssRNA enzymatic pre-treatments

For the T4 polynucleotide kinase (T4PNK) pre-treatment, a total of 100 ng of 17- to 50-nt sRNA (ssRNA fraction) was incubated in a 10 μ l reaction mixture containing 1 μ l 10x PNK buffer (New England Biolabs; B0201), 10 mM ATP (New England Biolabs; P0756S) and 1U T4PNK enzyme (New England Biolabs; M0201) at 37 °C for 1 h. Then, the enzyme was inactivated at 70 °C for 5 min and ssRNA were cleaned with the RNA Clean & Concentrator-5 kit (Zymo Research; R1015), according to the manufacturer's instructions.

For the combinatorial pre-treatment with the T4PNK enzyme and the demethylases (J. Shi et al., 2021), a total of 100 ng of 17- to 50-nt RNA (ssRNA fraction) was processed with the rtStar tRF&tiRNA pre-treatment kit (ArrayStar; AS-FS-005). ssRNA were mixed with 1 μ l RNase Inhibitor, 1 μ l Terminal Enzyme Mix, 3 μ l 10x Terminal enzyme reaction buffer, 3 μ l ATP (10mM) and nuclease-free water (up to 30 μ l of final volume) and incubated at 37 °C for 30 min, followed by an inactivation of the enzyme at 70 °C for 5 min. Then, ssRNA were column-purified with the RNA Clean & Concentrator-5 kit (Zymo Research; R1015). Afterwards, ssRNA fraction was incubated at 25 °C for 2 h in a 70 μ l reaction mixture containing 25 μ l of 4x Demethylation Reaction buffer, 5 μ l of Demethylase, 2 μ l of RNase inhibitor and 38 μ l of nuclease-free water. Demethylase enzyme was inactivated at 70 °C for 5 min and ssRNA were cleaned once more with the RNA Clean & Concentrator-5 kit (Zymo Research; R1015).

After enzymatic treatment, ssRNA samples were precipitated through incubation with 0.1 volumes of sodium acetate 3M (pH 4.8), 2.5 volumes of ethanol 100 % and 0.01 volumes of glycogen for 1 h at -80 $^{\circ}$ C and centrifuged for 30 min at 16000 g (4 $^{\circ}$ C). Finally, supernatant was removed, pellet was cleaned with ethanol 75 % and ssRNA were resuspended in nuclease-free water.

4.7 Quantitative reverse transcription PCR (RT-qPCR)

Different RT-qPCR technologies were applied in this thesis, chosen technology in each experiment is specified in the corresponding figure legend. For TaqMan and SYBR Green assays, total RNA from mouse striatum was treated with the TURBO DNase I kit (Invitrogen; AM1907) by adding 0.1 volumes of 10x TURBO DNAse buffer and 1 μ I of TURBO DNAse enzyme and incubating the mixture for 25 min at 37 °C in a thermomixer. Then, 0.1 volumes of DNAse Inactivation Reagent were added, incubated for 5 min (RT), centrifuged for 90 s at 10000 g (RT) and supernatant containing the RNA was collected. A total of 500 ng of RNA (in a final volume of 8 μ I) was used to generate cDNA with the First-strand cDNA Synthesis Kit (Cytiva; GE27-9261-01). Samples were first heated for 10 min at 65 °C and then, 5 μ I of bulk first stranded cDNA reaction mix, 1 μ I of DTT solution (200 mM) and 1 μ I of pd(N)6 primers (random hexadeoxynucleotides; 0.2 μ g/ μ I) were added to each sample. After these mixtures were incubated for 1 h at 37 °C, products were ready for PCR amplification.

4.7.1 TaqMan assay

Quantitative PCR (qPCR) was performed in 10 μ l of final volume containing 4.5 μ l cDNA, 0.5 μ l 20x TaqMan Gene Expression Assays and 5 μ l of 2x TaqMan Universal PCR Master Mix (Applied Biosystems; 4304437) per each sample. Determinations were performed in technical duplicates per cDNA sample on 384-well plates in an ABI Prism 7900 Sequence Detection system (Applied Biosystems) following supplier's parameters: 50 °C for 2 min, 95 °C for 10 min, and 40 cycles of 95 °C for 15 s and 60 °C for 1 min. Primers used are listed in Table 4. Data were processed by the Sequence Detection Software (SDS version 2.2.2; Applied Biosystems).

Taqivia	an assa	y prim	ers
---------	---------	--------	-----

Tagirian assi	.,	
Target gene	Gene full name	ID assay
Cxcl2	Chemokine ligand 2	Mm00436450_m1
II1b	Interleukin 1 beta	Mm00434228_m1
116	Interleukin 6	Mm00446190_m1
Ptgs2 FAM	Prostaglandin-endoperoxide synthase 2	Mm00478374_m1
Tnf	Tumor necrosis factor	Mm00443258_m1
Actb	Actin	Mm02619580_g1
Hprt1	Hypoxanthine-guanine phosphoribosyltransferase	Mm00446968_m1

Table 4. Primers and probes used for TaqMan qPCR assays in mouse brain samples. For each target gene, ID assays are provided.

4.7.2 SYBR Green assay

For qPCR, one μ l of diluted cDNA (1:10) was mixed with 5 μ l of PowerUp SYBR Green Master Mix (Applied Biosystems; A25742), 1 μ l of forward primer (10 μ M), 1 μ l of reverse primer (10 μ M) and 2 μ l of RNase-water. Primers used are listed in Table 5. Amplification was performed in a StepOnePlus Real-Time PCR System (Applied Biosystems) with the following cycling conditions: 95 °C for 10 min and 40 cycles of 95 °C for 15 s and 61 °C for 1 min. Melt curve (60-95 °C) analyses was performed at the end of each experiment. For each gene, determinations were performed in technical triplicates.

SYBR Green assay primers

Target gene	Gene full name	Sequence (5'-3')	Product length
Dlg4	Post-synaptic density protein 95	F : AGACGGTGACGCAGATGGAA R : TCGGGGAACTCGGAGAGAAG	100
II1b	Interleukin 1 beta	F: CCTTCCAGGATGAGGACATGA R: TCATCCCATGAGTCACAGAGGAT	79
116	Interleukin 6	F : CCTCTCTGCAAGAGACTTCCATCCA R : AGCCTCCGACTTGTGAAGTGGT	152
Ppp1r1b	Dopamine- and cAMP- regulated neuronal phosphoprotein of 32 kDa	F : AGATTCAGTTCTCTGTGCCCG R : GGTTCTCTGATGTGGAGAGGC	149
Ptpn5	Protein tyrosine phosphatase non-receptor type 5	F: TGGGTAGTTGGGGTAAAGACC R: ATGATCCAGACATGCGAACA	156
Actb	Actin	F: ACCTTCTACAATGAGCTGCG R: CTGGATGGCTACGTACATGG	147
Hprt	Hypoxanthine-guanine phosphoribosyltransferase	F: TGTTGTTGGATATGCCCTTG R: GGACGCAGCAACTGACATT	259

Table 5. Details of primers used for SYBR Green qPCR assays in mouse brain samples. For each target gene, forward (F) and reverse (R) primers and product length are provided.

4.7.3 miRCURY LNA custom PCR assay

A total of 10 ng of RNA from human putamen was used for reverse transcription with the miRCURY LNA RT Kit (Qiagen; 339340). For cDNA synthesis, 2 μ l of 5x miRCURY RT reaction buffer, 1 μ l of 10x miRCURY RT Enzyme Mix, 0.5 μ l of synthetic RNA spike-in U6 (UniSp6) and 4.5 μ l of RNase-free water were added to each RNA sample. UniSp6 was used as an internal reverse transcription control. Mixtures were incubated for 60 min at 42 °C, followed by an inactivation step for 5 min at 95 °C.

A 1:10 dilution of the obtained cDNA was required for qPCR using the miRCURY LNA SYBR Green PCR Kit (Qiagen; 339345). Briefly, 10 μ l of reaction mix were prepared by adding 3 μ l of cDNA, 5 μ l of 2x miRCURY SYBR Green Master Mix, 0.5 μ l of ROX Reference Dye, 1 μ l of PCR primer mix and 0.5 μ l of RNase-free water. Custom primers used are listed in Table 6. qPCR were carried out in a StepOnePlus Real-Time PCR System (Applied Biosystems) following the cycling conditions indicated by the manufacturer: 95 °C for 2 min and 40 cycles of 95 °C for 10 s and 56 °C for 1 min. Melt curve analysis was performed at the end of each experiment. For each condition, determinations were performed in triplicate.

miRCURY LNA custom PCR assay primers

Target tRF	Sequence (5'-3')
5'tRF-Ala-AGC	GGGGGTGTAGCTCAGTGGTAGAGCGCGTG
5'tRF-Glu-TTC	TCCCTGGTGGTCTAGTGGTTAGGATTCGGCG
5'tRF-Gly-CCC	GCGCCGCTGGTGTAGTGGTATCATGCAAGA
5'tRF-Val-TAC	GGTTCCATAGTGTAGTGGTTATCACGTCTGCTTT
J titl - val-TAC	ddirecaladidiadiddilaicaedicideili
Target gene	Sequence (5'-3')

Table 6. Details of primers used for miRCURY LNA custom qPCR assays in human and mouse brain samples. For each 5'tRF target, primer sequences are provided. For the housekeeping gene, forward (F) and reverse (R) primer sequences are given.

4.7.4 RT-qPCR quantifications

Relative quantification (RQ) was calculated with the $2\Delta\Delta$ Ct method (Livak & Schmittgen, 2001) using the appropriate reference gene in each case (specified in the corresponding figure legends) for normalization. For the analysis of RQ data, linear mixed-effects model (Steibel et al., 2009) was applied considering technical replicates.

4.8 RNA polyadenylation and PCR amplification of sCAG and HTT exon 1

The presence of sCAG and HTT exon 1 RNAs were evaluated in total RNA and sRNA purified fractions obtained from human putamen samples through RNA polyadenylation followed by PCR amplification. First, total RNA was treated with the TURBO DNase I kit (Invitrogen; AM1907), as described in section 4.7. For *in vitro* RNA polyadenylation, 1 µg of total RNA or 100 ng of purified sRNA were incubated with poly(A)-polymerase (Invitrogen; AM2030) and ATP (1 mM) at 37 °C for 1 h. Then, samples were annealed with a poly(T)-adapter primer (5'-CGA ATT CTA GAG CTC GAG GCA GGC GAC ATG GCT GGC TAG TTA AGC TTG GTA CCG AGC TCG GAT

Subsequently, PCR amplification was performed using a specific primer recognizing the poly(T)-adapter in combination with another primer recognizing sCAG or *HTT* exon 1 RNA. Amplification of miR-16 and *RNU66* were performed in parallel as internal controls. Primers used are listed in Table 7.

Primers for sCAG and HTT exon 1 detection

Target	Sequence (5'-3')
HTT exon 1	F: CCAAAAGACGGCAATATGGT
miR-16	F: ACACTCCAGCTGGGTAGCAGCACGTAAAT
RNU66	F: GTAACTGTGGTGATGGAAATGTG
sCAG	F: CAGCAGCAGCAGCAGCAG
Complementary to poly(T)-adapter	R: CGAATTCTAGAGCTCGAGGCAGG

Table 7. Details of primers used for sCAG and *HTT* **exon 1 detection in human samples.** For each target, forward (F) primer sequences are provided. Reverse (R) primer sequence recognizing the poly(T)-adapter used in all cases is detailed.

Finally, PCR products were resolved by electrophoresis in 2 % agarose gels and quantified using a computer-assisted densitometer (Gel-Pro Analyzer, version 4, Media Cybernetics). A synthetic oligonucleotide of (CAG)₇ repeats (21 nucleotides in total) mimicking sCAG species was loaded in the electrophoresis as a positive control.

4.9 RNA mass spectrometry (LC-MS/MS)

For the quantification of modified ribonucleosides in RNA molecules, liquid chromatography – tandem mass spectrometry (LC-MS/MS) was applied to the isolated specific-sized RNAs with a length between 50 to 70 nt. A total of 500 ng of 50- to 70-nt RNA from the putamen of control individuals and HD patients (n = 4/condition) were digested using 1 μ l of the Nucleoside Digestion Mix (New England Biolabs; M0649) and incubated for 1 h at 37 °C. Then, ribonucleosides were acidified with formic acid, desalted using HyperSep Hypercarb SPE Spin tips (Thermo Fisher Scientific; 60109-412) and analyzed using an Orbitrap Eclipse Tribrid mass spectrometer (Thermo Fisher Scientific; FSN04-10000) coupled to an EASY-nLC 1000 (Thermo Fisher Scientific; LC120) for online LC-MS/MS analysis.

4.10 Total protein extraction

4.10.1 Mouse and human brain samples

Animals were sacrificed by cervical dislocation at different stages of disease progression. Brains were quickly removed and striatum, motor cortex, hippocampus and cerebellum were dissected out and stored at -80 °C for further processing. Both mouse and human brain tissues were homogenized by sonication in ice-cold lysis buffer containing 50 mM Tris-HCl (pH 7.5), 10 mM EGTA, 150 mM NaCl and 1 % Triton X-100 supplemented with protease and phosphatase inhibitors: 2 mM PMSF (phenylmethylsulphonyl fluoride), 10 μ g/ μ l aprotinin, 1 μ g/ μ l leupeptin, 2 mM Na₃VO₄ and 100 mM NaF. Then, samples were centrifuged for 15 min at 16000 g (4 °C), supernatants were collected.

4.10.2 Cell cultures

Both WT (STHdh $^{Q7/Q7}$) and mutant (STHdh $^{Q111/Q111}$) cell cultures from passages 8 to 14 (P8-14) were used to obtain protein extracts. Cells were washed with phosphate-buffered saline (PBS), detached from plates using pre-warmed 2.5 % trypsin and centrifuged at 750 rpm for 5 min. Cell pellets were washed in ice-cold PBS and homogenized with an insulin syringe in lysis buffer containing 50 mM Tris-HCl (pH 7.5), 10 mM EDTA, 150 mM NaCl and 1 % Nonidet P40 Substitute (NP40; Sigma; 9016-45-9) supplemented with protease and phosphatase inhibitors: 2 mM PMSF, 10 μ g/ μ l aprotinin, 1 μ g/ μ l leupeptin and 2 mM Na₃VO₄. Then, samples were centrifuged for 15 min at 16000 g (4 °C) and supernatants were collected.

4.11 Protein quantification

After protein extraction, sample concentration was determined in a colorimetric assay using the Detergent-Compatible Protein Assay kit (BioRad; 5000116), following manufacturer instructions. As reference for protein concentration, serial dilutions of bovine serum albumin (BSA; from 0.5 μ g/ μ l to 16 μ g/ μ l) in proper lysis buffer were prepared. Each sample was measured in duplicates and quantifications with standard deviations <0.5 were accepted.

4.12 Western Blot (WB) analysis

Protein extracts (10 μ g for cell cultures and mouse samples and 20 μ g for human samples) were denatured in sample buffer containing 62.5 mM Tris-HCl (pH 6.8), 10 % glycerol, 2 % Sodium dodecyl sulphate (SDS), 140 mM β -mercaptoethanol and 0.1 % bromophenol blue. Then, protein extracts were heated at 100 °C for 5 min and resolved on 10-12 % SDS-polyacrylamide gels at 35 mA/gel for 75 min (RT). Afterwards, proteins were transferred to nitrocellulose membranes (Amersham; 10600002) at 90V for 90 min (4 °C). Membranes were stained using Ponceau S reagent to ensure protein transfer and then incubated with 5 % non-fat powdered milk and 5 % BSA in TBS-T (Tris-buffer saline 0.1 % Tween-20) for 1 h (RT). After

blocking non-specific binding sites, membranes were immunoblotted overnight in agitation (4 °C) with primary antibodies detailed in Table 8.

Primary antibodies

Printary antibodies					
Antigen	MW (kDa)	Host	Dilution	Source	Identifier
DARPP32 (clone 15)	32	Mouse	1:1000	BD Bioscience	611520
DNMT2 (clone D-9)	45	Mouse	1:400	Santa Cruz Biotechnology	sc-365001
DRD1 (H-109)	100	Rabbit	1:1000	Santa Cruz Biotechnology	sc-14001
DRD2	50	Rabbit	1:1000	Sigma	AB5084P
ENK	28	Rabbit	1:1000	Abcam	ab85798
NSun2 (for human)	87	Rabbit	1:500	Proteintech	20854-1-AP
NSun2 (for mouse)	77 and 85	Rabbit	1:1000	Invitrogen	702036
PHLPP1	150	Rabbit	1:1000	Cayman Chemical	10007191
PSD95 (7E3-1B8)	95	Mouse	1:1000	Thermo Fisher Scientific	MA1-046
RNase T2	29	Rabbit	1:500	Proteintech	13753-1-AP
STEP (clone 23E5)	46 and 61	Mouse	1:2000	Santa Cruz Biotechnology	sc-23892
GAPDH	34	Mouse	1:2000	Sigma	AB2302
Tubulin	55	Mouse	1:50000	Sigma	6074

Table 8. List of primary antibodies used for WB. Details of antigen molecular weights (kDa), host species, used dilutions, sources and identifiers of each antibody are provided. GAPDH and tubulin were used as loading controls.

The following day, after washing with TBS-T, membranes were incubated for 1 h (RT) with the appropriated horseradish peroxidase-conjugated secondary antibodies listed in Table 9. Immunoreactive bands were developed with the Western Blot Luminol Reagent (Santa Cruz Biotechnology; sc-2048), detected using the ChemiDoc Imaging System (BioRad; 12003153) or traditional films and finally quantified using a computer-assisted densitometer (Gel-Pro Analyzer, version 4, Media Cybernetics).

Secondary antibodies

Antigen	Dilution	Source	Identifier
Anti-mouse IgG	1:2000	Promega	W4021
Anti-rabbit IgG	1:2000	Promega	W4011

Table 9. List of secondary antibodies used for WB. Details of used dilution and source of each antibody are provided.

5. Morphological analysis

5.1 Tissue preparation

Animals were deeply and irreversibly anesthetized with pentobarbital (60 mg/kg) and transcardially perfused with ice-cold PBS for 5 min followed by 50 ml of 4 % formaldehyde (Casa Álvarez; FO090101). Alternatively, for sRNA-injected animals, as one cerebral hemisphere was dissected for protein or RNA extraction, half-brains were post-fixed in 4 % formaldehyde solution for 3 days (4 °C). After fixation, all samples were cryoprotected by immersion for 24 h in 15 % and 24 h in 30 % sucrose in PBS with 0.02 % sodium azide (4 °C). Then, samples were flash-frozen in dry ice-cooled 2-methylbutane for 1 min, embedded in OCT compound (Tissue-Tek; 4583) and 30- μ m serial coronal sections were obtained using a cryostat (Leica; CM3050S). Sections were collected in free-floating in 0.02 % sodium azide in PBS solution (4 °C) for further processing.

5.2 Nissl staining

For Nissl staining, coronal brain sections were placed in silane-coated slides and stained for 45 min in 0.1 % cresyl violet (Fluka; 61123) prepared in a 0.1 M acetic acid and 0.1 M sodium acetate solution. Then, samples were dehydrated by immersion in ethanol solutions of increasing concentrations (5 min each step: one step in 70 %, one step in 90 %, and two steps in 100 %) followed by two steps in xylene and mounted with DPX media (Sigma; 06522).

5.3 Immunohistochemistry

For DARPP32-immunoperoxidase staining, coronal brain slices were washed twice with PBS and endogenous peroxidase activity was quenched by incubating the tissue for 45 min in H_2O_2 in PBS (1:200; RT). Then, brain slices were rinsed in

blocking buffer containing 3 % normal horse serum (NHS; Pierce; 31874) in PBS for 1 h (RT). Then, samples were incubated overnight (4 °C) with mouse anti-DARPP32 (1:1000; BD Bioscience; 611520) in blocking buffer solution containing 0.02 % sodium azide. After primary incubation, ABC Peroxidase Standard Staining Kit (Thermo Fisher Scientific; 32020) was used following manufacturer's indications. Briefly, sections were first incubated with a biotinylated anti-mouse secondary antibody for 2 h (1:200; RT) diluted in blocking buffer and then with Reagent A (Avidin) and Reagent B (Biotinylated HRP), each of them diluted 1:56 in PBS, for 1.5 h (RT). As a peroxidase substrate, 3'-diaminobenzidine (DAB) was used by incubating the slices in DAB diluted at 1 x and H_2O_2 (1:200) in phosphate buffer (PB) 0.1 M for 3 min. Tissue sections were mounted onto silane-coated slides, dehydrated by immersion in ethanol solutions of increasing concentrations (5 min each step: one step in 70 %, one step in 90 %, and two steps in 100 %) followed by two steps in xylene and mounted with DPX media (Sigma; 06522). No signal was detected in control slices in which primary antibody was omitted.

5.4 Bright field image acquisition and analysis

For Nissl staining, neuronal cells were identified using morphological criteria previously described (García-Amado & Prensa, 2012; García-Cabezas et al., 2016). For each mouse, four images of the dorsal striatum from a minimum of three coronal slices of 30 μ m spaced 240 μ m apart were acquired at 10x magnification with the Olympus BX51 microscope. All bright field images were blinded to treatment and Nissl-positive cells contained in dorsal striata were manually counted using Fiji/ImageJ software.

For DARPP32-immunohistochemistry, stained cells in the dorsal striatum were examined in a minimum of four bright field images from six to eight coronal sections per animal spaced 240 μ m apart, covering the entire brain region. Stereological evaluation was performed in a blinded-to-treatment manner using a morphometric system consisting of an Olympus BX51 microscope equipped with a motorized stage and the Computer-Assisted Stereology Toolbox (CAST) software (Olympus). The mean number of stained cells per cubic millimetre of tissue was determined for each animal.

5.5 Immunohistofluorescence

Free-floating brain sections (30 μ m) were washed twice in PBS and tissue autoflorescence was quenched with an incubation with 50 mM NH₄Cl for 30 min (RT). Permeabilization was performed for 20 min (2x10 min) in 0.3 % Triton X-100 in PBS solution (RT). Then, tissue was blocked in a solution containing 5 % NHS (Pierce; 31874) and 0.3 % Triton X-100 in PBS for 2 h (RT). Afterwards, brain sections were incubated overnight in agitation (4 °C) in blocking solution with primary antibodies detailed in Table 10.

Primary antibodies

Antigen	Host	Dilution	Source	Identifier
ChAT	Goat	1:500	Sigma	AB144P
Cleaved caspase-3 (Asp175)	Rabbit	1:500	Cell Signalling	9661
Ctip2	Rat	1:400	Abcam	ab18465
lba1	Rabbit	1:500	Wako	019-19741
m ⁵ C (33D3)	Mouse	1:100	Abcam	ab10805
NPY	Rabbit	1:500	Abcam	ab30914
NSun2	Rabbit	1:300	Invitrogen	702036
Olig2	Rabbit	1:200	Sigma	AB9610
PARV	Rabbit	1:500	Swant	PV27
Sox9	Rabbit	1:500	Sigma	AB5535

Table 10. List of primary antibodies used for immunohistofluorescence. Details of host species, used dilutions, sources and identifiers of each antibody are provided.

After washing with PBS (2x10 min), tissue was incubated with specific fluorescent secondary antibodies (Table 11) diluted in blocking buffer for 2 h (RT). Consecutively, slices were washed with PBS (2x10 min), incubated for nuclear staining with Hoechst 33258 (1:5000; Invitrogen; H-3569) or DAPI (1:5000; Sigma; D9542) for 10 min (RT) and washed again (2x10 min). Finally, brain sections were mounted on slices and allowed to dry for 2 h (RT) prior mounting with Mowiol media (Sigma; 81381). As negative controls, slices were processed as described in the absence of primary antibodies and no signal was detected.

Secondary antibodies

Antigen	Dilution	Source	Identifier
AlexaFluor 488 Donkey Anti-Goat IgG	1:200	Jackson ImmunoResearch	705-545-003
AlexaFluor 488 Donkey Anti-Rabbit IgG	1:200	Jackson ImmunoResearch	711-545-152
AlexaFluor 555 Goat Anti-Rabbit IgG	1:200	Jackson ImmunoResearch	111-165-003
AlexaFluor 488 Goat Anti-Rat IgG	1:200	Jackson ImmunoResearch	112-545-003

Table 11. List of secondary antibodies used for immunohistofluorescence. Details of used dilutions, sources and identifiers of each antibody are provided.

For m^5C immunodetection, antigen retrieval was required prior to immunohistofluorescence. Antigen retrieval was performed by incubating the sections at 80 °C for 30 min in citrate buffer (10 mM sodium citrate, 0.05 % Tween-20, pH 6.0) in a thermomixer.

5.6 Confocal image acquisition and analysis

Images were obtained using an Olympus BX60 fluorescence microscope equipped with an Orca-ER cooled CCD camera (Hamamatsu Photonics) or a Zeiss LSM880 confocal laser scanning microscope with ZEN Software using a 63x objective and a standard pinhole (1 airy disk; 1AU). For intracellular sRNA tracking experiments, a minimum of 7 z-stacks were taken for each field and three-dimensional reconstructions were generated using Fiji/ImageJ software. For NSun2 and $\rm m^5C$ immunofluorescences, digital mosaics were performed tiling 4x6 images to cover the entire striatum. Images were processed through filtering and automatically thresholded using Fiji/ImageJ software. For a cell-type specific analysis, nuclei were segmented for Ctip2 or Hoechst signal and then nuclei area and nuclei intensity of NSun2 and $\rm m^5C$ were measured using a custom-made automatic macro. For each mouse, a minimum of four coronal slices of 30 μm spaced 240 μm apart were imaged, with an average of 300-400 cells analysed in each slice.

6. In vivo approaches

6.1 Intrastriatal cannula implantation

Mice were deeply anesthetized with a mixture of oxygen and isoflurane (5 % induction and 1 % maintenance) and placed into a stereotaxic apparatus in a flat skull position. During all procedures, body temperature was maintained constant using a heating pad. Stainless steel bilateral cannulas (26-gauge; Bilaney Consultants Ltd.) were implanted in dorsal striata at the following coordinates relative to bregma: anteroposterior (AP) + 0.6 mm, mediolateral (ML) ± 2 mm, and dorsoventral (DV) – 2 mm. Cannulas consisted of two single guide cannulas with a centre-to-centre distance of 4mm secured to a horizontal and thin plastic plate (Figure 10). Two mounting screws were located into the skull to serve as anchors and the assemblage was fixed in place with dental cement. Two removable occluding dummy cannulas (without projection) were inserted into the guide cannulas to prevent clogging and were only removed prior to infusions. After surgery, all animals received a subcutaneous injection of meloxicam (Metacam; 0.2 mL at 2 mg/mL) to provide postoperative analgesia and were kept on a warm place until recovered from anaesthesia.

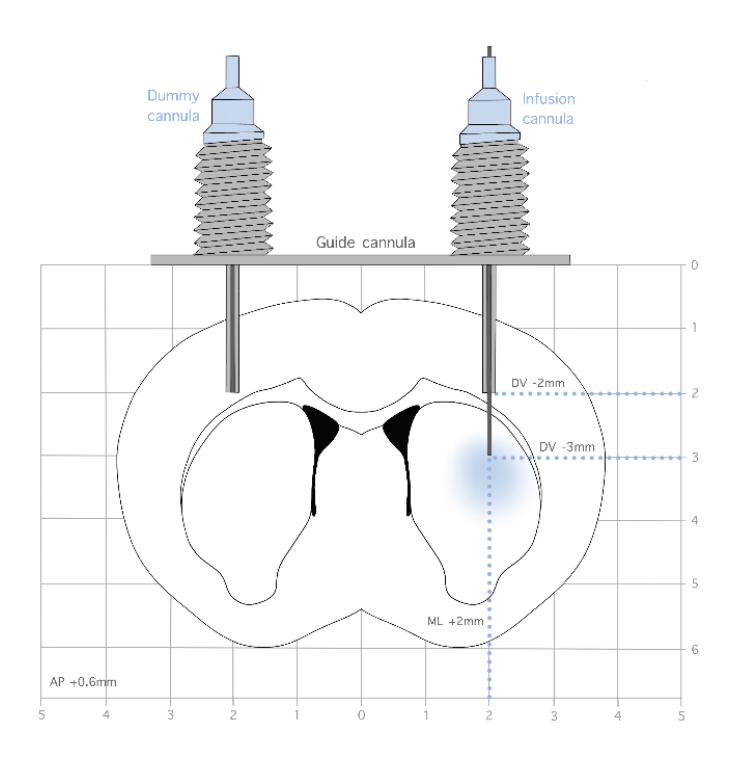


Figure 10. Schematic representation of an intrastriatal bilateral cannula positioned in the mouse brain. Specific coordinates of implantation of the guide cannula into dorsal striata with a dummy cannula (left) and an infusion cannula (right). Adapted from Allen mouse Brain Atlas.

6.2 Preparation of sRNA pools for in vivo injections

For *in vivo* intrastriatal treatments, human sRNA were purified from different brain regions of control individuals or HD patients, as described in sections 4.1 and 4.2, presenting a final concentration of 0.24 µg/µl. All the injected conditions are detailed in Table 12. Synthetic locked nucleic acid antisense oligonucleotides (LNA-ASO) were injected in combination with sRNA in a 1:2 quantity ratio. LNA-ASO complementary to the CAG repeat (LNA-CTG) consisted of a 21-nt length oligonucleotide (5'-CTGCTGCTGCTGCTGCTGCT-3') with an LNA located every third T nucleotide and a phosphorothioate-modified backbone. LNA-CTG and an analogous control scrambled LNA-modified sequence (LNA-SCB) GTGTAACACGTCTATACGCCCA-3') were custom designed and obtained from Exiqon. Synthetic RNA oligonucleotides mimicking sCAG species (sCAG: 5'-CAGCAGCAGCAGCAGCAGCAG-3') and comparable control scrambled RNA oligonucleotides (sSCB: 5'-GUGUAACACGUCUAUACGCCCA-3') were purchased from Thermo Fisher Scientific.

Material for intrastriatal injections

Condition abbreviation	Injected material	Genotype	Brain region	LNA
CTL-sRNA-PT	sRNA (<200nt)	Control	Putamen	-
HD-sRNA-PT	sRNA (<200nt)	HD	Putamen	-

CTL-sRNA-PT + LNA-SCB	sRNA (<200nt)	Control	Putamen	LNA-SCB
CTL-sRNA-PT + LNA-CTG	sRNA (<200nt)	Control	Putamen	LNA-CTG
HD-sRNA-PT + LNA-SCB	sRNA (<200nt)	HD	Putamen	LNA-SCB
HD-sRNA-PT + LNA-CTG	sRNA (<200nt)	HD	Putamen	LNA-CTG
CTL-sRNA-CTX	sRNA (<200nt)	Control	Cortex	-
HD-sRNA-CTX	sRNA (<200nt)	HD	Cortex	-
CTL-sRNA-CB	sRNA (<200nt)	Control	Cerebellum	-
HD-sRNA-CB	sRNA (<200nt)	HD	Cerebellum	-
sSCB	Oligonucleotides	-	-	-
sCAG	Oligonucleotides	-	-	-
Cy3-CTL-sRNA-PT	Cy3-sRNA (<200nt)	Control	Putamen	-
Cy3-HD-sRNA-PT	Cy3-sRNA (<200nt)	HD	Putamen	-
Cy3-CTL-sRNA-CTX	Cy3-sRNA (<200nt)	Control	Cortex	-
Cy3-HD-sRNA-CTX	Cy3-sRNA (<200nt)	HD	Cortex	-

Table 12. List of the different conditions of intrastriatal injections. Details of RNA purification and the source (genotype and brain region) of the injected material are provided.

6.3 Intrastriatal infusion

Intrastriatal infusions were performed in freely moving mice by removing dummy cannulas from guide cannulas and inserting infusion cannulas presenting 1mm projection from the guide to reach the specific injection coordinates (Figure 10). Infusion cannulas were paired with an infusion pump that allowed bilateral infusions of 2 μ l at 0.25 μ l/min. Infusion cannulas were left in place for 5 min after infusions to ensure a complete diffusion of the injected volume. Afterwards, infusion cannulas were removed, and dummy cannulas were positioned again. Artificial cerebrospinal fluid (aCSF) (in mM: 125 NaCl, 2.5 KCl, 1.2 NaH₂PO₄, 1.2 MgCl₂, 2.4 CaCl₂, 26 NaHCO₃, and 11 glucose; with pH adjusted to 7.2) was used as vehicle in all the experiments.

Infusions were administered in both hemispheres, twice per week with 48 h between infusions, and were preceded by a single vehicle infusion in the previous week (see experimental design in Figure 19A). Therefore, each animal received a total of eight sRNA infusions, four in each hemisphere. Mice body weight was recorded weekly along all the experiment. Animals were sacrificed 48 h after the last infusion, and the cerebral hemispheres were processed for histology and protein or RNA extraction.

For intracellular sRNA tracking, animals received a single infusion of Cy3-labelled sRNA and sacrificed 1 h later by transcardially perfusion. Mice brains were processed for further morphological analyses as described in sections 5.5 and 5.6.

6.4 Intrastriatal injection

Mice were deeply anesthetized with isoflurane (5 % induction and 1 % maintenance) and placed into a stereotaxic apparatus in a flat skull position for an intrastriatal injection. A single injection per animal in the dorsal striatum was performed at the following coordinates relative to bregma: AP + 0.6 mm, ML - 2 mm, and DV - 2 mm below the dural surface (Figure 11). Intrastriatal injections of 2 μ l were performed using a 5 μ l-Hamilton microliter syringe at an infusion rate of 250 nl/min. The needle was left in place for 5 min to ensure complete diffusion and then slowly retracted from the brain. Animals were sacrificed 24 h after the injection, brains were removed and injected striata were dissected out and flash frozen at -80 °C for further processing.

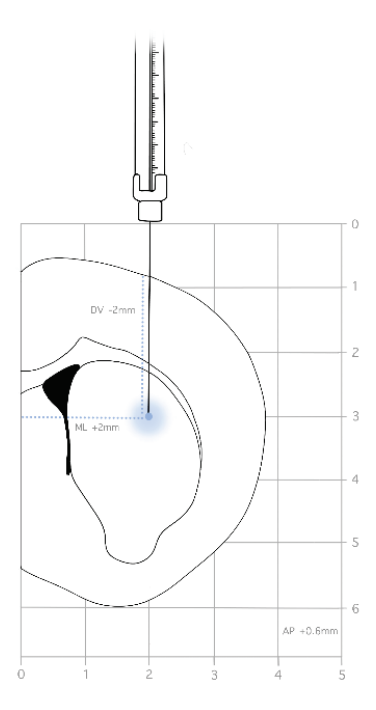


Figure 11. Schematic representation of an intrastriatal injection in the mouse brain. Specific coordinates of injection into the dorsal striatum using a Hamilton syringe. Adapted from Allen mouse Brain Atlas.

6.5 Behavioral analysis

6.5.1 Rotarod

Motor coordination was evaluated on the rotarod apparatus at distinct rotations per minute (rpm). Animals were placed on a motorized rod (30 mm diameter) and trained at different constant speeds (4, 8, 16, and 24 rpm) for 60 s to ensure they were familiar with the apparatus for subsequent assessments. The number of falls during the training test was recorded and no differences were detected between

groups during this period. After training, animals were evaluated once a week at 16, 24, and 32 rpm, and the latency to fall was registered. Trials in which mice put the 4 paws in the rod were the ones considered valid and subsequently registered. Final animal performance was measured as the mean latency to fall achieved during 3 trials at each speed. Animals were allowed to recover for 1 h between evaluations at the different speeds.

6.5.2 Balance beam

Motor coordination and balance were assessed by measuring the ability of mice to traverse a narrow beam as described in Anglada-Huguet et al., 2014, with brief modifications. The beam consisted of a long steel cylinder (50 cm) with a 15 mm-round diameter, placed horizontally, 40 cm above the floor and divided in 5 cm frames (Figure 12). Animals were allowed to walk for 2 min along the beam, while number of slips, total distance travelled, and latency to cover 30 frames were measured.



Figure 12. Schematic representation of a mouse performing the balance beam test. Mice were placed on the beam and evaluated while crossing the different beam frames (5 cm).

7. Sequencing approaches

7.1 sRNA-sequencing of human and mice samples

For sRNA-sequencing of human samples, a small amount of CTL-sRNA-PT, HD-sRNA-PT, CTL-sRNA-CTX, HD-sRNA-CTX, CTL-sRNA-CB and HD-sRNA-CB pools used for intrastriatal injections (see section 6.2) were directly processed.

For sRNA-sequencing of injected mice, total RNA was first isolated from the striatum of the animals injected with HD-sRNA-PT, CTL-sRNA-PT, or vehicle solution and subsequently DNAsed, as described in sections 4.1 and 4.7, respectively.

A total of 200 ng of human sRNA or 800 ng of total mice RNA of each condition were processed with NEBNext Small RNA Library Prep Set for Illumina (New England Biolabs; E7330S), following manufacturer's instructions. Then, size selection was performed using Novex Pre-Cast 6 % TBE PAGE gel (Thermo Fisher Scientific; EC62652BOX). Gel bands were separately excised as described: (a) 145–160 bp band (corresponding to adapter-ligated constructs derived from the 21 and 30 nt RNA fragments, respectively), (b) 160–180 bp band, (c) 180–200 bp band, (d) 200–300 bp band and (e) 300–500 bp band. This design permitted the inclusion of equimolar concentrations of RNAs of different sizes in the sequencing run in order to characterize the full set of RNAs injected into mice brains. However, deep

characterization was focused on the smaller fraction (sRNA <40 nt) because this is the size of sRNA generally related with a regulatory effect on gene expression.

Paired-end (2 × 50 bp, for CTL-sRNA-PT and HD-sRNA-PT samples) or single-end (1 × 50 bp, for CTL-sRNA-CTX, HD-sRNA-CTX, CTL-sRNA-CB, HD-sRNA-CB and mice samples) sequencing of indexed cDNA libraries were processed on a HiSeq 2500 platform (Illumina) using v4 SBS and Cluster Kits (Illumina; FC-401-4002). sRNA sequencing data are available at Gene Expression Omnibus with accession number GSE165667.

7.2 RNA sequencing of mice samples

For RNA sequencing of injected mice, total RNA was isolated from the striatum of the animals injected with HD-sRNA-PT, CTL-sRNA-PT, or vehicle solution and subsequently treated with a DNAse to prevent genomic DNA contamination, as described in sections 4.1 and 4.7, respectively. RNA integrity was assessed using a Bioanalyzer 2100 (Agilent Technologies) and samples presenting RIN > 8.5 were considered for further sequencing. TruSeq Stranded poly-A mRNA Library Prep (Illumina; 20020594) was used for indexed cDNA sequencing libraries preparation. Briefly, poly-A mRNA transcripts were captured from total RNA using poly-T beads and retrotranscribed into cDNA using random hexamer primers. Afterwards, paired-end sequencing (2 x 50 bp) of indexed cDNA libraries were carried out on a HiSeq 2500 platform (Illumina) using v4 SBS and Cluster Kits (Illumina; FC-401-4002). RNA sequencing data are available at Gene Expression Omnibus with accession number GSE165667.

7.3 PANDORA-sequencing of human samples

For human ssRNA-sequencing, a total of 100 ng of isolated ssRNA were obtained from the putamen of non-affected individuals and HD patients and pre-treated as detailed in sections 4.3 and 4.6, respectively, and then processed with NEBNext Small RNA Library Prep Set for Illumina (New England Biolabs; E7330S). Single-end sequencing (1 × 50 bp) of indexed cDNA libraries were processed on a NextSeq2000 platform (Illumina) using v4 SBS and Cluster Kits (Illumina; FC-401-4002).

8. Bioinformatic analysis

8.1 Quality control and adapter trimming

Coverage of the sequenced libraries was at least of 50 million reads per sample, except for PANDORAseq libraries that was ~ 10 million reads. Quality control of the sequenced fastq files was checked using Multiqc (Ewels et al., 2016) and FastQC softwares. Adapter trimming was performed using Cutadapt tool (M. Martin, 2011). In the case of RNAseq results, an estimation of ribosomal RNA in the raw data was obtained with riboPicker (Schmieder et al., 2012).

8.2 Alignment of reads and data analysis

For RNA-sequencing data, reads were aligned to the GENCODE release M14 of the mouse genome (version Ensemble GRHs38/hg38) using STAR aligner (version 2.7.9a; Dobin et al., 2013). Raw count of reads per gene were also obtained using STAR (–quantMode TranscriptomeSAM GeneCounts option).

For sRNA-sequencing data, trimmed reads were aligned to the human genome (version Ensemble hg19) or mouse genome (version Ensemble mm10) using STAR aligner (version 2.7.9a; Dobin et al., 2013). Sequencing reads that previously presented 3' adapters were annotated and quantified using the bcbio-nextgen smallRNA-seq pipeline, including Seqcluster (Pantano et al., 2011) and ExceRpt (NIH ExRNA Communication Consortium -ERCC-; Rozowsky et al., 2019) bioinformatic tools. Reads with no 3' adapters were processed through the bcbio-nextgen RNA-seq pipeline to measure RNA quality using qualimap (García-Alcalde et al., 2012) and to quantify gene expression of samples using sailfish (Patro et al., 2014). All software used for bioinformatic analyses are detailed in Table 13.

Softwares

Jultwares		
Resource	Source	Identifier
FastQC		http://www.bioinformatics.babraham.ac.uk/ projects/fastqc
Multiqc	Ewels et al., 2016	https://multiqc.info/
Qualimap	Garcia-Alcalde et al., 2012	http://qualimap.conesalab.org/
Cutadapt	Martin et al., 2011	https://doi.org/10.14806/ej.17.1.200
riboPicker	Schmieder et al., 2012	https://ribopicker.sourceforge.net/
STAR	Dobin et al., 2013	https://github.com/alexdobin/STAR
Seqbuster	Pantano et al., 2010	https://github.com/lpantano/seqbuster
Seqcluster	Pantano et al., 2011	https://github.com/lpantano/seqcluster
ExceRpt	Rozowsky et al., 2019	https://github.com/gersteinlab/exceRpt
Sailfish	Patro et al., 2014	http://www.cs.cmu.edu/~ckingsf/software/sailfish
DESeq2	Love et al., 2014	https://bioconductor.org/packages/DESeq2
R	R Core Team, 2017	https://www.r-project.org
DAVID	Huang et al., 2009	https://david.ncifcrf.gov/
MINTbase	Pliatsika et al., 2018	https://cm.jefferson.edu/MINTbase/
tsRBase	Zuo et al., 2021	http://www.tsrbase.org/

Table 13. List of the different resources used for bioinformatic analyses. Details of the source and the identifier are provided in each case.

Bcbio-nextgen smallRNA-seq pipeline was also used to detect human sRNA present in the brain of mice injected with vehicle (aCSF), CTL-sRNA-PT or HD-sRNA-PT. Sequencing reads that presented 3' adapters were mapped into the mouse (mm10) and the human (hg19) genomes using STAR aligner (Dobin et al., 2013). The number of mapped sequences in each genome was examined using statistics of the BAM files (aligned reads).

8.3 Downstream analysis of sequencing data

Differential gene expression

Prior to further analyses, genes were considered applying a threshold of a minimum of 2 raw counts in all samples tested while a cut-off of a minimum of 10 raw counts was used for sRNA read counts. Bioconductor package DESeq2 (Love et al., 2014) from R statistical software was used to assess differential expression analyses between experimental groups and only P values < 0.05 were considered. To control the False Discovery Rate, Benjamini-Hochberg correction of 0.05 % for multiple testing was applied. Gene ontology enrichment analyses of the differentially expressed genes (DEGs) were assessed using DAVID gene functional classification tool (D. W. Huang et al., 2009a, 2009b). The list of cell-type specific genes was obtained from previously published data (Merienne et al., 2019) and cell-type enrichment analysis was calculated using Chi-square test. Using the PANDORAseq strategy, pairwise comparison of differentially expressed (DE) sRNA among different ssRNA pre-treatments within the same sample was performed. All abovementioned bioinformatic resources used for sequencing analyses are also detailed in Table 13.

tsRNA annotation and analysis

SeqclusterViz tool was used to examine Seqcluster outputs allowing sRNA expression visualization along their precursors (Pantano et al., 2011). Specific tsRNA annotation was performed using MINTbase (Pliatsika et al., 2018) and tsRBase (Zuo et al., 2021) databases, generating unique identifiers for each of the transcripts based on the precursor tRNA isoacceptor mapped.

9. Statistical analysis

All data are presented as the mean \pm SEM and sample sizes are provided in the figure legends. Statistical analyses were performed using either Student's t-test, one- or two-way ANOVA test or linear mixed-effects model when technical replicates were considered (Steibel et al., 2009), followed by Bonferroni's post hoc test as appropriate and indicated in figure legends. A 95 % confidence interval was used and values of P < 0.05 were accepted as denoting statistical significance. Raw data was processed using Excel Microsoft Office and graphically represented using GraphPad Prism (v 8.0.2).

RESULTS

1. Study of the potential neurotoxic role of sRNA derived from HD patients' brains in vivo

1.1 Distribution of sRNA after their injection in the striatum of WT mice

To get insight into the sRNA transcriptome generated in the context of HD, purified fractions of sRNA (exclusively containing RNAs with less than 200 nt) were obtained from the putamen of control individuals (CTL-sRNA-PT) and HD patients (HD-sRNA-PT) (Figure 13A). Equivalent amounts of total RNA were mixed to obtain representative pools of CTL-RNA-PT (n= 10-14) and HD-RNA-PT (n= 11-14). Next, sRNA from each pool were purified in parallel using size exclusion columns. Validation of sRNA purification was performed using RNA electrophoresis, confirming the absence of RNAs with more than 200 nt in length in sRNA pools in comparison to total RNA pools in both conditions (Figure 13B).

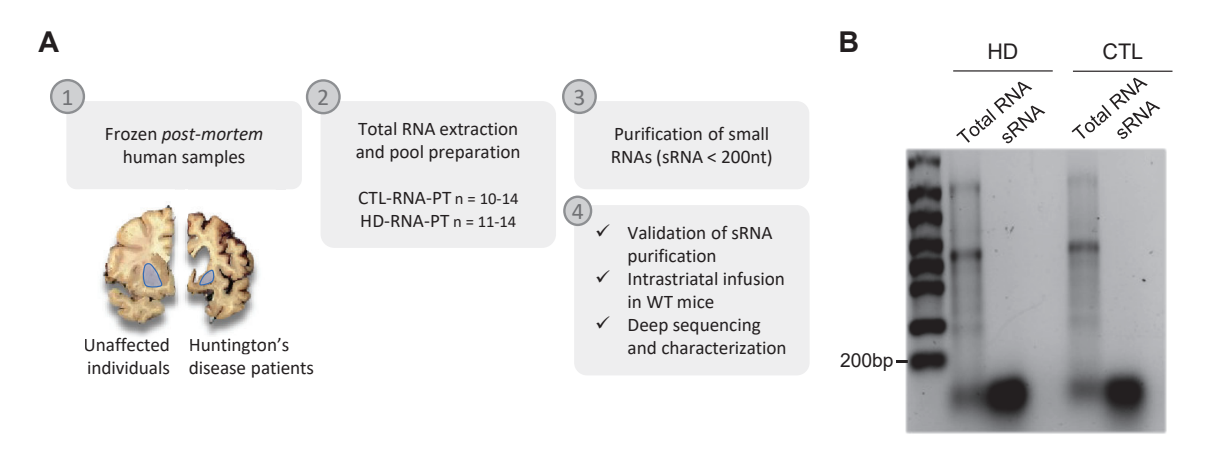


Figure 13. Overview of the experimental design and validation of sRNA purification. (A) Schematic diagram of the followed experimental plan. (B) Total RNA and column-purified sRNA obtained from the putamen of control individuals (CTL) or HD patients (HD) were size-separated by agarose gel electrophoresis for its visualization.

To investigate whether sRNA generated in the brain of HD patients could play a neurotoxic role *in vivo*, a mouse model was generated whereby sRNA purified from human brain tissue were intrastriatally injected. However, the correct location of bilateral cannula implantation and the capability of cells to incorporate human sRNA were first analyzed through an infusion of fluorescently labelled CTL-sRNAs (Cy3-sRNA) into the striatum of WT mice together with an evaluation of their localization after the infusion by fluorescence microscopy (Figure 14). Analysis of sRNA intracellular distribution were performed 30 min, 1 h, 24 h and 48 h after Cy3-sRNA infusions. However, the best fluorescent signal was detected at 30 min and 1 h time points, with similar results among these conditions.

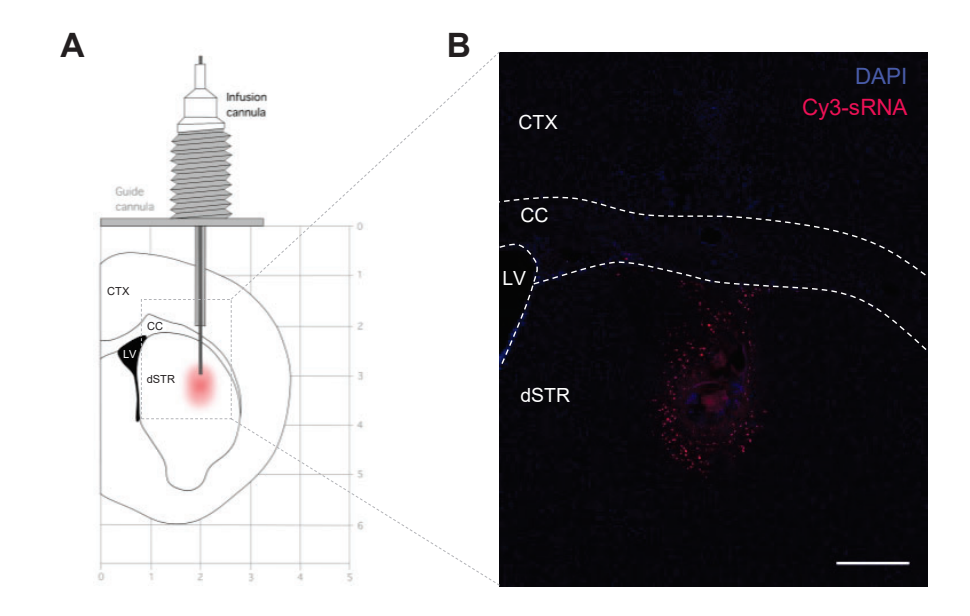
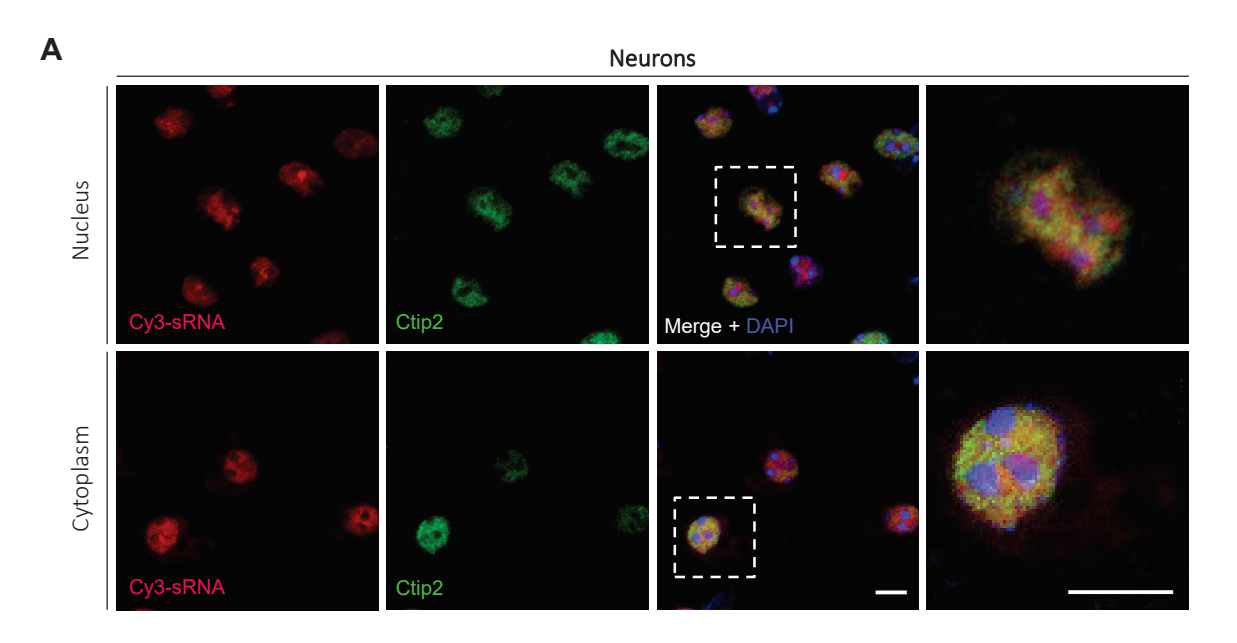


Figure 14. Intrastriatally injected Cy3-sRNA can be observed in the dorsal striatum of WT mice. (A) Schematic representation of the intrastriatal cannula positioned in the mouse brain. (B) Confocal image illustrating the specific labelling of Cy3-sRNA (in red) and cell nuclei (in blue) one hour after sRNA infusion using intrastriatal bilateral cannulas. Multiple brain areas are indicated: cortex (CTX), corpus callosum (CC), lateral ventricle (LV) and dorsal striatum (dSTR). Scale bar: 250 μm.

sRNA species were found to colocalize with Ctip2-positive cells indicating that MSNs, as the main neuronal population in the striatum, were able to incorporate these sRNA (Figure 15A). In addition, Iba1 staining revealed that microglial cells were also integrating Cy3-sRNA (Figure 15B). Interestingly, in both cases there was a preferential localization in the nucleus although Cy3-sRNA immunofluorescence signal was also detected in the cytoplasm of these cells.



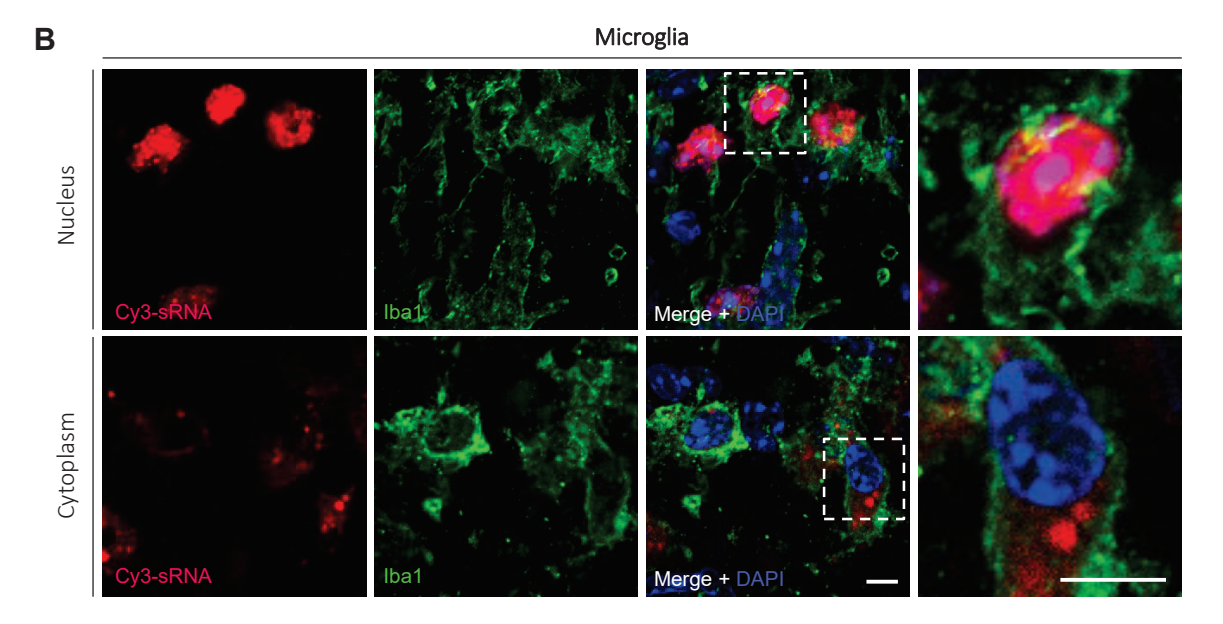


Figure 15. Cy3-sRNA are incorporated by neurons and microglia after intrastriatal injection. One hour after sRNA infusion into the dorsal striatum of WT mice, Cy3-sRNA distribution (in red) was visualized in striatal brain sections by immunohistofluorescence against the specific cell-type markers (A) Ctip2 or (B) Iba1 (in green), for MSNs and microglial cells, respectively. Cell nuclei are labelled in blue. Nuclear (top panel) and cytosolic (bottom panel) images of (A) MSNs and (B) microglial cells are shown. Panels on the right show a magnification of the boxed areas in white illustrating the appearance of Cy3-sRNA distribution in the double positive cells. Scale bar: 10 μ m.

In contrast, one-hour post-injection Cy3-sRNA were not incorporated by Sox9- and Olig2-positive cells, as markers of astrocytes and oligodendrocytes respectively (Figure 16). However, it is important to note that these results were observed one hour after Cy3-sRNA infusion and although there was an initial preference for neuronal and microglial cells, it could not be ruled out the incorporation of these sRNA by other cell types at later time points.

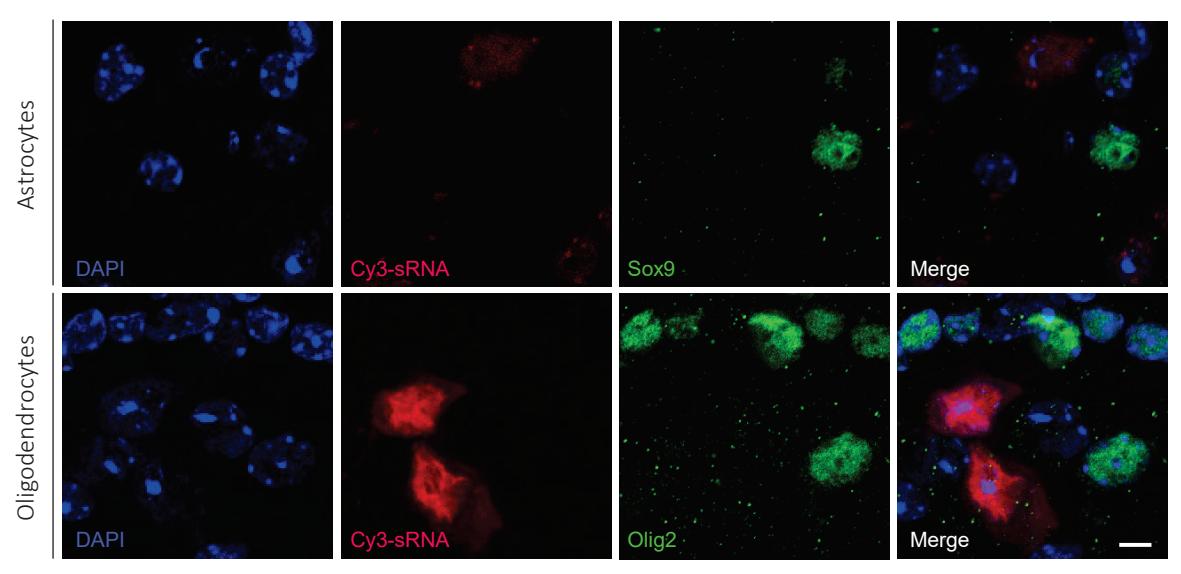


Figure 16. Cy3-sRNA do not colocalize with astrocytes nor oligodendrocytes one hour after

RESULTS

intrastriatal injection. Confocal representative images of immunohistofluoresces in striatal brain slices of Cy3-sRNA-injected mice against Sox9 and Olig2 (in green), as astrocyte and oligodendrocyte specific cell-type markers respectively. Cell nuclei are labelled in blue. Scale bar: $10~\mu m$.

In order to determine whether Cy3-sRNA were incorporated by striatal GABAergic or cholinergic interneurons, immunohistofluorescences against different markers for these cell-types were performed. No colocalization of Cy3-sRNA with NPY-, PARV- nor ChAT-positive cells was detected (Figure 17). Therefore, these findings indicated that exogenous sRNA species were preferentially incorporated and integrated by striatal MSNs and microglia, at least in the evaluated conditions.

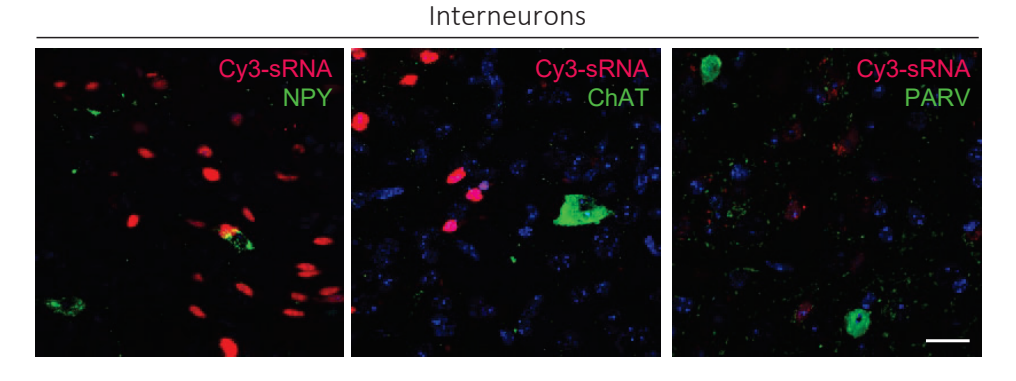


Figure 17. Cy3-sRNA do not colocalize with striatal interneurons one hour after intrastriatal injection. Representative images of immunohistofluorescences against NPY, ChAT and PARV (in green) interneuron markers in striatal brain slices of Cy3-sRNA-injected mice (in red). Cell nuclei are labelled in blue. Scale bar: 15 μm.

To further evaluate whether differential distributions were dependent on the source of the sRNA, intrastriatal infusions were performed using Cy3-labelled sRNA obtained from the putamen of non-affected individuals (Cy3-CTL-sRNA-PT) and HD patients (Cy3-HD-sRNA-PT) and localization studies were carried out one hour later. This experiment showed that the percentage of MSNs incorporating sRNA was significatively increased when these were obtained from HD patients (Cy3-HDsRNA-PT) compared to Cy3-CTL-sRNA-PT (Figure 18A and G). In contrast, Ctip2negative cells, namely interneurons and glial cells of the striatum, did not exhibit a preference among sRNA sources (Figure 18A). When only considering Ctip2positive cells, we could confirm the increased proportion of MSNs incorporating sRNA whenever they were produced in the HD brain (Figure 18B). In addition, a higher intensity of Cy3-sRNA was also detected within Ctip2-positive cells when injecting Cy3-HD-sRNA-PT in comparison to Cy3-CTL-sRNA-PT infusions (Figure 18C). To validate that these results were a consequence of sRNA produced in the HD context, we intrastriatally injected sRNA isolated from another brain region, namely the cortex, of both control subjects and HD patients. Hence, we observed analogous results to the ones obtained using putamen-derived sRNA (Figure 18D-G).

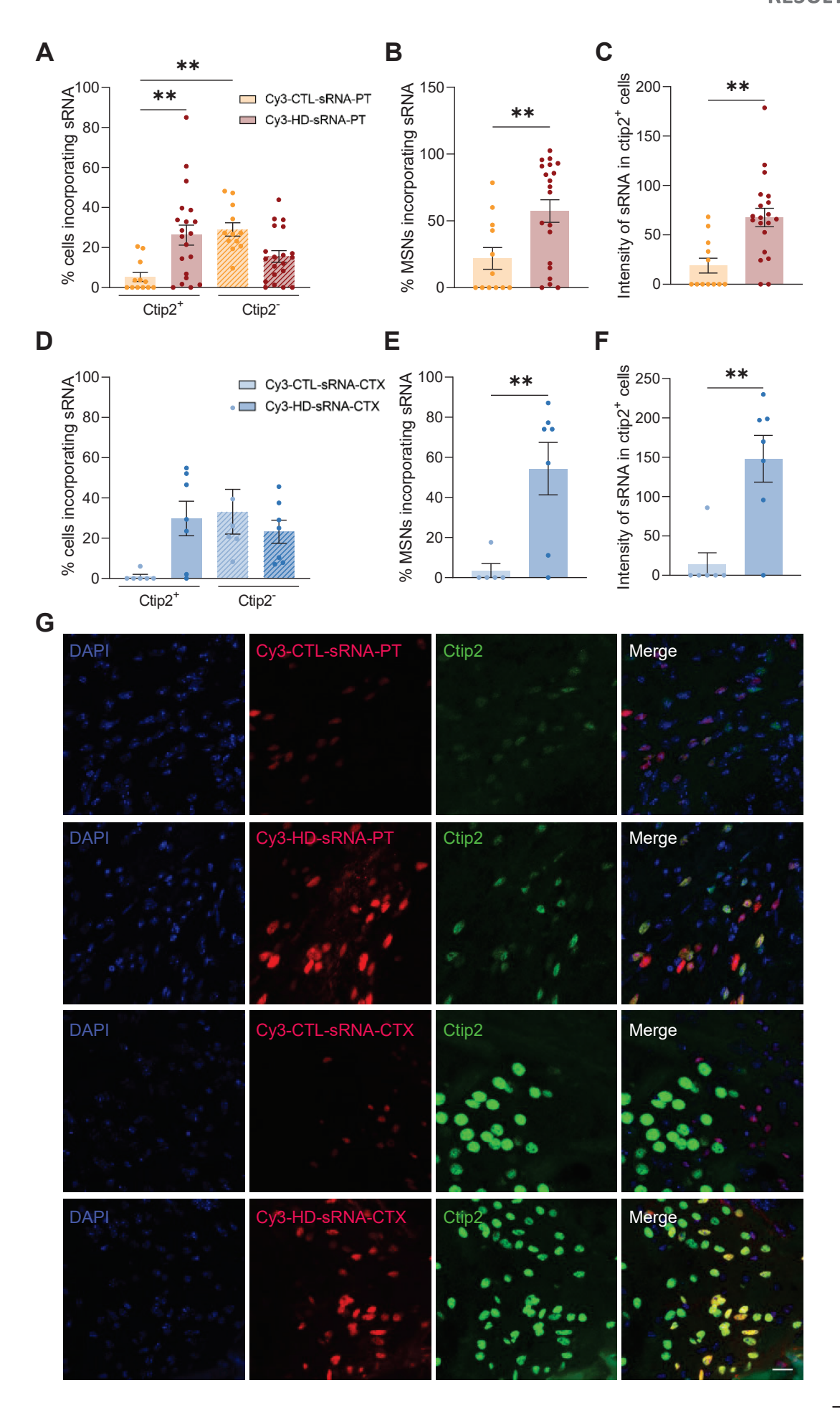


Figure 18. MSNs preferentially incorporate HD-sRNA-PT, while other cell types do not show any preference. (A,D) Graphs showing the proportion of sRNA-positive cells in Cy3-sRNA-injected striata considering all cellular nuclei. (B,E) Graphs showing the proportion of double-labelled cells for Ctip2 and sRNA in relation to the total population of Ctip2-positive cells. (C,F) Quantifications of Cy3-sRNA mean intensities in Ctip2-positive cells located in the striatum of injected mice. In (A-F), each point represents data from an independent field and values are shown as mean \pm SEM. **P < 0.01 versus the indicated groups; calculated by one-way ANOVA followed by Bonferroni *post hoc* test in (A,D) and two-tailed unpaired Student's t-test in (B,C,E,F). (G) Representative images of Ctip2 (in green) immunohistofluorescence in the striatum of Cy3-sRNA-injected animals. Cy3-sRNA-PT and Cy3-sRNA-CTX obtained from non-affected subjects (CTL) or HD patients are labelled in red and cell nuclei in blue. Scale bar: 15 µm.

1.2 Intrastriatal injection of HD-sRNA-PT alters motor function in WT mice

On the basis that previous studies in the field have described a strong sRNA expression dysregulation in the putamen of HD patients (Martí et al., 2010) and on the fact that alterations of motor coordination present in HD patients have also been linked with the dysfunction, or even loss, of striatal MSNs (Vonsattel & DiFiglia, 1998), we sought to unravel whether HD-sRNA-PT could be participating in this process and, in turn, compromise motor behavior. To explore this hypothesis, vehicle (aCSF), CTL-sRNA-PT or HD-sRNA-PT were bilaterally injected into the striatum of WT mice, twice a week for two weeks. Then, mice were assessed weekly by using the rotarod and the balance beam tests known to be sensitive to motor abnormalities and balance alterations, respectively (Figure 19A). We observed that HD-sRNA-PT-injected mice showed significant motor alterations in both tasks in comparison with CTL-sRNA-PT- or vehicle-injected mice. It is important to note that motor perturbations in the rotarod test were already detected after the two first injections and worsened with the two subsequent ones in all the speeds evaluated (Figure 19B). To further confirm that infusion itself was not responsible for changes in the behavior of animals in the rotarod, all mice were infused with vehicle solution prior to sRNA infusions and no alterations in their performance in the rotarod test were observed (Figure 19B).

In parallel, the balance beam test revealed coordination and balance impairments in HD-sRNA-PT-injected mice shown by significant alterations in the number of slips per frame (Figure 19C). Remarkably, CTL-sRNA-PT-injected mice performed similarly to mice injected with vehicle, confirming that CTL-sRNA-PT have no adverse effects on motor function. In addition, no significant changes in mice body weight were detected under any treatment or procedure throughout all the study confirming the suitability of the executed experimental design and the fact that exerted motor abnormalities were not due to a general poor condition of the animals (Figure 19D). Altogether, these results suggest that intrastriatal injection of sRNA derived from the putamen of HD patients alter motor function in WT mice.

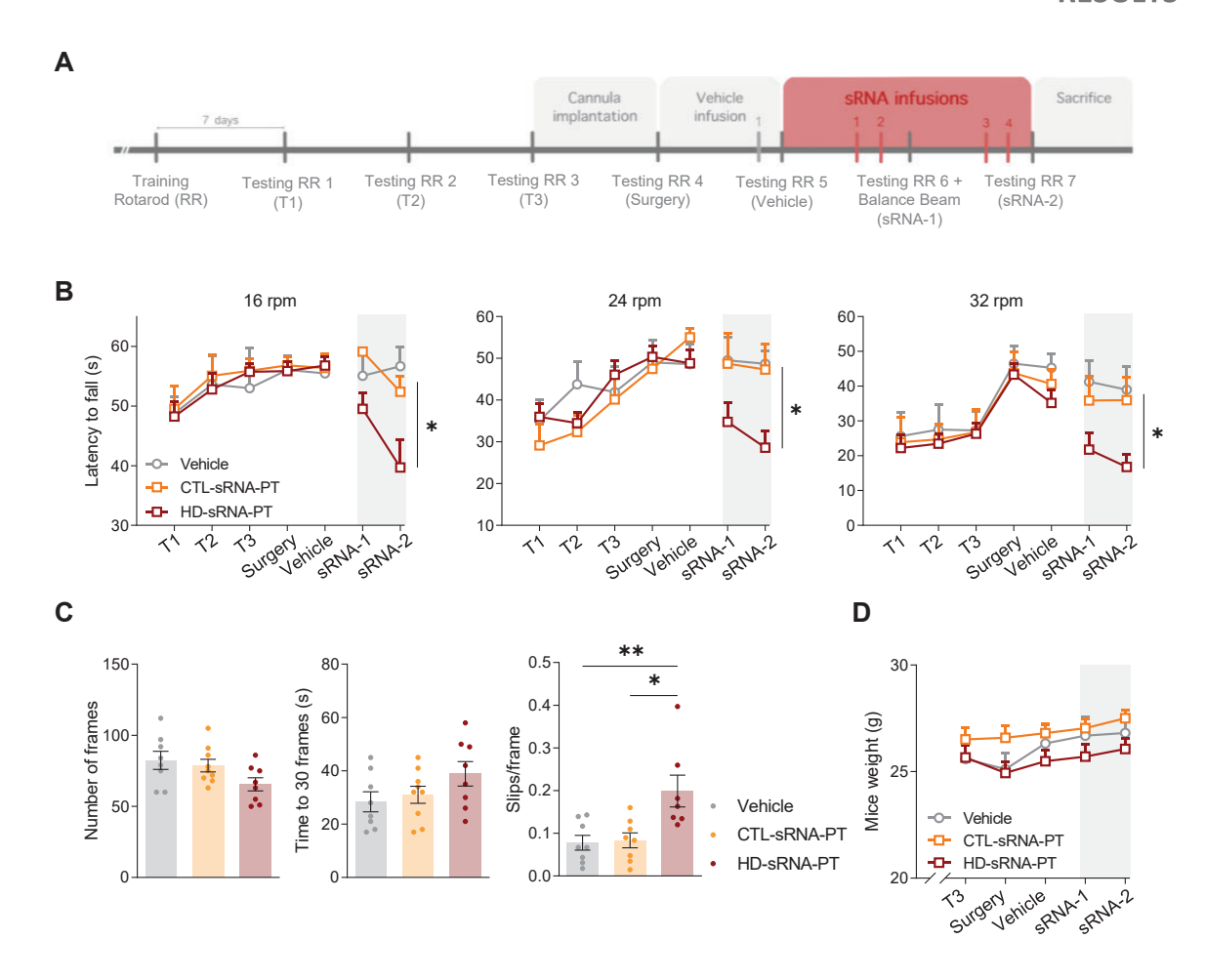


Figure 19. Intrastriatal injection of HD-sRNA-PT alters motor behavior in WT mice. (A) Timeline of the followed experimental procedure including intrastriatal infusions of vehicle and sRNA (CTL-sRNA or HD-sRNA) in freely moving mice together with their behavioral phenotyping. Fixed rotarod test was performed every week whereas the balance beam test was only conducted after the first week of sRNA infusions. Animals received four sRNA infusions in total and were sacrificed 48 h after the fourth infusion. (B) Motor performance was evaluated in the rotarod test at 16, 24 and 32 rpm. Vehicle n = 8; CTL-sRNA-PT n = 16; HD-sRNA-PT n = 16. Graphs show the latency to fall at each speed as mean \pm SEM. *P < 0.05 versus all other groups; calculated by two-way ANOVA followed by Bonferroni post hoc test. (C) Total number of crossed frames, time to traverse 30 frames and number of slips were registered in the balance beam test. Vehicle n = 8; CTL-sRNA-PT n = 8-9; HD-sRNA-PT n = 7-8. Each point represents data from an individual mouse. Data are shown as mean ± SEM. **P < 0.01, *P < 0.05 versus the indicated groups; calculated by one-way ANOVA followed by Bonferroni post hoc test. (D) Mice body weight was controlled throughout all the experimental procedure. Vehicle n = 8; CTL-sRNA-PT n = 19; HD-sRNA-PT n = 18. Graphs show animal weight as mean ± SEM.

1.3 HD-sRNA-PT induce selective gene expression alterations in WT mice striatum concordant with an HD-associated transcriptional signature

An early feature displayed in HD that contributes to the neuropathology is the transcriptional dysregulation affecting a variety of cellular processes, leading to alterations in neuronal function and survival (Heinz et al., 2021; Kumar et al., 2014; Zuccato et al., 2010). These gene expression abnormalities have been found across multiple HD models in parallel to human patients associated to CAG repeat length and dependent on the brain region (Langfelder et al., 2016).

To get insight into the pathways underlying the detrimental effects observed after HD-sRNA-PT injection, RNA-sequencing analysis was performed to examine overall gene expression profiles in the striatum of injected animals. Specifically, mice treated with vehicle, CTL-sRNA-PT or HD-sRNA-PT were sacrificed 48 h after the last infusion, when motor alterations were obvious, and striatal tissue was processed for sequencing.

Prior to further analyses, we first sought to validate the presence of sRNA with human origin in the injected striata. The proportion of sRNA mouse reads that mapped onto the human genome was a 6-10% higher in animals injected with human sRNA (CTL-sRNA-PT or HD-sRNA-PT, respectively) than in animals injected with vehicle solution (Table 14), confirming the presence of human specific sRNA in mice striata. As an additional control, the fraction of sRNA mouse reads mapping onto mouse genome was examined and over a 96% of alignment was achieved in all cases.

	Vehicle	CTL-sRNA-PT	HD-sRNA-PT
Fraction mapping onto human genome	0.7827	0.8427	0.8832
Fraction mapping onto mouse genome	0.9646	0.9771	0.9859

Table 14. Fractions of sRNA obtained from the striatum of injected animals mapping onto the different genomes.

Further differential enrichment analysis of RNA sequencing results showed a total of 1846 upregulated genes and 1358 downregulated genes in HD-sRNA-PT- versus vehicle-injected mice (n= 8 animals per group), using an adjusted P < 0.05 and a fold change > 1.5 or < 1.5 as a screening threshold (Figure 20A). Moreover, these differentially expressed genes (DEGs) were not significantly dysregulated when comparing CTL-sRNA-PT- versus vehicle-injected mice (n= 8 animals per group, adjusted P > 0.05) (Figure 20B).

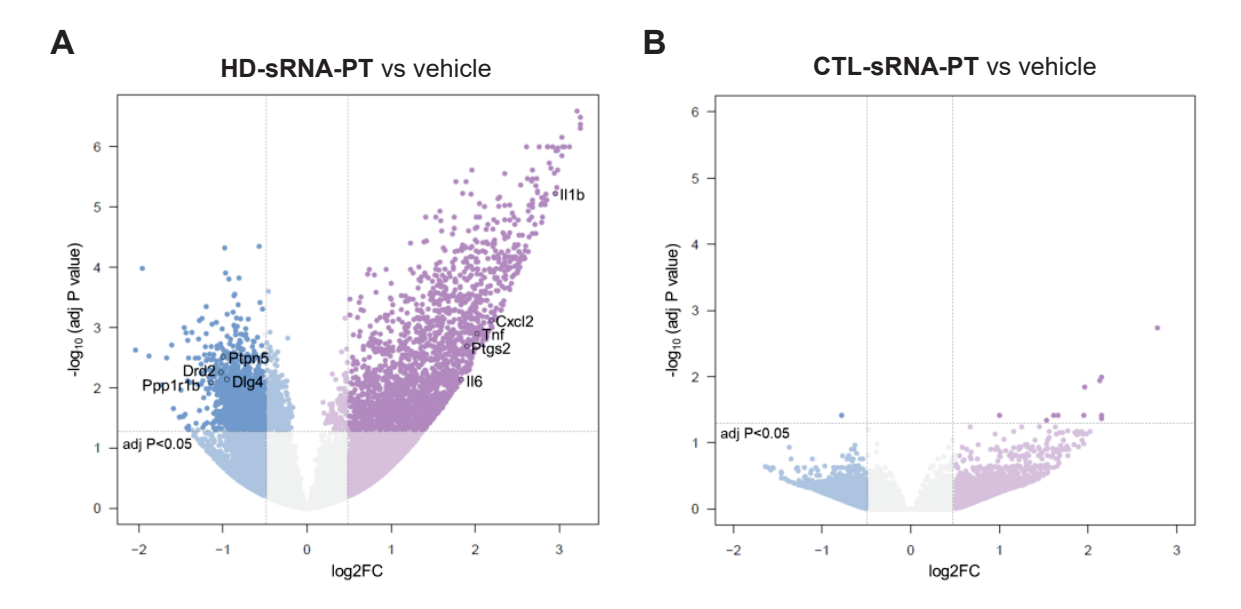


Figure 20. Intrastriatal HD-sRNA-PT injections induce transcriptional abnormalities in the striatum of WT animals. Volcano plots of the DEGs 48 h after the last infusion between (A) HD-sRNA-PT- and vehicle-injected mice and between (B) CTL-sRNA-PT- and vehicle-injected animals. Dark purple dots highlight the significantly upregulated genes (log2 fold change > 0.58 and adjusted P < 0.05) while dark blue dots illustrate the downregulated genes (log2 fold change < 0.58 and adjusted P < 0.05). Dots representing selected genes are labelled. FC: fold change.

Next, we explored whether the dysregulated transcriptome present in injected striata was associated to distinct functional signatures. Hence, David functional annotation tool (D. W. Huang et al., 2009b, 2009a) was used to identify specifically enriched gene groups among the DEGs between HD-sRNA-PT- and vehicle-injected mice. Functional annotation of the downregulated DEGs revealed an enrichment for the gene ontology (GO) biological process terms linked to neuronal pathways (Figure 21A; see Annex for Supplementary Table 1 and 2). In contrast, upregulated genes showed a clear association with immune system and inflammatory response terms (Figure 21B; see Annex for Supplementary Table 3 and 4). It is important to note that these results are in line with the transcriptional signatures that have been previously described in different HD models (Han et al., 2010; Langfelder et al., 2016; Merienne et al., 2019; Sapp et al., 2001).

Notably, the enrichment of immune response-related genes was the only pathway significantly altered when comparing the DEGs of HD-sRNA-PT versus CTL-sRNA-PT conditions (adjusted P < 0.05; see Annex for Supplementary Table 5 and 6), suggesting that these are the genes more consistently dysregulated by HD-sRNA-PT infusions. Further analysis of these DEGs revealed an aberrant interferon (INF) signaling resulting in the upregulation of multiple interferon-stimulated genes (ISGs), namely *Isg15*, *Usp18*, *Cxcl10*, among others, in the striatum of HD-sRNA-PT-injected mice (Figure 21C).

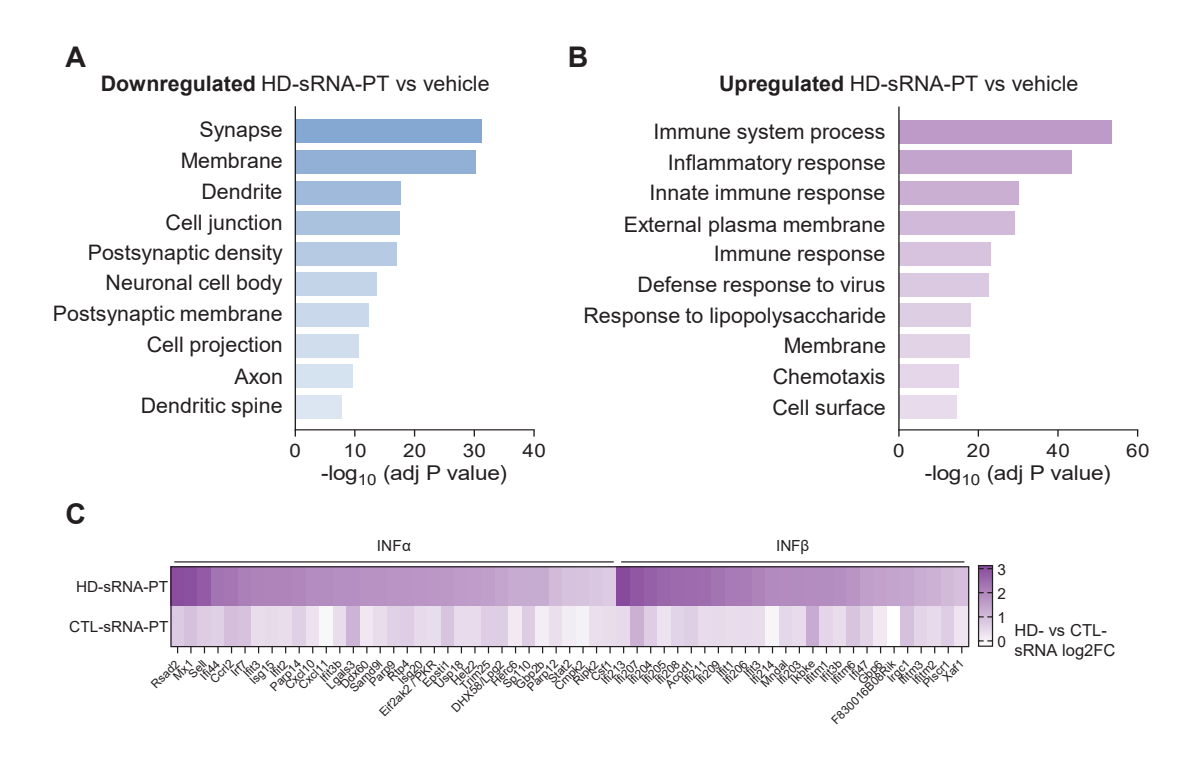


Figure 21. Intrastriatal injections of HD-sRNA-PT lead to transcriptional alterations resembling the HD-associated transcriptome. Bar plots showing -log10 values (adjusted P) of representative GO biological processes associated with (A) downregulated and (B) upregulated DEGs when comparing HD-sRNA-PT versus vehicle-injected mice. (C) Heatmap representing the log2 fold changes of multiple genes related to INF response pathways, both INF α and INF β , between HD- and CTL-sRNA-PT-injected mice. FC: fold change.

Due to the fact that both neuronal and glial cells have been implicated in different aspects of the pathophysiology of HD, it was important to unravel the specific contribution of each cell type (Allaman et al., 2011). Therefore, we took advantage of cell-type-specific gene expression profiles from adult mouse striatum published in the bibliography (Merienne et al., 2019) to determine whether specific cell types were affected. Intersection of these data with the previously identified HD-sRNA-PT upregulated and downregulated DEGs confirmed highly selective cell-type signatures. In particular, we identified up to a 17.6% of the downregulated DEGs specifically overlapping with neuronal genes together with a 18.1% of the upregulated DEGs specifically overlapping with glial genes (Figure 22A). Significantly downregulated transcripts in HD-sRNA-PT-injected striatum were specific genes from the subpopulation of MSNs expressing the dopamine D2 receptor (D2-MSNs; P value = 2.2e-15; Figure 22B and C), being the first population to degenerate in HD (Bergonzoni et al., 2021; Y. P. Deng et al., 2004; Reiner et al., 1988; Sapp et al., 1995). In contrast, the upregulated genes corresponded to glialspecific genes, with a special enrichment in microglial-related transcripts (P value < 2e-20; Figure 22B and D).

Altogether, these findings suggest that HD-sRNA-PT are contributing to specific neuronal subpopulation loss and microglial activation, both well-defined hallmarks present in the putamen of HD patients (Crotti & Glass, 2015; Gerfen, 1988; Sapp et al., 2001; Vonsattel et al., 1985).

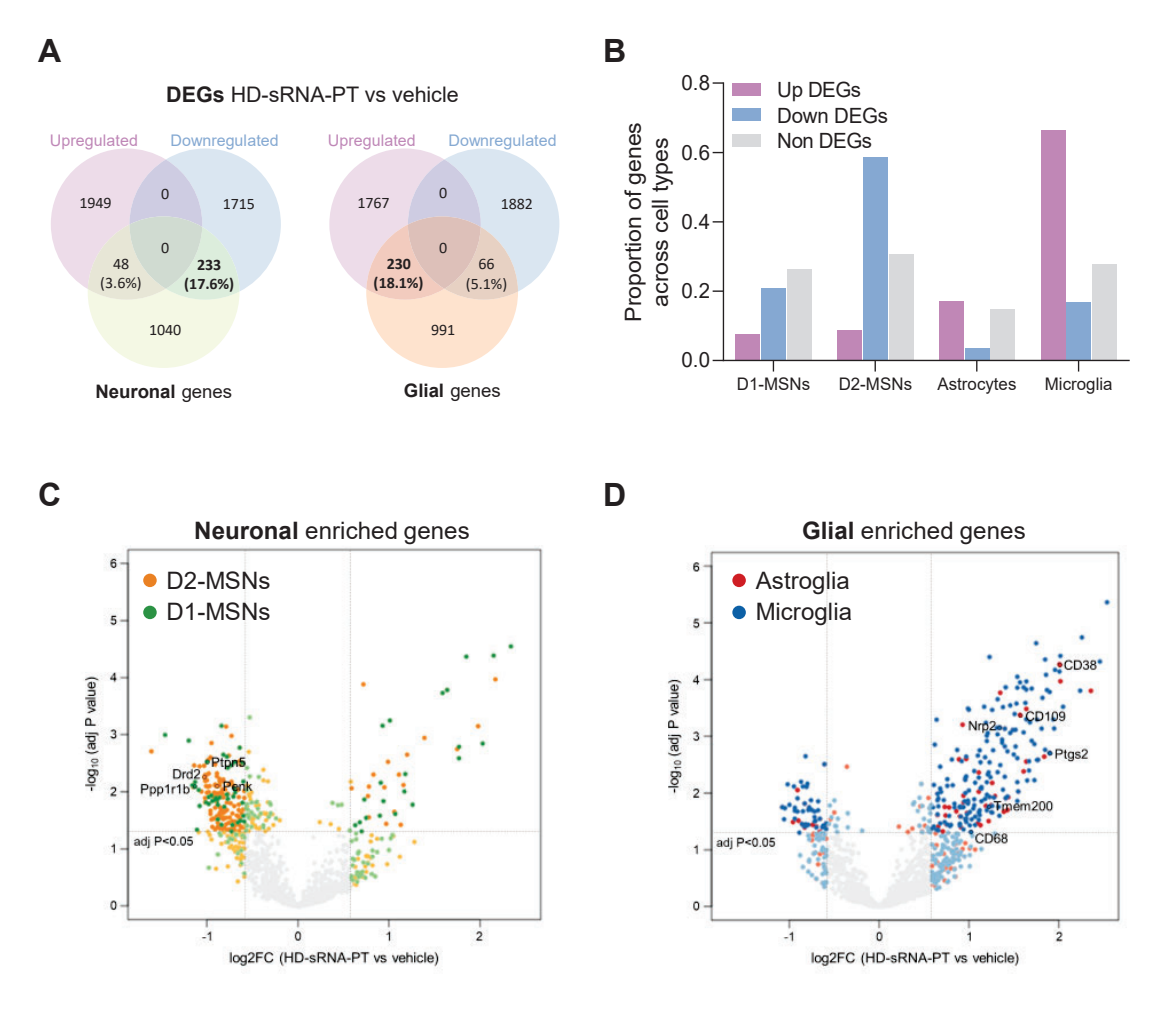


Figure 22. Transcriptional dysregulation associated to HD-sRNA-PT injections is cell-type specific. (A) Venn diagrams showing the overlap between neuronal and glial genes with the detected DEGs. (B) Bar plot showing the proportion of upregulated DEGs, downregulated DEGs and non-differentially expressed genes overlapping with each cell-type specific cluster of genes. (C-D) Volcano plots showing the (C) neuronal-enriched and (D) glial-enriched DEGs among all differentially expressed genes, 48 h after the last infusion between HD-sRNA-PT-and vehicle-injected mice. In (C), green dots represent genes corresponding to D1-MSNs, orange dots represent genes corresponding to D2-MSNs and grey dots represent non-differential expressed genes. In (D), red dots represent genes belonging to astroglia, blue dots represent genes belonging to microglia and grey dots represent non-differential expressed genes. Differential enrichment of cell-type specific genes was calculated using a Chi-square test. Screening threshold: fold change > 1.5 or < 1.5 (log2 fold change > 0.58 or < 0.58) and adjusted P < 0.05 in dark colors. FC: fold change.

Considering the obtained results, we were interested in evaluating how HD-sRNA-PT signature resembles the HD-associated transcriptome. To assess this, we compared our DEGs with existing transcriptomic datasets from both the putamen

of HD patients (Durrenberger et al., 2015; Hodges et al., 2006) and the striatum of a KI HD mouse model (Langfelder et al., 2016). Analogous DEGs expression patterns were found in all cases, showing a significant overlap in the dysregulated genes (Figure 23A and B) and suggesting that HD-sRNA-PT *per se* are able to recapitulate comparable transcriptomic alterations to those observed along HD pathogenesis.

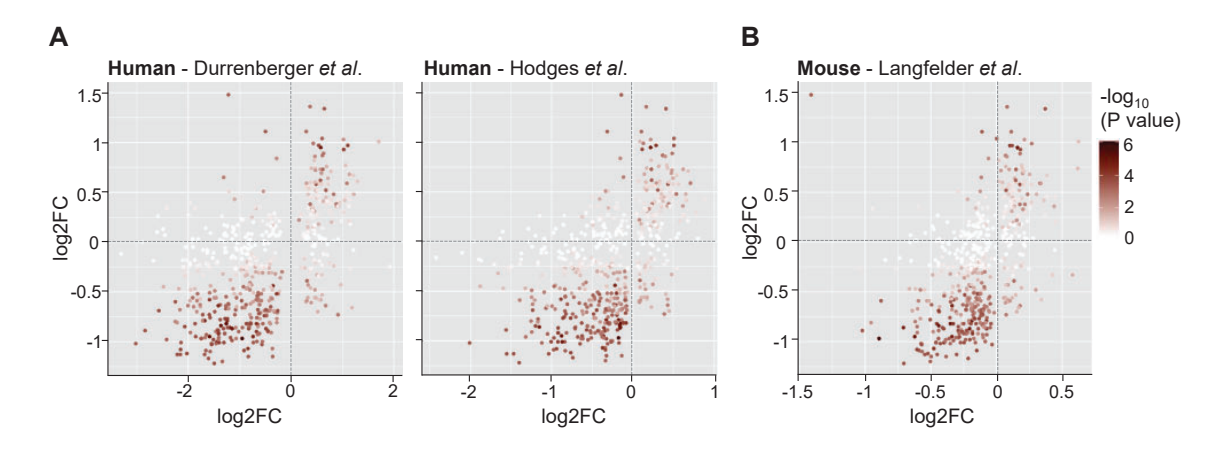
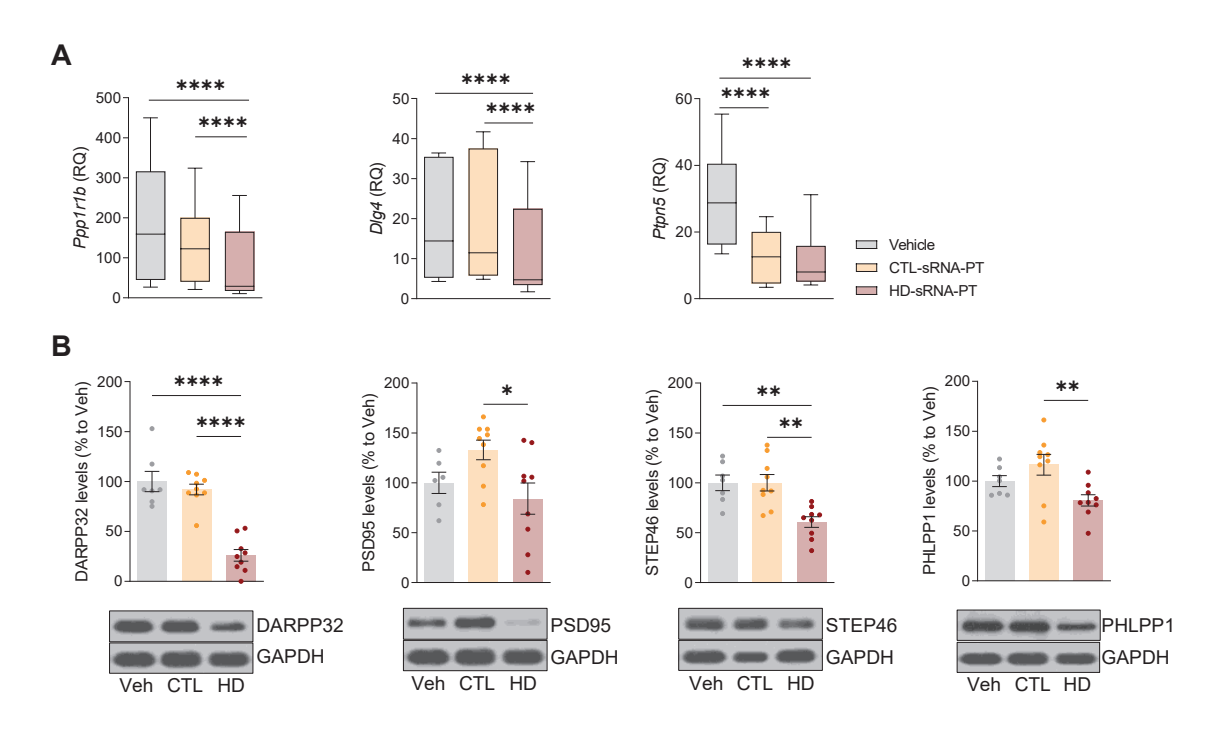


Figure 23. HD-sRNA-PT injections induce analogous transcriptomic alterations to those described in HD context. (A) Correlation of the DEGs between HD-sRNA-PT versus vehicle-injected mice and the DEGs found within the putamen in two independent HD human transcriptomic datasets. **(B)** Correlation of the DEGs between HD-sRNA-PT versus vehicle-injected mice and the striatal DEGs described in a HD mouse model transcriptomic dataset.

1.4 HD-sRNA-PT induces specific neuronal degeneration in WT mice striatum

Based on the described transcriptomic alterations, we asked whether the downregulation in neuronal markers could be validated by qPCR and whether it was paralleled by perturbations at the protein level. Therefore, we examined the expression levels of multiple neuronal markers characteristically decreased in the striatum of HD: DARPP32 (*Ppp1r1b* gene; Bibb et al., 2000; Van Dellen et al., 2000), PSD95 (*Dlg4* gene; Fourie et al., 2014; Torres-Peraza et al., 2008), STEP46 (*Ptpn5* gene; Desplats et al., 2006; Luthi-Carter et al., 2000; Saavedra et al., 2011) and PHLPP1 (Rué et al., 2016; Saavedra et al., 2010). While mRNA expression levels of DARPP32 and PSD95 were significantly decreased in the striatum of HD-sRNA-PT-injected mice in comparison to animals injected with vehicle or CTL-sRNA-PT, STEP46 showed a reduction in its expression both in CTL-sRNA-PT and HD-sRNA-PT-injected mice (Figure 24A). However, a decrease in protein levels was observed in HD-sRNA-PT-injected animals for all the striatal markers analyzed compared to control conditions (Figure 24B).



As it has been mentioned, HD is characterized by a specific loss of striatal neurons, an important hallmark that is poorly recapitulated by HD mouse models (Ferrante, 2009; Naver et al., 2003). To assess whether HD-sRNA-PT could have an impact on cell viability, we performed a morphometric analysis of MSNs present in the striatum of injected mice. Nissl staining and DARPP32 immunohistochemistry revealed a reduction in the number of Nissl-positive neuronal cells and DARPP-32-positive cells in striatal brain slices of HD-sRNA-PT-injected mice in comparison to vehicle- and CTL-sRNA-PT-injected animals (Figure 25A-D), which was in line with a significant increase of cleaved caspase-3-positive nuclei in the same animals (Figure 25E-F).

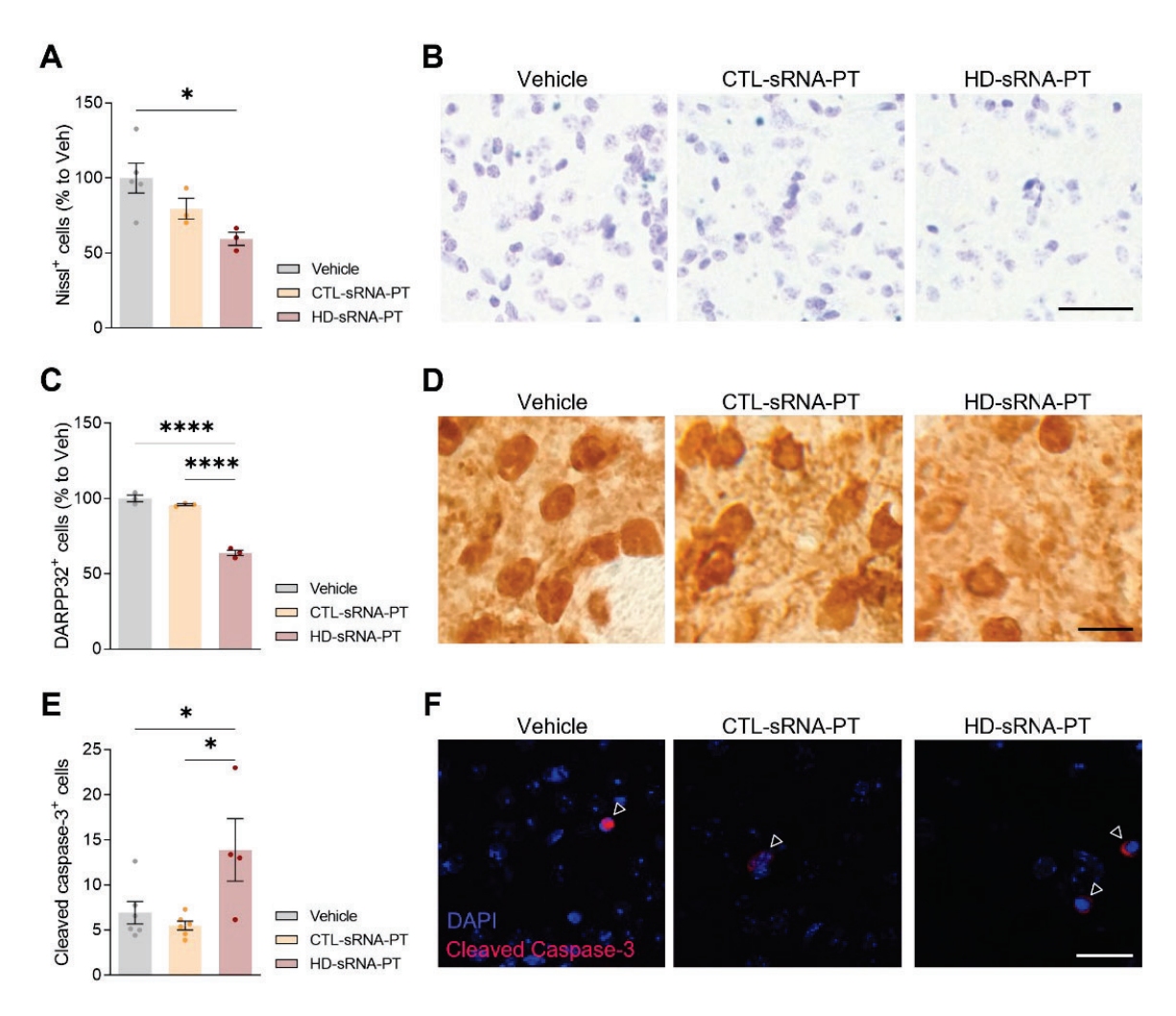


Figure 25. HD-sRNA-PT intrastriatal injection induces neuronal loss in the striatum of WT mice. (A) Quantification of the number of neurons using Nissl staining in the striatum of injected mice. Vehicle n = 5; CTL-sRNA-PT n = 3; HD-sRNA-PT n = 3. (B) Representative images of NissI staining in the striatum of injected mice. Scale bar: 20 μm. (C) Quantification of DARPP32-positive cells in the striatum of injected mice. Vehicle n = 3; CTL-sRNA-PT n = 3; HD-sRNA-PT n = 3. In (A) and (C), values are expressed as percentage to vehicle-injected animals, shown as mean ± SEM and each point represents an individual mouse. *P < 0.05 and ****P < 0.0001 versus the indicated groups; calculated by one-way ANOVA followed by Bonferroni post hoc test. (D) Representative images of DARPP-32 immunostained MSNs in the striatum of injected mice. Scale bar: 20 µm. (E) Quantification of the number of cleaved caspase-3-positive cells in the striatum of injected mice. Vehicle n = 6; CTL-sRNA-PT n = 6; HD-sRNA-PT n = 4. Each point represents data from an individual mouse. Data are shown as mean ± SEM. *P < 0.05 versus the indicated groups; calculated by one-way ANOVA followed by Bonferroni post hoc test. (F) Representative images of cleaved caspase-3 immunostained coronal striatal sections of injected mice. Cleaved caspase-3 is shown in red and DAPI in blue. Arrowheads indicate examples of cleaved caspase-3-positive cells. Scale bar: 25 μm.

In line with the transcriptomic analysis results showing an important reduction of D2-MSNs-specific genes (Figure 22), we evaluated the protein levels of different markers classically related to the indirect and direct pathways of striatal MSNs. The protein levels of the indirect pathway markers, DRD2 and ENK, were significantly

decreased in HD-sRNA-PT-injected animals in comparison with the other treatments (Figure 26A). In contrast, we could not detect any alterations in DRD1 protein levels with the different treatments, as a specific marker of the direct pathway of striatal MSNs.

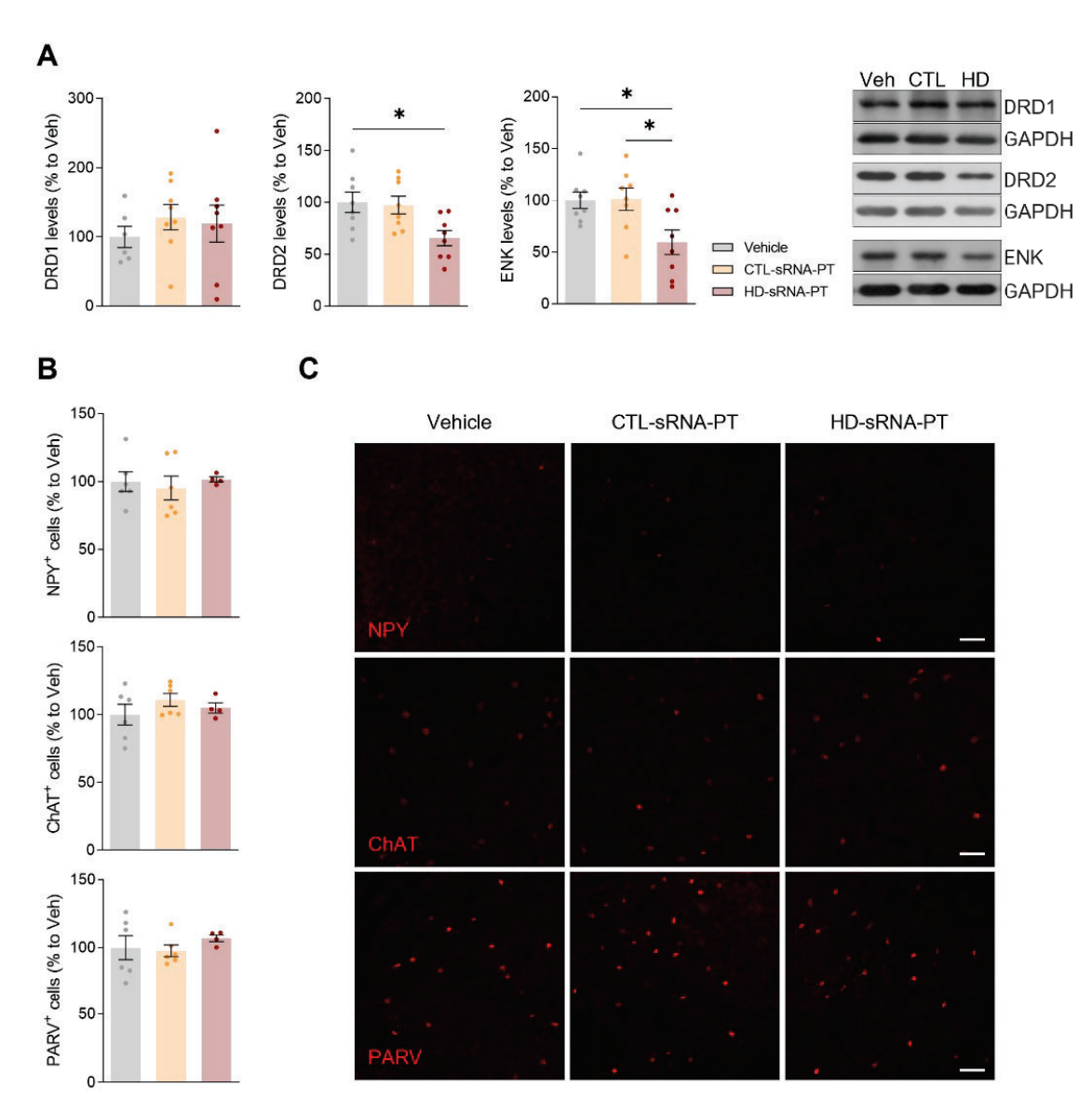


Figure 26. Intrastriatal injection of HD-sRNA-PT selectively affects the indirect pathway of the basal ganglia. (A) Protein levels of DRD1, DRD2 and ENK were analyzed by WB in striatal lysates from injected animals. GAPDH was used as a loading control. Representative immunoblots are shown. Vehicle n = 6-8; CTL-sRNA-PT n = 8; HD-sRNA-PT n = 8. Each point represents data from an individual mouse. Values are expressed as percentage to vehicle-injected animals and shown as mean \pm SEM. *P < 0.05 versus the indicated groups; calculated by one-way ANOVA followed by Bonferroni *post hoc* test. (B) Quantification of the total number of NPY-, ChAT- and PARV-positive cells in the striatum of injected mice. Vehicle n = 6; CTL-sRNA-PT n = 6; HD-sRNA-PT n = 4. Each point represents data from an individual mouse. Values are expressed as percentage to vehicle-injected animals and shown as mean \pm SEM. (C) Representative images of NPY, ChAT and PARV immunostained striatal interneurons in coronal brain sections of injected mice. Scale bar: 50 μ m.

Although MSNs are the principal neuronal population in the striatum, GABAergic and cholinergic interneurons are also present in this brain region (Ferrante et al., 1987; Zuccato et al., 2010). Therefore, morphological analyses by immunohistofluorescence of GABAergic interneurons expressing NPY or PARV markers and cholinergic interneurons expressing ChAT were performed. No obvious differences in the number of NPY-, PARV- and ChAT-positive cells were detected in the striatum of the HD-sRNA-PT treated animals (Figure 26B and C). These results support the idea that HD-sRNA-PT may not have a broad deleterious effect since only minor alterations were detected in the less affected cell types by disease progression, namely striatal interneurons (Rikani et al., 2014).

Consistently with HD-sRNA-PT-related transcriptomic perturbations, all these findings suggest that HD-sRNA-PT could compromise neuronal functionality and viability *in vivo*, specially suggesting a deleterious effect on the indirect pathway of the basal ganglia (D2-MSNs), which is the striatal neuronal population primarily affected throughout HD progression (Bergonzoni et al., 2021; Han et al., 2010).

1.5 HD-sRNA-PT induces striatal inflammation in WT mice

To further confirm the upregulation of inflammatory and immune-related genes observed by RNA-sequencing, we validated multiple top dysregulated inflammation markers by RT-qPCR. *Cxcl2*, *Tnf*, *Il6*, *Il1b* and *Ptgs2* expression levels were increased in the striatum of HD-sRNA-PT-injected mice in comparison to vehicle- and CTL-sRNA-PT-injected animals (Figure 27A and B). These findings pointed sRNA as contributors to the abnormal immune activation reported in the HD brain (Pavese et al., 2006; Tai et al., 2007).

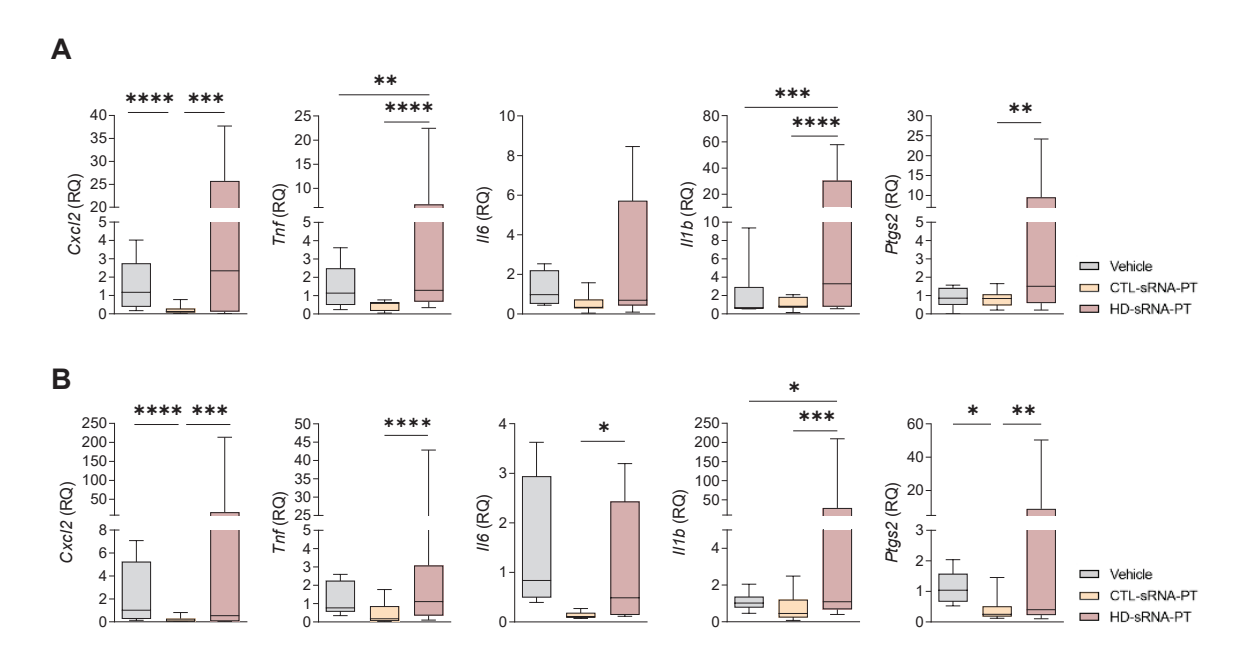


Figure 27. HD-sRNA-PT intrastriatal injection induces inflammation in the striatum of WT mice. Expression levels of *Cxcl2*, *Tnf*, *ll6*, *ll1b* and *Ptgs2* in the striatum of injected animals

were determined by RT-qPCR using TaqMan technology. **(A)** *Actin* and **(B)** *Hprt* were used as reference genes. Relative quantification (RQ) was calculated with the $2\Delta\Delta$ Ct method. Vehicle n = 6; CTL-sRNA-PT n = 8; HD-sRNA-PT n = 8. Boxplots show medians (horizontal lines), 25^{th} to 75^{th} percentiles (boxes) and minimum to maximum (whiskers). ****P < 0.0001, ***P < 0.001, **P < 0.01, *P < 0.05 versus all other groups; calculated using a linear mixed-effects model followed by Bonferroni *post hoc* test.

In an attempt to unravel whether inflammation was an early event during the neurotoxicity observed, we performed a single injection of HD-sRNA-PT in the striatum of WT mice and 24 h later, we analyzed a set of inflammation and neuronal markers previously found to be dysregulated in the striatum of the animals that underwent the experimental design described in Figure 19A. Hence, 24 h after an intrastriatal injection, we detected an increase in the expression levels of *II1b* and *II6* in the striatum of HD-sRNA-PT compared to CTL-sRNA-PT- and vehicle-injected animals (Figure 28A). In contrast, the neuronal markers *Ppp1r1b* and *Dlg4* did not show any significant differences between conditions (Figure 28B), indicating that the sRNA-triggered inflammatory environment was preceding neurodegeneration and could be enhancing the neurotoxic effects exerted by sRNA *per se*.

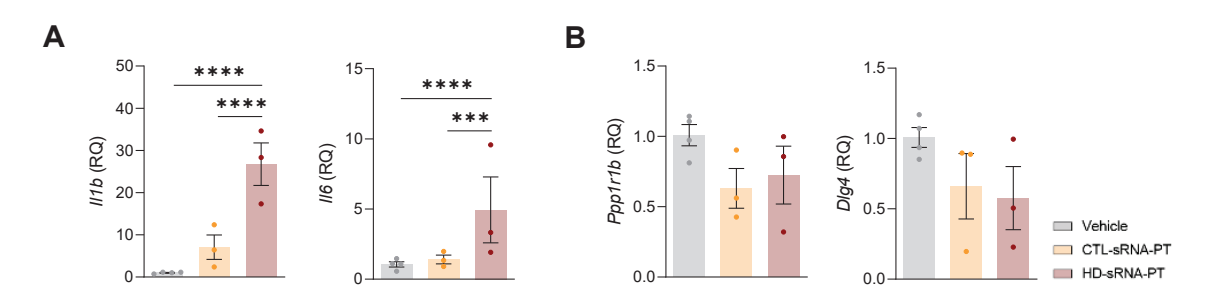


Figure 28. Intrastriatal injection of HD-sRNA-PT induce inflammation prior to neurodegeneration. Expression levels of **(A)** *II1b* and *II6* and **(B)** *Ppp1r1b* and *Dlg4* were determined in the striatum 24 h after the injection by RT-qPCR using SYBR Green technology. *Actin* was used as reference gene. Relative quantification (RQ) was calculated with the $2\Delta\Delta$ Ct method. Vehicle n = 4; CTL-sRNA-PT n = 3; HD-sRNA-PT n = 3. Each point represents data from an individual mouse. ****P < 0.0001 and ***P < 0.001 versus all other groups; calculated using a linear mixed-effects model followed by Bonferroni *post hoc* test.

1.6 HD-sRNA from different brain regions differentially affect motor function but do not recapitulate HD molecular abnormalities in WT mice striatum

Specific mechanisms underlying selective vulnerability of certain HD brain regions is still poorly understood. In what regards to sRNA generation in the HD context, we wondered whether harmful HD-sRNA are preferentially produced in the most vulnerable brain areas or analogously produced in regions typically not considered to be primary sites of neuropathology. To elucidate this, we obtained HD-sRNA from the frontal cortex (as affected) and the cerebellum (as less affected) of both control individuals and HD patients (Rosas et al., 2003). Next, HD-sRNA from the different brain regions were injected into the striatum of WT mice in parallel with

a behavioral analysis to examine whether they could differently compromise mice motor function. Specifically, animals were infused with vehicle solution, CTL-sRNA or HD-sRNA isolated from the frontal cortex (CTL- or HD-sRNA-CTX) or the cerebellum (CTL- or HD-sRNA-CB) of human post-mortem brain tissue following the same experimental plan depicted in Figure 19A. Similar motor impairment was detected in the rotarod test in animals injected with HD-sRNA-CTX to those observed in HD-sRNA-PT-injected mice (Figure 29A). However, HD-sRNA-CB infusions seemed to have milder effects as significant motor deficits were only detected at the most demanding speeds (Figure 29B). Consistently with the results obtained in the previous experiments, CTL-sRNA obtained from the cortex and the cerebellum did not alter mice execution in the rotarod test, which performed similarly to vehicle-injected animals. In contrast, no differences between treatments were observed in the balance beam test (Figure 29C), further confirming the previously anticipated milder effects in comparison to HD-sRNA-PT treatment. Lastly, no alterations in mice body weight were observed during this experimental procedure (Figure 29D).

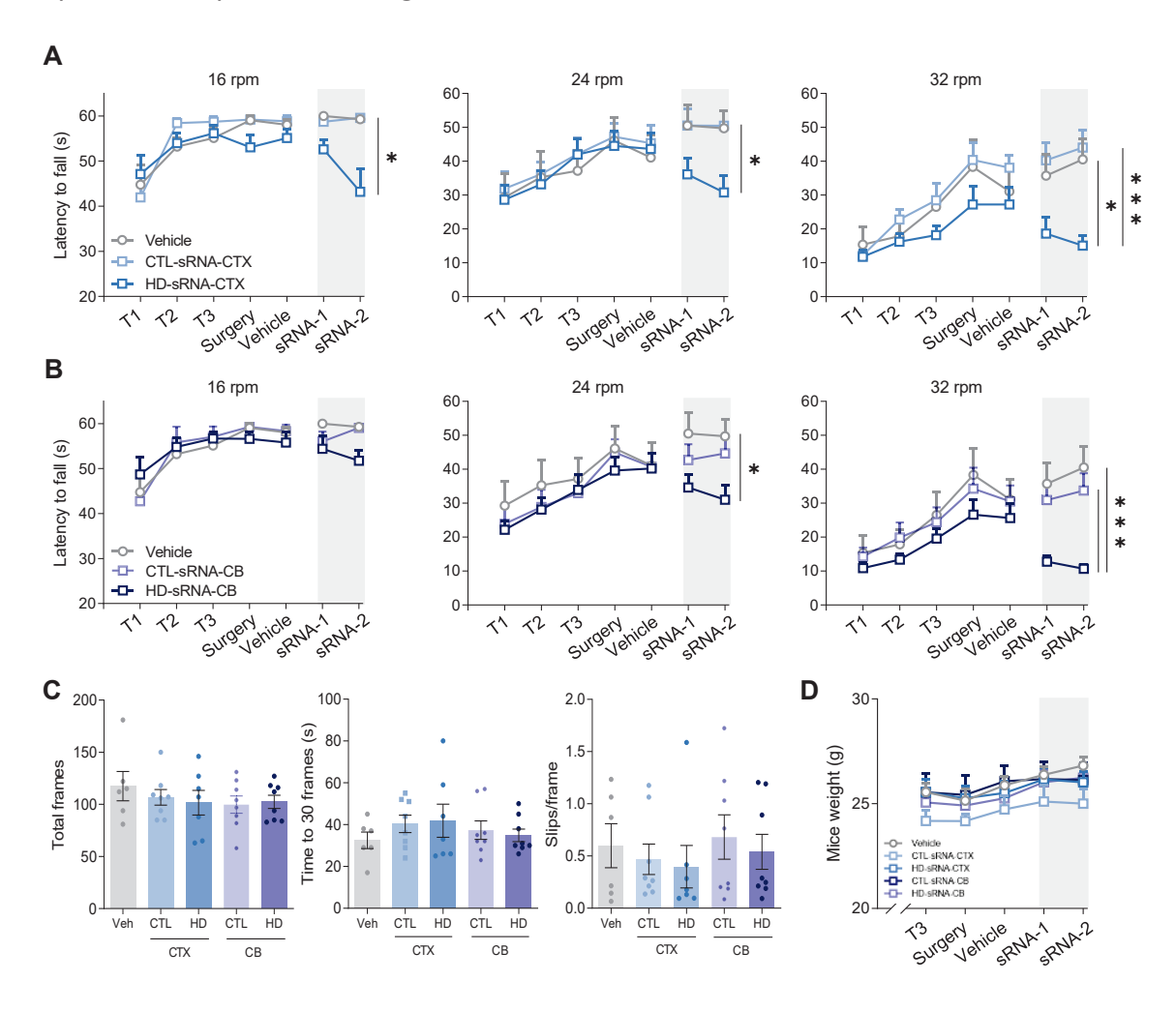


Figure 29. Intrastriatal injection of HD-sRNA from distinct brain regions differently compromises motor performance in WT mice. (A-B) Motor performance was evaluated in

the rotarod test at 16, 24 and 32 rpm in animals injected with sRNA obtained from human (A) cortex or (B) cerebellum. Vehicle n=6; CTL-sRNA-CTX n=8; HD-sRNA-CTX n=13; CTL-sRNA-CB n=8; HD-sRNA-CB n=14. Graphs show the latency to fall at each speed as mean \pm SEM. ***P < 0.001 and *P < 0.05 versus all other groups; calculated by two-way ANOVA followed by Bonferroni *post hoc* test. (C) Total number of crossed frames, time to traverse 30 frames and number of slips were registered in the balance beam test. Vehicle n=6; CTL-sRNA-CTX n=8; HD-sRNA-CTX n=7; CTL-sRNA-CB n=8; HD-sRNA-CB n=8. Each point represents data from an individual mouse. Data are shown as mean \pm SEM. (D) Mice body weight was controlled throughout all the experimental procedure. Vehicle n=14; CTL-sRNA-CTX n=4; HD-sRNA-CTX n=9; CTL-sRNA-CB n=4; HD-sRNA-CB n=10. Graphs show animal weight as mean \pm SEM.

As in previous experiments, striata of injected animals were further processed for subsequent biochemical analyses. However, no changes in the protein levels of different neuronal markers were detected in sRNA-CTX- (Figure 30A) and sRNA-CB-injected mice (Figure 30B) regardless of whether sRNA were obtained from tissue of control individuals or HD patients.

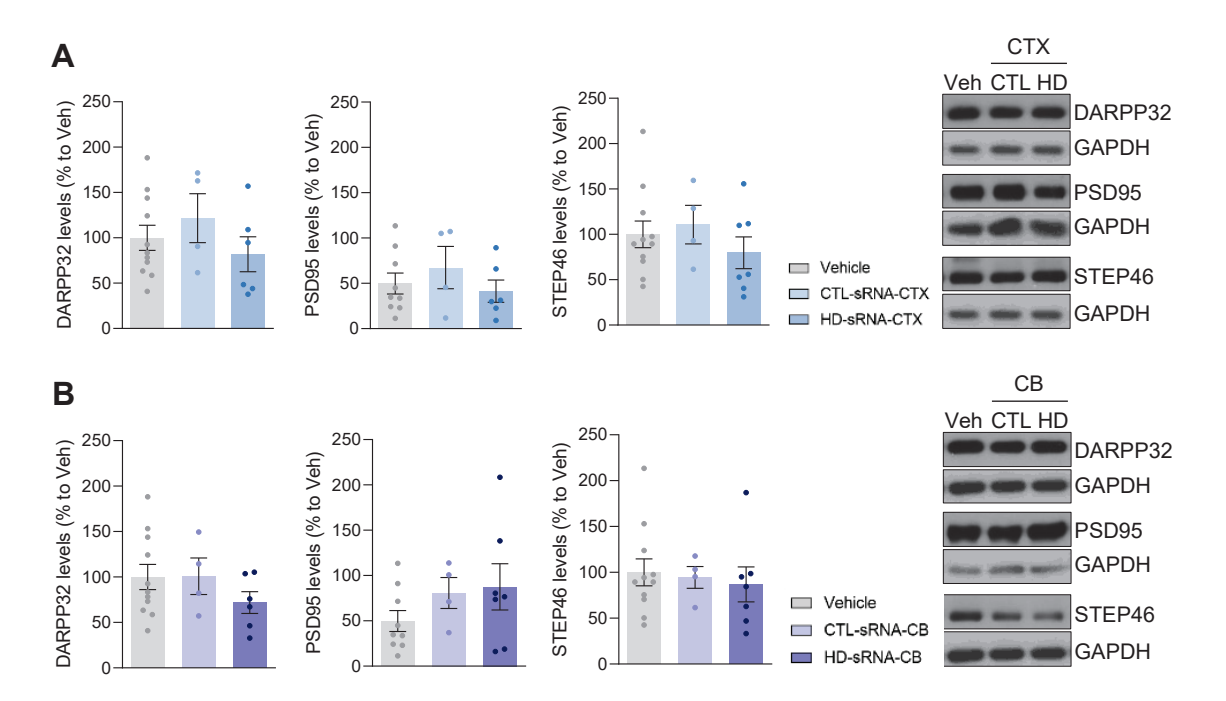


Figure 30. Intrastriatal injection of HD-sRNA obtained from the cortex or the cerebellum do not reproduce the alterations in neuronal markers observed after HD-sRNA-PT injections. Protein levels of DARPP32, PSD95 and STEP46 were analyzed by WB in striatal lysates from animals injected with (A) CTX-derived sRNA and (B) CB-derived sRNA. GAPDH was used as a loading control. Representative immunoblots are shown. Vehicle n = 9-11; CTL-sRNA-CTX n = 4; HD-sRNA-CTX n = 6-7; CTL-sRNA-CB n = 4; HD-sRNA-CB n = 6-7. Each point represents data from an individual mouse. Values are expressed as percentage to vehicle-injected animals and shown as mean \pm SEM.

Moreover, RT-qPCR analyses in the striatum of injected animals showed a lack of a consistent pro-inflammatory response in HD-sRNA-injected animals in comparison to CTL-sRNA or vehicle-injected animals, neither with sRNA obtained from the

human cortex nor the cerebellum (Figure 31A and B), as any of these conditions reproduced the upregulation of cytokine expression levels observed after HD-sRNA-PT injections (Figure 27).

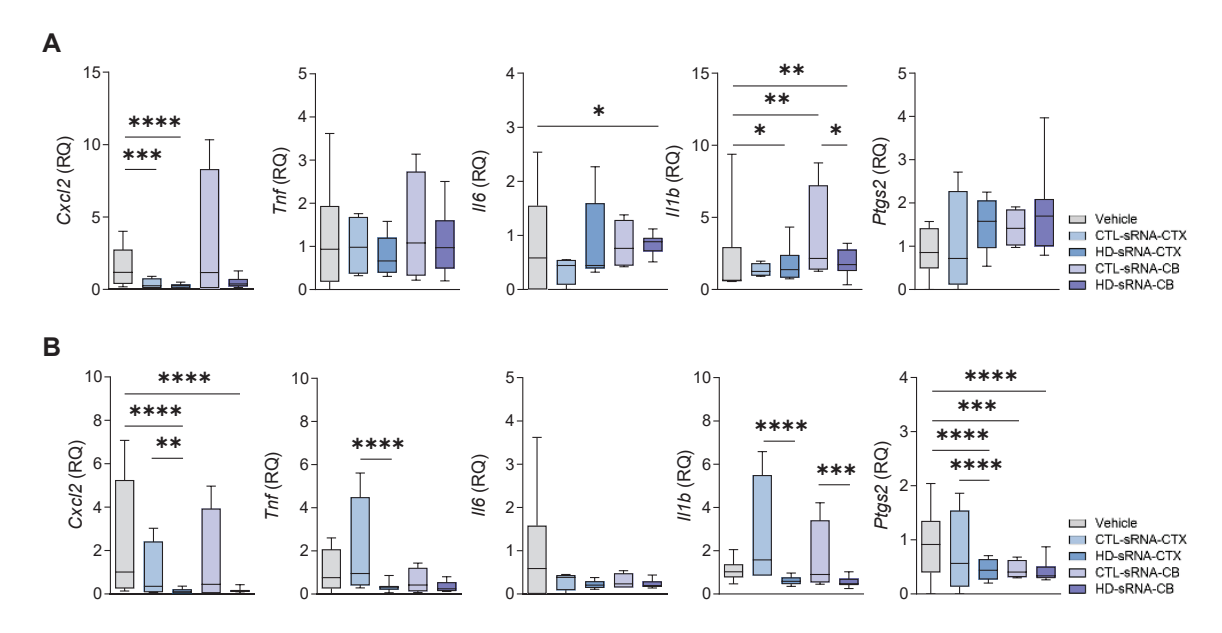


Figure 31. HD-sRNA obtained from human cortex or cerebellum do not induce striatal inflammation in WT mice. Expression levels of *Cxcl2*, *Tnf*, *Il6*, *Il1b* and *Ptgs2* in the striatum of injected animals were determined by RT-qPCR using TaqMan technology. **(A)** *Actin* and **(B)** *Hprt* were used as reference genes. Relative quantification (RQ) was calculated with the $2\Delta\Delta$ Ct method. Vehicle n = 6; CTL-sRNA-CTX n = 4; HD-sRNA-CTX n = 8; CTL-sRNA-CB n = 4; HD-sRNA-CB n = 8. Boxplots show medians (horizontal lines), 25^{th} to 75^{th} percentiles (boxes) and minimum to maximum (whiskers). ****P < 0.0001, ***P < 0.001, **P < 0.05 versus all other groups; calculated using a linear mixed-effects model followed by Bonferroni *post hoc* test.

Conversely, when we performed a single injection of HD-sRNA-CTX in the striatum of WT mice and analyzed inflammation levels 24 h later, we observed an acute immune activation in HD-sRNA-CTX-injected mice in comparison to both vehicle-and CTL-sRNA-CTX-injected animals (Figure 32), analogously to HD-sRNA-PT injection (Figure 28A).

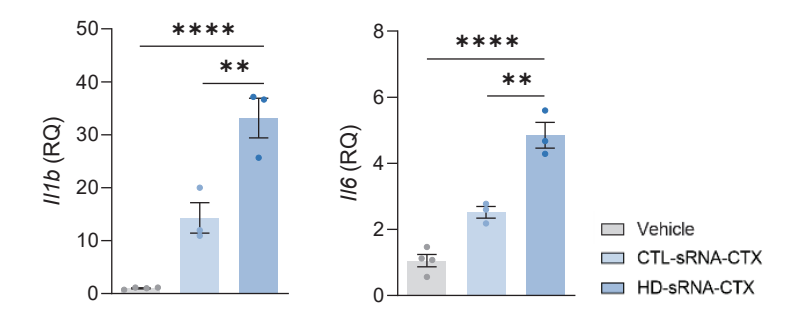


Figure 32. Intrastriatal injection of HD-sRNA-CTX induce inflammation prior to neurodegeneration. Expression levels of *II1b* and *II6* were determined in the striatum 24 h after the injection by RT-qPCR using SYBR Green technology. *Actin* was used as reference

gene. Relative quantification (RQ) was calculated with the $2\Delta\Delta$ Ct method. Vehicle n = 4; CTL-sRNA-CTX n = 3; HD-sRNA-CTX n = 3. Each point represents data from an individual mouse. ****P < 0.0001 and **P < 0.01 versus all other groups; calculated using a linear mixed-effects model followed by Bonferroni *post hoc* test.

Overall, these results indicate that the most affected brain areas in HD present intrinsic biochemical properties that may underlie the biogenesis of detrimental sRNA giving rise to HD-specific sRNA profiles associated to regional vulnerability.

1.7 sCAG are partial contributors to the detrimental effects of HD-sRNA-PT

It has been previously reported that the expression of CAG-expanded HTT leads to an increase in sCAG species, which are elevated in the putamen of HD patients and could compromise cell viability *in vitro* (Bañez-Coronel et al., 2012). On the basis of these studies, we sought to validate the presence of sCAG species in the purified fractions of sRNA used in the previous experiments. RNA polyadenylation followed by PCR amplification confirmed the presence of sCAG species in the purified pools of sRNA (CTL-sRNA-PT and HD-sRNA-PT), with a moderate increase in the pool obtained from HD putamen (Figure 33A and B). Amplification of miR-16 was performed as a reference sRNA presenting similar levels in both purified pools.

Moreover, we confirmed that whereas the pool of total RNA obtained from the putamen of HD patients (HD-total-RNA-PT) contained long expanded *HTT* exon 1, this transcript was undetectable in the injected HD-sRNA-PT purified fraction (Figure 33C), as anticipated from previous studies (Bañez-Coronel et al., 2012). This validation guaranteed that the detrimental effects caused by CAG repeats after HD-sRNA-PT injection should be attributed to short CAG repeats, namely sCAG species.

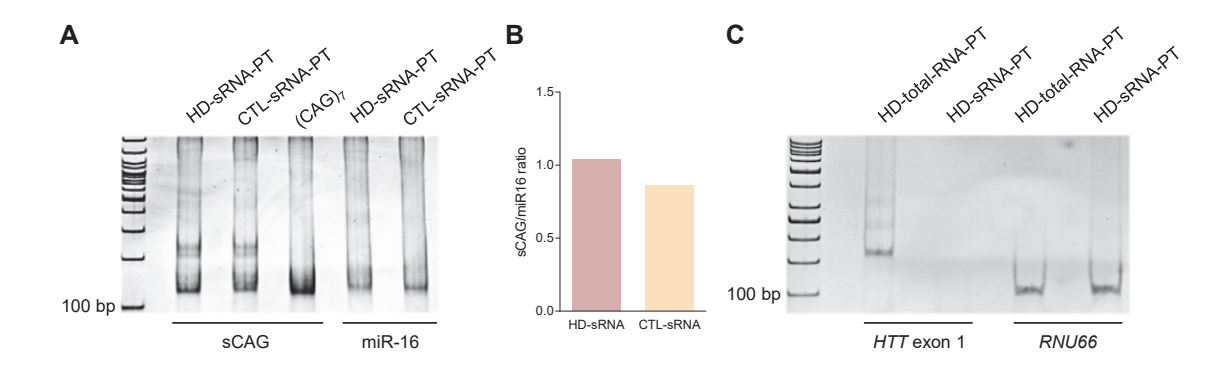


Figure 33. Validation of sCAG species presence and HTT exon 1 absence in sRNA-PT purified pools. (A) Gel electrophoresis of sCAG and miR-16 PCR amplification products in the purified fractions of sRNA (CTL-sRNA-PT and HD-sRNA-PT). A synthetic oligonucleotide containing 7 CAG repeats (CAG)₇ was used as a positive control. (B) Densitometric quantification of the specific PCR amplification products in the gel. For sCAG levels quantification, miR-16 was used as the reference sRNA. (C) Gel electrophoresis of *HTT* exon 1 and RNU66 PCR amplification products contained in the pool of total RNA obtained from the putamen of HD patients (HD-total-RNA-PT) and in the HD-sRNA-PT purified fraction. *RNU66* was used as an internal control.

Given the observed alterations in motor behavior and neuronal toxicity derived from HD-sRNA-PT injection, we sought to determine to what extent sCAG species were contributing. To this end, we took advantage of a locked nucleic acid antisense oligonucleotide specifically targeting the CAG repeats (LNA-CTG), as it has been demonstrated that intrastriatal injection of LNA-CTG in the striatum of R6/2 mice improved their motor performance (Rué et al., 2016). Hence, we evaluated HD-sRNA-PT injection consequences in the presence of the LNA-CTG or an analogous control scrambled oligonucleotide (LNA-SCB), following the experimental design depicted in Figure 19A.

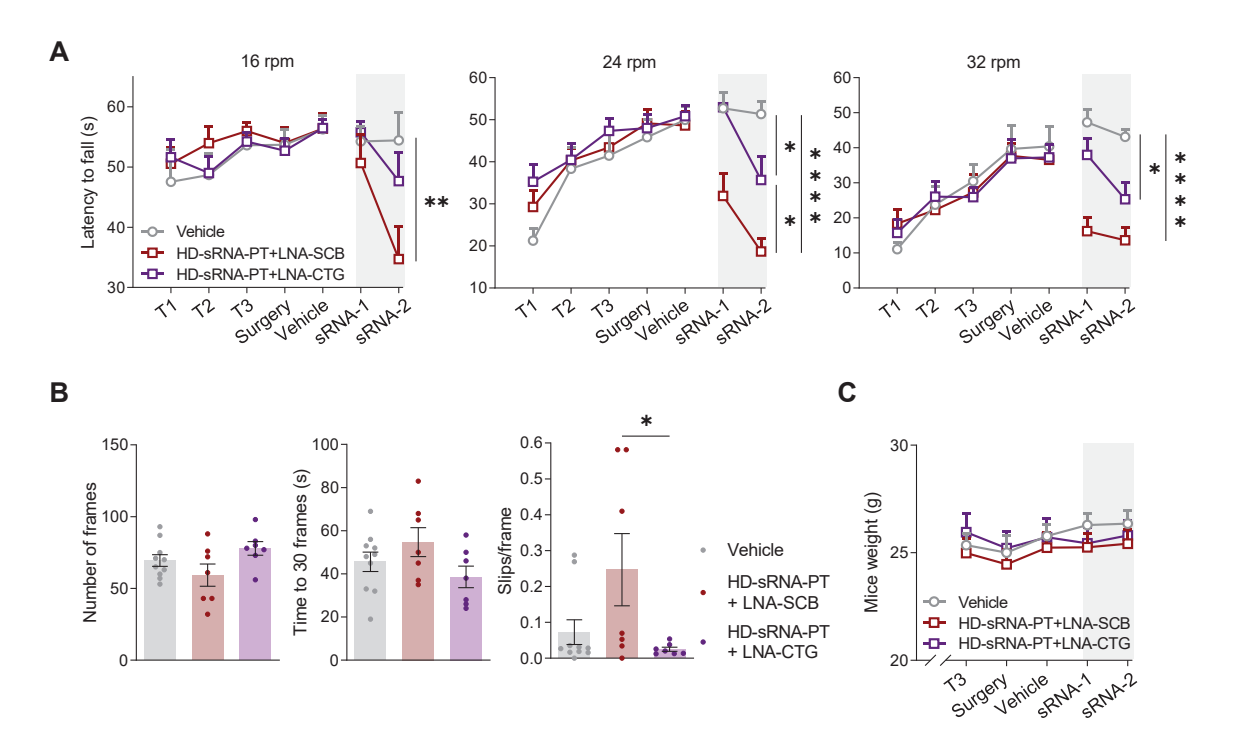


Figure 34. Motor deterioration in WT mice intrastriatally injected with HD-sRNA-PT is delayed by the blockage of sCAG. (A) Motor performance was evaluated in the rotarod test at 16, 24 and 32 rpm. Vehicle n = 8; HD-sRNA-PT + LNA-SCB n = 8; HD-sRNA-PT + LNA-CTG n = 8. Graphs show the latency to fall at each speed as mean \pm SEM. ****P < 0.0001, **P < 0.01, *P < 0.05 versus all other groups; calculated by two-way ANOVA followed by Bonferroni *post hoc* test. (B) Total number of crossed frames, time to traverse 30 frames and number of slips were registered in the balance beam test. Vehicle n = 10; HD-sRNA-PT + LNA-SCB n = 7; HD-sRNA-PT + LNA-CTG n = 7. Each point represents data from an individual mouse. Data are shown as mean \pm SEM. *P < 0.05 versus the indicated groups; calculated by one-way ANOVA followed by Bonferroni *post hoc* test. (C) Mice body weight was controlled throughout all the experimental procedure. Vehicle n = 9; HD-sRNA-PT + LNA-SCB n = 9; HD-sRNA-PT + LNA-CTG n = 9. Graphs show animal weight as mean \pm SEM.

Rotarod tests performed after sRNA intrastriatal infusions evidenced a significant delay in the onset of motor deterioration in HD-sRNA-PT + LNA-CTG-injected animals compared to the HD-sRNA-PT + LNA-SCB-injected mice at all tested speeds (Figure 34A). It is important to note that HD-sRNA-PT injections caused a rapid

decrease in the latency to fall immediately after the first week of infusions (Figure 34A). In contrast, HD-sRNA-PT + LNA-CTG-injected animals did not start presenting significant motor abnormalities until the second week of infusions (Figure 34A). Consistently with these findings, only HD-sRNA-PT + LNA-SCB-injected animals presented coordination alterations in the balance beam test, performed after one week of injections (Figure 34B). Finally, no obvious changes in body weight were detected in any mice group during all the study (Figure 34C).

To decipher the molecular basis of the delay in the appearance of motor deterioration, transcriptomic, biochemical, and morphological analyses of the striatum of injected mice were performed. Remarkably, mice injected with HD-sRNA-PT + LNA-CTG did not show significant changes in the levels of transcripts strongly dysregulated in HD-sRNA-PT-injected animals, suggesting a post-transcriptional mechanism of action of LNA-CTG (Table 15). Moreover, this result indicated that sRNA species present in HD-sRNA-PT pool, other than sCAG, were responsible for the transcriptomic alterations observed.

	HD-sRNA-PT vs vehicle		HD-sRNA-PT vs HD-sRNA-PT+LNA-CTG			
Gene	log2FC	P value	Adjusted P	log2FC	P value	Adjusted P
Mefv	3.253	1.957E-11	3.268E-07	1.703	0.000499	0.200608
Thbs1	3.249	3.855E-11	4.291E-07	1.607	0.001173	0.258813
Ccr1	3.248	5.957E-11	4.974E-07	1.820	0.000264	0.175665
Sirpb1b	3.205	7.729E-12	2.581E-07	1.541	0.000896	0.247989
Ifi213	3.120	2.137E-10	1.008E-06	1.769	0.000340	0.180077
Ms4a4c	3.062	3.850E-10	1.008E-06	1.628	0.000957	0.254185
Spp1	3.044	1.968E-10	1.008E-06	0.935	0.053348	0.906576
Oas2	3.032	1.050E-10	7.010E-07	1.250	0.008496	0.497838
Rsad2	3.028	7.242E-10	1.423E-06	1.677	0.000706	0.229543
Mx1	2.984	5.170E-10	1.151E-06	1.406	0.003757	0.403248
Ighg3	-2.037	5.420E-05	0.002376	0.242908	0.630933	1
Gm13536	-1.961	6.100E-07	0.000105	-0.188976	0.663624	1
Krt75	-1.877	7.472E-05	0.002989	-0.074750	0.880381	1
Myod1	-1.738	0.000408	0.009023	-0.534202	0.287082	1
Mir132	-1.670	8.241E-05	0.003208	-0.041630	0.927120	1
Prss56	-1.611	4.069E-05	0.001964	0.449960	0.268193	1
Tfap2d	-1.595	0.001701	0.022157	-1.330011	0.009056	0.509474
Gm27169	-1.523	0.002856	0.030753	-0.532573	0.294691	1
lghv1-18	-1.502	0.002833	0.030615	-0.344381	0.488829	1

Gm28883 -1.497 0.000551 0.011008 -0.204987 0.658801 1

Table 15. Differential gene expression between HD-sRNA-PT- versus HD-sRNA-PT+LNA-CTG-injected animals in the top ten upregulated and downregulated genes in HD-sRNA-PT- versus vehicle-injected mice.

Next, we examined the expression levels of the different neuronal markers previously analyzed. Whereas *Ppp1r1b* mRNA levels (DARPP32) remained unaltered with the LNA-CTG treatment (Figure 35A), the decrease in DARPP32 protein levels was prevented (Figure 35B). Other markers strongly altered by HD-sRNA-PT injection, such as PSD95, STEP46, PHLPP1, DRD2 and ENK showed a trend to decrease their protein levels in the striatum of HD-sRNA-PT + LNA-SCB-injected mice, while LNA-CTG administration did not affect their levels (Figure 35C). In addition, neither LNA-SCB nor LNA-CTG modified DRD1 protein levels in injected mice.

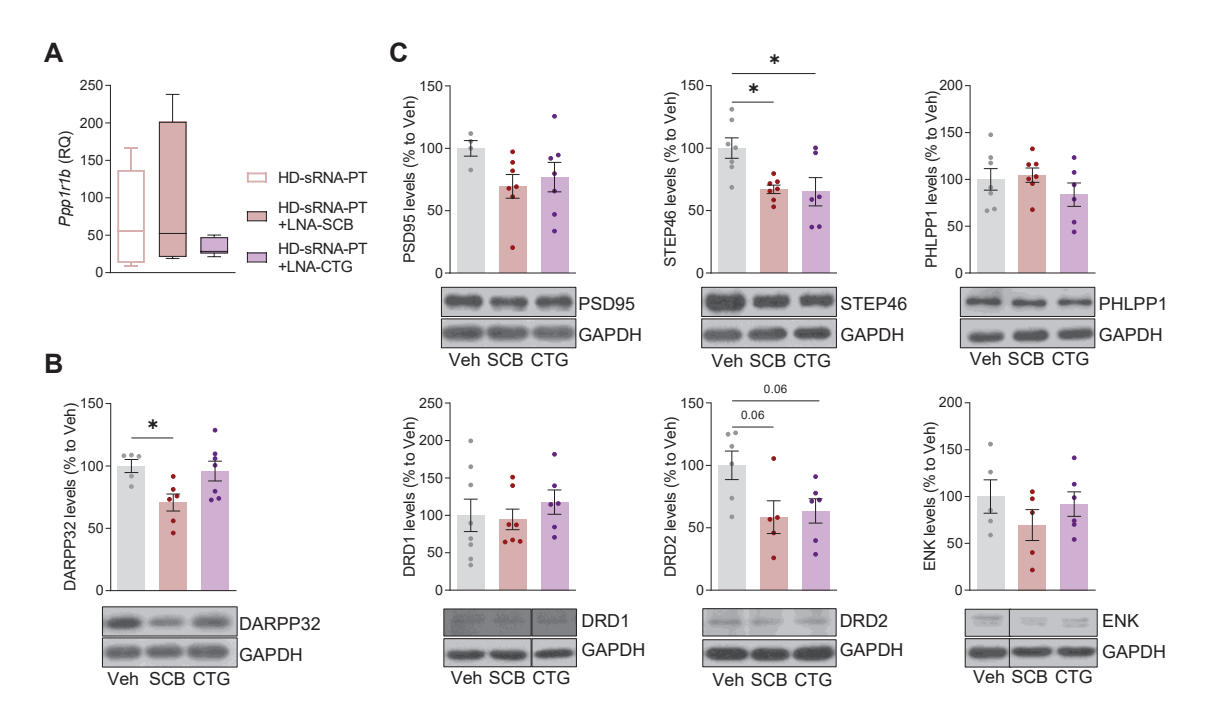


Figure 35. Blockage of sCAG does not prevent most of the detrimental effects caused by HD-sRNA-PT injection. (A) Expression levels of DARPP32 (Ppp1r1b) in the striatum of injected animals were determined by RT-qPCR using SYBR Green technology. Hprt was used as a reference gene. HD-sRNA-PT n = 12; HD-sRNA-PT + LNA-SCB n = 7; HD-sRNA-PT + LNA-CTG n = 7. Boxplots show medians (horizontal lines), 25^{th} to 75^{th} percentiles (boxes) and minimum to maximum (whiskers). (B-C) Protein levels of DARPP32, PSD95, STEP46, PHLPP1, DRD1, DRD2 and ENK were analyzed by WB in striatal lysates from injected animals. GAPDH was used as a loading control. Representative immunoblots are shown. Vehicle n = 4-8; HD-sRNA-PT + LNA-SCB n = 5-7; HD-sRNA-PT + LNA-CTG n = 6-7. Each point represents data from an individual mouse. Values are expressed as percentage to vehicle-injected animals and shown as mean \pm SEM. *P < 0.05 and P < 0.06 versus the indicated groups; calculated by one-way ANOVA followed by Bonferroni *post hoc* test.

The reduction in the number of neurons observed in the Nissl-stained sections was prevented in the striatum of HD-sRNA-PT + LNA-CTG-injected animals (Figure 36A and B), as well as the decrease in the number of DARPP32-positive cells (Figure 36C and D), which was in line with DARPP32 protein levels (Figure 35B). Nevertheless, we could not detect changes in the number of cleaved caspase-3-positive cells in the striatum of HD-sRNA-PT + LNA-SCB- and HD-sRNA-PT + LNA-CTG-injected mice (Figure 36E and F). Altogether, these data suggest that sCAG species could be contributing to the observed effects, yet do not explain many important pathogenic effects exerted by HD-sRNA-PT.

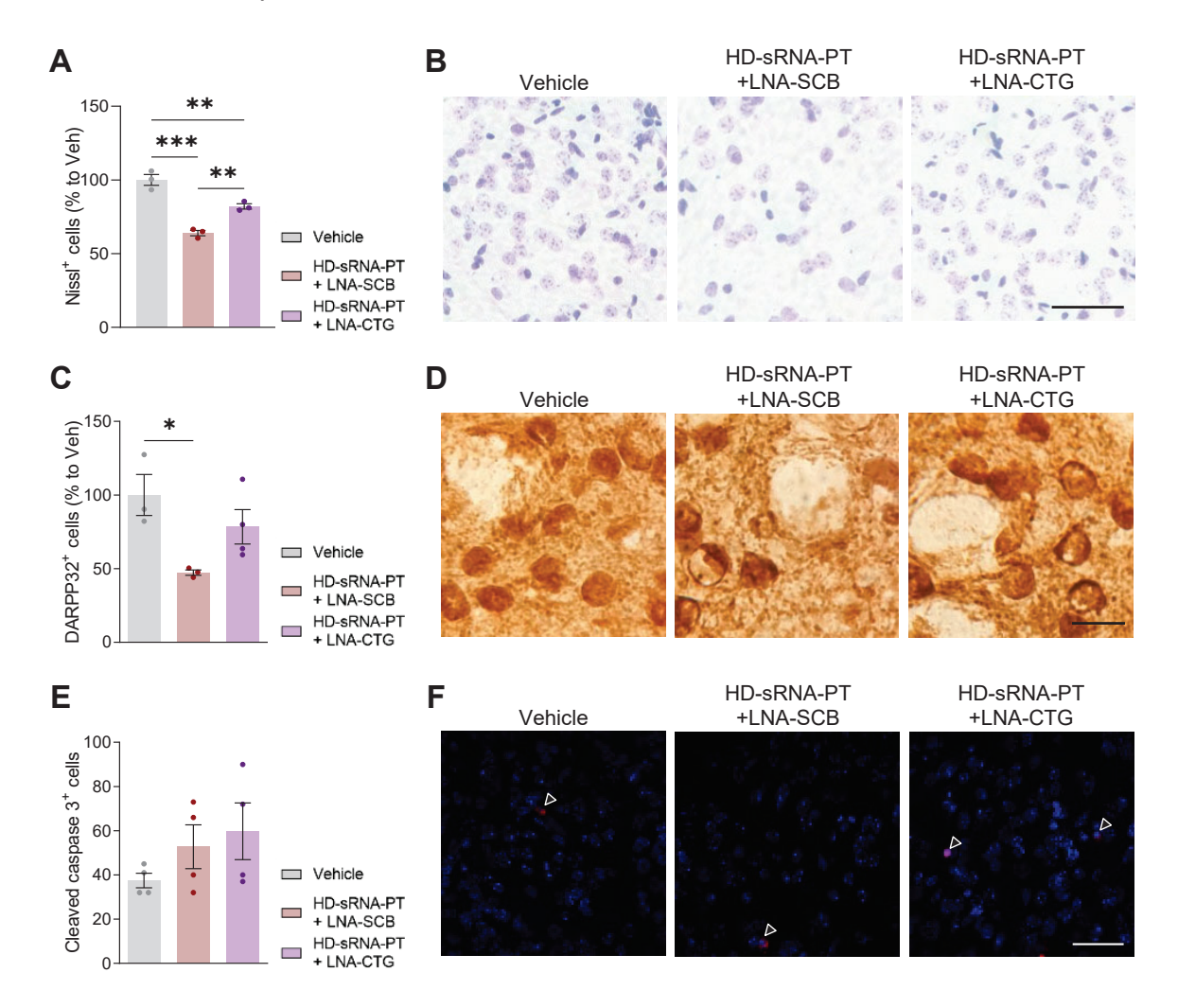


Figure 36. LNA-CTG administration prevents neuronal loss in the striatum of HD-sRNA-PT-injected mice. (A) Quantification of the number of neurons using Nissl staining in the striatum of injected mice. Vehicle n=3; HD-sRNA-PT + LNA-SCB n=3; HD-sRNA-PT + LNA-CTG n=3. (B) Representative images of Nissl staining in the striatum of injected mice. Scale bar: 20 µm. (C) Quantification of DARPP32-positive cells in the striatum of injected mice. Vehicle n=3; HD-sRNA-PT + LNA-SCB n=3; HD-sRNA-PT + LNA-CTG n=4. In (A) and (C), values are expressed as percentage to vehicle-injected animals, shown as mean \pm SEM and each point represents an individual mouse. ***P < 0.001, **P < 0.01 and *P < 0.05 versus the indicated groups; calculated by one-way ANOVA followed by Bonferroni *post hoc* test. (D) Representative images of DARPP-32 immunostained MSNs in the striatum of injected

mice. Scale bar: 20 μ m. **(E)** Quantification of the number of cleaved caspase-3-positive cells in the striatum of injected mice. Vehicle n = 4; HD-sRNA-PT + LNA-SCB n = 4; HD-sRNA-PT + LNA-CTG n = 4. Each point represents data from an individual mouse. Data are shown as mean \pm SEM. **(F)** Representative images of cleaved caspase-3 immunostained coronal striatal sections of injected mice. Cleaved caspase-3 is shown in red and DAPI in blue. Arrowheads indicate examples of cleaved caspase-3-positive cells. Scale bar: 25 μ m.

In parallel, we showed that injections of CTL-sRNA-PT together with LNA-CTG or LNA-SCB did not affect mice performance in the rotarod test (Figure 37A) nor alter the protein levels of DARPP32, PSD95, STEP46, PHLPP1, DRD1, DRD2 and ENK (Figure 37B). Therefore, we could conclude that the observed effects of CTL-sRNA-PT are not influenced by LNA-ASOs.

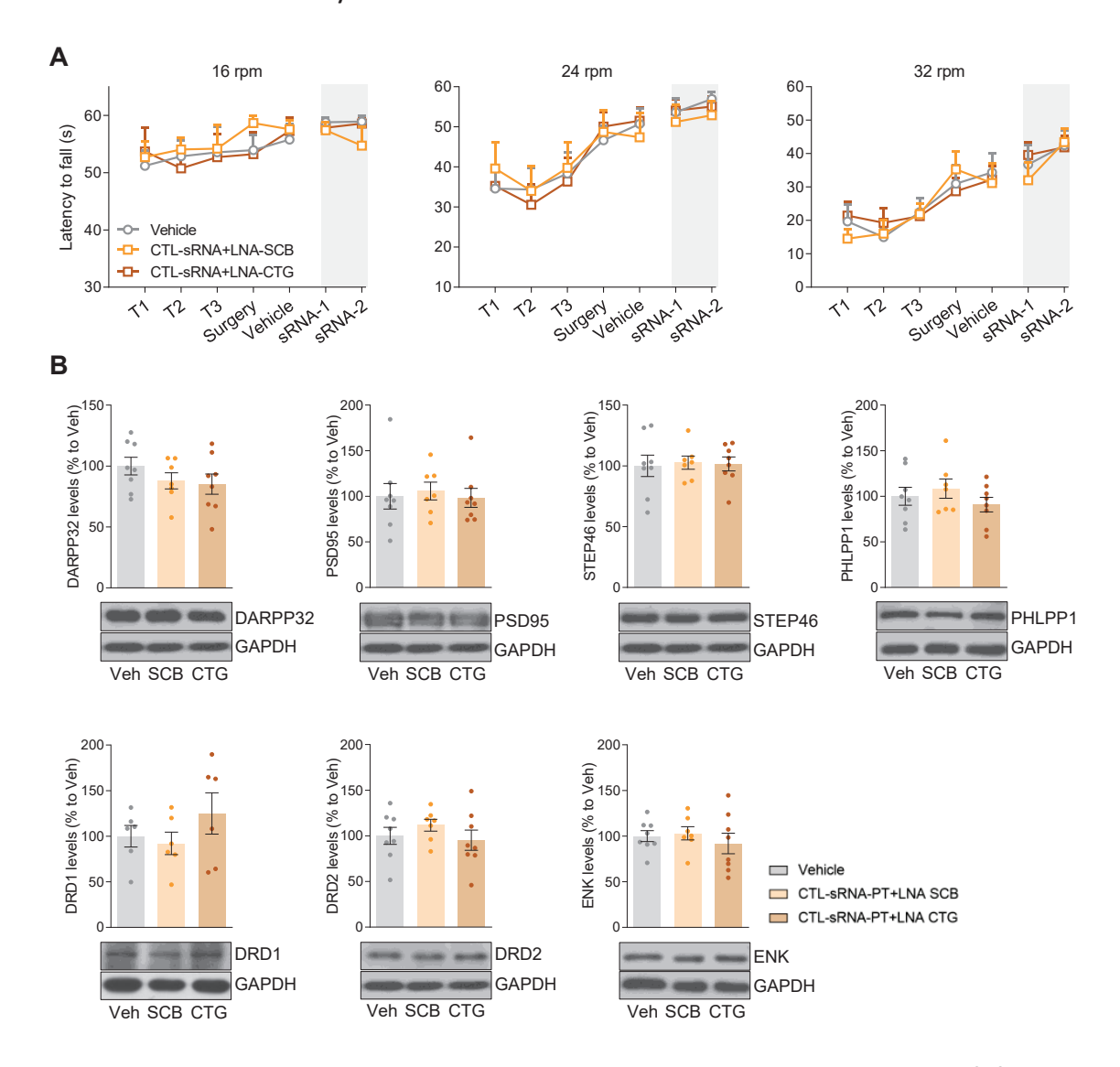


Figure 37. LNA-ASOs do not affect putative CTL-sRNA-PT outcomes. (A) Motor performance was evaluated in the rotarod test at 16, 24 and 32 rpm. Vehicle n = 8; CTL-sRNA-PT + LNA-SCB n = 8; CTL-sRNA-PT + LNA-CTG n = 10. Graphs show the latency to fall at each speed as mean \pm SEM. (B) Protein levels of DARPP32, PSD95, STEP46, PHLPP1, DRD1, DRD2 and ENK were analyzed by WB in striatal lysates from injected animals. GAPDH was used as a loading control. Representative immunoblots are shown. Vehicle n = 6-8; CTL-

 $sRNA-PT + LNA-SCB \ n = 6-7$; CTL- $sRNA-PT + LNA-CTG \ n = 6-8$. Each point represents data from an individual mouse. Values are expressed as percentage to vehicle-injected animals and shown as mean \pm SEM.

On the basis of the partial prevention of the deleterious effects caused by the coadministration of LNA-CTG with HD-sRNA-PT, we aimed to further confirm the detrimental effects of sCAG species in vivo by using a different approach. Synthetic RNA oligonucleotides of 21 nt mimicking sCAG species (sCAG) and comparable control scrambled RNA oligonucleotides (sSCB) were infused into the striatum of WT mice following the experimental plan described in Figure 38A. Rotarod test revealed a motor impairment in animals infused with sCAG in comparison to vehicle- and sSCB-injected mice, however this was only detected at the most demanding speed (32 rpm) (Figure 38B, data from 16 and 24 rpm not shown). In the balance beam test, alterations in motor coordination and balance were also observed in sCAG-injected animals, as shown by a reduction in the total number of frames travelled, an increase in the time required to cross 30 frames and a higher number of slips compared to animals in the control groups (Figure 38C). In accordance with the results obtained after HD-sRNA-PT infusions (Figure 19B and C), sCAG-injected animals started presenting behavioral alterations after the first week of infusions while the differences with the other treatments appeared to be more significant after four infusions. Finally, mice body weight was not substantially altered under any treatment or procedure (Figure 38D).

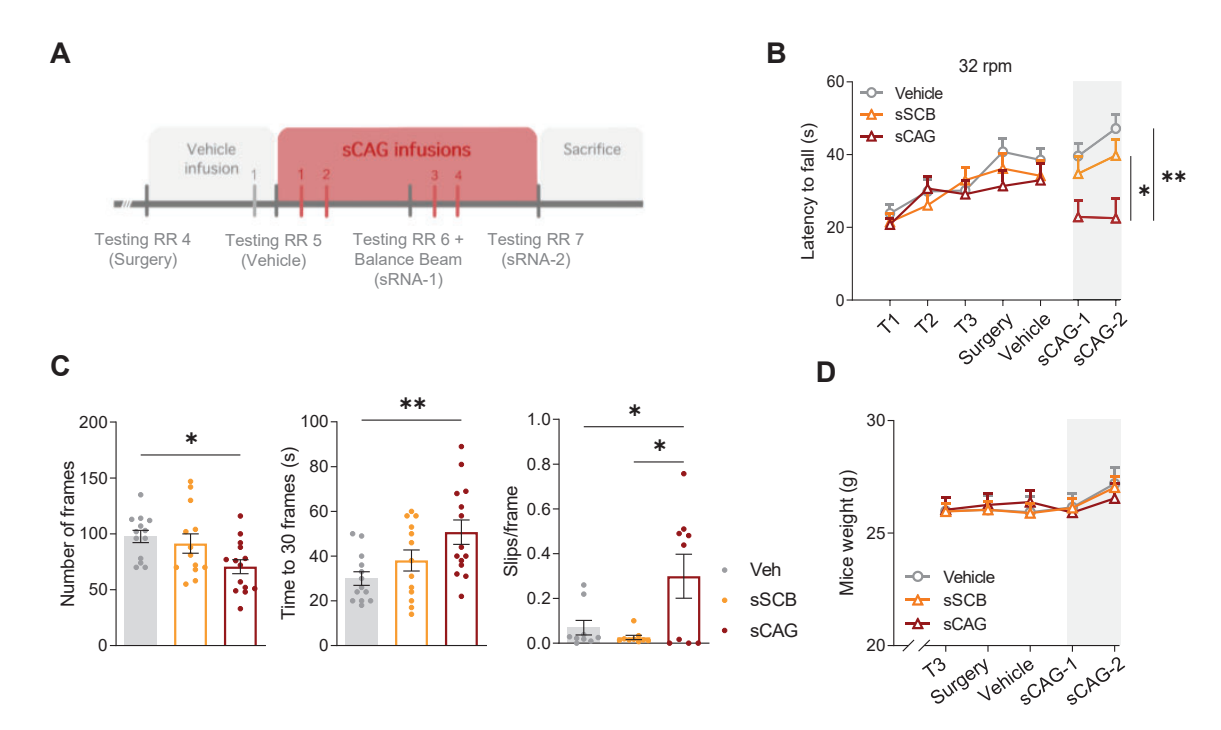


Figure 38. Intrastriatal infusions of synthetic sCAG species induce motor deficits in WT mice. (A) Timeline of the followed experimental procedure including intrastriatal infusions of vehicle, sSCB and sCAG synthetic oligonucleotides in freely moving mice together with their behavioral phenotyping. Fixed rotarod test was performed every week whereas the

balance beam test was only conducted after the first week of injections. Animals received four infusions in total and were sacrificed 48 h after the fourth infusion. (B) Motor performance was evaluated in the rotarod test performed at 32 rpm. Vehicle n = 16; sSCB n = 18; sCAG n = 18. Graphs show the latency to fall at each speed as mean \pm SEM. **P < 0.01 and *P < 0.05 versus all other groups; calculated by two-way ANOVA followed by Bonferroni *post hoc* test. (C) Total number of crossed frames, time to traverse 30 frames and number of slips were registered in the balance beam test. Vehicle n = 9-13; sSCB n = 9-13; sCAG n = 9-14. Each point represents data from an individual mouse. Data are shown as mean \pm SEM. **P < 0.01 and *P < 0.05 versus the indicated groups; calculated by one-way ANOVA followed by Bonferroni *post hoc* test. (D) Mice body weight was controlled throughout all the experimental procedure. Vehicle n = 17; sSCB n = 18; sCAG n = 18. Graphs show animal weight as mean \pm SEM.

After behavioral characterization, we wondered whether the observed motor alterations were paralleled by analogous molecular abnormalities to those caused by HD-sRNA-PT infusions. Despite the general trend of the different markers to decrease, DARPP32 was the only neuronal marker with significantly reduced protein levels in the striatum of mice injected with synthetic sCAG species (Figure 39).

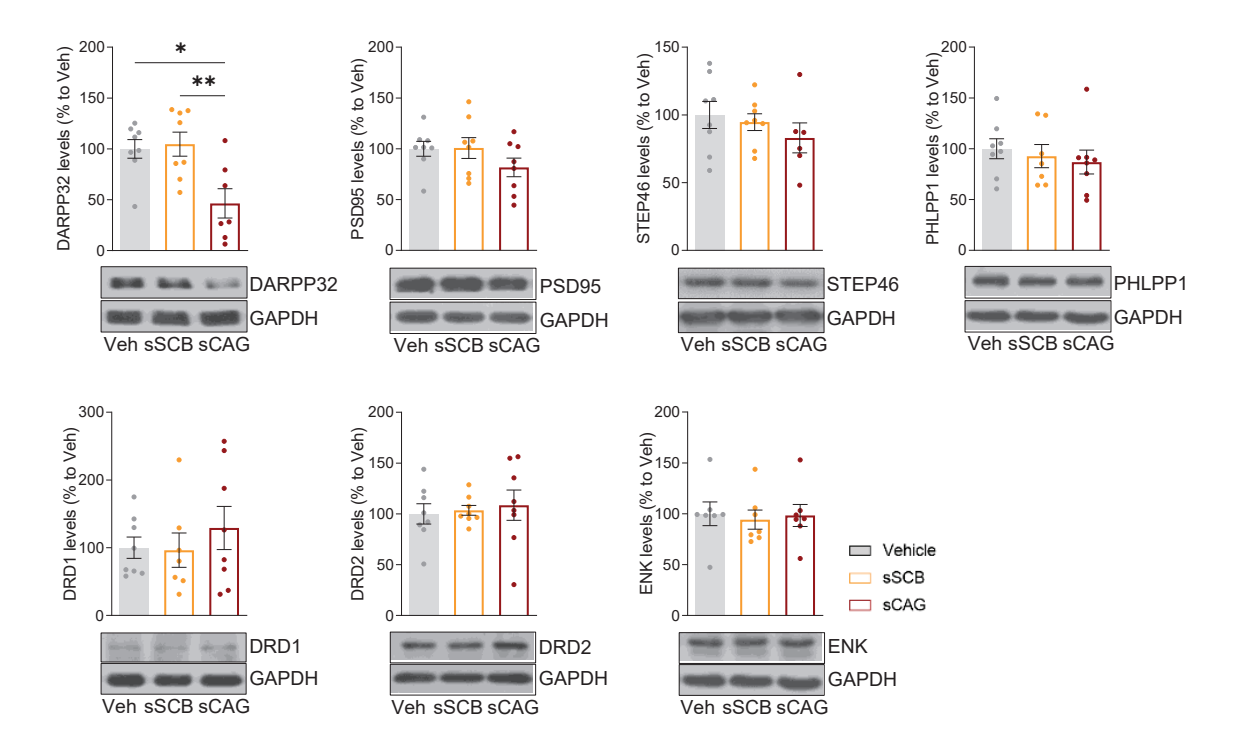


Figure 39. sCAG intrastriatal injections do not reproduce the alterations in neuronal markers observed after HD-sRNA-PT injections. Protein levels of DARPP32, PSD95, STEP46, PHLPP1, DRD1, DRD2 and ENK were analyzed by WB in striatal lysates from injected animals. GAPDH was used as a loading control. Representative immunoblots are shown. Vehicle n=7-8; sSCB n=7-8; sCAG n=6-8. Each point represents data from an individual mouse. Values are expressed as percentage to vehicle-injected animals and shown as mean \pm SEM. **P < 0.01 and *P < 0.05 versus the indicated groups; calculated by one-way ANOVA followed by Bonferroni *post hoc* test.

In contrast, no differences in the total number of DARPP32-positive neurons were detected by immunohistochemistry (Figure 40A and B), accordingly with an unaltered quantification of apoptotic cell death (Figure 40C and D) among the different conditions. These results suggest that the harmful activity of sCAG species must be complemented by other sRNA species containing CAG repeats that are present in the HD human putamen and are presumably targeted by LNA-CTG.

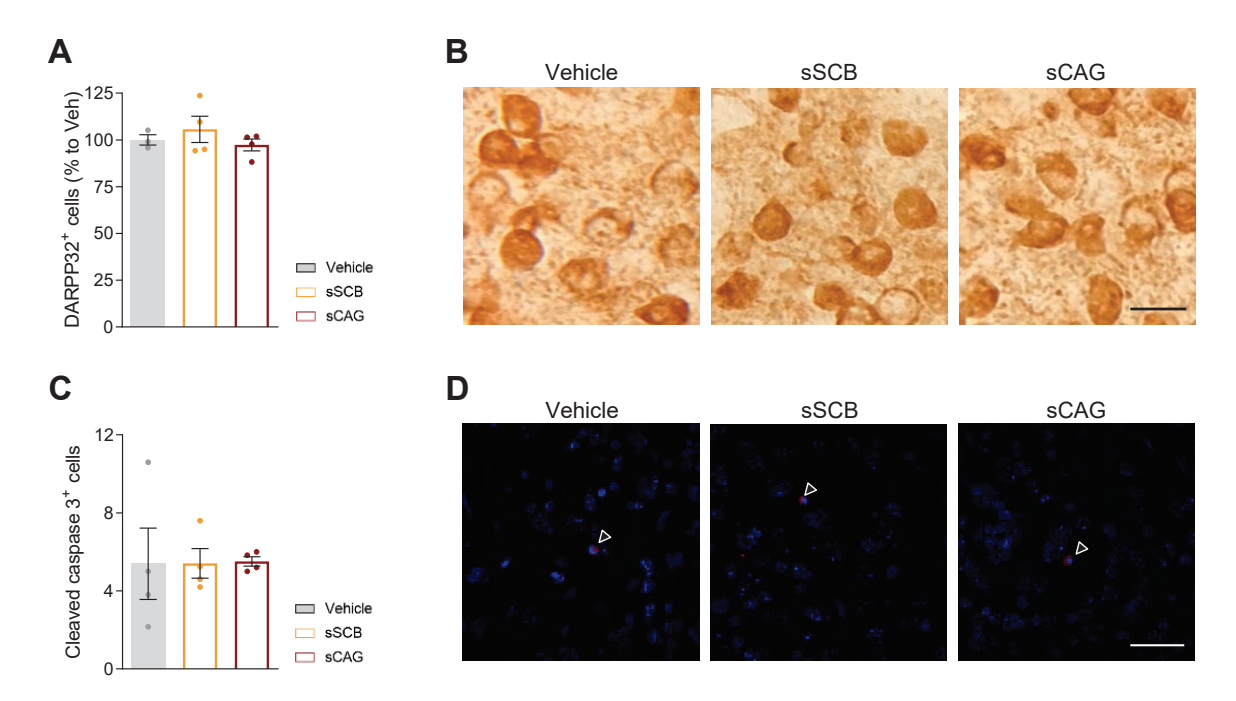


Figure 40. Intrastriatal injections of synthetic sCAG species fail to induce neuronal loss in the striatum of WT mice. (A) Quantification of DARPP32-positive cells in the striatum of injected mice. Vehicle n=3; sSCB n=4; sCAG n=4. Each point represents data from an individual mouse. Values are expressed as percentage to vehicle-injected animals and shown as mean \pm SEM. (B) Representative images of DARPP-32 immunostained MSNs in the striatum of injected mice. Scale bar: 20 μ m. (C) Quantification of the number of cleaved caspase-3-positive cells in the striatum of injected mice. Vehicle n=4; sSCB n=4; sCAG n=4. Each point represents data from an individual mouse. Data are shown as mean \pm SEM. (D) Representative images of cleaved caspase-3 immunostained coronal striatal sections of injected mice. Cleaved caspase-3 is shown in red and DAPI in blue. Arrowheads indicate examples of cleaved caspase-3-positive cells. Scale bar: 25 μ m.

Overall, these data support the idea that sCAG species are playing a role in the sRNA toxicity observed, in line with previous published data (Bañez-Coronel et al., 2012). However, there are specific mechanisms of neuronal dysfunction underlying motor impairments that cannot be explained solely by sCAG species and are potentially caused by other sRNA contained in the HD-sRNA-PT pool.

2. Characterization of the sRNA transcriptome in different areas of HD brains and potential roles in HD pathogenesis

2.1 Different areas of the HD brain present dysregulated sRNA signatures, with an overproduction of tsRNA

All the altered outcomes observed after intrastriatal injections prompted us to extensively characterize the sRNA transcriptome and identify which sRNA species, besides of sCAG, were enriched in the HD brain and could be responsible for both the neurotoxic effects and the transcriptomic dysregulation observed.

Thus, to obtain a detailed profile of sRNA transcriptome associated to HD, CTL-sRNA-PT and HD-sRNA-PT pools were characterized through deep sequencing. Subsequently, Sequently, Sequently and used to identify clusters of co-expressed sRNA consistently and non-redundantly mapping onto the same RNA precursor, therefore enabling the annotation and quantification of many different classes of sRNA (Pantano et al., 2011).

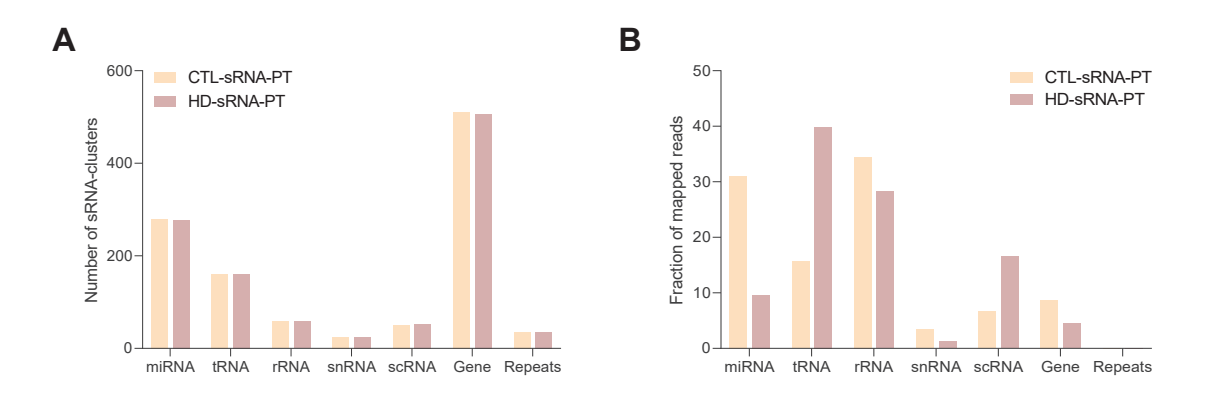


Figure 41. Seqcluster tool reveals a differential biotype composition of sRNA pools between CTL- and HD-sRNA-PT samples. (A) Total number of sRNA-clusters classified by sRNA biotypes within CTL-sRNA-PT and HD-sRNA-PT pools. **(B)** Fraction of mapped reads in each sRNA-PT pool annotating onto the different sRNA biotypes.

In CTL- and HD-sRNA-PT samples, around 1200 different clusters were identified corresponding to different sRNA biotypes. Gene- and miRNA-clusters were the most abundant biotypes followed by tRNA- and rRNA-clusters (Figure 41A). Notably, both analyzed conditions showed equal distributions in terms of total number of sRNA-clusters detected. However, considering the relative abundance of annotated reads in each sample, miRNA-and rRNA-clusters were the most predominant biotypes in CTL-sRNA-PT sample while tRNA-clusters were the most abundant within the HD-sRNA-PT pool (Figure 41B).

Next, we analyzed the length distribution of sRNA reads among both samples which evidenced the presence of two different clusters based on sRNA lengths. The first set was less abundant and contained sRNA with >40 nt in length that predominantly mapped onto rRNA. In contrast, the other cluster was highly concentrated with

sRNA presenting <40 nt and mapping onto a diverse variety of biotypes. Focusing on this sRNA <40 nt fraction, deep sRNA profiling revealed a differential composition between CTL-sRNA-PT and HD-sRNA-PT samples. While CTL-sRNA-PT showed a high abundance of sequences with 21-22 nt in length mapping onto miRNAs, the most abundant species in HD-sRNA-PT sample presented 32-33 nt in length and were annotated as tRNA (Figure 42).

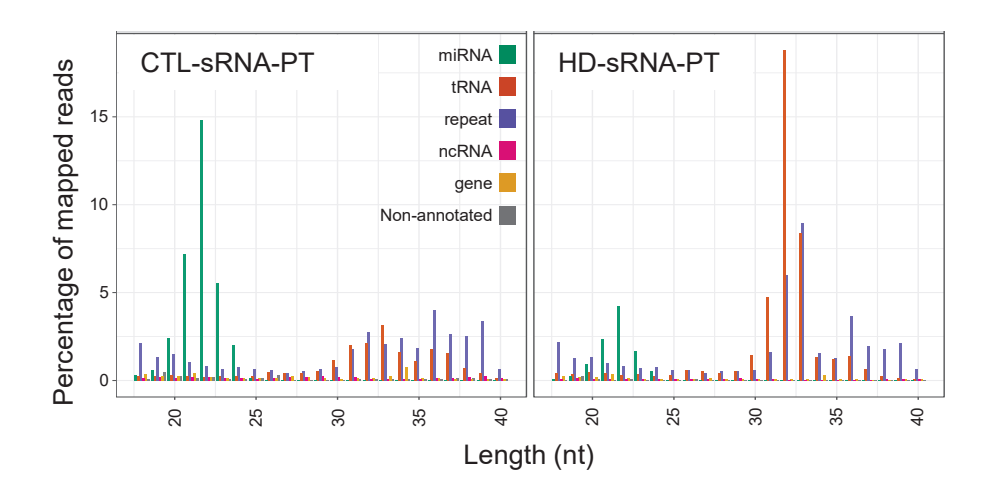


Figure 42. Differential read length distribution and biotype composition is observed among CTL- and HD-sRNA-PT pools. Histogram showing length distribution by biotype of the sRNA <40 nt fraction contained in CTL-sRNA-PT and HD-sRNA-PT samples. Abundances (in %) are relative to all sRNA with <40 nt sequenced.

Further analysis of tRNA-clusters displayed abundant short sequences specifically annotating onto particular regions of different tRNA precursors, with this defining tRNA-derived small RNAs (tsRNA). In order to comprehend the abundances of tsRNA subtypes within samples, we annotated the specific sequences of the obtained reads into the MINTbase database (Pliatsika et al., 2018). This approach highlighted the differential tsRNA fragmentation signatures between samples with an overrepresentation of tsRNA derived from the 5'-end of the precursor tRNA (5'tRFs and 5'halves) in the HD-sRNA-PT pool compared to the CTL-sRNA-PT sample (Figure 43A). When focusing on the precursor tRNA isoacceptors from which tsRNA had been generated, we detected different abundances between conditions with higher proportions of tRFs derived from tRNA^{Glu}, tRNA^{Gly} and tRNA^{Val} in the HDsRNA-PT pool (Figure 43B). Finally, length distribution analyses revealed a differential distribution within samples with two predominant read lengths at 33 and 36 nt within the HD-sRNA-PT and the CTL-sRNA-PT pools. A massive increase in sequences of 33 nt in length was detected in the HD-sRNA-PT sample compared to the CTL-sRNA-PT pool, although similar abundances among conditions were observed for the 36 nt length peak (Figure 43C).

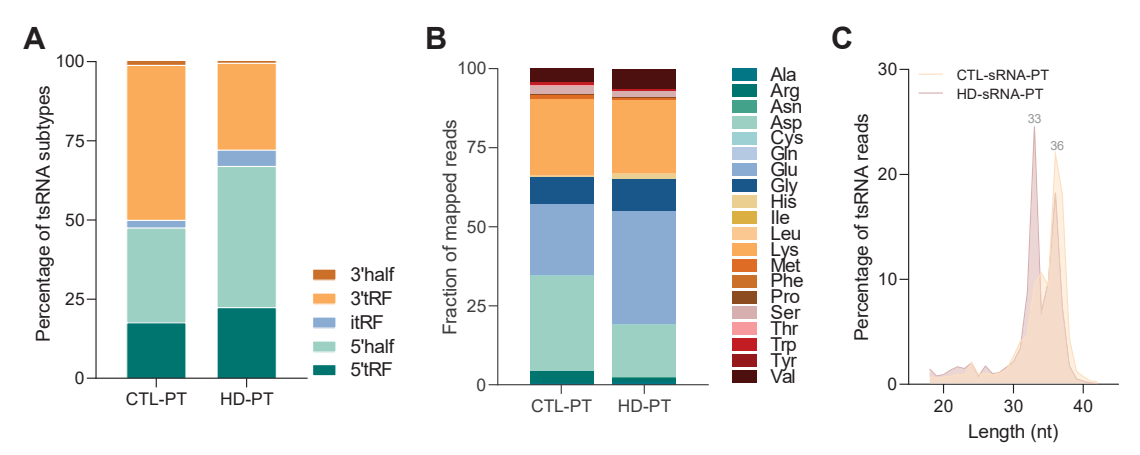
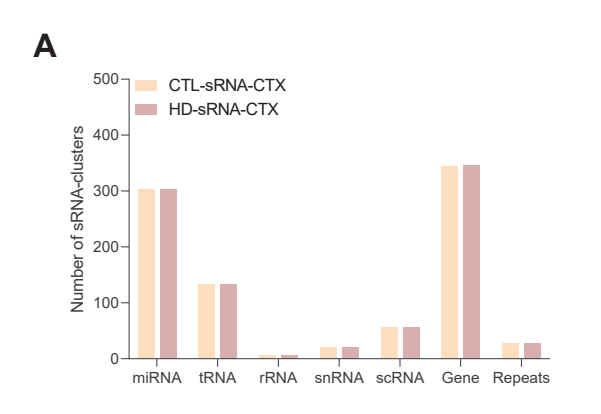
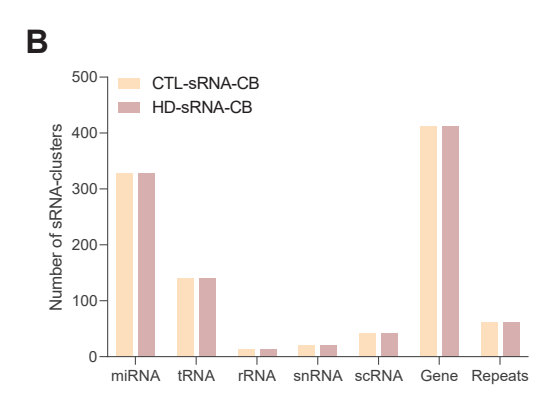


Figure 43. CTL- and HD-sRNA-PT pools display distinct proportions in terms of tsRNA subtypes, tsRNA isoacceptors and tsRNA read lengths. (A) Abundance of tsRNA mapped reads corresponding to different subtypes of tsRNA in CTL-sRNA-PT and HD-sRNA-PT samples. (B) Abundance of tsRNA mapped reads within CTL-sRNA-PT and HD-sRNA-PT pools classified according to precursor tRNA isoacceptors. (C) Length distribution profiles of the mapped tsRNA reads within CTL-sRNA-PT and HD-sRNA-PT pools.

In order to evaluate whether sRNA transcriptome dysregulation was brain region specific, analogous sRNA-sequencing analyses were performed in samples obtained from the frontal cortex and cerebellum of HD patients together with their corresponding controls. Segcluster tool revealed a total of around 980 clusters in the CTL- and HD-sRNA-CTX pools, most of which were identified as miRNA- and gene-clusters (Figure 44A). In the case of sRNA pools obtained from the cerebellum, we detected around 1100 different clusters, with miRNA- and gene-clusters being also the most abundant mapped biotypes (Figure 44B). However, regarding the fraction of mapped reads within each sample, miRNA- and tRNA-clusters presented the greatest abundance in both sRNA-CTX and sRNA-CB samples. Specifically, miRNA-clusters were the predominant biotype observed in CTL-sRNA-CTX and CTLsRNA-CB whereas tRNA-clusters were the most abundant representatives in HDsRNA-CTX and HD-sRNA-CB pools (Figure 44C and D). Therefore, similar biotype distribution patterns were observed in sRNA pools obtained from all the examined brain areas, including the putamen (Figure 41B). Yet, differences between HD-sRNA and CTL-sRNA conditions were less pronounced in the frontal cortex and cerebellum compared to the putamen, especially regarding tRNA-clusters.





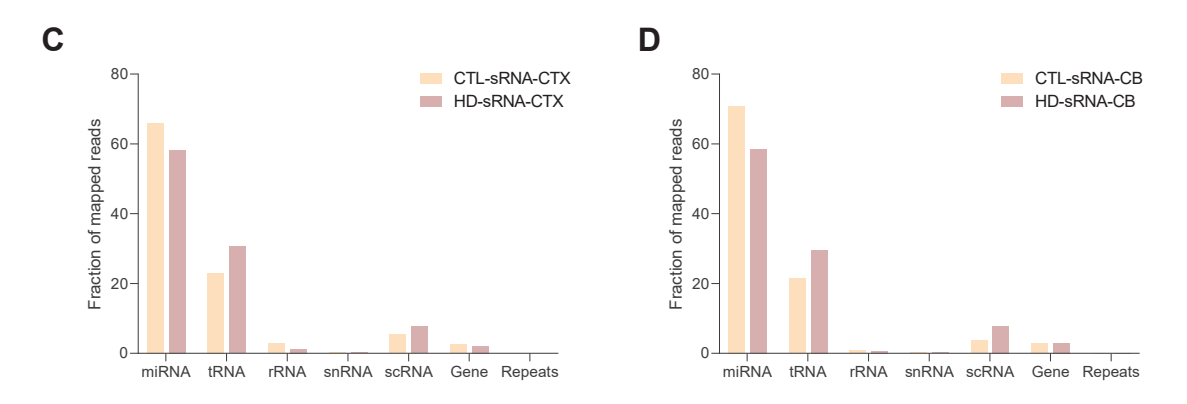
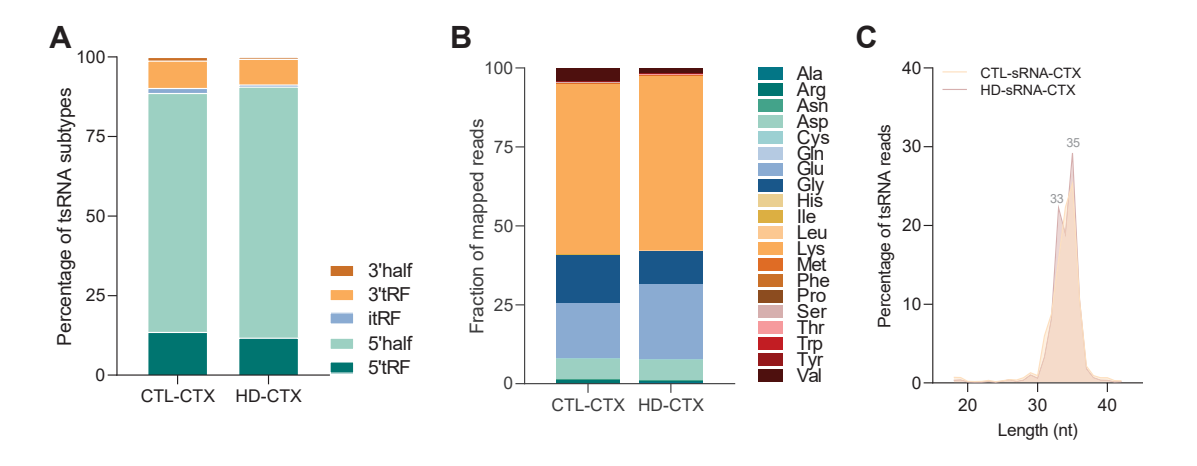


Figure 44. Distinct biotype distributions are observed between CTL- and HD-sRNA pools but not among the frontal cortex and the cerebellum. (A-B) Total number of sRNA-clusters classified by sRNA biotypes in human *post-mortem* samples obtained from the (A) frontal cortex and (B) cerebellum. (C-D) Fraction of mapped reads annotating onto the different sRNA biotypes in (C) CTL- and HD-sRNA-CTX pools and in (D) CTL- and HD-sRNA-CB pools.

Subsequently, MINTbase database (Pliatsika et al., 2018) was used to annotate the sequences of the obtained reads identified as tRNA into different tsRNA subtypes and isoacceptors. Consistently with the results observed in the HD-sRNA-PT samples, a massive overrepresentation of 5'tRFs and 5'halves was observed in HD-sRNA-CTX and HD-sRNA-CB pools (Figure 45A and D). However, we could not detect any differences between CTL- and HD-sRNA in none of the two examined brain areas. Similar findings were obtained when analyzing the precursor tRNA isoacceptors that served as tsRNA source, where tRFs derived from tRNA^{Asp}, tRNA^{Glu}, tRNA^{Gly} and tRNA^{Lys} were predominantly represented in all the conditions analyzed (Figure 45B and E). Next, length distribution analyses showed analogous read lengths along all samples revealing the presence of two main read lengths of 33 and 35 nt (Figure 45C and F).



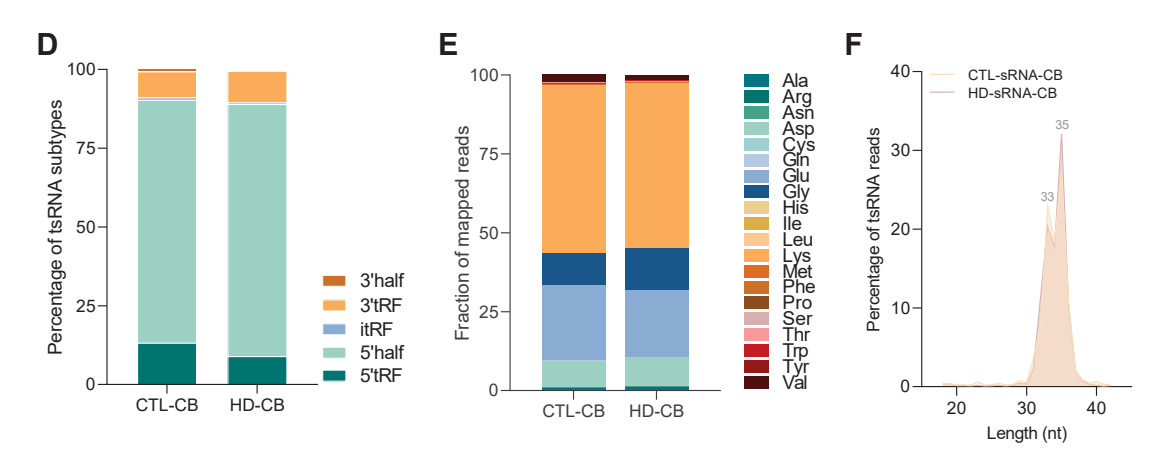


Figure 45. tsRNA subtypes, tsRNA isoacceptors and tsRNA read lengths show similar proportions between CTL- and HD-sRNA pools derived from frontal cortex or cerebellum. (A,D) Abundance of tsRNA mapped reads corresponding to different subtypes of tsRNA in (A) CTL- and HD-sRNA-CTX pools and in (D) CTL- and HD-sRNA-CB pools. (B,E) Abundance of tsRNA mapped reads classified according to precursor tRNA isoacceptors within (B) CTL- and HD-sRNA-CTX pools and (E) CTL- and HD-sRNA-CB pools. (C,F) Length distribution profiles of the mapped tsRNA reads within (C) CTL- and HD-sRNA-CTX pools and in (F) CTL- and HD-sRNA-CB pools.

Having defined the specific tsRNA profiles in the putamen, frontal cortex and cerebellum of HD patients compared to non-affected individuals, we wondered whether analogous dysregulations were observed throughout different brain regions under pathological conditions. A heatmap of tsRNA expression patterns across the abovementioned brain areas showed that both upregulation and downregulation of certain tsRNA derived from the same tRNA isoacceptors was more pronounced in the putamen compared to the frontal cortex and the cerebellum of HD patients (Figure 46). These findings are consistent with previous evidence linking stress-induced tRNA fragmentation to neurodegeneration (Blanco et al., 2014; Hanada et al., 2013; Pantano et al., 2016).

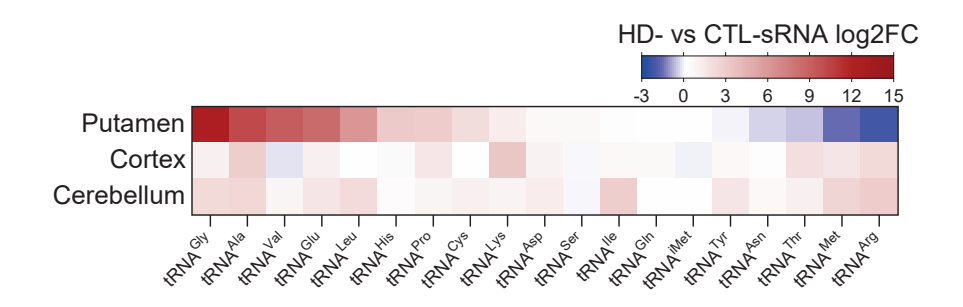


Figure 46. Divergent tsRNA expression profiles are observed across differently affected brain regions. Heatmap representing the log2 fold changes of the tRNA clusters comparing HD- and CTL-sRNA from the putamen, frontal cortex, and cerebellum. All tRNA clusters mapping onto each tRNA isotype were represented together.

Next, read coverage along each position of the mature tRNA isoacceptor was examined using the SeqclusterViz tool (Pantano et al., 2011) to compare tsRNA sequences mapping and abundance within CTL- and HD-sRNA pools. As a result of this analysis, we identified specific tsRNA sequences that were overrepresented in the HD-sRNA-PT pool in comparison to the CTL-sRNA-PT sample. tRFs produced from tRNA^{Ala}, tRNA^{Gly}, tRNA^{Val} and tRNA^{Glu} displayed the highest fold changes between conditions (Figure 47A). In addition, the expression levels of the selected tRFs were further validated in the putamen of an independent cohort of control individuals and HD patients by RT-qPCR. Consistently with sRNA-sequencing data, 5'tRF-Ala, 5'tRF-Glu, 5'tRF-Gly and 5'tRF-Val were significantly upregulated in the putamen of HD patients compared to control subjects (Figure 47B).

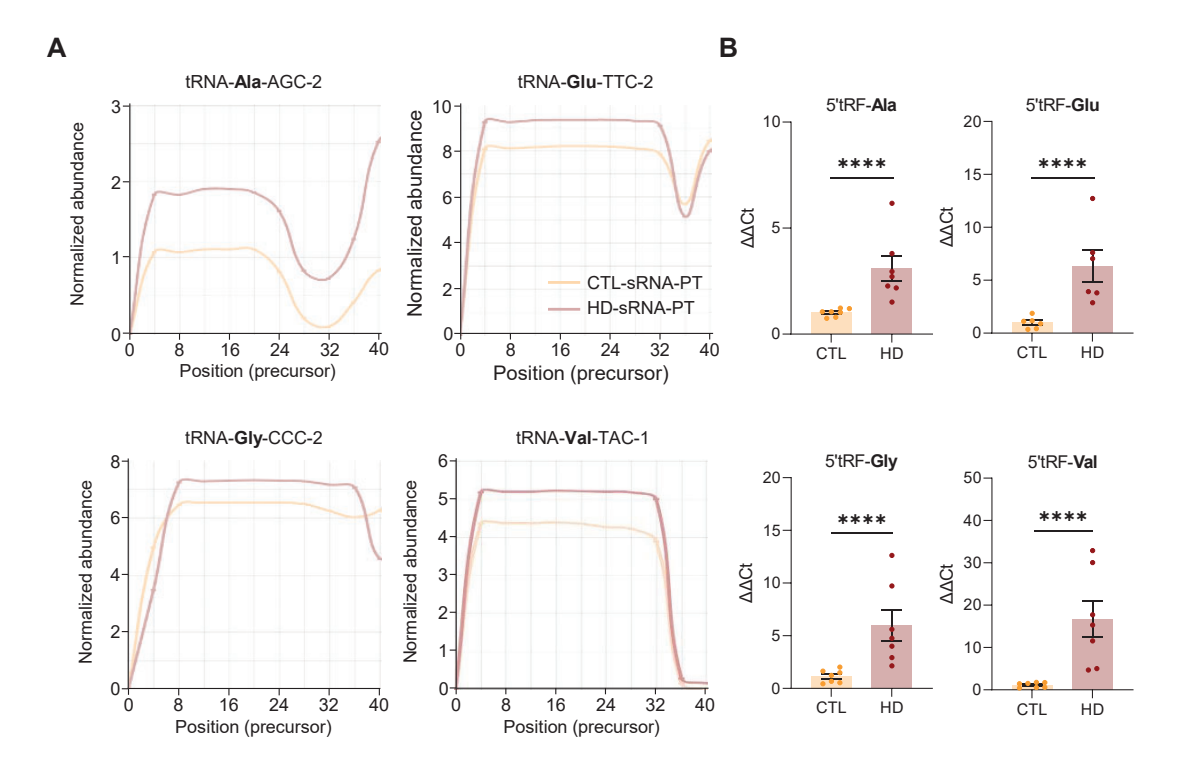


Figure 47. The putamen of HD patients shows an overrepresentation of specific 5'tRFs. (A) Normalized abundance profiles of different tsRNA along the length of the corresponding mature tRNA precursors. tsRNA detected in CTL- and HD-sRNA-PT pools and derived from tRNA-Ala-AGC-2, tRNA-Glu-TTC-2, tRNA-Gly-CCC-2 and tRNA-Val-TAC-1 are represented. (B) Expression levels of the selected 5'tRF candidates in the putamen of control individuals (CTL) and HD patients (HD) were determined by RT-qPCR using miRCURY LNA custom PCR assays. r18S was used as a reference gene. Relative quantification (RQ) was calculated with the 2ΔΔCt method. CTL-sRNA-PT n = 6-7; HD-sRNA-PT n = 6-7. Each point represents data from an individual subject. Values are shown as mean ± SEM. ****P < 0.0001 versus the indicated group; calculated using a linear mixed-effects model followed by Bonferroni post hoc test.

In parallel, SeqclusterViz tool revealed that tsRNA expression profiles presented certain differences between CTL- and HD-sRNA pools obtained from the frontal cortex and the cerebellum compared to the putamen. In fact, milder changes in

comparison to their respective controls or even no changes between conditions were detected in sRNA-CTX (Figure 48A) and sRNA-CB pools (Figure 48B). This result is consistent with the observed tsRNA expression profiles across differently affected brain regions in Figure 46 strengthening the idea that these areas present intrinsic and specific biochemical characteristics underlying tsRNA biogenesis.

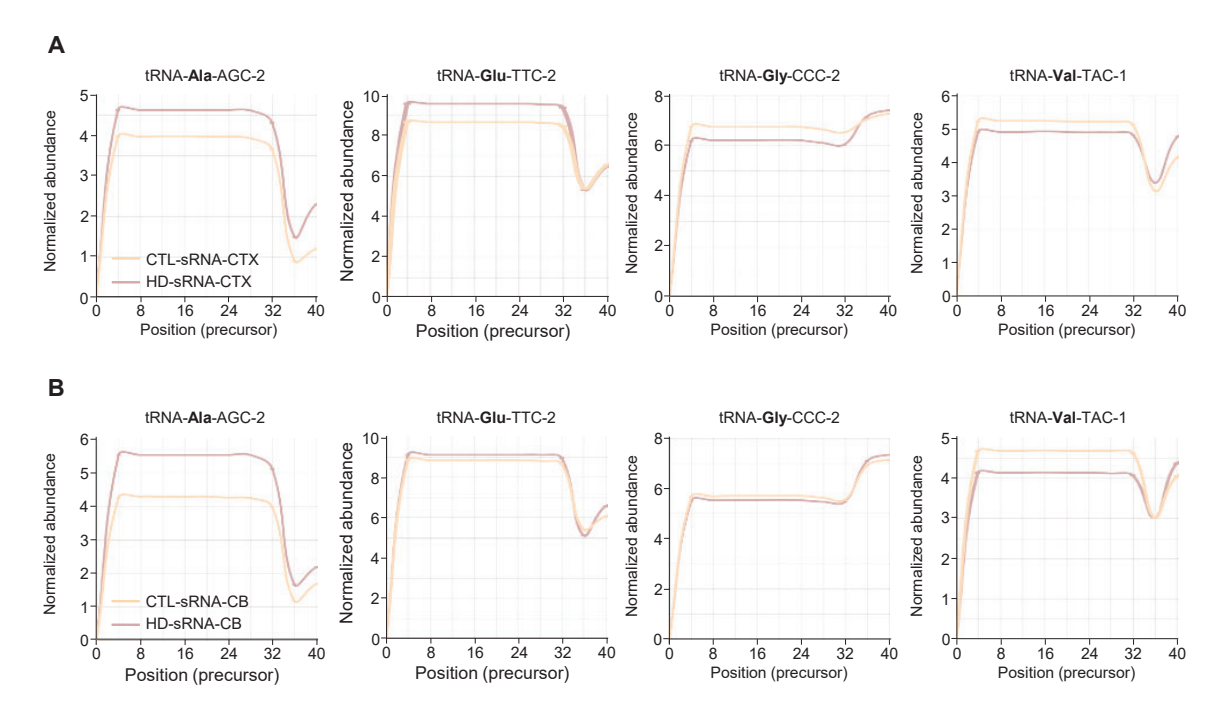


Figure 48. tsRNA expression patterns in HD present differences depending on the examined brain region. Normalized abundance profiles of selected tsRNA along the length of the corresponding mature tRNA precursors in **(A)** sRNA-CTX and **(B)** sRNA-CB pools. tsRNA belonging to tRNA-Ala-AGC-2, tRNA-Glu-TTC-2, tRNA-Gly-CCC-2 and tRNA-Val-TAC-1 are shown.

2.2 Specific tsRNA species which are overproduced in HD putamen display neurotoxic effects

Given the fact that specific 5'tRFs have been shown to regulate neural response to stress (Blanco et al., 2014; Hanada et al., 2013; Ivanov et al., 2014) and are also overexpressed in HD-sRNA-PT, we wondered if these species could be participating in the neurotoxicity widely described in HD. To explore the effect of specific 5'tRFs in neurons, primary cultured WT striatal neurons were treated with synthetic RNA oligonucleotides mimicking different HD-sRNA-PT-overrepresented 5'tRFs, namely 5'tRF-Ala, 5'tRF-Val and 5'tRF-Gly, and cell viability was evaluated using the MTS assay (Figure 49A). Uptake of the RNA oligonucleotides by cultured cells was performed without any transfection reagents in a process called gymnosis, in order to resemble the *in vivo* experiments performed. As internal controls, antisense sequences of the selected 5'tRF oligonucleotides were used. Moreover, treatment with hydrogen peroxide (H_2O_2) was included as a positive control for cell death. Treatment with 5'tRF-Ala in the sense version resulted in decreased cell viability

whereas other 5'tRF did not present any effect at the time and dose assessed (Figure 49B). Additionally, a dose response assay was performed for the 5'tRF-Ala using both sense and antisense oligonucleotides at different concentrations and cell viability was measured following the same experimental design described in Figure 49A. Dosages over 30 ng of 5'tRF-Ala were able to dramatically decrease cell viability in comparison to the treatment with the antisense sequence at equal concentrations (Figure 49C). Altogether, these data suggest that specific 5'tRFs, which are overexpressed in HD patients' putamen, induce striatal neuronal death and could be contributing to the neurotoxicity observed after HD-sRNA injections together with other sRNA species.

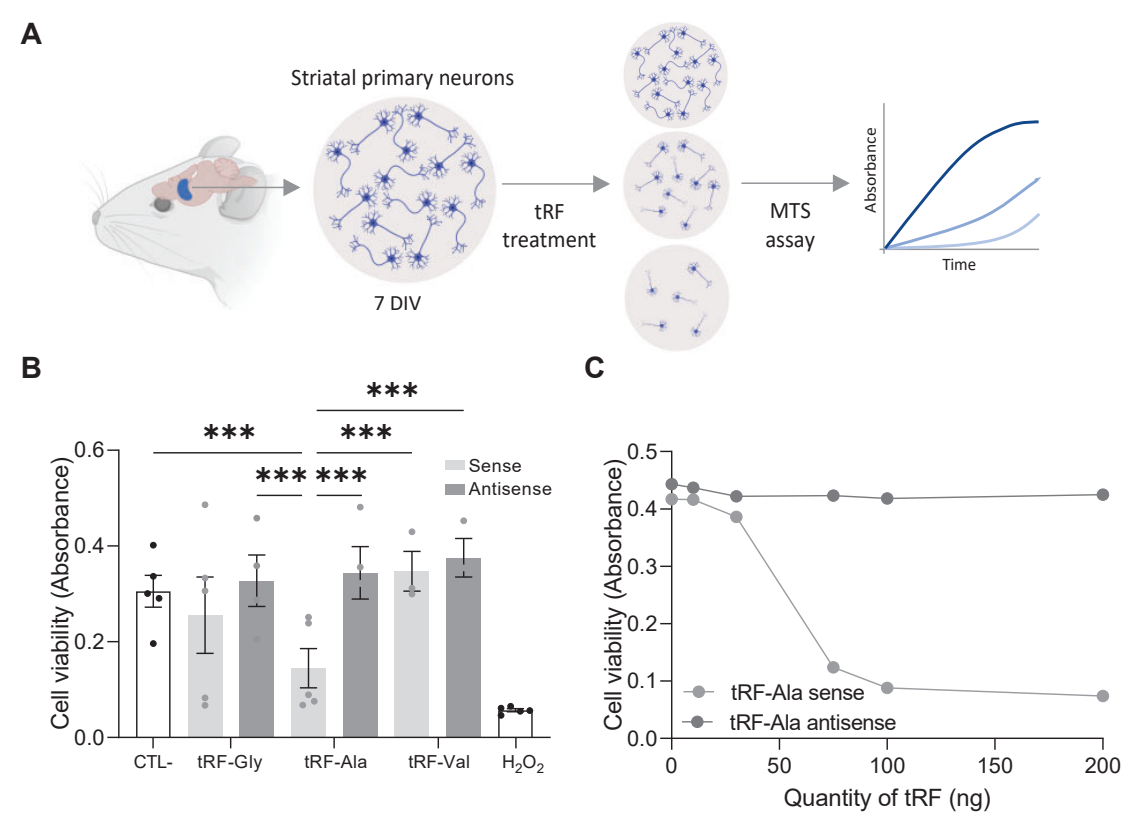


Figure 49. Specific 5'tRFs compromise neuronal viability. (A) Schematic representation of the experimental design. Striatal primary neuronal cultures at 7 DIV were treated with synthetic RNA oligonucleotides mimicking HD-sRNA-PT-dysregulated 5'tRFs in the sense version. Antisense sequences of the same oligonucleotides were used as controls. Cell viability was measured using MTS assay 1 h after treatment. (B) Cell viability determination after treatment with 5'tRF sense and antisense oligonucleotides (200ng). Treatment with H_2O_2 was used as positive control. Non-treated (CTL-) n = 5; Gly sense n = 5; Gly antisense n = 4; Ala sense n = 6; Ala antisense n = 4; Val sense n = 3; Val antisense n = 3; H_2O_2 n = 5. Each point represents data from an independent culture. ***P < 0.001 versus all other groups; calculated using a linear mixed-effects model followed by Bonferroni *post hoc* test. (C) Dose response assay determined after treatment with 5'tRF-Ala sense and antisense oligonucleotides at different concentrations (0, 10, 30, 75, 100 and 200 ng/well) for 1 h. In (B-C), values are expressed as the difference in absorbance 15 min and 3 h after MTS exposure in each well and shown as mean \pm SEM.

3. Study of the contribution of key players involved in tsRNA biogenesis in HD pathogenesis

3.1 The RNA methyltransferase NSun2 is altered in HD patients and several HD models

It has been widely described that tRNA can be processed into tsRNA by different ribonucleases under specific stimuli (R. Magee & Rigoutsos, 2020). Thus, to investigate whether these enzymes could be altered in HD brains, we analyzed their protein levels by WB in two brain regions differentially affected by the disease. Although tRNA fragmentation depends on several ribonucleases, ANG and RNAse T2 ribonucleases did not present altered levels in the putamen nor in the frontal cortex of HD patients in comparison to control individuals (Figure 50A and B). However, alterations in the activity of these enzymes could not be discarded.

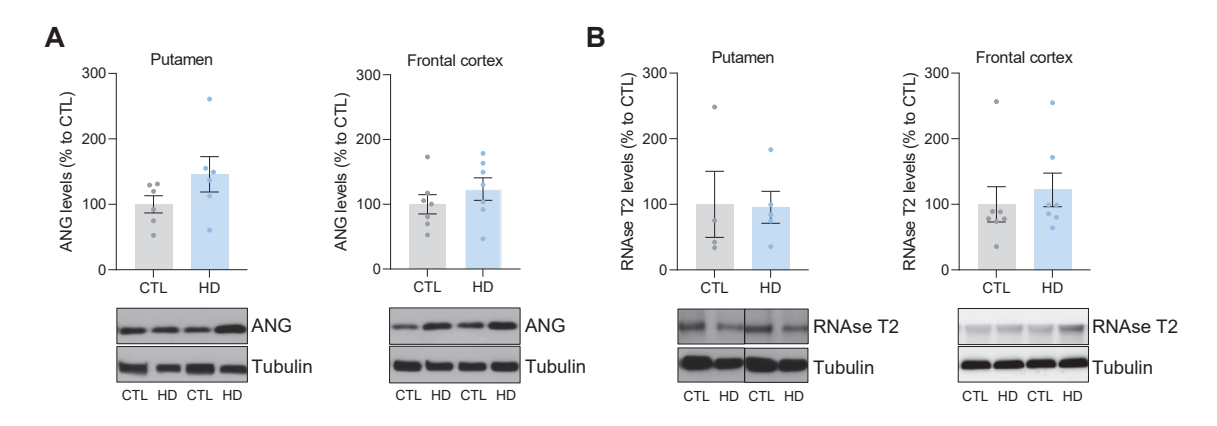


Figure 50. ANG and RNAse T2 protein levels are not altered either in HD putamen or frontal cortex. Protein levels of (A) ANG and (B) RNAse T2 were analyzed by WB in protein extracts from the putamen and the frontal cortex of HD patients and non-affected individuals. Tubulin was used as loading control. Representative immunoblots are shown. CTL n = 4-7; HD n = 5-7. Each point represents data from an individual subject. Values are expressed as percentage to control samples and shown as mean \pm SEM.

After establishing that the overproduction of tsRNA in HD was not associated with increased levels of tRNA fragmentation enzymes, we wondered whether tRNA stability could be affected. Cytosine-5 tRNA methylation has been described as an important epitranscriptomic modification that contributes to tRNA stability and, in turn, is able to regulate tsRNA production (Blanco et al., 2014; Lyons et al., 2018; Tuorto et al., 2012). In fact, the loss of particular tRNA modifications enhances the sensitivity to different stressors (Begley et al., 2007; Jablonowski et al., 2006; M. Schaefer et al., 2010). Therefore, we wondered whether the levels of the cytosine-5 methyltransferase NSun2 were modified in HD, leading to the massive increase in tsRNA observed in the putamen. WB analysis revealed significantly decreased protein levels of NSun2 in the putamen of HD patients compared to non-affected individuals (Figure 51A). Besides, a tendency toward reduced NSun2 levels was observed in the other brain regions analyzed in comparison to analogous brain

areas of control subjects, although it did not reach significance in any case (Figure 51B-D). Next, we wondered whether NSun2 alterations were associated to subjects' age or disease progression. However, no significant correlation was found between NSun2 protein levels and the age of the examined HD subjects (r = 0.349; P value = 0.063; Figure 51E) or the Vonsattel stage (r = -0.09; P value = 0.78; Figure 51F).

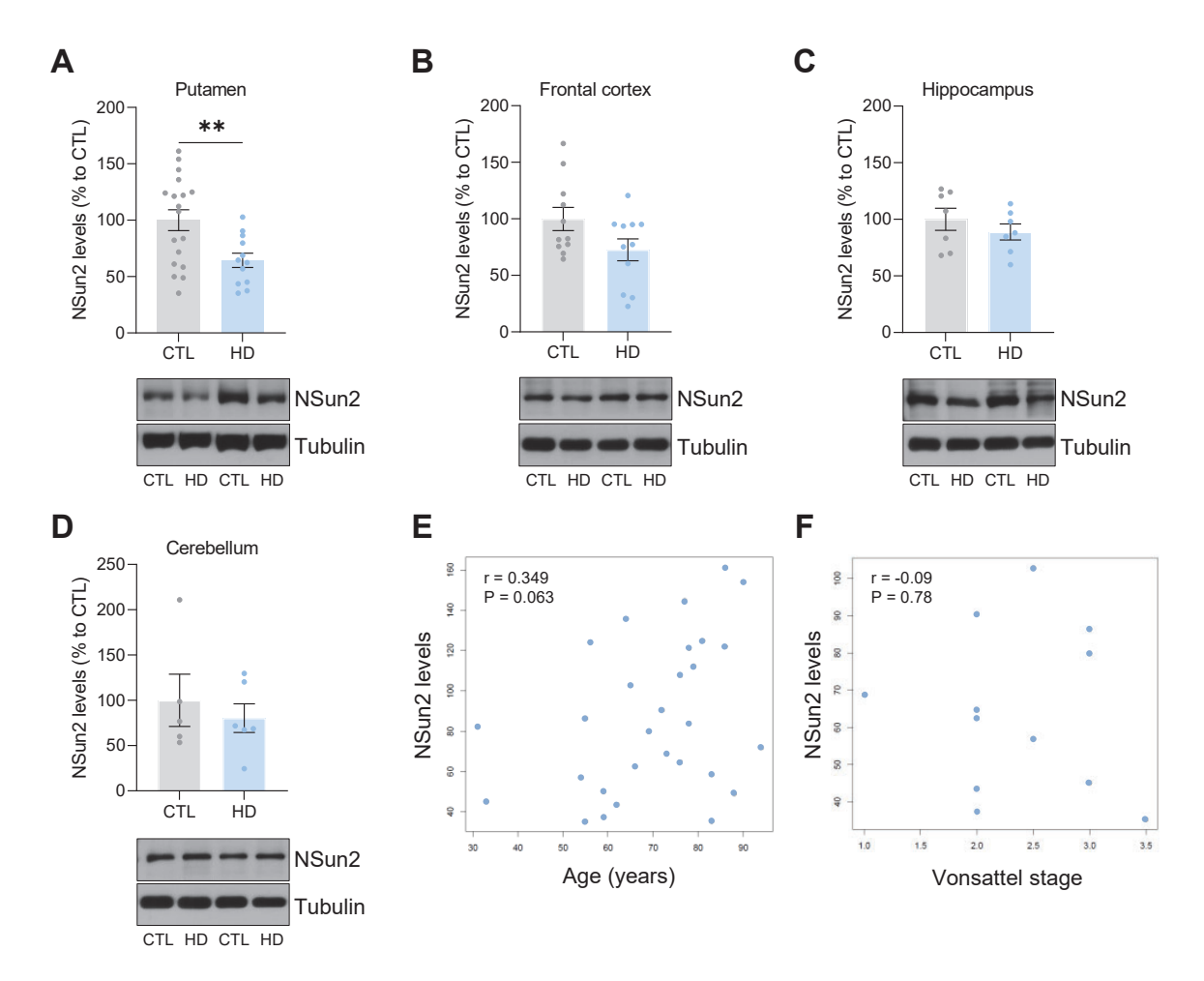


Figure 51. NSun2 protein levels are decreased in the putamen of HD patients. (A-D) Protein levels of NSun2 were analyzed by WB in protein extracts from the (A) putamen, (B) frontal cortex, (C) hippocampus and (D) cerebellum of HD patients and non-affected individuals. Tubulin was used as loading control. Representative immunoblots are shown. CTL n = 6-18; HD n = 6-12. Each point represents data from an individual subject. Values are expressed as percentage to control samples and shown as mean \pm SEM. **P < 0.01 versus the indicated group; calculated by two-tailed unpaired Student's t-test. (E-F) Correlation analysis between NSun2 protein levels and (E) age or (F) Vonsattel stage, determined by simple linear regression in putamen samples from HD patients. P values and Pearson correlation coefficients (r) are indicated in the graphs.

Next, we examined whether there was an increased abundance in the HD-sRNA-PT pool of some tsRNA produced from tRNA described as NSun2 methylation targets (Auxilien et al., 2012; Brzezicha et al., 2006; Khoddami & Cairns, 2013; Squires et al., 2012; Tuorto et al., 2012). In agreement with our hypothesis, different NSun2-

targeted tRNA were found fragmented and overrepresented in the putamen of HD patients in comparison to non-affected individuals using SeqclusterViz tool (Figure 52). Therefore, our analyses suggested that many of the tsRNA overrepresented in HD are dependent on the methylation status of the mature tRNA precursor.

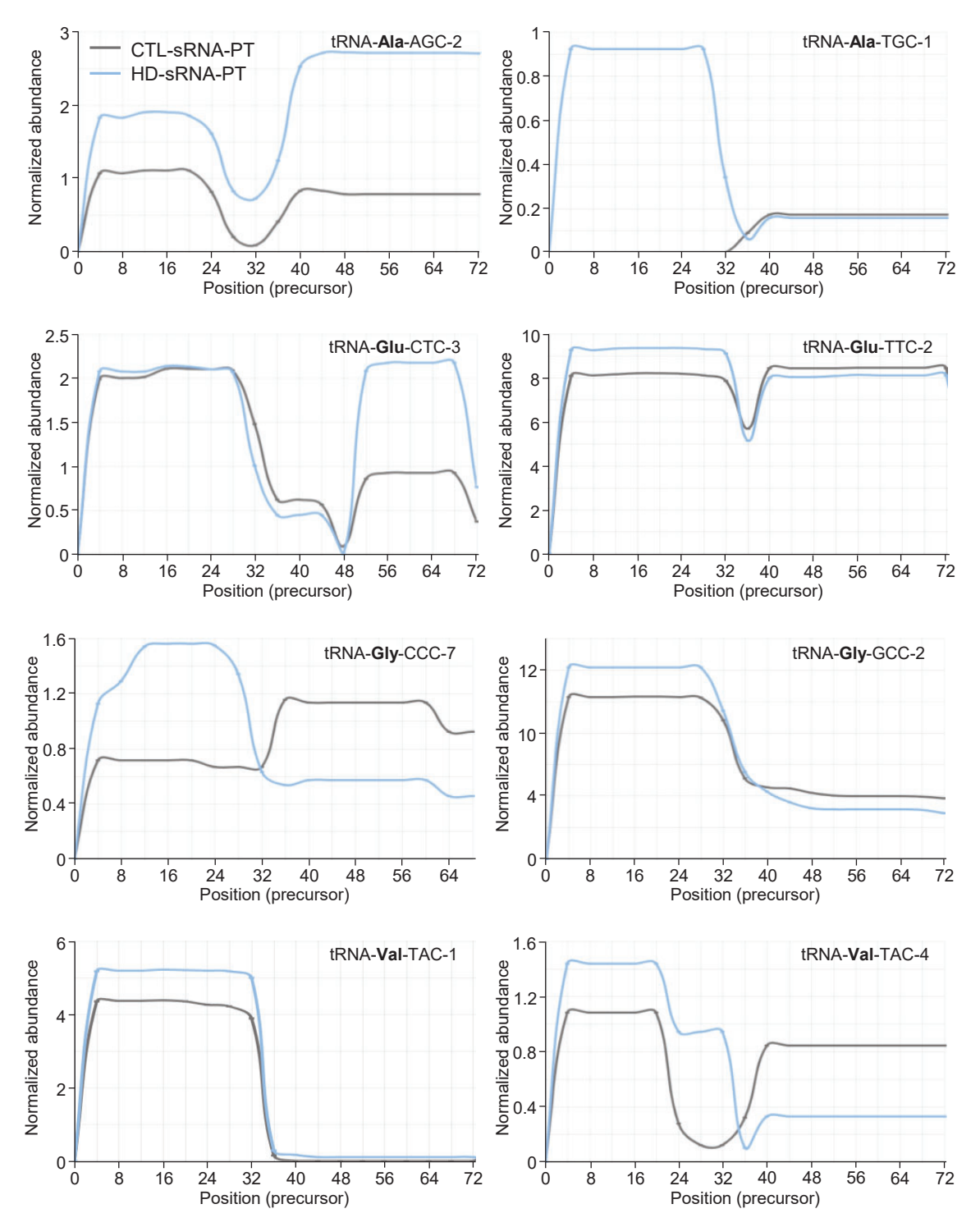


Figure 52. Overrepresentation of specific tsRNA derived from NSun2-targeted tRNA in the putamen of HD patients. Normalized abundance profiles of different tsRNA along each position of the mature tRNA isoacceptor. tsRNA derived from tRNA-Ala-AGC-2, tRNA-Ala-TGC-1, tRNA-Glu-CTC-3, tRNA-Glu-TTC-2, tRNA-Gly-CCC-7, tRNA-GCC-2, tRNA-Val-TAC-1 and tRNA-Val-TAC-4 and detected in CTL- and HD-sRNA-PT pools are represented.

On the basis of these results, we decided to evaluate whether NSun2 alterations were also reproduced in different HD models, both *in vivo* and *in vitro*. To this end, we started by analyzing protein lysates obtained from the striatum of WT and R6/1 male and female mice by WB. Several ages were tested to evaluate alterations throughout the disease progression (from post-natal day 6 to 30 weeks of age).

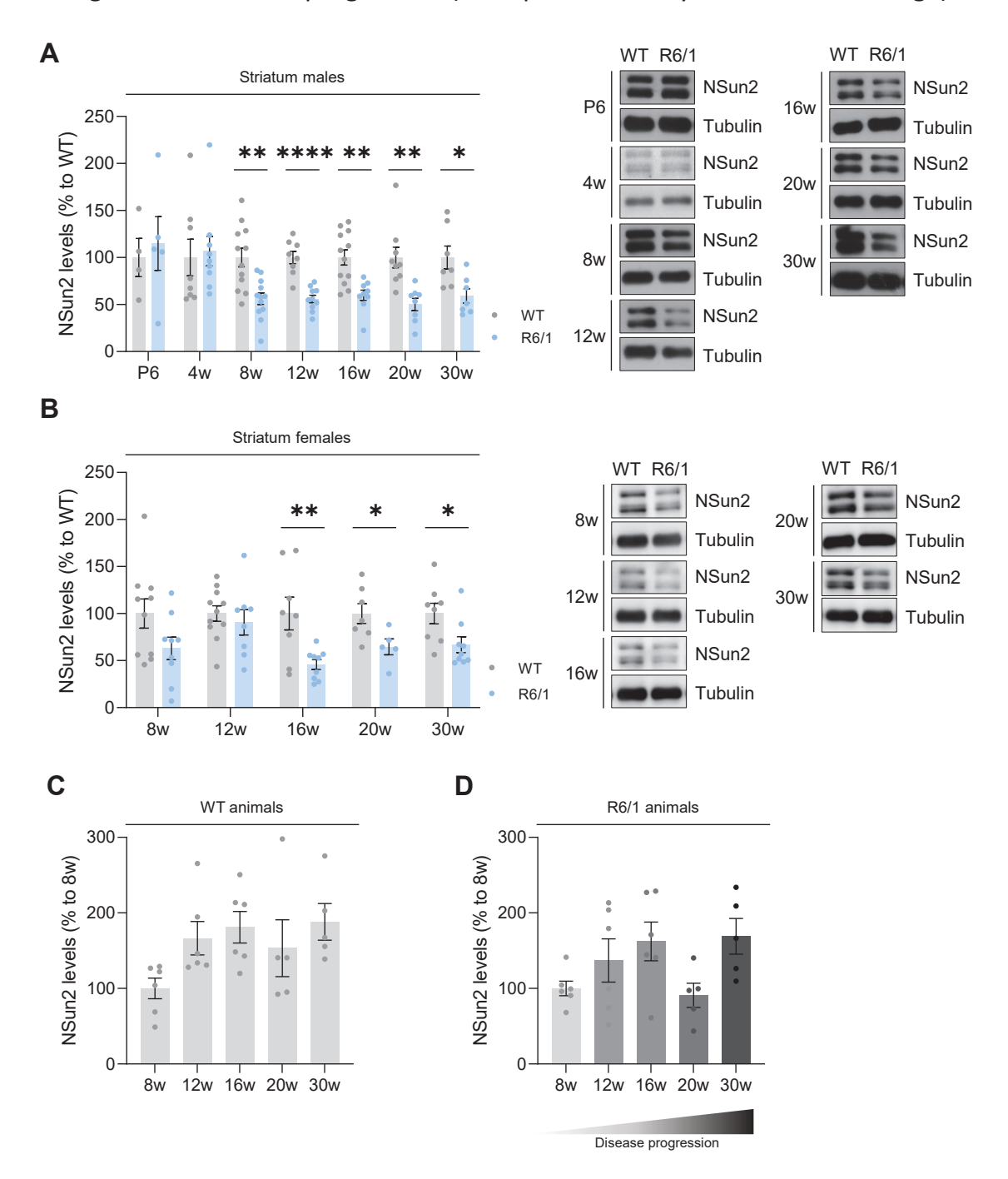
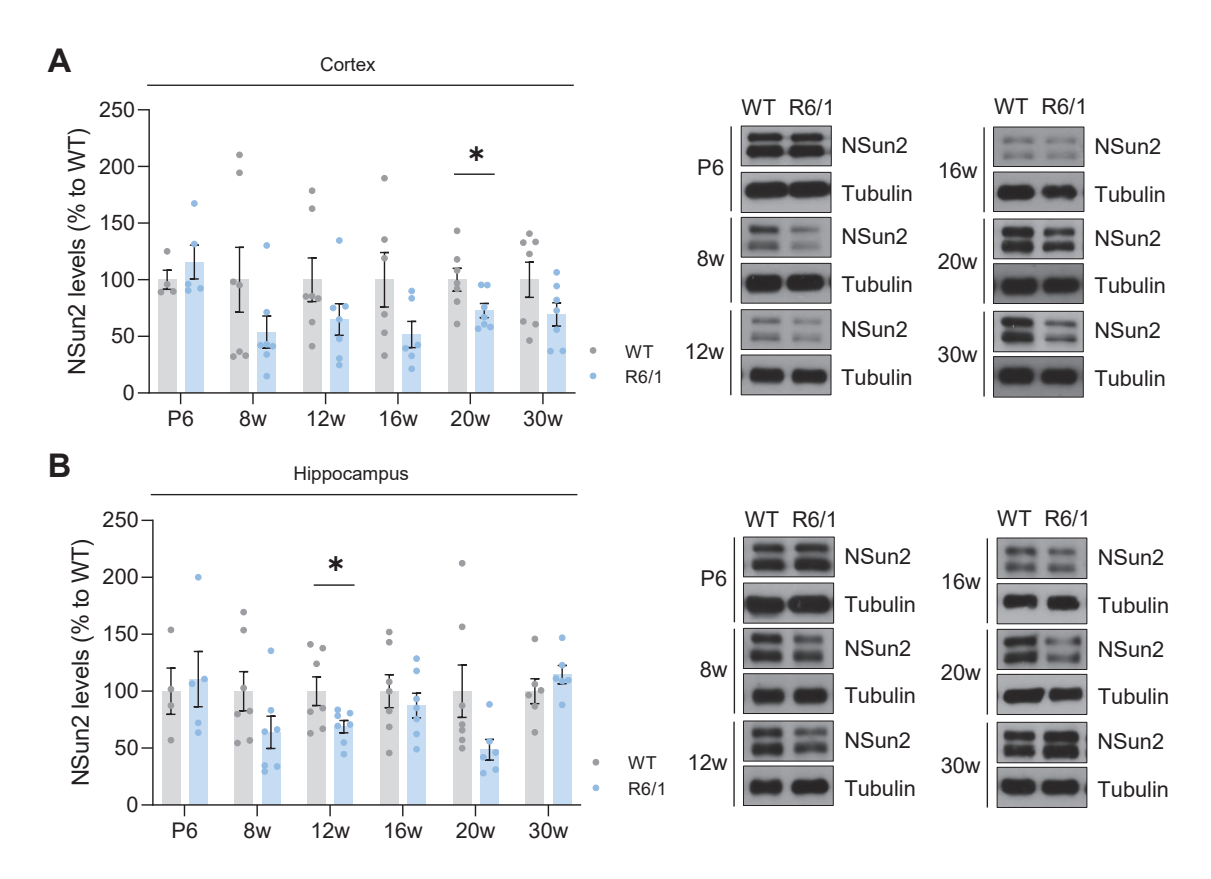


Figure 53. NSun2 protein levels are decreased in the striatum of R6/1 mice. Protein levels of NSun2 were analyzed by WB in striatal lysates from WT and R6/1 animals. (A) For males, post-natal day 6 (P6), 4, 8, 12, 16, 20 and 30 weeks (w) of age were evaluated. (B) For females, 8, 12, 16, 20 and 30 w were analyzed. (C-D) For the time course, males of 8, 12, 16, 20 and 30 w were examined. Tubulin was used as a loading control. Representative immunoblots are shown. WT males n = 4-12; R6/1 males n = 5-12; WT females n = 7-11;

R6/1 females n = 5-9. Each point represents data from an individual mouse. Values are expressed as percentage to WT animals in **(A-B)** and to 8 w mice in **(C-D)** and shown as mean \pm SEM. ****P < 0.0001, **P < 0.01 and *P < 0.05 versus the indicated groups; calculated by two-tailed unpaired Student's t-test.

In line with the results obtained in HD patients, we detected a significant decrease in NSun2 protein levels in the striatum of R6/1 mice compared to their corresponding WT littermates, starting from pre-symptomatic stages of the disease (Figure 53A and B). However, time course analyses in the striatum did not show significant changes in protein levels along ageing in WT mice (Figure 53C) or along disease progression in R6/1 mice (Figure 53D), reinforcing the idea that NSun2 reduction is tightly associated with HD pathophysiological mechanisms.

Subsequently, total protein lysates of cortex, hippocampus and cerebellum obtained from the same animals were also analyzed by WB. In contrast to the results obtained in the striatum, no consistent differences between R6/1 and WT mice were observed in these brain areas along disease progression, although a tendency to decrease was observed in many cases (Figure 54).



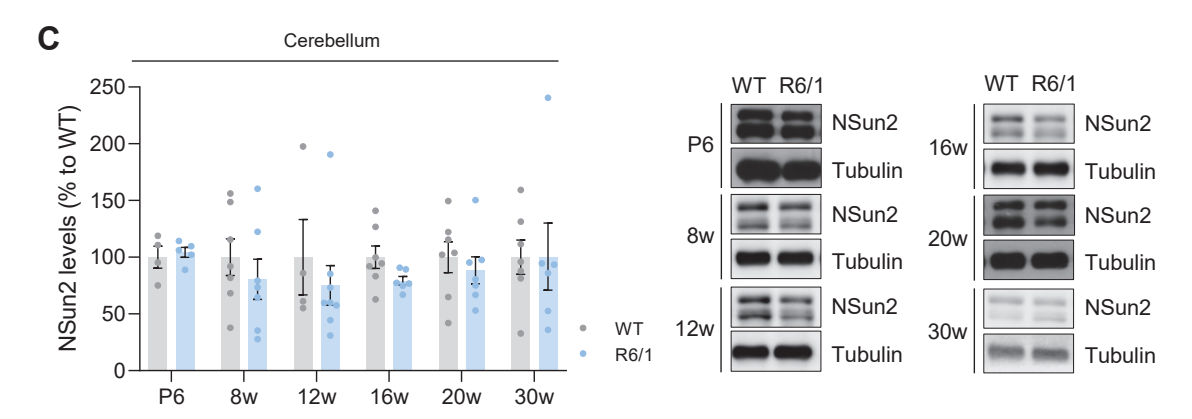


Figure 54. NSun2 protein levels are not altered in the cortex, hippocampus, and cerebellum of R6/1 mice. Protein levels of NSun2 were analyzed by WB in total lysates from the (A) cortex, (B) hippocampus and (C) cerebellum of WT and R6/1 animals. For each genotype, post-natal day 6 (P6), 8, 12, 16, 20 and 30 weeks (w) of age were evaluated. Tubulin was used as a loading control. Representative immunoblots are shown. WT n = 4-7; R6/1 n = 5-8. Each point represents data from an individual mouse. Values are expressed as percentage to WT animals and shown as mean \pm SEM. *P < 0.05 versus the indicated groups; calculated by two-tailed unpaired Student's t-test.

Finally, analogous WB studies were performed in a different HD mouse model to validate the obtained results. Specifically, both the striatum of Hdh^{Q7/Q111} KI mice and the striatal cell line STHdh^{Q111/Q111} were analyzed. Consistently with the R6/1 mouse model, a significant lowering in the striatum of KI male mice compared to WT animals was detected since initial stages of the disease (Figure 55A). A similar reduction was also observed in STHdh^{Q111/Q111} in comparison to STHdh^{Q7/Q7} cells (Figure 55B).

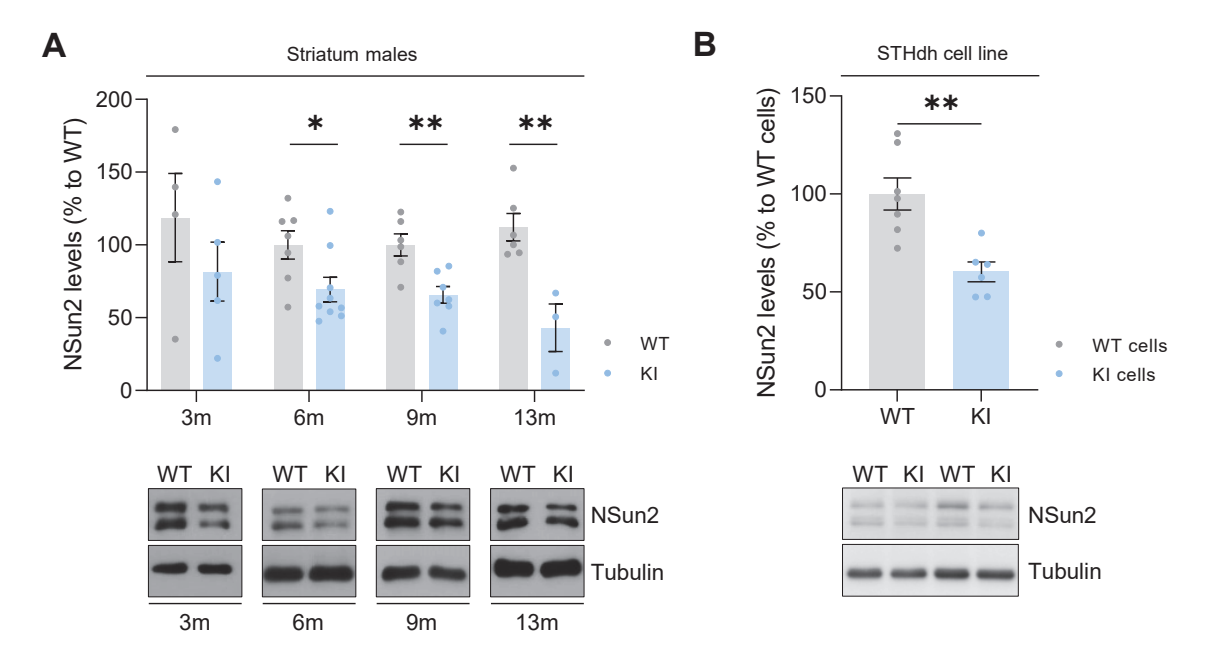


Figure 55. NSun2 protein levels are decreased in the striatum of KI mice and in STHdh^{Q111/Q111} striatal cells. (A) Protein levels of NSun2 were analyzed by WB in striatal

lysates from male WT and KI animals. For each genotype, 3, 6, 9 and 13 months (m) of age were evaluated. WT n = 4-7; KI n = 3-9. **(B)** Protein levels of NSun2 were analyzed by WB in total lysates from WT (STHdh $^{Q7/Q7}$) and KI (STHdh $^{Q111/Q111}$) cells. WT n = 7; KI n = 6. In **(A-B)**, tubulin was used as a loading control and representative immunoblots are shown. Each point represents data from an individual mouse or a different cell passage. Values are expressed as percentage to WT animals or cells, and shown as mean \pm SEM. **P < 0.01 and *P < 0.05 versus the indicated group; calculated by two-tailed unpaired Student's t-test.

Given the previous findings, the next step was to explore whether Dnmt2, the other widely studied cytosine-5 tRNA methyltransferase in higher eukaryotes (Tuorto et al., 2012), presented similar alterations. To assess this, striatal protein lysates from WT and R6/1 male and female mice were used for WB analyses. Although several stages of the disease were tested (from 8 to 30 weeks of age), no significant alterations in Dnmt2 protein levels were observed (Figure 56A and B). Unaltered levels of Dnmt2 point to a lack of compensation of NSun2 reduction and reinforce the idea of a loss of cytosine-5 tRNA methylation as a potential contributor to tsRNA biogenesis in the HD context.

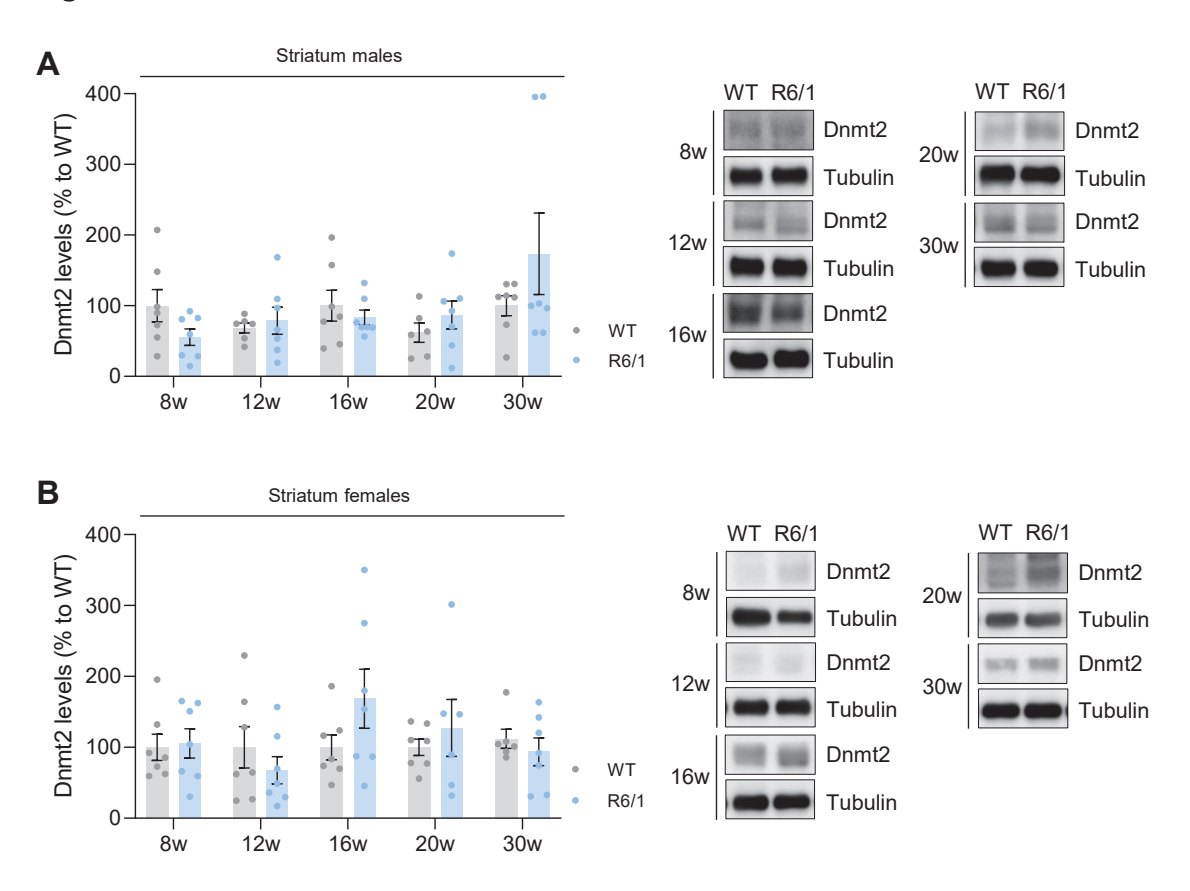


Figure 56. Dnmt2 protein levels remain unaltered in the striatum of male and female R6/1 mice along disease progression. Protein levels of Dnmt2 were analyzed by WB in striatal lysates from WT and R6/1 animals, both (A) males and (B) females. For each genotype, 8, 12, 16, 20 and 30 weeks (w) of age were evaluated. Tubulin was used as a loading control. Representative immunoblots are shown. WT males n = 6-7; R6/1 males n = 7; WT females n = 6-7; R6/1 females n = 6-7. Each point represents data from an individual mouse. Values are expressed as percentage to WT animals and shown as mean \pm SEM.

Having validated the decreased NSun2 protein levels in the striatum of R6/1 mice, we took advantage of this mouse model to investigate whether it was general reduction or a cell-type specific alteration. Moreover, since it has been described that MSNs represent the main neuronal population in the striatum (Gerfen, 1988) and are the most affected cell type in HD (Bergonzoni et al., 2021; Y. P. Deng et al., 2004; Reiner et al., 1988; Sapp et al., 1995), we focused on the analysis of this specific neuronal population. Hence, we performed double immunohistofluorescence against NSun2 and Ctip2 in order to specifically distinguish MSNs nuclei (Alcalá-Vida et al., 2021; Arlotta et al., 2008) among other striatal cell types. Selected striatal brain slices corresponded to 15-weeks-old WT and R6/1 mice, a disease stage where animals already present cognitive and initial motor alterations together with NSun2 reduced levels. Confirming the results obtained by WB analysis (Figure 53), a general reduction in NSun2 mean intensity was detected in the striatum of R6/1 mice compared to WT animals (Figure 57A and B). Additionally, specific analysis of Ctip2-positive nuclei showed that MSNs subpopulation was affected by this reduction in NSun2 levels (Figure 57C and D).

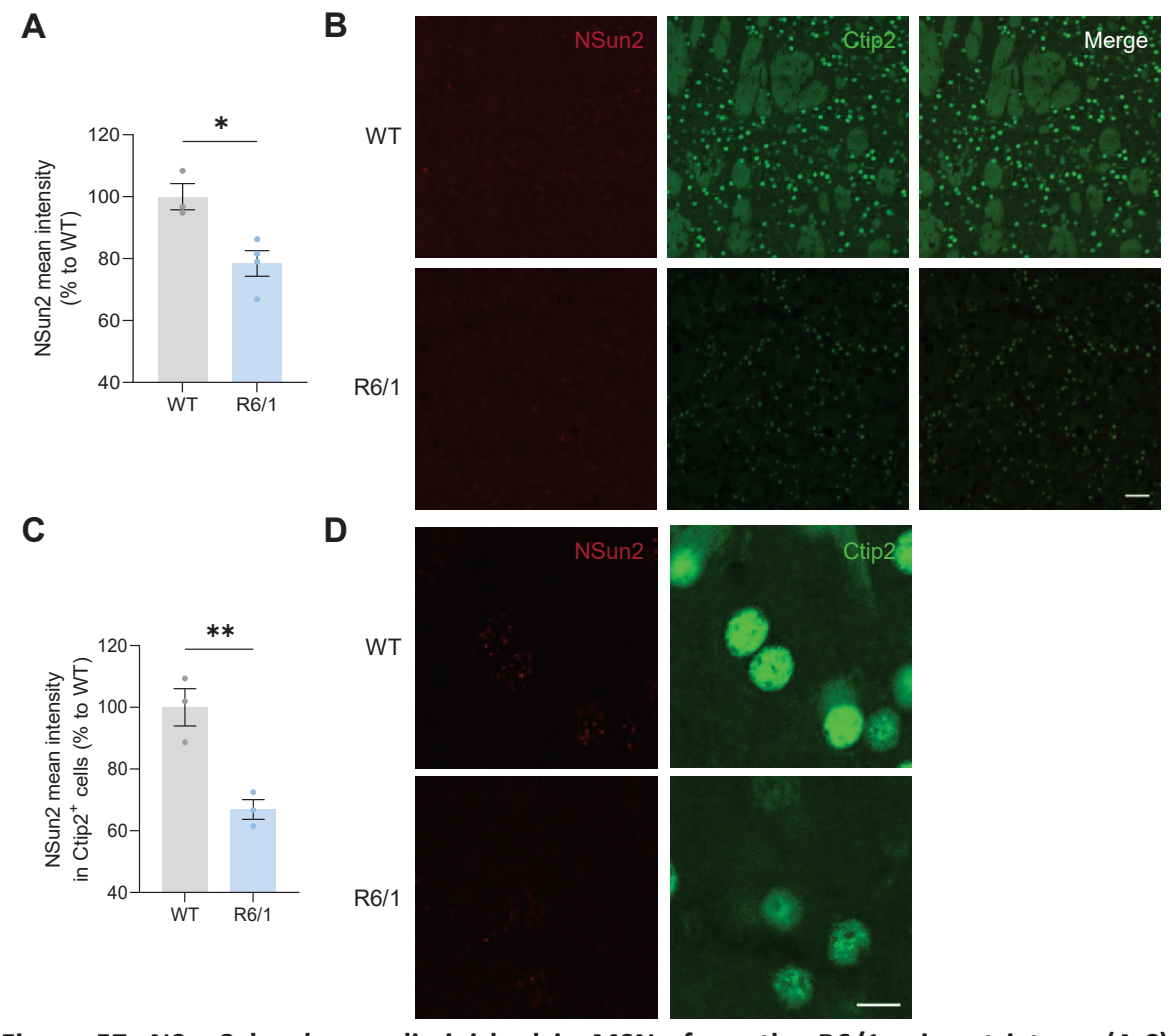


Figure 57. NSun2 levels are diminished in MSNs from the R6/1 mice striatum. (A,C) Quantification of NSun2 mean intensity (A) in the whole striatum and (C) only in Ctip2-positive nuclei from the striatum of WT and R6/1 male animals at 15 weeks of age. WT n = 100

3; R6/1 n = 3-4. Each point represents data from an individual mouse. Values are expressed as percentage to WT animals and shown as mean \pm SEM. *P < 0.05 versus the indicated groups; calculated by two-tailed unpaired Student's t-test. (B) Representative images of NSun2 (in red) and Ctip2 (in green) immunohistofluorescence in the striatum of WT and R6/1 mice. Scale bar: 50 μ m. (D) Panels showing a magnification of Ctip2-positive nuclei illustrating the appearance of NSun2 intensity in the double positive cells. Scale bar: 10 μ m.

The RNA methyltransferase NSun2 introduces m⁵C methylations within tRNA and other small ncRNAs (Frye & Watt, 2006; Khoddami & Cairns, 2013; Y. A. Kim et al., 2022). To assess whether NSun2 reduced levels led to a loss in RNA methylation in the brain of the R6/1 mouse model, we performed an immunostaining against m⁵C together with the MSNs marker Ctip2 in coronal brain slices from 15-weeks-old WT and R6/1 mice, when NSun2 alterations were already evident. In line with the bibliography (Blanco et al., 2014; Blaze et al., 2021; Tuorto et al., 2012), striatal reduction of NSun2 protein levels was correlated with a significant decrease in m⁵C intensity detected in the nucleus of all striatal cells of R6/1 compared to WT mice (Figure 58A and D). In addition, a similar trend was observed when only focusing on the nuclei of striatal Ctip2-positive cells (Figure 58B and D). Conversely, no alterations in m⁵C intensity were observed in the nuclei of cortical cells in R6/1 mice compared to WT animals at 15 weeks of age (Figure 58C and E). Therefore, these results correlated with the changes in NSun2 protein levels found in this mouse model and with the contribution of NSun2 to m⁵C epitranscriptomic modifications.

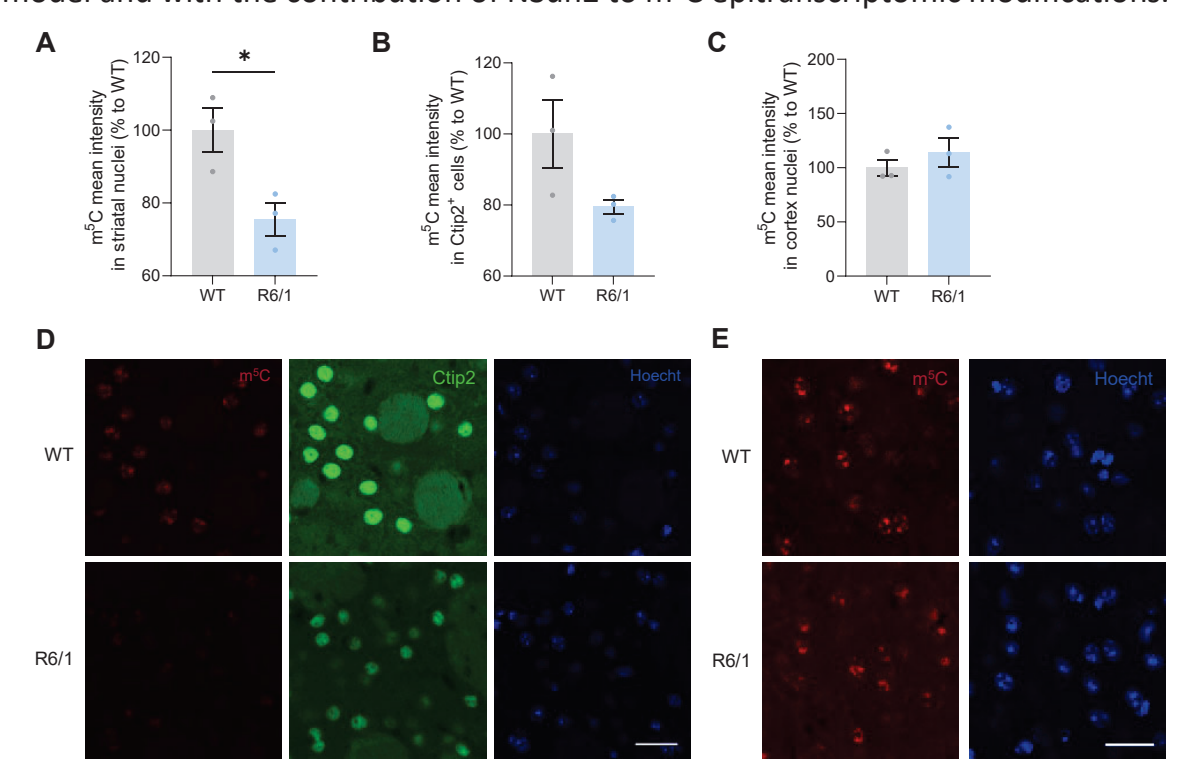


Figure 58. m^5 C levels are decreased in the striatum, but not in the cortex, of R6/1 mice. (A-C) Quantification of m^5 C mean intensity (A) in the striatum, (B) in Ctip2-positive striatal cells or (C) in the cortex of WT and R6/1 male mice at 15 weeks of age. WT n = 3; R6/1 n = 3. Each point represents data from an individual mouse. Values are expressed as percentage

to WT animals and shown as mean \pm SEM. *P < 0.05 versus the indicated groups; calculated by two-tailed unpaired Student's t-test. (**D-E**) Representative images of m⁵C (in red) and Ctip2 (in green) immunohistofluorescence in the (**D**) striatum and (**E**) cortex of WT and R6/1 mice. Cell nuclei are labelled in blue. Scale bar: 25 μ m.

3.2 Overcoming RNA modifications expands the repertoire of detected tsRNA

Overall, many findings pointed to a potential implication of tsRNA and, in turn, of their modifications in HD pathogenic mechanisms. However, it has been demonstrated that traditional library preparation and sRNA sequencing present some limitations in the detection of these sRNA species since they harbor post-transcriptional modifications in their sequences interfering with these processes (Cozen et al., 2015; G. Zheng et al., 2015). To better uncover HD-associated sRNA transcriptome, we took advantage of the PANDORAseq strategy, which is based on different enzymatic treatment protocols during sRNA-sequencing library preparation (J. Shi et al., 2021). The step of adapter ligation is improved using T4 polynucleotide kinase (T4PNK) allowing the detection of all sRNA sequences that presented multiple 5' and 3' ends, different from the 5' monophosphate (5'-P) and the 3' hydroxyl group (3'-OH). In parallel, the reverse transcription is also enhanced by using AlkB demethylase that removes sRNA internal modifications (Figure 59).

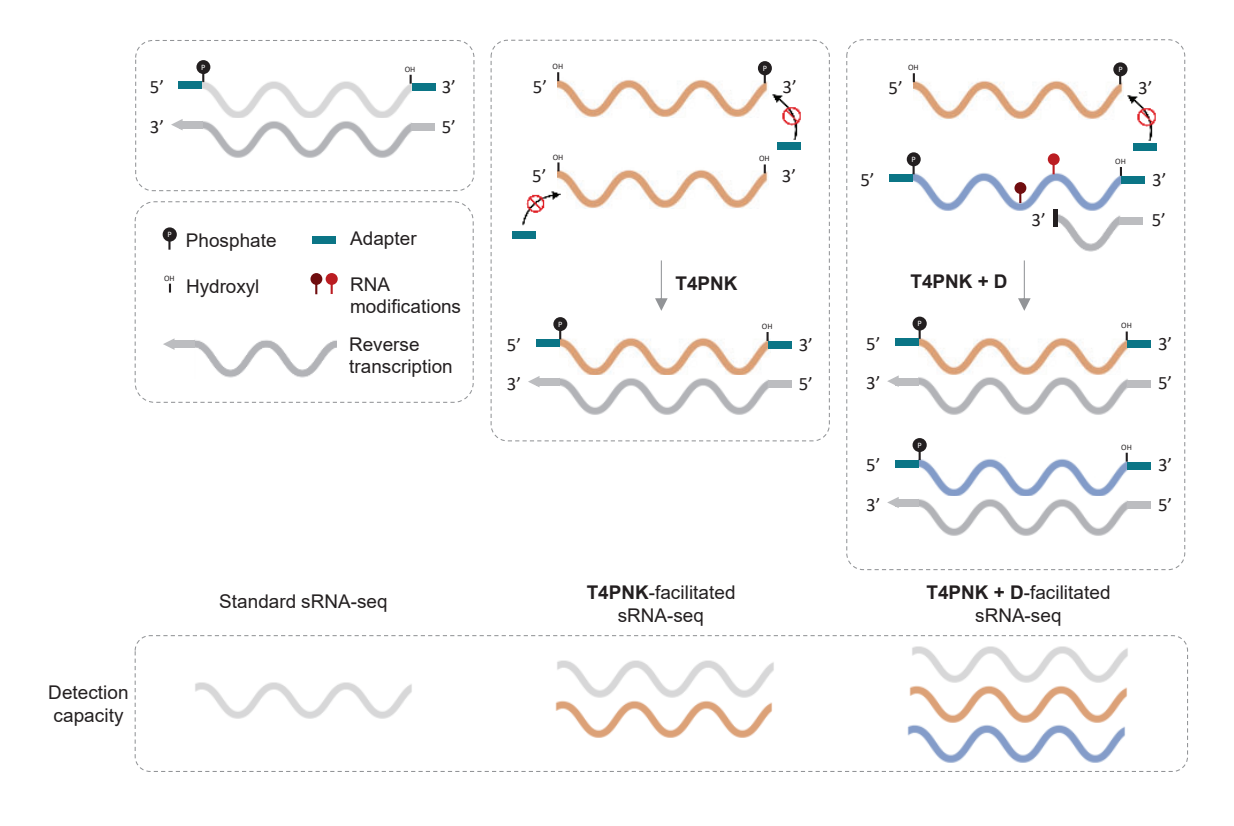


Figure 59. Schematic overview of sRNA sequences and their modifications together with T4PNK and T4PNK+D pre-treatments to enhance library preparation for sRNA-sequencing.

First, we performed bioanalyzer analysis of the purified sRNA pools (<200 nt) which showed that they contained approximately a 20-25% of sRNA with a length below

50 nt while the resting 75-80% corresponded to sRNA of 50 to 200 nt (Figure 60A). Besides, this distribution was maintained across sRNA pools obtained from different brain regions and subject genotypes (Figure 60B).

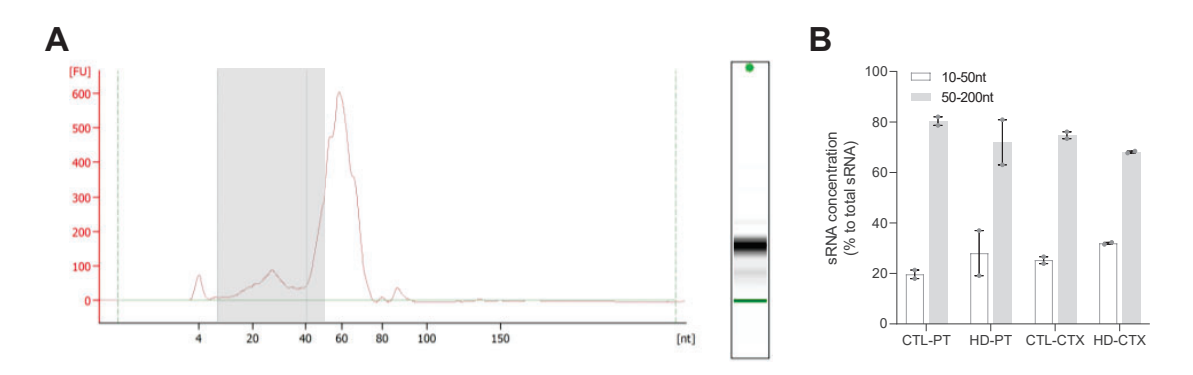


Figure 60. sRNA pools present similar length profiles according to bioanalyzer. (A) Electropherogram obtained using bioanalyzer showing concentration and length distribution of a column purified sample of sRNA (<200 nt). (B) Histogram based on bioanalyzer results showing sRNA concentrations of different sRNA lengths within sRNA pools obtained from human samples.

It has been widely described that sRNA biotypes that could be participating in the transcriptomic alterations and the neurotoxicity observed in the *in vivo* experiments mostly correspond to miRNA and tsRNA species (Blaze & Akbarian, 2022; Esteller, 2011; B. Liu et al., 2021; Salta & De Strooper, 2012), all of them presenting a length below 50 nt. Therefore, we performed pre-size-selection to purify sRNA with a length from 17 to 50 nt (ssRNA) from purified sRNA pools. It is worth mentioning that this selection also avoided the potential tRNA degradation after demethylase treatment leading to the production of additional tsRNA in the small RNA library representing an artefact, which is a phenomenon that has been recently described (J. Shi et al., 2021). As a result, the removal of an artificial tsRNA source, namely tRNA present in the sRNA pools, guaranteed a more reliable result.

To confirm that the combinatorial treatment of ssRNA was expanding the discovery of sRNA sequences in our samples, we performed sRNA sequencing of the same sample under different conditions: without pre-treatment, pre-treated with T4PNK enzyme and pre-treated with a combination of T4PNK enzyme together with different demethylases (T4PNK+D). Mapping, annotation and analysis of the sRNA sequencing data using Seqcluster displayed that ssRNA pre-treatments expanded tsRNA and rRNA detection, with T4PNK+D pre-treatment showing an enhanced effect in comparison to T4PNK alone in the case of tsRNA mapped reads (Figure 61A). Specifically, tsRNA derived from all the isoacceptors showed an increase in their relative levels with both pre-treatments in comparison to the non-treated sample (Figure 61B). However, it is worth noting that improvements in tsRNA detection with the different pre-treatments were dependent on the tRNA

isoacceptor, suggesting differential end-modifications in sRNA sequences and methylations depending on the original tRNA.

While miRNAs are one of the predominant biotypes detected by standard sRNA sequencing, represented by the non-treated sample, both pre-treatments substantially increased the reads of other sRNA biotypes without losing information as the total number of clusters detected in all cases remained unchanged (Figure 61C). Therefore, it was validated that T4PNK+D pre-treatment allowed a better coverage of ssRNA diversity, especially favoring tsRNA detection.

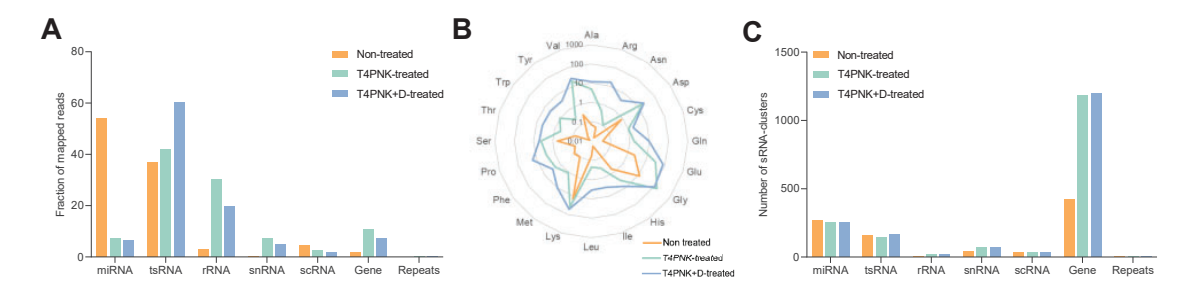


Figure 61. Combinatorial enzyme pre-treatment with T4PNK+D reveals a tsRNA-enriched landscape. (A) Fraction of mapped reads annotating onto the different sRNA biotypes according to different ssRNA pre-treatments. **(B)** Radar plot showing the sensibilities of tsRNA derived from the different isoacceptors to the pre-treatments. Levels of tsRNA were normalized to total miRNA reads. The scale on the radius represents log values. **(C)** Total number of sRNA-clusters classified by sRNA biotypes within each ssRNA pre-treatment.

Further characterization of tsRNA mapped reads was performed using the MINTbase database (Pliatsika et al., 2018) to annotate the obtained reads into the corresponding tRNA. Notably, this strategy increased the detection of 3'halves, 3'tRFs and itRFs (Figure 62A) and expanded the repertoire of tsRNA corresponding to different tRNA isoacceptors (Figure 62B) in comparison to the non-treated sample. Length distribution analysis displayed a differential detection of sequences between conditions, with different predominant lengths observed depending on the ssRNA pre-treatment applied (Figure 62C). Moreover, SeqclusterViz tool revealed an increased mapping of tsRNA onto their corresponding mature tRNA precursors especially after T4PNK+D ssRNA pre-treatment (Figure 62D and E). These results confirmed the fact that under standard library preparation conditions, the analyzed tsRNA harboured both terminal adapter ligation-blocking modifications and internal reverse-transcription-preventing modifications.

In conclusion, these findings demonstrated that pre-size-selection of ssRNA followed by a combinatorial enzymatic treatment of samples constituted an improved and optimized protocol that could be applied to examine the tsRNA landscape in HD human brains.

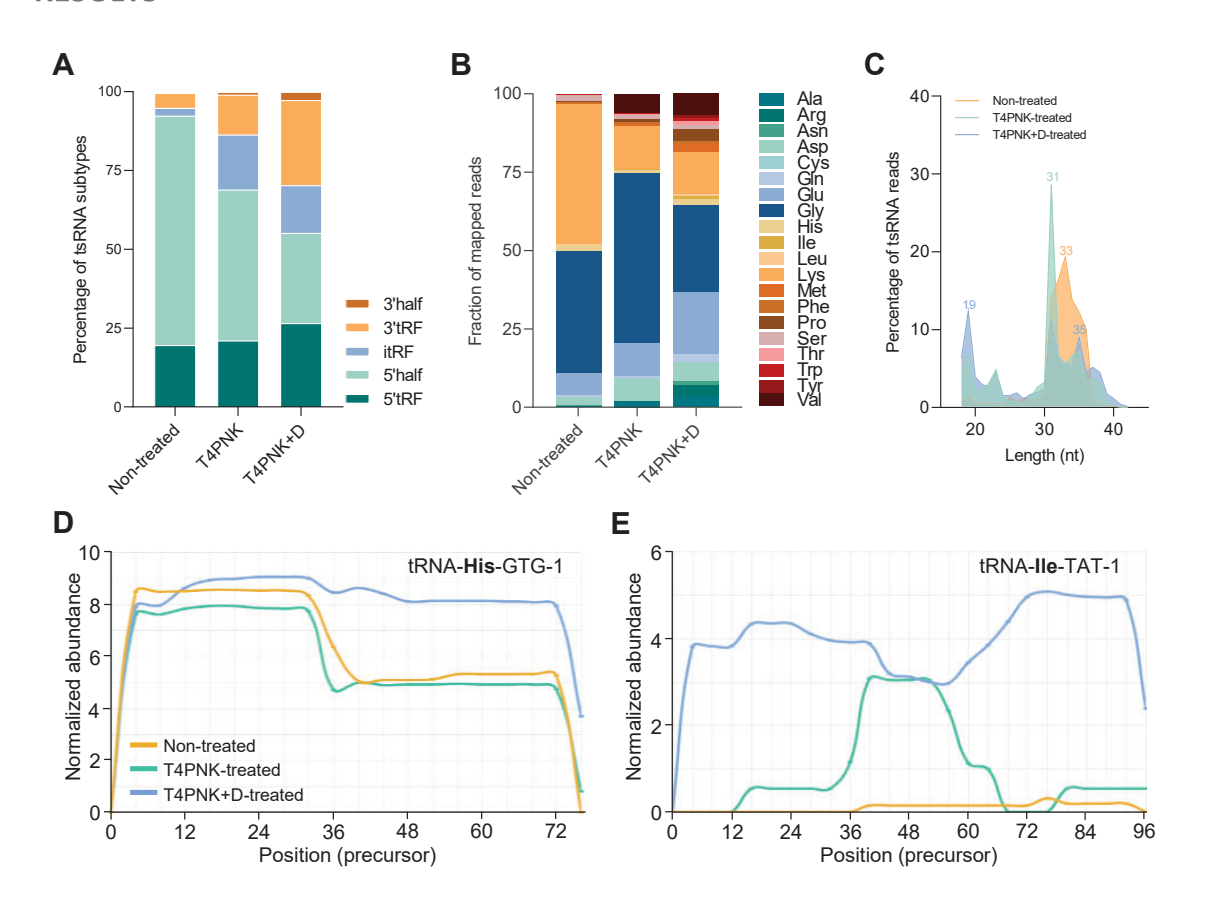


Figure 62. Overcoming RNA modifications with ssRNA pre-treatments expands the repertoire of identified tsRNA. (A) Abundance of tsRNA mapped reads corresponding to different subtypes of tsRNA depending on ssRNA pre-treatment. (B) Abundance of tsRNA mapped reads classified according to precursor tRNA isoacceptors within each ssRNA pre-treatment. (C) Length distribution profiles of the mapped tsRNA reads depending on ssRNA pre-treatment. (D-E) Normalized abundance profiles of tsRNA along the length of the corresponding mature tRNA precursors depending on ssRNA pre-treatment. tsRNA belonging to (D) tRNA-His-GTG-1 and (E) tRNA-Ile-TAT-1 clusters are shown.

3.3 Epitranscriptomic tRNA modifications regulate specific tsRNA biogenesis in HD

In an attempt to unravel transcriptional alterations present in HD pathogenesis in parallel to dysregulations in sRNA methylations, we performed sRNA-seq with purified ssRNA samples (17-50 nt) obtained from the putamen of HD patients (HD-ssRNA-PT) and non-affected individuals (CTL-ssRNA-PT). sRNA libraries were prepared from ssRNA directly purified or adding a pre-treatment with T4PNK or T4PNK+D and subsequently sequenced at 50 nt single end. Using this strategy, we obtained a more detailed profile of the sRNA transcriptome of the putamen, including the features of sRNA termini (comparing non-treated versus T4PNK pre-treated samples) and also an indirect readout of the general methylation levels present in sRNA sequences (comparing T4PNK versus T4PNK+D pre-treated samples).

Importantly, it has been described that treatment of total RNA with demethylases can lead to degradation due to alterations in RNA structure resulting in increased non-specific fragmentation (J. Shi et al., 2021). Although we performed an isolation of specific-sized RNAs to avoid this phenomenon, sRNA-sequencing data suggested that no further degradation occurred using sRNA-sequencing data. In fact, sequences of interest (short; 17-42 nt in length) represented around a 90% of total reads in all samples while the percentage of sequences corresponding to degradation products (too short; <17 nt in length) remained insignificant, therefore validating the followed strategy (Figure 63).

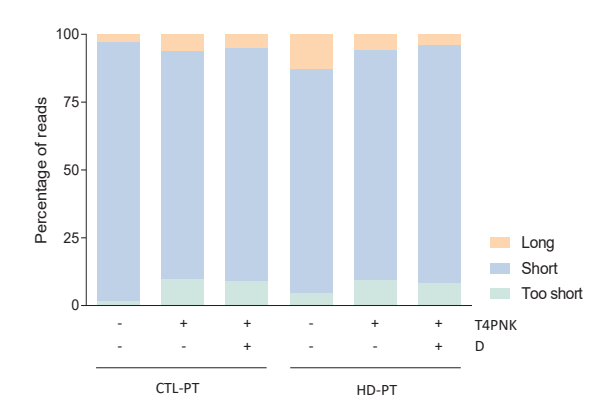


Figure 63. Pre-treatment of sRNA-sequencing samples with T4PNK and T4PNK+D does not induce significant sRNA degradation. Abundance of reads corresponding to sequences of interest (short), degradation products (too short) and longer sequences not classified as sRNA (long) depending on ssRNA pre-treatment and genotype.

Analysis of the sRNA-sequencing data using the Seqcluster pipeline showed a total of around 1800 clusters identified in all pre-treated samples, duplicating the number of clusters detected without any pre-treatment (see Figure 41A and Figure 44A and B). Classification of clusters among sRNA biotypes displayed that the most abundant clusters corresponded to gene-clusters in the two pre-treatments analyze (Figure 64A). While the number of gene-clusters was obviously increased upon T4PNK and T4PNK+D pre-treatments, the total number of clusters of each sRNA biotypes was similar among non-treated and pre-treated conditions (Figure 64A). These results point to the existence of gene derived fragments with end configurations other than 5'-P and 3'-OH and consequently they are only revealed using the different pre-treatments.

Regarding the abundance of the different sRNA biotypes, T4PNK and T4PNK+D pretreatments resulted in an increased detection of rRNA-, snRNA- and gene-clusters and especially tsRNA-clusters in a genotype-independent manner (Figure 64B), consistently with previous results (Figure 61A). The increased abundance of these diverse biotypes led to a decreased proportion of miRNA, as this biotype is less sensitive to T4PNK pre-treatment (Figure 64B).

Of note, the abundance distribution profiles showed that tsRNA are the sequences presenting the highest sensibility to demethylation, as they are the only sRNA biotype displaying an increased relative abundance after T4PNK+D pre-treatment compared to T4PNK alone. Furthermore, analysis of the sequencing data using ExceRpt pipeline (Rozowsky et al., 2019) confirmed a clear higher proportion of sequences mapping onto tsRNA in T4PNK+D pre-treated samples compared to the non-treated and the T4PNK pre-treated ones (Figure 64C), validating the tsRNA-enriched landscape observed using Seqcluster.

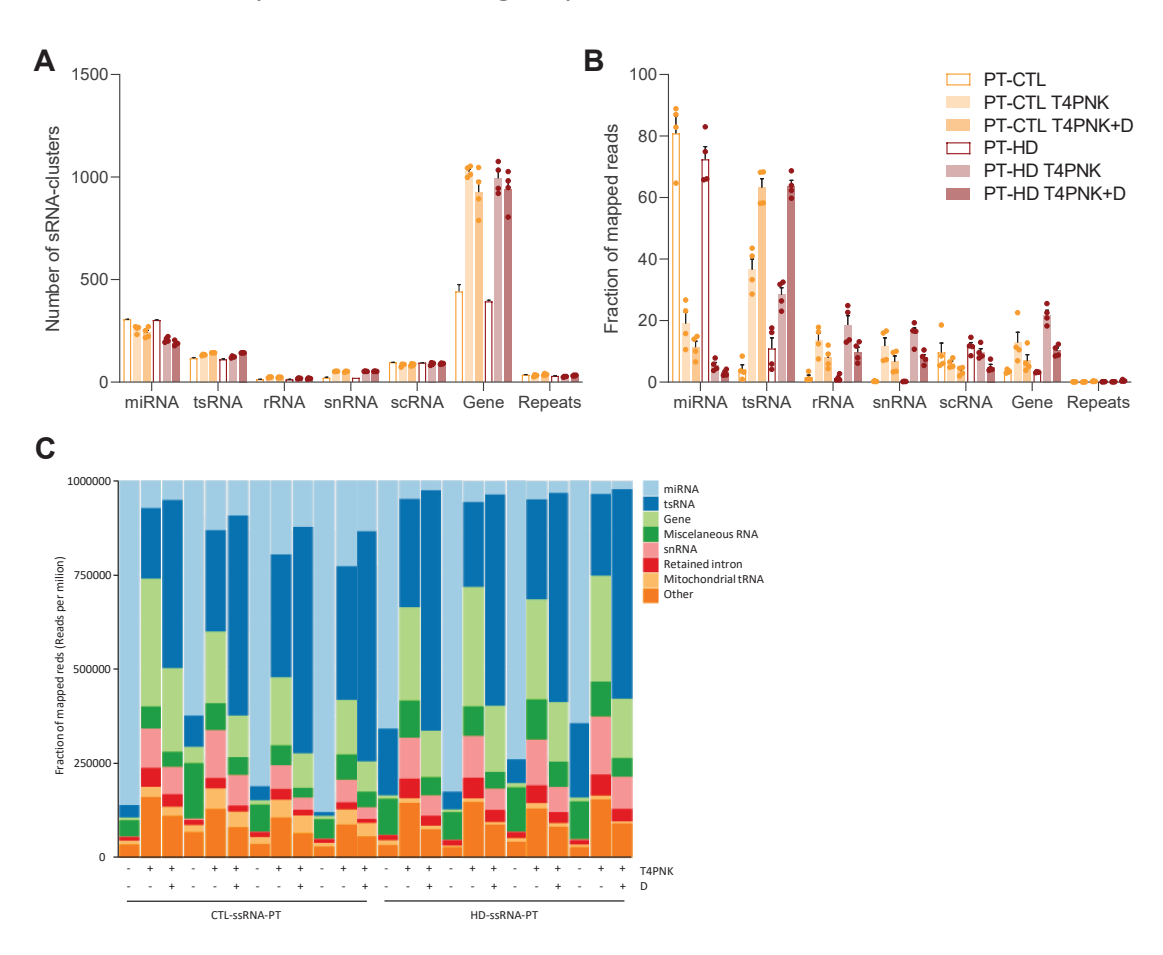


Figure 64. tsRNA species display the most prominent sensibility to demethylation, regardless of the genotype. (A) Total number of sRNA-clusters classified by sRNA biotypes within CTL-ssRNA-PT and HD-ssRNA-PT samples, according to Seqcluster. (B) Fraction of mapped reads in each sample annotating onto the different sRNA biotypes depending on the pre-treatment applied, according to Seqcluster. In (A-B), CTL-ssRNA-PT n = 4; HD-ssRNA-PT n = 4 and each point represents data from an individual subject. Values are shown as mean ± SEM. (C) Abundance of ssRNA mapped reads corresponding to the different biotypes depending on ssRNA pre-treatment (non-treated, T4PNK or T4PNK+D) and genotype (CTL- or HD-ssRNA-PT), according to ExceRpt tool.

Deep sRNA profiling confirmed a differential composition of ssRNA samples between genotypes. Notably, pre-treatment of samples highlighted tsRNA of 21, 34-39 nt in both genotypes. However, different tsRNA length distributions were observed in HD samples, within all conditions analyzed. For instance, we observed

an increased percentage of tsRNA with lengths of 33-34 nt in non-treated HD-ssRNA-PT samples while the percentage of tsRNA species of 35-36 nt was duplicated in HD-ssRNA-PT samples applying any of the pre-treatments (Figure 65A and B). Therefore, this finding confirmed an increased tsRNA biogenesis in the putamen of HD patients, in line with the results observed in non-treated sRNA pools (Figure 42).

Regarding miRNA species, we did not detect many significant changes in their profiles after enzymatic treatments, apart from a general decreased coverage. Specifically, we observed that CTL-ssRNA-PT samples displayed a high abundance of reads with 21-22 nt in length, while sequences of 22 nt were less abundant within HD-ssRNA-PT samples in all cases (Figure 65A and B). In what regards to other sRNA biotypes, we detected higher percentages of gene fragments and scRNA in HD-ssRNA-PT compared to CTL-ssRNA-PT samples, but only when using pre-treatments (Figure 65A and B).

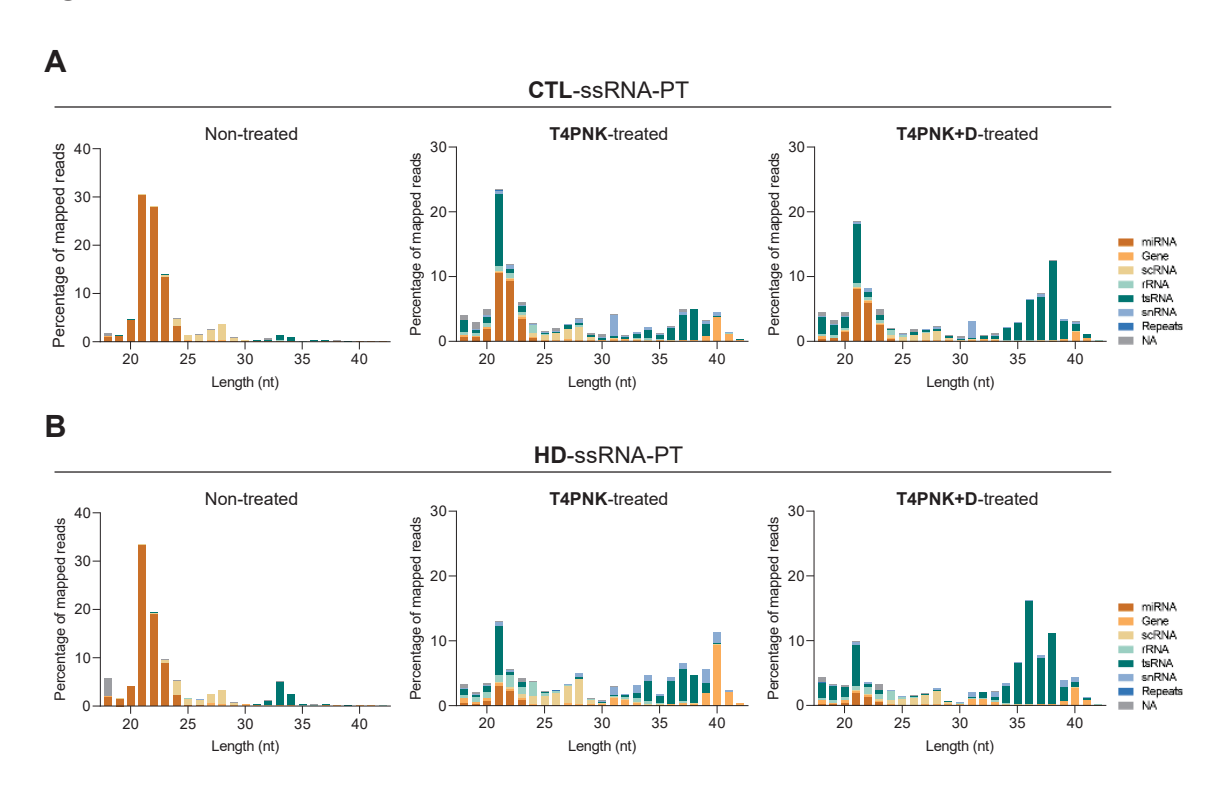


Figure 65. Differential read length distributions and biotype compositions are observed between CTL- and HD-ssRNA-PT samples using T4PNK and T4PNK+D pre-treatments. Histograms showing length distributions by biotypes contained in (A) CTL-ssRNA-PT and (B) HD-ssRNA-PT samples without pre-treatment or applying T4PNK and T4PNK+D pre-treatments. Abundances (in %) are relative to total ssRNA sequenced within each sample.

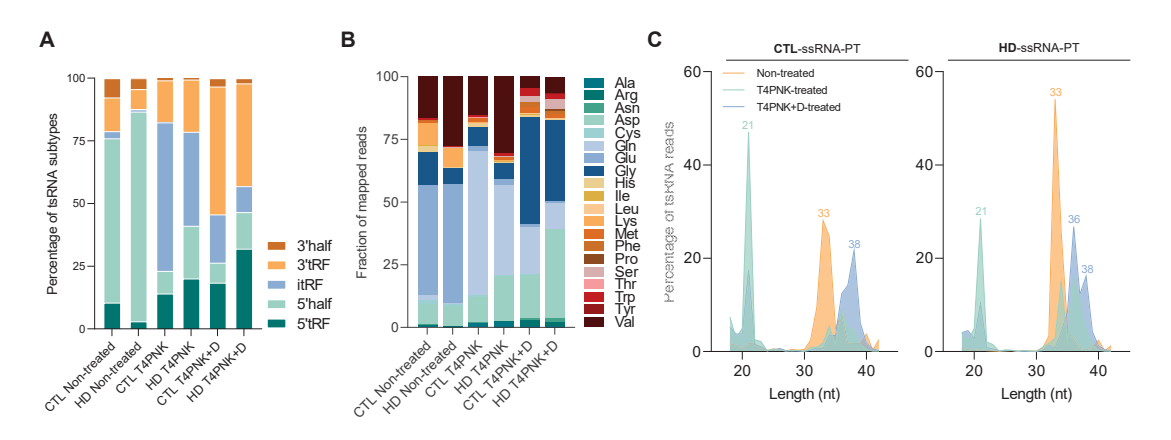
Considering the enhanced tsRNA coverage upon pre-treatments, we sought to further characterize tsRNA sequences within the different conditions. We annotated the obtained reads into the MINTbase (Pliatsika et al., 2018) and tsRBase (Zuo et al., 2021) databases. This approach highlighted differential tsRNA signatures

in the putamen of HD patients and non-affected individuals. Particularly, we confirmed an increased abundance in 5'-end derived tsRNA (5'tRF and 5'halves) in HD-ssRNA-PT under non-treated conditions (Figure 66A and D). Although both pretreatments increased the discovery of itRFs and 3'-end derived tsRNA (3'tRF and 3'halves), a higher percentage of 5'-end derived tsRNA was maintained in HD- in comparison to CTL-ssRNA-PT samples (Figure 66A and D).

Focusing on the precursor tRNA isoacceptors, T4PNK+D pre-treatment increased the number of isoacceptors detected to a greater extend compared with T4PNK alone (Figure 66B and E). Besides, different proportions of isoacceptors were detected depending on the genotype, with an increased detection of tRNA^{Asp} and tRNA^{Val} in parallel with a decreased mapping of tRNA^{Gln} and tRNA^{Gly} in HD-ssRNA-PT T4PNK and T4PNK+D pre-treated samples compared to the respective pre-treatments in CTL-ssRNA-PT samples (Figure 66B and E).

Next, length distribution analyses revealed a differential distribution depending on the pre-treatment applied but also highlighted the presence of different ssRNA species within genotypes. In fact, in non-treated samples, we observed a sharp peak of sequences of 33 nt in length. In contrast, while T4PNK pre-treatment revealed tsRNA sequences presenting 21 nt, T4PNK+D pre-treatment additionally uncovered sequences of 36-38 nt in length (Figure 66C and F). Notably, different proportions of these tsRNA sequences were observed in each condition when comparing genotypes (Figure 66C and F).

Radar plots confirmed a different relative response of each tsRNA subcategory to T4PNK and T4PNK+D pre-treatments compared to non-treated conditions (Figure 66G and H), revealing genotype- and isoacceptor-specific patterns. Finally, it is important to remark that the abovementioned results were equally observed when mapping onto both databases, corroborating the obtained findings.



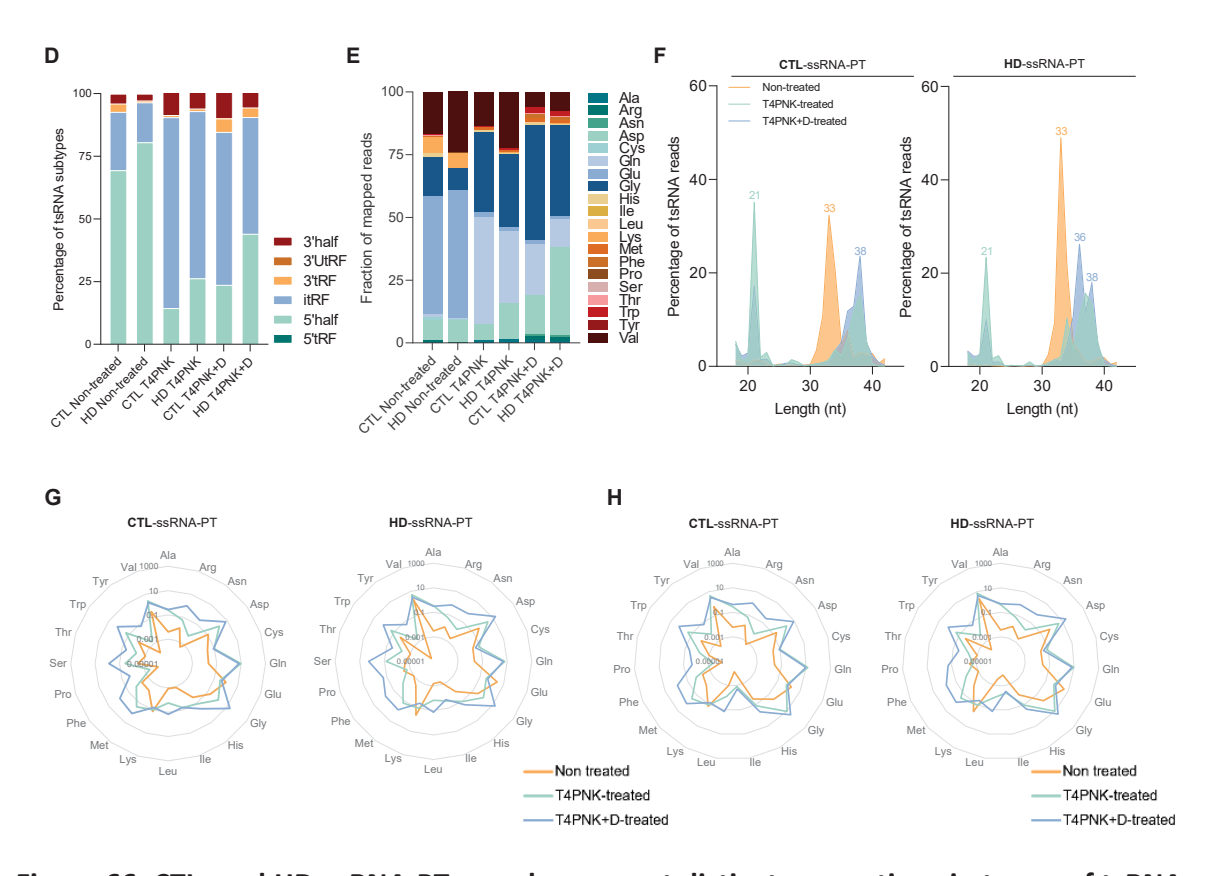


Figure 66. CTL- and HD-ssRNA-PT samples present distinct proportions in terms of tsRNA subtypes, tsRNA isoacceptors and tsRNA read lengths, which can be observed upon different ssRNA pre-treatments. (A,D) Abundance of tsRNA mapped reads corresponding to different subtypes of tsRNA within CTL-ssRNA-PT and HD-ssRNA-PT samples depending on the pre-treatment used, according to (A) MINTbase and (D) tsRBase databases. (B,E) Abundance of tsRNA mapped reads within CTL-ssRNA-PT and HD-ssRNA-PT samples classified according to precursor tRNA isoacceptors annotated into (B) MINTbase and (E) tsRBase databases. (C,F) Length distribution profiles of the mapped tsRNA reads within CTL-ssRNA-PT and HD-ssRNA-PT samples, according to (C) MINTbase and (F) tsRBase databases. (G,H) Radar plots showing the sensitivities of tsRNA derived from the different isoacceptors to the pre-treatments upon annotation into (G) MINTbase and (H) tsRBase databases. Levels of tsRNA were normalized to total miRNA reads. The scale on the radius represents log values.

Subsequently, differential expression analyses in non-treated samples confirmed the presence of multiple DE sRNA clusters in HD- compared to CTL-ssRNA-PT samples (Figure 67A; adjusted P < 0.05 and a fold change < 1.5 or > 1.5 as screening thresholds). Particularly, miRNA- and gene-clusters displayed an important number of significantly downregulated clusters. Besides, these sRNA biotypes together with tsRNA and scRNA also presented a considerable number of significantly upregulated clusters. Regarding tsRNA, DE analyses in T4PNK- and T4PNK+D-pretreated samples showed a shift in the number of dysregulated clusters in comparison to non-treated samples, presenting more significantly downregulated tsRNA clusters than upregulated ones (Figure 67B; see Annex for Supplementary Table 7, 8 and 9). These findings pointed to the fact that tsRNA species from CTL-

ssRNA-PT samples are more sensible to pre-treatments, preferentially increasing the detection of novel species, whereas tsRNA discovery in HD-ssRNA-PT samples remained unaltered, suggesting that HD-ssRNA-PT samples mainly contain tsRNA species with 5'-P and 3'-OH ends, and thus leading to the observed shift in DE tsRNA sequences.

Taking into account that the more likely detrimental species contributing to HD-associated pathological mechanisms are those specifically upregulated in HD putamen, we centered the analysis on the significantly upregulated tsRNA clusters in HD putamen. Hence, we observed that while the majority of tsRNA clusters were only detected in non-treated conditions, some specific clusters were shared among conditions (Figure 67C and Table 16), reinforcing the idea of a differential sensibility to the type of pre-treatment applied.

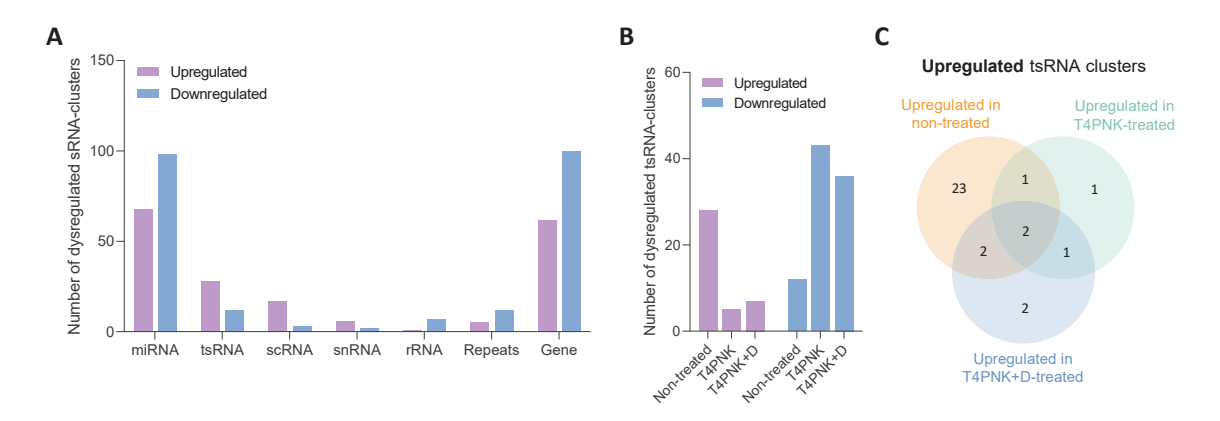


Figure 67. T4PNK and T4PNK+D pre-treatments affect differential expression analyses, reducing the number of significantly dysregulated tsRNA clusters. (A) Total number of significantly dysregulated sRNA-clusters in non-treated HD- versus CTL-ssRNA-PT samples classified by sRNA biotypes. **(B)** Total number of significantly dysregulated tsRNA-clusters in HD- versus CTL-ssRNA-PT samples depending on the pre-treatment applied. **(C)** Venn diagram showing the overlap between significantly upregulated tsRNA clusters detected using each pre-treatment. Screening threshold: fold change > 1.5 or < 1.5 and adjusted P < 0.05.

tRNA cluster	Pre-treatment	log2FC	P value	Adjusted P
	Non-treated	2.264820	2.50E-07	3.19E-06
tRNA-Asp-GTC-2-3	T4PNK	1.089808	0.008024	0.026892
	T4PNK+D	1.586983	0.000107	0.000924
	Non-treated	4.992531	2.27E-12	1.03E-10
tRNA-Val-TAC-2-1	T4PNK	1.250826	0.009239	0.029589
	T4PNK+D	1.293240	0.005140	0.021369
tRNA-Asp-GTC-1-1	Non-treated	1.210344	0.012585	0.034062

tRNA-Asp-GTC-4-1 Non-treated 3.401694 0.000106 0.000634 tRNA-Asp-GAC/GAT* TAPNK+D 1.722196 0.001791 0.009160 tRNA-Asp-GAC/GAT* TAPNK+D 1.638711 0.003771 0.016867 tRNA-Asp-GAC/GAT* TAPNK+D 1.848476 0.008366 0.030558 tRNA-Arg-GAC-3-1 TAPNK 4.078403 7.46€-08 1.32E-06 tRNA-Arg-AGA* TAPNK 2.456025 6.48E-05 0.000470 tRNA-Arg-AGA* TAPNK 2.456025 4.06E-05 0.000282 tRNA-Asr-GTT-2-6 Non-treated 1.522551 4.06E-05 0.000282 tRNA-Asr-GTT-2-6 Non-treated 1.073534 0.006472 0.019624 tRNA-Ser-GCT-3-1 Non-treated 1.082520 0.014722 0.037942 tRNA-Gly-CCC-2-1 Non-treated 1.319645 0.001745 0.006732 tRNA-Gly-CCC-1-2 Non-treated 1.405878 0.006642 0.02031 tRNA-Lys-TT-2-3 Non-treated 1.541920 0.00160 0.004767		T4PNK+D	1.463951	0.000619	0.003979
tRNA-Asp-GAC/GAT* T4PNK+D 1.722196 0.001791 0.009160 tRNA-Asp-GAC/GAT* T4PNK+D 1.638711 0.003771 0.016867 tRNA-Asp-GAC/GAT* T4PNK 1.848476 0.008366 0.030558 tRNA-Arg-AGA* T4PNK 4.078403 7.46E-08 1.32E-06 tRNA-Arg-AGA* T4PNK 2.456025 6.48E-05 0.000490 tRNA-Arg-AGA* T4PNK 2.456025 6.48E-05 0.000471 tRNA-Arg-TCT-1-1 Non-treated 1.522551 4.06E-05 0.000282 tRNA-Ser-GCT-3-1 Non-treated 1.073534 0.006472 0.019624 tRNA-Ser-GCT-3-1 Non-treated 1.305836 0.014722 0.037336 tRNA-Gly-CCC-2-1 Non-treated 1.319645 0.001745 0.006732 tRNA-Gly-CCC-2-2 Non-treated 1.405878 0.006642 0.02031 tRNA-Heu-TAG-3-1 Non-treated 1.541920 0.00160 0.004767 tRNA-Glu-TCC-1-3 Non-treated 1.541920 0.00160 0.004767 <	ADNIA Asia CTC 4.4	Non-treated	3.401694	0.000106	0.000634
trnna-asp-gac/gat* T4PNK+D 1.848476 0.008366 0.030558 trna-Ala-CGC-3-1 T4PNK 4.078403 7.46E-08 1.32E-06 trna-Arg-AGA* T4PNK 2.116175 5.06E-05 0.000490 trna-Arg-AGA* T4PNK 2.456025 6.48E-05 0.000471 trna-Arg-TCT-1-1 Non-treated 1.522551 4.06E-05 0.000282 trna-Arg-TCT-1-6 Non-treated 1.073534 0.006472 0.019624 trna-Ala-TGC-2-1 Non-treated 1.082520 0.014722 0.037942 trna-Gly-CCC-1 Non-treated 1.305836 0.014289 0.037336 trna-Gly-CCC-1 Non-treated 1.405878 0.00642 0.006732 trna-Gly-CCC-1 Non-treated 1.478952 0.006880 0.02033 trna-Leu-TaG-3-1 Non-treated 1.580111 6.52E-05 0.000423 trna-Glu-GAG* Non-treated 1.797660 0.013511 0.035657 trna-Glu-GAG* Non-treated 2.139902 0.001671 0.006510	tkNA-Asp-GTC-4-1	T4PNK+D	1.722196	0.001791	0.009160
tRNA-Ala-CGC-3-1 T4PNK 4.078403 7.46E-08 1.32E-06 tRNA-Ala-CGC-3-1 T4PNK+D 2.116175 5.06E-05 0.000490 tRNA-Arg-AGA* T4PNK 2.456025 6.48E-05 0.000471 tRNA-Arg-TCT-1-1 Non-treated 1.522551 4.06E-05 0.000282 tRNA-Arg-TCT-1-6 Non-treated 1.073534 0.006472 0.019624 tRNA-Ala-TGC-2-1 Non-treated 1.082520 0.014722 0.037942 tRNA-Ala-TGC-2-1 Non-treated 1.305836 0.014289 0.037336 tRNA-Gly-CCC-2-2 Non-treated 1.319645 0.001745 0.006732 tRNA-Gly-CCC-1-1 Non-treated 1.405878 0.006642 0.02031 tRNA-Heu-TAG-3-1 Non-treated 1.541920 0.00160 0.004767 tRNA-Leu-TAG-3-1 Non-treated 1.580111 6.52E-05 0.000423 tRNA-Glu-GAG* Non-treated 1.797660 0.013511 0.035657 tRNA-Glu-GAG* Non-treated 2.09695 0.001671 0.005610	tRNA-Asp-GAC/GAT*	T4PNK+D	1.638711	0.003771	0.016867
tRNA-Ala-CGC-3-1 T4PNK+D 2.116175 5.06E-05 0.000490 tRNA-Arg-AGA* T4PNK 2.456025 6.48E-05 0.000471 tRNA-Arg-AGA* T4PNK 1.522551 4.06E-05 0.000282 tRNA-Arg-TCT-1-1 Non-treated 1.527453 0.008735 0.028410 tRNA-Ser-GCT-3-1 Non-treated 1.073534 0.006472 0.019624 tRNA-Ala-TGC-2-1 Non-treated 1.082520 0.014722 0.037942 tRNA-Gly-CC-2-1 Non-treated 1.319645 0.001745 0.006732 tRNA-Gly-CC-2-2 Non-treated 1.408878 0.00642 0.02031 tRNA-Met-CAT-1-3 Non-treated 1.541920 0.001160 0.004767 tRNA-Gly-TCC-1-1 Non-treated 1.580111 6.52E-05 0.000423 tRNA-Glu-GGA* Non-treated 1.580111 6.52E-05 0.000423 tRNA-Glu-GGG* Non-treated 1.797660 0.013511 0.035657 tRNA-Glu-GGA* Non-treated 2.098081 0.002790 0.009745 <th>tRNA-Asp-GAC/GAT*</th> <th>T4PNK+D</th> <th>1.848476</th> <th>0.008366</th> <th>0.030558</th>	tRNA-Asp-GAC/GAT*	T4PNK+D	1.848476	0.008366	0.030558
TAPNK+D 2.116175 5.06E-05 0.000490 tRNA-Arg-AGA* T4PNK 2.456025 6.48E-05 0.000471 tRNA-Arg-AGA* T4PNK 1.522551 4.06E-05 0.000282 tRNA-Arg-TCT-1-1 T4PNK 1.257453 0.008735 0.028410 tRNA-Asn-GTT-2-6 Non-treated 1.073534 0.006472 0.019624 tRNA-GCT-3-1 Non-treated 1.082520 0.014722 0.037942 tRNA-Gly-TCC-1-1 Non-treated 1.305836 0.014289 0.037336 tRNA-Gly-CCC-2-2 Non-treated 1.319645 0.001745 0.006732 tRNA-Gly-CCC-1-1 Non-treated 1.405878 0.006642 0.020031 tRNA-Gly-TCC-1-1 Non-treated 1.541920 0.00160 0.004767 tRNA-Trp-CCA-2-1 Non-treated 1.580111 6.52E-05 0.000423 tRNA-Glu-GAG* Non-treated 1.797660 0.013511 0.035657 tRNA-Glu-GAG* Non-treated 2.103661 0.007669 0.022470 tRNA-Glu-TTC-1 </th <th>*DNA Al- CCC 2.1</th> <th>T4PNK</th> <th>4.078403</th> <th>7.46E-08</th> <th>1.32E-06</th>	*DNA Al- CCC 2.1	T4PNK	4.078403	7.46E-08	1.32E-06
trna-Arg-TCT-1-1 Non-treated 1.522551 4.06E-05 0.000282 trna-Arg-TCT-1-1 T4PNK 1.257453 0.008735 0.028410 trna-Asn-GTT-2-6 Non-treated 1.073534 0.006472 0.019624 trna-Ser-GCT-3-1 Non-treated 1.082520 0.014722 0.037942 trna-Gly-CC-2-1 Non-treated 1.305836 0.014289 0.037336 trna-Gly-CC-2-2 Non-treated 1.319645 0.001745 0.006732 trna-Gly-CC-1-1 Non-treated 1.405878 0.006642 0.020031 trna-Met-CAT-1-3 Non-treated 1.478952 0.006880 0.020530 trna-Gly-CC-2-1 Non-treated 1.541920 0.001160 0.004767 trna-Glu-Trp-CC-2-1 Non-treated 1.580111 6.52E-05 0.000423 trna-Glu-GAG* Non-treated 1.797660 0.013511 0.035657 trna-Glu-GGG* Non-treated 2.103661 0.007669 0.022470 trna-Glu-TC-1-1 Non-treated 2.290695 0.001671 0.	TRINA-Ald-CGC-5-1	T4PNK+D	2.116175	5.06E-05	0.000490
tRNA-Arg-TCT-1-1 T4PNK 1.257453 0.008735 0.028410 tRNA-Asn-GTT-2-6 Non-treated 1.073534 0.006472 0.019624 tRNA-Ser-GCT-3-1 Non-treated 1.082520 0.014722 0.037942 tRNA-GI-TGC-2-1 Non-treated 1.305836 0.014289 0.037336 tRNA-GI-TGC-2-1 Non-treated 1.319645 0.001745 0.006732 tRNA-GI-TCC-1-1 Non-treated 1.405878 0.006642 0.020031 tRNA-Met-CAT-1-3 Non-treated 1.478952 0.006880 0.020530 tRNA-Leu-TAG-3-1 Non-treated 1.541920 0.001160 0.004767 tRNA-GI-GA-3-1 Non-treated 1.580111 6.52E-05 0.000423 tRNA-GIL-GAG* Non-treated 1.602206 0.00348 0.010475 tRNA-GIL-GAG* Non-treated 2.098081 0.002790 0.009745 tRNA-GIL-GAG* Non-treated 2.103661 0.002790 0.002470 tRNA-GIL-TTC-1-1 Non-treated 2.290695 0.001671 0.006510<	tRNA-Arg-AGA*	T4PNK	2.456025	6.48E-05	0.000471
T4PNK 1.257453 0.008735 0.028410 tRNA-Asn-GTT-2-6 Non-treated 1.073534 0.006472 0.019624 tRNA-Ser-GCT-3-1 Non-treated 1.082520 0.014722 0.037942 tRNA-GIV-CC-2-1 Non-treated 1.305836 0.014289 0.037336 tRNA-GIV-CC-2-2 Non-treated 1.319645 0.001745 0.006732 tRNA-GIV-TCC-1-1 Non-treated 1.478952 0.006642 0.020031 tRNA-Het-CAT-1-3 Non-treated 1.541920 0.00160 0.004767 tRNA-Leu-TAG-3-1 Non-treated 1.580111 6.52E-05 0.000423 tRNA-GIu-GAC* Non-treated 1.602206 0.003048 0.010475 tRNA-GIu-GAG* Non-treated 2.098081 0.002790 0.009745 tRNA-GIu-GAG* Non-treated 2.139902 0.001671 0.006510 tRNA-Giu-TTC-1-1 Non-treated 2.290695 0.000134 0.000766 tRNA-Giu-TTC-8-1 Non-treated 2.296661 0.002028 0.007516	tPNA_Arg_TCT_1_1	Non-treated	1.522551	4.06E-05	0.000282
tRNA-Ser-GCT-3-1 Non-treated 1.082520 0.014722 0.037942 tRNA-Ala-TGC-2-1 Non-treated 1.305836 0.014289 0.037336 tRNA-Gly-CCC-2-2 Non-treated 1.319645 0.001745 0.006732 tRNA-Gly-TCC-1-1 Non-treated 1.405878 0.006642 0.020031 tRNA-Met-CAT-1-3 Non-treated 1.478952 0.006880 0.020530 tRNA-Leu-TAG-3-1 Non-treated 1.541920 0.001160 0.004767 tRNA-Leu-TAG-3-1 Non-treated 1.580111 6.52E-05 0.000423 tRNA-Glu-GAG-2 Non-treated 1.602206 0.003048 0.010475 tRNA-Glu-GAG* Non-treated 1.797660 0.013511 0.035657 tRNA-Glu-GCTC-1-3 Non-treated 2.098081 0.002790 0.009745 tRNA-Glu-TTC-1 Non-treated 2.139902 0.001671 0.006510 tRNA-Glu-TTC-8-1 Non-treated 2.296661 0.002028 0.007516 tRNA-Glu-TTC-4-2 Non-treated 2.312178 0.002104		T4PNK	1.257453	0.008735	0.028410
tRNA-Ala-TGC-2-1 Non-treated 1.305836 0.014289 0.037336 tRNA-Gly-CCC-2-2 Non-treated 1.319645 0.001745 0.006732 tRNA-Gly-TCC-1-1 Non-treated 1.405878 0.006642 0.020031 tRNA-Met-CAT-1-3 Non-treated 1.478952 0.006880 0.020530 tRNA-Leu-TAG-3-1 Non-treated 1.541920 0.001160 0.004767 tRNA-Trp-CCA-2-1 Non-treated 1.580111 6.52E-05 0.000423 tRNA-Glu-GS-TTT-3-2 Non-treated 1.602206 0.03048 0.010475 tRNA-Glu-GAG* Non-treated 1.797660 0.013511 0.035657 tRNA-Glu-GAG* Non-treated 2.098081 0.002790 0.009745 tRNA-Glu-TC-1-3 Non-treated 2.139902 0.001671 0.006510 tRNA-Lys-CTT-2-5 Non-treated 2.290695 0.000134 0.00766 tRNA-Glu-TTC-8-1 Non-treated 2.312178 0.002104 0.007721 tRNA-Glu-TTC-2-1 Non-treated 2.445590 0.000165	tRNA-Asn-GTT-2-6	Non-treated	1.073534	0.006472	0.019624
tRNA-Gly-CCC-2-2 Non-treated 1.319645 0.001745 0.006732 tRNA-Gly-TCC-1-1 Non-treated 1.405878 0.006642 0.020031 tRNA-Met-CAT-1-3 Non-treated 1.478952 0.006880 0.020530 tRNA-Leu-TAG-3-1 Non-treated 1.541920 0.001160 0.004767 tRNA-Trp-CCA-2-1 Non-treated 1.580111 6.52E-05 0.000423 tRNA-Lys-TTT-3-2 Non-treated 1.602206 0.03048 0.010475 tRNA-Glu-GG* Non-treated 1.797660 0.013511 0.035657 tRNA-Glu-GTC-1-3 Non-treated 2.098081 0.002790 0.009745 tRNA-Glu-TG-1 Non-treated 2.103661 0.007669 0.022470 tRNA-Glu-TTC-1 Non-treated 2.290695 0.00134 0.000766 tRNA-Glu-TTC-8-1 Non-treated 2.312178 0.002104 0.007721 tRNA-Glu-TTC-2-1 Non-treated 2.445590 0.000165 0.000919 tRNA-Arg-CCG-1-2 Non-treated 2.655349 0.007040 <th< th=""><th>tRNA-Ser-GCT-3-1</th><th>Non-treated</th><th>1.082520</th><th>0.014722</th><th>0.037942</th></th<>	tRNA-Ser-GCT-3-1	Non-treated	1.082520	0.014722	0.037942
tRNA-Gly-TCC-1-1 Non-treated 1.405878 0.006642 0.020031 tRNA-Met-CAT-1-3 Non-treated 1.478952 0.006880 0.020530 tRNA-Leu-TAG-3-1 Non-treated 1.541920 0.001160 0.004767 tRNA-Trp-CCA-2-1 Non-treated 1.580111 6.52E-05 0.000423 tRNA-Lys-TTT-3-2 Non-treated 1.602206 0.003048 0.010475 tRNA-Glu-GAG* Non-treated 1.797660 0.013511 0.035657 tRNA-Glu-GGAG* Non-treated 2.098081 0.002790 0.009745 tRNA-Glu-TTC-1-3 Non-treated 2.103661 0.007669 0.022470 tRNA-Glu-TTC-1-1 Non-treated 2.139902 0.001671 0.006510 tRNA-Lys-CTT-2-5 Non-treated 2.290695 0.000134 0.000766 tRNA-Glu-TTC-8-1 Non-treated 2.312178 0.002104 0.007721 tRNA-Glu-TTC-2-1 Non-treated 2.446642 5.56E-05 0.000376 tRNA-Arg-CCG-1-2 Non-treated 2.655349 0.007040	tRNA-Ala-TGC-2-1	Non-treated	1.305836	0.014289	0.037336
tRNA-Met-CAT-1-3 Non-treated 1.478952 0.006880 0.020530 tRNA-Leu-TAG-3-1 Non-treated 1.541920 0.001160 0.004767 tRNA-Trp-CCA-2-1 Non-treated 1.580111 6.52E-05 0.000423 tRNA-Lys-TTT-3-2 Non-treated 1.602206 0.003048 0.010475 tRNA-Glu-GG* Non-treated 1.797660 0.013511 0.035657 tRNA-Glu-GG* Non-treated 2.098081 0.002790 0.009745 tRNA-Glu-GG* Non-treated 2.103661 0.007669 0.022470 tRNA-Glu-TTC-1-1 Non-treated 2.290695 0.000134 0.000510 tRNA-Glu-TTC-8-1 Non-treated 2.296661 0.002028 0.007516 tRNA-Glu-TTC-4-2 Non-treated 2.312178 0.002104 0.0007721 tRNA-Val-TAC-3-1 Non-treated 2.445590 0.000165 0.000919 tRNA-Glu-GAG* Non-treated 2.655349 0.007040 0.020898 tRNA-Glu-GAG* Non-treated 2.701290 0.000124 0.000	tRNA-Gly-CCC-2-2	Non-treated	1.319645	0.001745	0.006732
tRNA-Leu-TAG-3-1 Non-treated 1.541920 0.001160 0.004767 tRNA-Trp-CCA-2-1 Non-treated 1.580111 6.52E-05 0.000423 tRNA-Lys-TTT-3-2 Non-treated 1.602206 0.003048 0.010475 tRNA-Glu-GAG* Non-treated 1.797660 0.013511 0.035657 tRNA-Glu-GAG* Non-treated 2.098081 0.002790 0.009745 tRNA-Glu-GAG* Non-treated 2.103661 0.007669 0.022470 tRNA-Glu-TTC-1-1 Non-treated 2.139902 0.001671 0.006510 tRNA-Lys-CTT-2-5 Non-treated 2.290695 0.000134 0.000766 tRNA-Glu-TTC-8-1 Non-treated 2.312178 0.002028 0.007516 tRNA-Glu-TTC-2-1 Non-treated 2.406642 5.56E-05 0.000376 tRNA-Val-TAC-3-1 Non-treated 2.445590 0.000165 0.000919 tRNA-Glu-GAG* Non-treated 2.655349 0.000124 0.000714	tRNA-Gly-TCC-1-1	Non-treated	1.405878	0.006642	0.020031
tRNA-Trp-CCA-2-1 Non-treated 1.580111 6.52E-05 0.000423 tRNA-Lys-TTT-3-2 Non-treated 1.602206 0.003048 0.010475 tRNA-Glu-GAG* Non-treated 1.797660 0.013511 0.035657 tRNA-Glu-GAG* Non-treated 2.098081 0.002790 0.009745 tRNA-Glu-GAG* Non-treated 2.103661 0.007669 0.022470 tRNA-Glu-TTC-1-1 Non-treated 2.139902 0.001671 0.006510 tRNA-Glu-TTC-8-1 Non-treated 2.290695 0.000134 0.000766 tRNA-Glu-TTC-8-1 Non-treated 2.312178 0.002028 0.007516 tRNA-Glu-TTC-2-1 Non-treated 2.406642 5.56E-05 0.000376 tRNA-Val-TAC-3-1 Non-treated 2.445590 0.000165 0.000919 tRNA-Glu-GGG* Non-treated 2.655349 0.007040 0.020898 tRNA-Glu-GGG* Non-treated 2.701290 0.000124 0.000714	tRNA-Met-CAT-1-3	Non-treated	1.478952	0.006880	0.020530
tRNA-Lys-TTT-3-2 Non-treated 1.602206 0.003048 0.010475 tRNA-Glu-GAG* Non-treated 1.797660 0.013511 0.035657 tRNA-Glu-CTC-1-3 Non-treated 2.098081 0.002790 0.009745 tRNA-Glu-GAG* Non-treated 2.103661 0.007669 0.022470 tRNA-Glu-TTC-1-1 Non-treated 2.139902 0.001671 0.006510 tRNA-Lys-CTT-2-5 Non-treated 2.290695 0.000134 0.000766 tRNA-Glu-TTC-8-1 Non-treated 2.296661 0.002028 0.007516 tRNA-Glu-TTC-4-2 Non-treated 2.406642 5.56E-05 0.000376 tRNA-Val-TAC-3-1 Non-treated 2.445590 0.000165 0.000919 tRNA-Glu-GAG* Non-treated 2.655349 0.007040 0.020898 tRNA-Glu-GAG* Non-treated 2.701290 0.000124 0.000714	tRNA-Leu-TAG-3-1	Non-treated	1.541920	0.001160	0.004767
tRNA-Glu-GAG* Non-treated 1.797660 0.013511 0.035657 tRNA-Glu-CTC-1-3 Non-treated 2.098081 0.002790 0.009745 tRNA-Glu-GAG* Non-treated 2.103661 0.007669 0.022470 tRNA-Glu-TTC-1-1 Non-treated 2.139902 0.001671 0.006510 tRNA-Lys-CTT-2-5 Non-treated 2.290695 0.000134 0.000766 tRNA-Glu-TTC-8-1 Non-treated 2.296661 0.002028 0.007516 tRNA-Glu-TTC-4-2 Non-treated 2.312178 0.002104 0.007721 tRNA-Glu-TTC-2-1 Non-treated 2.406642 5.56E-05 0.000376 tRNA-Val-TAC-3-1 Non-treated 2.445590 0.000165 0.000919 tRNA-Glu-GAG* Non-treated 2.655349 0.007040 0.020898 tRNA-Glu-GAG* Non-treated 2.701290 0.000124 0.000714	tRNA-Trp-CCA-2-1	Non-treated	1.580111	6.52E-05	0.000423
tRNA-Glu-CTC-1-3 Non-treated 2.098081 0.002790 0.009745 tRNA-Glu-GAG* Non-treated 2.103661 0.007669 0.022470 tRNA-Glu-TTC-1-1 Non-treated 2.139902 0.001671 0.006510 tRNA-Lys-CTT-2-5 Non-treated 2.290695 0.000134 0.000766 tRNA-Glu-TTC-8-1 Non-treated 2.296661 0.002028 0.007516 tRNA-Glu-TTC-4-2 Non-treated 2.312178 0.002104 0.007721 tRNA-Glu-TTC-2-1 Non-treated 2.406642 5.56E-05 0.000376 tRNA-Val-TAC-3-1 Non-treated 2.445590 0.000165 0.000919 tRNA-Glu-GAG* Non-treated 2.655349 0.007040 0.020898 tRNA-Glu-GAG* Non-treated 2.701290 0.000124 0.000714	tRNA-Lys-TTT-3-2	Non-treated	1.602206	0.003048	0.010475
tRNA-Glu-GAG* Non-treated 2.103661 0.007669 0.022470 tRNA-Glu-TTC-1-1 Non-treated 2.139902 0.001671 0.006510 tRNA-Lys-CTT-2-5 Non-treated 2.290695 0.000134 0.000766 tRNA-Glu-TTC-8-1 Non-treated 2.296661 0.002028 0.007516 tRNA-Glu-TTC-4-2 Non-treated 2.312178 0.002104 0.007721 tRNA-Glu-TTC-2-1 Non-treated 2.406642 5.56E-05 0.000376 tRNA-Val-TAC-3-1 Non-treated 2.445590 0.000165 0.000919 tRNA-Arg-CCG-1-2 Non-treated 2.655349 0.007040 0.020898 tRNA-Glu-GAG* Non-treated 2.701290 0.000124 0.000714	tRNA-Glu-GAG*	Non-treated	1.797660	0.013511	0.035657
tRNA-Glu-TTC-1-1 Non-treated 2.139902 0.001671 0.006510 tRNA-Lys-CTT-2-5 Non-treated 2.290695 0.000134 0.000766 tRNA-Glu-TTC-8-1 Non-treated 2.296661 0.002028 0.007516 tRNA-Glu-TTC-4-2 Non-treated 2.312178 0.002104 0.007721 tRNA-Glu-TTC-2-1 Non-treated 2.406642 5.56E-05 0.000376 tRNA-Val-TAC-3-1 Non-treated 2.445590 0.000165 0.000919 tRNA-Arg-CCG-1-2 Non-treated 2.655349 0.007040 0.020898 tRNA-Glu-GAG* Non-treated 2.701290 0.000124 0.000714	tRNA-Glu-CTC-1-3	Non-treated	2.098081	0.002790	0.009745
tRNA-Lys-CTT-2-5 Non-treated 2.290695 0.000134 0.000766 tRNA-Glu-TTC-8-1 Non-treated 2.296661 0.002028 0.007516 tRNA-Glu-TTC-4-2 Non-treated 2.312178 0.002104 0.007721 tRNA-Glu-TTC-2-1 Non-treated 2.406642 5.56E-05 0.000376 tRNA-Val-TAC-3-1 Non-treated 2.445590 0.000165 0.000919 tRNA-Arg-CCG-1-2 Non-treated 2.655349 0.007040 0.020898 tRNA-Glu-GAG* Non-treated 2.701290 0.000124 0.000714	tRNA-Glu-GAG*	Non-treated	2.103661	0.007669	0.022470
tRNA-Glu-TTC-8-1 Non-treated 2.296661 0.002028 0.007516 tRNA-Glu-TTC-4-2 Non-treated 2.312178 0.002104 0.007721 tRNA-Glu-TTC-2-1 Non-treated 2.406642 5.56E-05 0.000376 tRNA-Val-TAC-3-1 Non-treated 2.445590 0.000165 0.000919 tRNA-Arg-CCG-1-2 Non-treated 2.655349 0.007040 0.020898 tRNA-Glu-GAG* Non-treated 2.701290 0.000124 0.000714	tRNA-Glu-TTC-1-1	Non-treated	2.139902	0.001671	0.006510
tRNA-Glu-TTC-4-2 Non-treated 2.312178 0.002104 0.007721 tRNA-Glu-TTC-2-1 Non-treated 2.406642 5.56E-05 0.000376 tRNA-Val-TAC-3-1 Non-treated 2.445590 0.000165 0.000919 tRNA-Arg-CCG-1-2 Non-treated 2.655349 0.007040 0.020898 tRNA-Glu-GAG* Non-treated 2.701290 0.000124 0.000714	tRNA-Lys-CTT-2-5	Non-treated	2.290695	0.000134	0.000766
tRNA-Glu-TTC-2-1 Non-treated 2.406642 5.56E-05 0.000376 tRNA-Val-TAC-3-1 Non-treated 2.445590 0.000165 0.000919 tRNA-Arg-CCG-1-2 Non-treated 2.655349 0.007040 0.020898 tRNA-Glu-GAG* Non-treated 2.701290 0.000124 0.000714	tRNA-Glu-TTC-8-1	Non-treated	2.296661	0.002028	0.007516
tRNA-Val-TAC-3-1 Non-treated 2.445590 0.000165 0.000919 tRNA-Arg-CCG-1-2 Non-treated 2.655349 0.007040 0.020898 tRNA-Glu-GAG* Non-treated 2.701290 0.000124 0.000714	tRNA-Glu-TTC-4-2	Non-treated	2.312178	0.002104	0.007721
tRNA-Arg-CCG-1-2 Non-treated 2.655349 0.007040 0.020898 tRNA-Glu-GAG* Non-treated 2.701290 0.000124 0.000714	tRNA-Glu-TTC-2-1	Non-treated	2.406642	5.56E-05	0.000376
tRNA-Glu-GAG* Non-treated 2.701290 0.000124 0.000714	tRNA-Val-TAC-3-1	Non-treated	2.445590	0.000165	0.000919
	tRNA-Arg-CCG-1-2	Non-treated	2.655349	0.007040	0.020898
tRNA-Val-TAC-1-1 Non-treated 2.769647 0.000110 0.000648	tRNA-Glu-GAG*	Non-treated	2.701290	0.000124	0.000714
	tRNA-Val-TAC-1-1	Non-treated	2.769647	0.000110	0.000648

tRNA-Pro-TGG-3-3	Non-treated	4.147417	1.50E-10	5.63E-09
tRNA-Thr-AGT-6-1	Non-treated	6.127961	0.001123	0.004704

Table 16. Significantly upregulated tsRNA clusters in HD-ssRNA-PT versus CTL-ssRNA-PT samples considering the pre-treatment applied. *Clusters mapping onto specific tRNA isoacceptors according to Repeat Masker in UCSC Genome Browser on human (GRCh38/hg38) with a variable percentage of divergence (7.9-27.8%) depending on the number of insertions and deletions observed in the sequences contained within each cluster.

To gain insight into the specific tsRNA that contributed to tsRNA dysregulation at the cluster level, we sought to analyze individual tsRNA sequences. Therefore, we took advantage of the MINTbase database (Pliatsika et al., 2018) in order to annotate the tsRNA sequences detected. Further differential enrichment analysis showed a total of 69 significantly upregulated tsRNA species in HD putamen, considering the results obtained applying all different pre-treatments (Table 17).

					_	_	_
	Туре	Isoacceptor	tsRNA sequence	Pre-treatment	log2FC	P value	Adj P
				Non-treated	5.757385	7.23E-13	6.62E-11
1	5'half	ProCGG	GGCTCGTTGGTCT AGGGGTATGATTC TCGCTT	T4PNK	2.463407	1.90E-05	0.000508
				T4PNK+D	3.459374	1.75E-08	3.18E-06
2	5'half	ValTAC	GGTTCCATAGTGT AGCGGTTATCACG TCTGCTTT	Non-treated	5.201118	3.26E-13	3.98E-11
3	5'half	ValTAC	GGTTCCATAGTGT AGTGGTTATCACG TCTGCTTT	Non-treated	4.570808	3.37E-10	2.47E-08
4	itRF	GlyCCC	CATTCTTGCGACC CGGGTT	Non-treated	4.009309	9.67E-06	0.000153
5	5'half	ValTAC	GGTTCCATAGTGT AGTGGTTATCACA TCTGCTTT	Non-treated	4.007645	6.28E-09	2.55E-07
6	5'half	AspGTC	TCCTCGTTAGTAT AGTGGTTAGTATC CCCGCCTGT	Non-treated	4.000208	1.01E-14	1.85E-12
7	5'half	ValTAC	GGTTCCATAGTGT AGCGGTTATCACG TCTGCTT	Non-treated	3.903881	3.53E-07	9.30E-06
8	3'tRF	AspGTC	CGGGAGACCGGG GTTCGATTCCCCG ACGGGGAGC	Non-treated	3.810647	2.21E-15	8.08E-13
9	itRF	GlnTTG	AATCCAGCGATCC	T4PNK	3.627629	1.46E-08	2.72E-06
J	ILNF	GIIIIG	GAGTTC	T4PNK+D	2.929931	2.94E-07	2.68E-05
10	5'half	AspGTC	TCCTCGTTAGTAT AGTGGTGAGTATC CCCGCCTGT	Non-treated	3.526687	1.81E-09	1.10E-07

11	5'half	GlyCCC	GCGCCGCTGGTGT AGTGGTATCATGC AAGATT	Non-treated	3.363874	3.67E-09	1.92E-07	
12	5'tRF	ArgTCT	GGCTCCGTGGCGC	T4PNK	2.428853	5.02E-05	0.000983	
12	ז נגר	Aigici	AATGG	T4PNK+D	2.755635	2.50E-07	2.68E-05	
13	3'tRF	SerTGA	GAATCCTGCCGAC TACGC	T4PNK	2.466488	3.94E-06	0.000183	
14	itRF	CysGCA	ATAGCTCAGTGGT	T4PNK	2.345886	0.000147	0.002108	
14	TCINI	Сузасл	AGAGCATTTGACT	T4PNK+D	2.052001	0.003619	0.030638	
15	itRF	F GInCTG	CTGAATCCAGCGA TCCGAGTTC	T4PNK	2.288490	3.51E-06	0.000183	
	ICINI			T4PNK+D	2.153560	0.000160	0.003234	
16	3'tRF	SerAGA	CGAATCCTGCCGA CTACGC	T4PNK	2.257928	1.20E-06	0.000148	
17	5'tRF	ArgTCT	GGCTCCGTGGCGC	T4PNK	2.199060	0.000828	0.008323	
	J IN		AATGGA	T4PNK+D	2.038973	0.000278	0.005057	
18	5'half			GGTTCCATAGTGT AGCGGTTATCACG	T4PNK	2.184419	2.37E-06	0.000183
10	3 man		TCTGCT	T4PNK+D	2.189801	1.03E-06	7.48E-05	
19	3'tRF	AspGTC	GGGAGACCGGGG TTCGATTCCCCGA CGGGGAGC	T4PNK+D	2.178544	9.17E-05	0.002086	
20	itRF	HisGTG	TGGTTAGTACTCT GCGTTGT	T4PNK	2.146995	0.008370	0.047369	

Table 17. Top twenty upregulated tsRNA sequences in HD- versus CTL-ssRNA-PT samples, according to MINTbase annotation.

Next, we analyzed the subtypes and tRNA-derived isoacceptors corresponding to the upregulated tsRNA sequences when applying the different pre-treatments. Hence, we observed that 5'-end derived tsRNA species (5'tRF and 5'halves) are the most upregulated sequences in HD-ssRNA-PT samples upon the different pre-treatments (Figure 68A). However, an increased number of upregulated itRF and 3'tRFs was also uncovered using T4PNK and T4PNK+D pre-treatments (Figure 68A). Considering the precursor tRNA isoacceptors from which tsRNA sequences have been generated, a reduced variety in the corresponding isoacceptors of tsRNA sequences was detected using ssRNA pre-treatments compared to non-treated conditions (Figure 68B).

Ultimately, overlapping of the upregulated tsRNA sequences in each condition showed a differential sensibility to pre-treatment among tsRNA species (Figure 68C). On the one hand, we found a group of tsRNA sequences that were

upregulated in HD-ssRNA-PT within all conditions, therefore demonstrating a consistent upregulation independently of the pre-treatment applied. On the other hand, there were tsRNA sequences that were only detected upon T4PNK or T4PNK+D pretreatment, or a combination of both. Consequently, we could infer that alternative ends and/or multiple methylations are present in these tsRNA sequences.

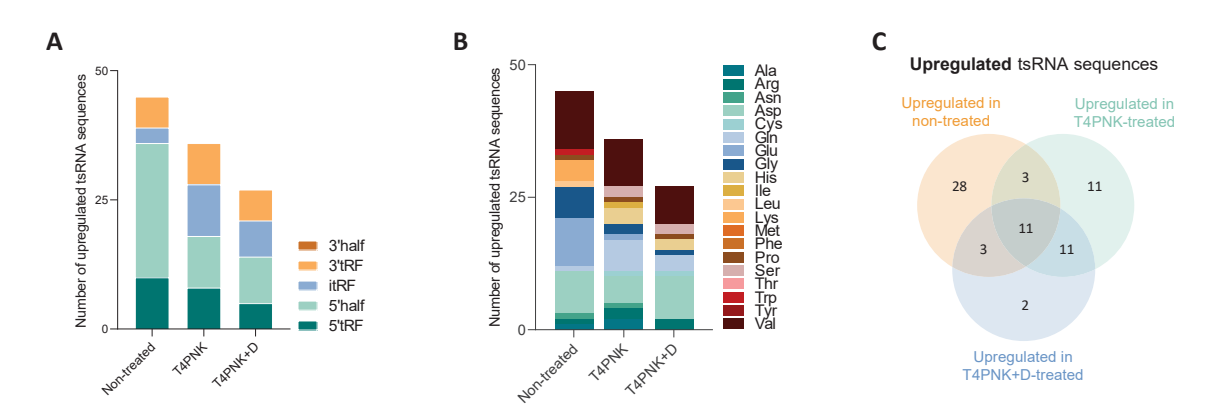


Figure 68. T4PNK and T4PNK+D pre-treatments affect differential expression analyses, reducing the number and complexity of significantly upregulated tsRNA sequences. (A-B) Total number of significantly upregulated tsRNA sequences in HD- compared to CTL-ssRNA-PT samples using the different pre-treatments and classified according to (A) tsRNA subtypes and (B) tRNA-derived isoacceptors. (C) Venn diagram showing the overlap between significantly upregulated tsRNA sequences detected using each pre-treatment. Screening threshold: fold change > 1.5 or < 1.5 and adjusted P < 0.05.

Considering the obtained results, we next focused on the relationship between differential methylation profiles associated to HD and tsRNA biogenesis. To explore this, we analyzed all methylations and other modifications present in the tRNA of the same HD patients and non-affected individuals used for sRNA-sequencing. We obtained purified fractions of sRNA of approximately 80 nt in length, mostly corresponding to tRNA, and analyzed them by LC-MS/MS. This characterization revealed multiple epitranscriptomic modifications that were significantly altered in tRNA from HD putamen. In particular, we detected a decrease in 5-formylcytosine (5 fC), 6-methyladenosine (6 A) and 1-methylinosine (1 I) modifications and an increase in 3-(3-amino-3-carboxypropyl)uridine (acp 3 U), dihydrouridine (D) and pseudouridine (Y) modifications in HD- in comparison to CTL-tRNA-PT (Figure 69).

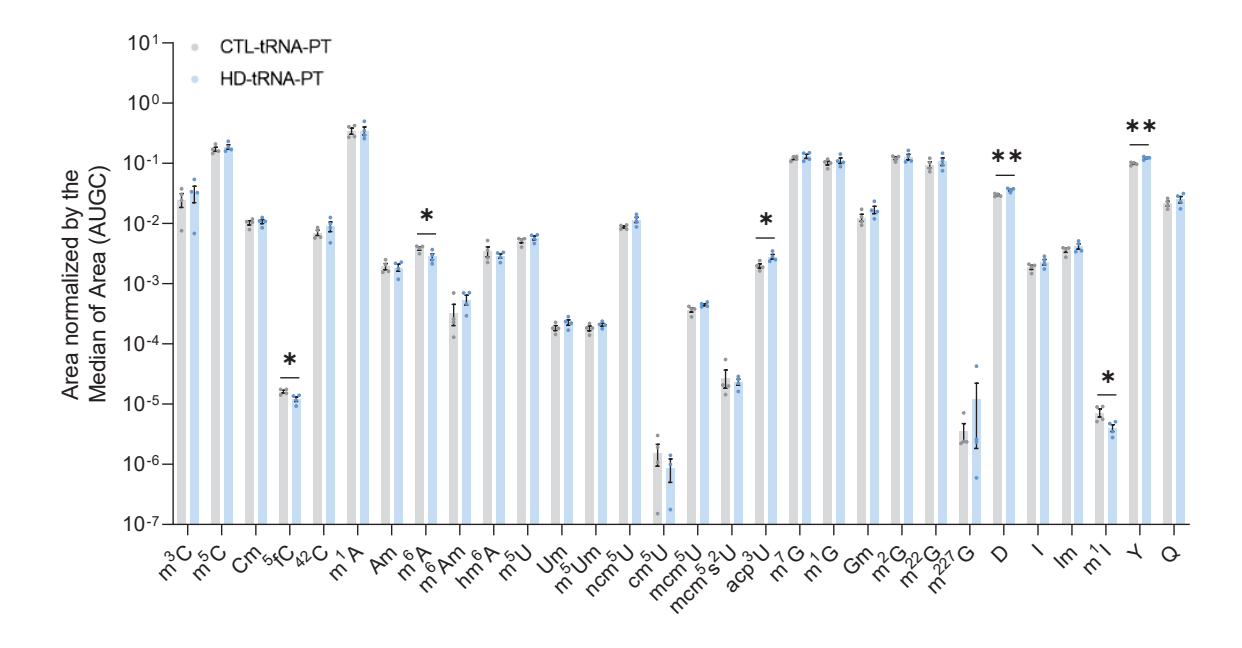


Figure 69. Levels of epitranscriptomic modifications present in purified tRNA from the putamen of HD patients and non-affected individuals. Histogram shows the levels of multiple RNA modifications within tRNA isolated from the putamen of HD patients (HD-tRNA-PT) and non-affected subjects (CTL-tRNA-PT) measured using LC-MS/MS. CTL n = 4; HD n = 4. Each point represents data from an individual subject. **P < 0.01 and *P < 0.05 versus the indicated group; calculated by two-tailed unpaired Student's t-test.

Specific epitranscriptomic modifications have been widely associated to tRNA stability and fragmentation (Lyons et al., 2018). A clear example is the selective m¹I methylation catalyzed by ADAT1 and Trm5 in the position 37 of tRNA^{Ala}, which has only been reported in this specific tRNA in eukaryotes (Björk et al., 2001; Grosjean et al., 1996; Keegan et al., 2000; Torres, Piñeyro, et al., 2014). Using SegclusterViz, we detected a general increase in the coverage of the tRNA^{Ala}, both in the 5'half and in the 3'half, when samples were pre-treated with T4PNK+D compared to T4PNK treatment alone, indicating the presence of methylations along the tRNA^{Ala} sequence (Figure 70A). Furthermore, mass spectrometry results showed a significant decrease in m¹I methylations in HD-tRNA-PT samples (log2FC = -0.84, P value = 0.038; Figure 69) in parallel with higher levels of tsRNA in HD-ssRNA-PT compared to CTL-ssRNA-PT T4PNK+D pre-treated samples (log2FC = 2.12, adjusted P = 0.0005; Figure 70A). Therefore, these results associated m¹I hypomethylation in HD with an increased biogenesis of tsRNA derived from tRNA^{Ala}, in line with the hypothesis that hypomethylated tRNA are less stable and pointing to a differential tsRNA biogenesis between genotypes.

In contrast, we observed other tsRNA species which did not present any noticeable sensibility to T4PNK+D pre-treatment in comparison to T4PNK alone, suggesting a lack of methylations along their sequences that interfered with library preparation. One example was found in the tRNA^{Val} that presented similar profiles

independently of the pre-treatment applied (Figure 70B). Consistently, tsRNA annotating into the tRNA^{val} were significantly upregulated in HD-ssRNA-PT samples in non-treated conditions and using both pre-treatments (log2FC and P values indicated in Figure 70B).

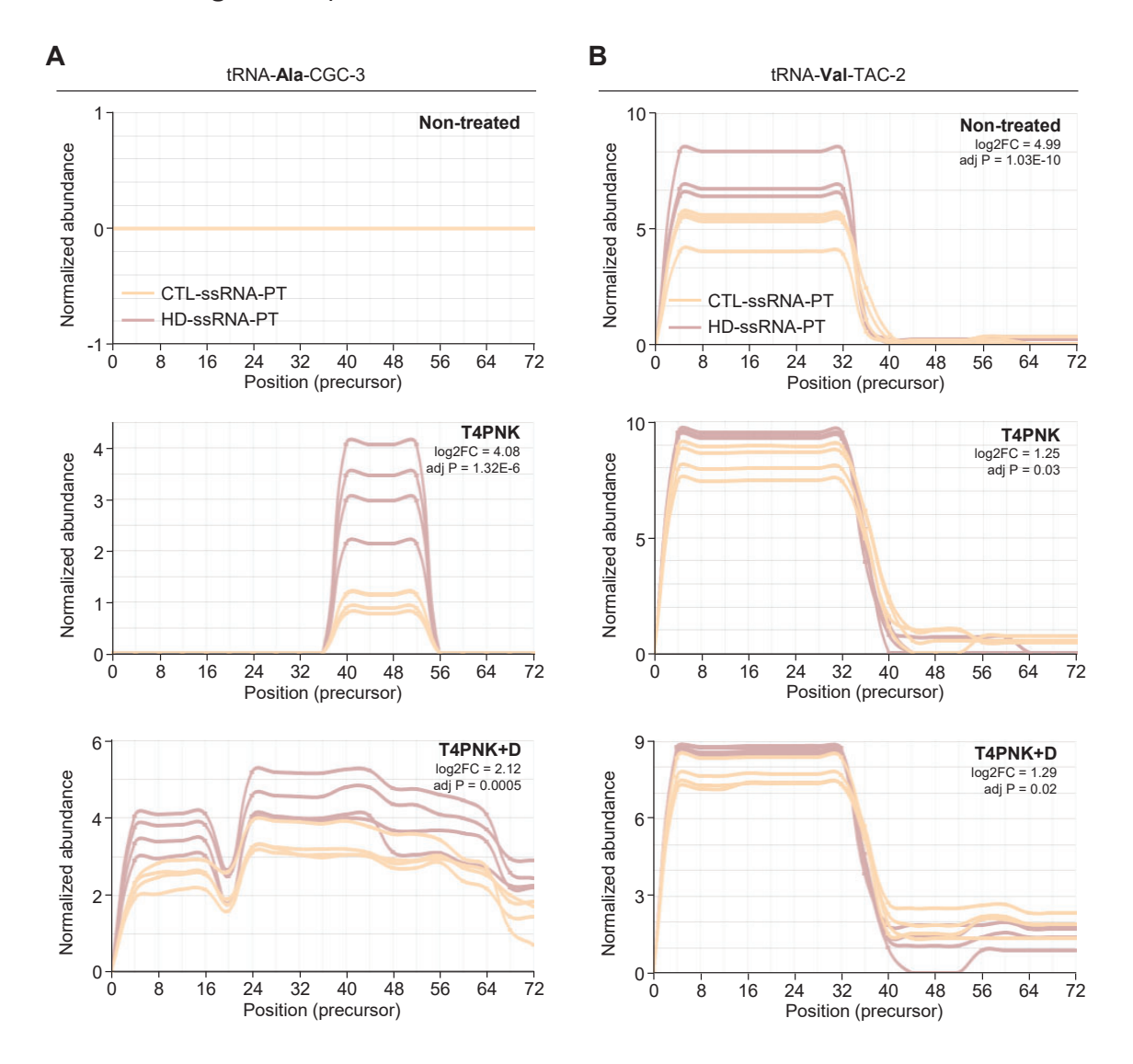


Figure 70. T4PNK and T4PNK+D pre-treatments are useful tools to decipher the complex tsRNA landscape present in the putamen of HD patients. Normalized abundance profiles of different tsRNA along each position of the mature tRNA isoacceptor. tsRNA derived from (A) tRNA-Ala-CGC-3 and (B) tRNA-Val-TAC-2 detected in CTL- and HD-ssRNA-PT samples are represented. Non-treated condition, T4PNK or T4PNK+D pre-treatment of the samples is indicated in each graph. Differential expression between conditions is shown by log2 fold changes and adjusted P specified in each graph. FC: fold change.

In conclusion, these experiments suggest that differential methylation signatures in tRNA derived from the putamen of HD patients could contribute to the increased tsRNA biogenesis observed in this brain region.

DISCUSSION

Important gaps remain in understanding the molecular basis underlying neurodegeneration in HD. In addition to the disruption of multiple cell processes induced by mHTT protein with expanded polyQ, here we provide evidence that both transcribed CAG repeat RNAs (reviewed in Martí, 2016) together with other classes of sRNA species that are strongly perturbed in HD directly participate in the pathophysiology of this disease. Neurotoxicity produced by CAG repeat RNAs of different lengths may be complemented by detrimental effects of strongly perturbed sRNA, such as tsRNA, as well as RAN translation products, thus adding complexity to the mechanisms causing neurodegeneration. In fact, although conflicting observations have been reported regarding the neurotoxic activity of RAN translation in HD (Bañez-Coronel et al., 2015; S. Yang et al., 2020), this discovery has hindered the differentiation between the toxicity produced by expanded CAG repeat-containing RNA and RAN polypeptides.

Several model systems of different neurological disorders have shown RNA toxicity due to expanded CAG repeats. *Drosophila melanogaster* was one of the first models showing neurodegeneration when elongated translated and untranslated CAG tracks were expressed (L. B. Li et al., 2008; Z. Yu et al., 2011). Subsequent studies have evidenced multiple RNA toxic mechanisms, including *HTTexon1* production, sCAG biogenesis, RAN translation or even sequestration of many RBPs leading to nucleolar stress, RNA transport impairments and alterations in alternative splicing, among others (Heinz et al., 2021; Malik et al., 2021; Martí, 2016). However, it remains to be elucidated to what extend the CAG-repeat expanded RNA and the expanded polyQ protein/peptides are contributing to the pathogenesis.

Focusing on HD, there is compelling evidence that suggests that RNA toxicity observed in this disease is not only caused by the expanded CAG RNA but also by other sRNA species. First, it has been described that sCAG are pathogenic RNA species and they are produced in HD brains from the expanded CAG RNA (Bañez-Coronel et al., 2012). However, the reversion of motor symptoms and the recovery of different protein markers strongly decreased in the R6/2 mouse model were only partial using a specific LNA blocking the expanded CAG-repeat RNA activity (Rué et al., 2016). Importantly, a strong dysregulation in the sRNA transcriptome has been observed in the most affected brain regions in HD (Martí et al., 2010), suggesting that sRNA, different from sCAG, could also be participating in the pathogenic mechanisms of HD. Therefore, to evaluate whether an altered sRNA transcriptome is an important contributor to the pathogenesis, we isolated, directly from the putamen of HD patients, a sRNA-enriched fraction containing different RNAs shorter than 200 nucleotides, that was subsequently injected in the striatum of WT mice. This approach allowed us to ensure that injected sRNA maintained the structures and the modifications present in the actual human pathologic situation. Our results showing motor alterations in HD-sRNA-PT-injected mice indicated that

DISCUSSION

HD-associated sRNA, without mHTT protein or its derivatives, are playing an important role that could be explained by multiple different sRNA-linked mechanisms. Hence, HD-sRNA-PT are able to induce a disease phenotype, accordingly with studies showing DM1-like histological and behavioral impairments in mice expressing a non-coding CAG-expanded RNA (Hsu et al., 2011).

1. Involvement of HD-sRNA-PT in HD neuropathology

Transcriptional alterations induced by HD-sRNA-PT

It is important to note that sRNA effects can be exerted both in the nucleus and in the cytoplasm (Quan et al., 2017; Qureshi & Mehler, 2012; Salta & De Strooper, 2012), highlighting the extensive potential of sRNA in carrying out their functions while dynamically modulating gene expression. In fact, experiments using fluorescently labelled Cy3-sRNA showed a widespread intracellular distribution with a mainly nuclear localization but also present in the cytoplasm, as it was expected due to their extensive area of action. Further characterization revealed that one hour after their injection, sRNA were localized within different types of cells, with an initial preference for striatal MSNs and microglial cells. It is worth mentioning that in this experiment we only analyzed samples up to one hour postinjection due to labelling detection limitations. Therefore, an eventual incorporation into other cell types at later timepoints and upon repetitive injections cannot be discarded.

It has been reported that extracellularly delivered RNAs can reach cells, be internalized and eventually regulate gene expression, facilitating cell-to-cell communications (Thomou et al., 2017; Vickers et al., 2011). Notably, the vast majority of these sRNA are not secured within extracellular vesicles but protected from degradation though their binding to proteins or forming secondary structures that provide resistance to nucleases (Tosar & Cayota, 2020; Vickers et al., 2011). The exact mechanisms by which the different extracellularly delivered and naked sRNA are incorporated in cells remain quite elusive (reviewed in Torres & Martí, 2021). Some uptake pathways have been proposed involving the recognition of specific motifs or certain secondary structures in sRNA by multiple RBPs (Pong & Gullerova, 2018; Prud'homme et al., 2016; Woolnough et al., 2015). Additionally, internalization of sRNA via clathrin- and raftlin-dependent endocytosis (Itoh et al., 2008; Watanabe et al., 2011) and even spontaneous uptake (Ivanov et al., 2014) have also been observed. After sRNA intrastriatal injections, we observed an increased incorporation of these sRNA into MSNs when these were produced both in the putamen and in the cortex of HD patients compared to the ones generated in the brain of non-affected individuals. This result suggested a differential composition of sRNA between genotypes and led us to hypothesize that sRNA produced in the HD brain present different motifs and/or secondary structures that favor its specific recognition and internalization by MSNs.

Regarding HD-sRNA-PT-induced effects, we found major gene expression changes in the striatum of injected mice that reflected neuronal dysfunction and immune activation, which eventually could be underlying the observed motor alterations. Downregulated genes were enriched in neuronal pathways, including synaptic transmission, axon guidance, and nervous system development. Furthermore, the group of downregulated genes highlighted perturbations analogous to those found in HD mouse models and patients (Ament et al., 2018; Becanovic et al., 2010; Brochier et al., 2008; Durrenberger et al., 2015; Han et al., 2010; Hervás-Corpión et al., 2018; Hodges et al., 2006; Labadorf et al., 2015; Langfelder et al., 2016, 2018; Le Gras et al., 2017; Merienne et al., 2019; Novati et al., 2018). In fact, defects in axonal guidance have been pointed by multiple studies showing HD-associated downregulated genes underlying this defect (Hodges et al., 2006) but also upregulated miRNA targeting this pathway (Martí et al., 2010). Additionally, upregulated genes mainly corresponded to microglial-specific transcripts, pointing to a microgliosis in the striatum of injected mice, which is an HD hallmark present in the most affected brain regions (Crotti & Glass, 2015; Pavese et al., 2006; Tai et al., 2007; Valadão et al., 2020). It is worth noting that the massive inflammation observed after HD-sRNA-PT injections was not so obvious when CTL-sRNA-PT were used, indicating that sRNA species generated in HD brains can specifically activate these processes. However, determining how microglial activation in response to sRNA is linked to neurodegenerative mechanisms is still a matter of study.

The most consistently dysregulated transcripts in HD-sRNA-PT-injected animals compared to other conditions were associated to immune response activation and inflammatory pathways, with a special enrichment in transcripts related to interferon signaling. As abovementioned, extracellular sRNA can be captured by cells through endocytosis. In this process, the receptor for advanced glycation endproducts (RAGE), which is expressed on the cell surface of neuronal and microglial cells (Kierdorf & Fritz, 2013), binds to sRNA in a sequence-independent manner enhancing cellular RNA uptake into endosomes (Bertheloot et al., 2016). Notably, RNAs internalized via RAGE are able to activate TLRs that are localized within endosomes and function as single stranded RNA-sensors triggering the induction of INF responses (G. Q. Liu & Gack, 2020). Taking into account that HD-sRNA-PT are delivered extracellularly as a consequence of the injection strategy used and also that mice displayed increased activation of INF pathways in the striatum, it is tempting to speculate that these species exert their functions via activation of TLRs that specifically sense these sRNA. Our data indicate that specific TLRs are strongly induced by HD-sRNA-PT, particularly TLR1, TLR2, TLR4, TLR5, TLR6, TLR7, TLR8 and TLR13, suggesting that both single and double-stranded sRNA may mediate downstream proinflammatory signaling. Furthermore, the activation of different TLRs by host sRNA, such as miRNA and tsRNA, leading to INF responses has been

DISCUSSION

associated not only with an immune activation and cytokine production but also with neurotoxicity and apoptosis (Coleman et al., 2017; Lehmann et al., 2012; Pawar et al., 2020). However, the exact signaling cascade linking TLR activation and caspase-3 cleavage leading to apoptosis remains to be elucidated, although some candidates such as Jun N-terminal kinase have been proposed to be involved (S. C. Tang et al., 2008).

Importantly, downregulated transcripts induced by HD-sRNA-PT injection were specifically enriched in striatal MSNs of the indirect pathway, in line with a reduction of ENK and DRD2 protein levels in the striatum of those animals. Conversely, HD-sRNA-PT injections did not exert any neurotoxic effect over striatal interneurons, which is consistent with their already described resistance to neurodegeneration in HD (Ferrante et al., 1987; Vonsattel & DiFiglia, 1998). Therefore, these results suggest a selective detrimental activity of HD-sRNA-PT preferentially affecting D2-MSNs, the striatal neuronal population to first degenerate in human HD patients (Bergonzoni et al., 2021; Reiner et al., 1988; Richfield et al., 1995; Rikani et al., 2014; Sapp et al., 1995), but poorly recapitulated by HD mouse models (Ferrante, 2009; Naver et al., 2003).

It has been speculated that cell-type-specific traits account for the differential modulation of toxicity in HD, including specific requirements for survival signaling, energy demand, neurochemical content, glutamate neurotransmission and axonal transport (Han et al., 2010). Our data indicate that HD-sRNA-PT injection was able to significantly alter genes related to glutamatergic synapse function and axon guidance, which could contribute to the impairment of neuronal pathways and especially impact on striatal D2-MSNs normal function. Additionally, cell-typespecific gene expression studies have associated mitochondrial RNA release in D2-MSNs leading to innate immune activation as a process that may contribute to their enhanced vulnerability (H. Lee et al., 2020). This would be consistent with the preferential sensitivity of D2-MSNs and the overactivation of the immune response observed after HD-sRNA-PT injections. In fact, it has been described that many interferon-responsive genes are selectively upregulated in D2-MSNs of the striatum in different HD mouse models (H. Lee et al., 2020), which is in line with the differentially upregulated transcripts found in HD-sRNA-PT-injected mice. However, we did not detect a significant overrepresentation of mitochondrialderived sRNA in the HD-sRNA-PT-injected pools, suggesting that additional sRNA biotypes are contributing to this response. An overactivation of PKR, an RNA sensor that triggers the activation of the interferon pathway, has been observed in the striatum of HD mice (H. Lee et al., 2020) and also in our injected animals, as well as directly associated to cell death (Chung et al., 2018), suggesting a mechanistic link between HD-derived sRNA, D2-MSNs vulnerability and the aberrant immune response observed.

Overall, these findings strongly point to the participation of sRNA in the general transcriptomic alterations associated with the disease. Additionally, one may hypothesize that endogenous sRNA released during neuronal degeneration might cause further spread of damage in the central nervous system through a paracrine activity. Given the relevance of sRNA in regulating cell homeostasis, their dysregulation and neurotoxic activity could be envisioned as a general mechanism in neurodegeneration. Whether cell-autonomous or non-autonomous sRNA detrimental signaling occurs in HD and other neurodegenerative conditions requires additional research.

Specific neurodegeneration induced by HD-sRNA-PT

Having defined the transcriptomic alterations caused by HD-sRNA-PT injections, we wondered whether changes in gene expression were translated into alterations at the protein level. Indeed, HD-sRNA-PT contributed to a pronounced decline in the levels of numerous striatal neuronal markers severely impaired in HD. One example is found in STEP, a phosphatase that is highly expressed in the striatum and whose levels and activity are reduced in the presence of mHTT in vivo (Saavedra et al., 2011). Hence, diminished levels of STEP, as well as of other markers, in HD-sRNA-PT-injected mice in the absence of mHTT protein and its derivatives reinforces the idea of a toxic mechanism at the RNA level. Considering that DARPP32 is a classical hallmark of MSNs, whose loss determines the different grades of the disease (Vonsattel et al., 1985), it is important to remark that the striatum of HD-sRNA-PTinjected mice also presented a reduction in the number of DARPP32-positive cells corroborated by diminished levels of this protein by WB analysis, pointing to distinctive alterations commonly found in HD. In summary, changes in the expression of these proteins may reflect the neurotoxic effect of HD-sRNA-PT leading to an alteration of striatal neuronal function, consistent with the poor performance in the behavioral tests exerted by injected mice.

Moreover, we showed that the loss of striatal neuronal markers was accompanied by a significant increase in cleaved caspase-3-positive cells in the striatum of HD-sRNA-PT-injected animals, indicating an activation of apoptotic cell death, which has been also shown in the striatum of HD patients (Pattison et al., 2006). Consistently, it has been described that sRNA, such as miRNA and tsRNA, are able to regulate rRNA biogenesis (H. K. Kim et al., 2017, 2019; Talimur Reza & Yuan, 2021) and also that rRNA perturbations induce nucleolar stress (Tsoi et al., 2012; Tsoi & Chan, 2014), which has been linked to apoptosis and neurodegeneration in different paradigms (Kalita et al., 2008; Parlato et al., 2008; Pietrzak et al., 2011; Rieker et al., 2011; Tsoi et al., 2012; Tsoi & Chan, 2013).

However, there are multiple alternative mechanisms by which sRNA may trigger apoptotic cell death. As it has been mentioned, activation of TLR-associated

DISCUSSION

pathway could mediate neuronal death comprising the induction of cleaved caspase-3 (Lehmann et al., 2012; S. C. Tang et al., 2008). In fact, due to the broad expression of TLRs in neurons along the nervous system and their implication in various pathological conditions (T. Liu et al., 2010; Préhaud et al., 2005), including AD, PD, ALS and MS in which no infectious pathogens are involved (Bsibsi et al., 2002; Letiembre et al., 2009; Prinz et al., 2006; Walter et al., 2007), TLRs have even been proposed as death receptors in neurodegenerative disorders (Lehmann et al., 2012; S. C. Tang et al., 2008). Notably, a deficiency of TLR2, TLR3 and TLR4 in a HD mouse model has been associated with longer life expectancies (Griffioen et al., 2018). Therefore, the identification of sRNA that act as specific TLR ligands leading to innate immune activation and eventually to neurotoxicity, opens a new avenue that requires further investigation.

HD neuropathology represents the outcome of a cascade of events in which neurons are differentially vulnerable. Although the dramatic reduction of MSNs in the striatum is the most visible hallmark (Vonsattel et al., 1985), cortical cell loss has been also reported (Rosas et al., 2003; Vonsattel & DiFiglia, 1998). In contrast, other brain areas such as the cerebellum typically display little to no detectable cell loss or volume changes (Rosas et al., 2003). In terms of transcriptomics, these different brain areas show distinct regional patterns that parallel the neuropathology, with major dysregulations in the striatum and cortex and minor changes in the cerebellum (Hodges et al., 2006). Indeed, an extensive characterization of transcriptomic signatures in different brain regions along disease progression in KI mice has been reported, showing CAG length-dependent and brain region-associated miRNA dysregulations (Langfelder et al., 2018). However, similar studies considering additional sRNA biotypes also need to be addressed.

Our data show that HD-sRNA obtained from the different HD brain areas, when injected in mice striata, are sufficient to produce HD-like motor perturbations in WT mice. Furthermore, our results suggest that sRNA from the most affected brain regions, namely putamen and cortex, are more toxic compared with sRNA generated in less-affected brain areas such as the cerebellum, accordingly with the differential regional vulnerability that has been observed in HD (Han et al., 2010). In conclusion, our findings point to intrinsic characteristics of the most affected brain areas underlying the formation of harmful sRNA species and leading to region-specific sRNA signatures associated to differential vulnerability. However, a potential selective differential sensitivity of the brain region in front of different sRNA species still needs further exploration.

Role of HD-sRNA-PT in inflammation

Although progressive dysfunction and eventual loss of neurons represents the main hallmark in neurodegenerative disorders, another common feature among them is a chronic immune activation, in particular of microglial cells, leading to detrimental consequences despite of the triggering initial event (Amor et al., 2010). In parallel, multiple ncRNAs have been implicated in inflammation processes specifically regulating cytokine and chemokine production in both physiological and pathological conditions (Ashrafizadeh et al., 2022). Here, we observed an aberrant striatal inflammation induced by HD-sRNA-PT injections, which was evidenced by the increased levels of multiple pro-inflammatory factors, such as Cxcl2, Tnf, Il6, Il1b and Ptgs2.

Interestingly, NLRP3 inflammasome is an intracellular protein complex activated by TLRs whose function entails caspase activation that, in turn results in IL1b and IL18 production. Notably, NLRP3 aberrant signaling has been associated with different neurodegenerative diseases, such as AD and PD, where its regulation has been postulated as a strategy for alleviating, or even blocking, certain detrimental processes (E. Lee et al., 2018; Nakanishi et al., 2018; Stancu et al., 2019). Accordingly, it has been also shown that there is an enhanced expression of the NLRP3 inflammasome in the striatum of R6/2 mice as well as in HD-sRNA-PTinjected mice, which could be contributing to the detected increase in caspase 1, Il18 and Il1b levels in their striata. However, an evaluation of their protein levels would be required to validate this hypothesis. Notably, a treatment inhibiting NLRP3 inflammasome assembly induced a reduction in gliosis together with an improved neuronal survival in the striatum of R6/2 mice, ameliorating motor dysfunction and extending animals life span (K.-P. Chen et al., 2021). Although this study associates NLRP3 activation to mHTT protein aggregation, our findings point to a role of sRNA as additional contributors which are sufficient to induce the activation of NLRP3 expression. Therefore, further characterization of the mechanisms underlying NLRP3-triggered inflammation and cell death will provide important insights that could facilitate the development of novel therapeutic agents by targeting upstream activators such as sRNA.

However, a major unsolved question in our model is whether sRNA-associated inflammation is an early event preceding neurodegeneration or a consequence of it. To shed light on the temporal pattern of these processes, we performed an acute injection of HD-sRNA-PT in the striatum of WT mice and we observed an increased inflammation prior to neuronal alterations. Accordingly, studies in this field have also described that microglial cells produce inflammatory cytokines upon exposure to certain extracellularly delivered miRNA (Coleman et al., 2017; Feng et al., 2017; Lehmann et al., 2012; Pawar et al., 2020). In fact, there are multiple widely reported miRNA that have been associated to inflammation activation, such as let-7, miR-

DISCUSSION

155, miR-132, among others (Das & Rao, 2022; Slota & Booth, 2019). However, none of them have been found upregulated in HD-sRNA-PT injected pools, pointing to other sRNA biotypes as main drivers of the neuroinflammation observed. Strikingly, microglial activation has been demonstrated to be non-essential for the miRNA-triggered neurodegenerative effects in purified neuronal cultures (Lehmann et al., 2012). In summary, accumulating evidence suggests that sRNA-associated initial pro-inflammatory environment could be enhancing the neurotoxic effects of sRNA *per se*, although not being the primary cause.

Finally, although the pattern of cytokine expression favors a pro-inflammatory phenotype, no significant increases in Iba1 and GFAP levels were detected (data not shown). We hypothesize that complete glial activation might occur at later timepoints, since studies on neuroinflammation show a sequential activation of microglial- and astrocyte-cytokine expression, preceding that of Iba1 and GFAP (Norden et al., 2016).

2. Identification of HD-sRNA-PT neurotoxic species

Contribution of sCAG to the overall effects of HD-sRNA-PT

Several studies have demonstrated the ability of expanded CAG RNA to exert toxicity though multiple mechanisms (reviewed in Heinz et al., 2021; Malik et al., 2021; Martí, 2016). One strategy is based on the aberrant folding into long hairpin structures formed by the expanded triplet repeats included in the mutated genes implicated in several TREDs (Michlewski & Krzyzosiak, 2004; Napierala et al., 2005; Napierala & Krzyzosiak, 1997; Sobczak & Krzyzosiak, 2004, 2005; Tian et al., 2000). Dicer-dependent processing of these hairpins results in sCAG biogenesis, which has been reported in multiple neurodegenerative paradigms, including HD, and has been associated with neurotoxicity (Bañez-Coronel et al., 2012; Krol et al., 2007; Lawlor et al., 2011; Z. Yu et al., 2011). However, it remains to be elucidated the extend of sCAG-associated detrimental impact on the overall RNA toxicity.

Our results point to a partial role of sCAG in the global pathogenic alterations produced by HD-sRNA-PT injection into the mouse striatum. For instance, motor perturbations were partially prevented by intrastriatal injection of LNA-CTG whereas the direct injection of pure sCAG in the striatum induced moderate motor coordination deficits. Accordingly, previous studies of our group demonstrated that the inhibition of *mHTT* RNA expression using LNA-CTG was able to reverse motor deficits in the R6/2 HD mouse model (Rué et al., 2016). Although the LNA-CTG used presents a remarkable biological stability due to their phosphorothioate-modified backbones (Bennett & Swayze, 2010), further experiments are required to explore how the observed prevention and the described reversal of motor impairments are modulated in the long term.

We hypothesize that sCAG species derived from human HD brains may contribute to motor dysfunction by targeting DARPP32 positive neurons, since LNA-CTG significantly prevented the loss of DARPP32 levels induced by HD-sRNA-PT injection and pure sCAG infusion decreased striatal DARPP-32 protein levels. These results are in line with a prevention of DARPP32 protein levels reduction in LNA-CTGtreated R6/2 mice (Rué et al., 2016) as well as with the detrimental effects induced by sCAG species in diverse cell models (Bañez-Coronel et al., 2012; Murmann et al., 2018) and reinforce the idea of sCAG as contributors to the disease as its specific blockage confers neuroprotection. It has been reported that the neurotoxic activity of sCAG in cell models is dependent on the RISC gene-silencing machinery (Bañez-Coronel et al., 2012). However, the present data suggest a post-transcriptional mechanism of action, since LNA-CTG beneficial effects do not induce major changes in the transcriptome of HD-sRNA-PT-injected striatum. Considering the fact the expanded CAG RNA is able to bind multiple RBPs (Heinz et al., 2021; Malik et al., 2021; Martí, 2016), additional similar functions involving sCAG species should be explored. In the case of miRNA, an alternative mechanism for gene expression modulation has been described where miRNA directly binds to RBPs inhibiting their functions (Eiring et al., 2010). Hence, the characterization of sCAG capacity for binding proteins may shed light to potential novel sRNA-associated pathogenic mechanisms.

In addition, LNA-CTG did not prevent HD-sRNA-PT-induced decrease in the protein levels of diverse neuronal markers, nor in the glial reactive response, which agrees with the effect elicited by the injection of pure sCAG. Furthermore, the lack of effect of sCAG in the number of DARPP32 and cleaved caspase-3-positive cells suggests that sCAG are not primarily responsible for the HD-sRNA-PT-induced apoptotic cell death. In line with this, genetic mouse models expressing versions of the HTT exon 1 with expanded CAG repeats (Turmaine et al., 2000) or longer versions of the *mHTT* gene (Hodgson et al., 1999; Reddy et al., 1998; Z. X. Yu et al., 2003) differ in the severity and onset of the motor symptoms, but do not show prominent striatal cell death.

Therefore, these observations are consistent with the idea that sCAG species are contributors to the sRNA toxicity (Figure 71), accordingly with previous published data regarding HD pathogenesis (Bañez-Coronel et al., 2012) and underlie common phenotypes within other TREDs, such as DM1 (Z. Yu et al., 2011). However, it must not be forgotten that as *mHTT* is ubiquitously expressed throughout the body, sCAG biogenesis may occur in multiple tissues where the effects seem to be negligible, suggesting differential cell type-specific vulnerabilities to these species and/or differential biogenesis. In fact, a selective modulation of Dicer activity contributing to a differential production of sCAG has been proposed (Bañez-Coronel et al., 2012), although a selective downregulation of Dicer has also been reported in HD

DISCUSSION

putamen (Petry et al., 2022). Moreover, when focusing in the most affected brain areas, neurodegeneration appears as a progressive process pointing to a long term and/or accumulative detrimental effect of sCAG species, integrated with many other pathological processes occurring in the HD brain. Overall, we hypothesize that sRNA, besides of sCAG, produced in human HD putamen expressing full-length mHTT, may also participate in important HD pathological hallmarks, including striatal neuronal dysfunction, glial activation and transcriptomic dysregulation and thus, fitting with the idea of a complex combination of pathogenic sRNA inducing toxicity.

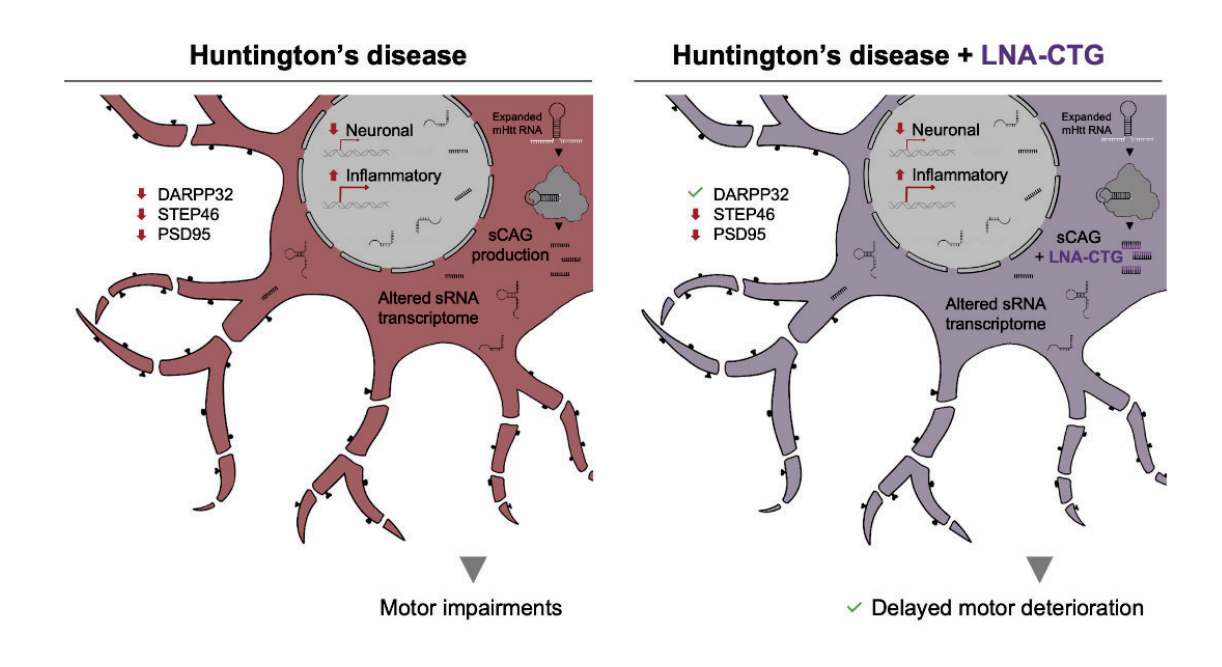


Figure 71. sCAG species contribute to sRNA-associated pathogenic mechanisms in HD. Schematic representation of how the altered sRNA transcriptome found in HD putamen, which includes a dysregulation in sCAG production as well as in many other sRNA biotypes, is able to induce transcriptomic alterations underlying neurodegeneration and neuroinflammation leading to motor alterations. A specific blockage of sCAG species using an LNA-CTG demonstrates their contribution to neuronal dysfunction and consequently to motor impairment.

Contribution of non-sCAG species to the overall effects of HD-sRNA-PT

The more likely detrimental species contributing to the HD-like neuropathology observed are those specifically expressed in the HD-sRNA-PT pool and virtually absent in CTL-sRNA-PT pool. In order to obtain a proper characterization of the full sRNA transcriptome, we used the Seqcluster bioinformatic tool (Pantano et al., 2011, 2016) that deals with multi-mapping events, therefore ensuring an unbiased count-based differential expression analysis. This was particularly important because multi-mapping phenomenon represents a major drawback in the analysis and quantification of sRNA, especially tRNA and other ncRNA genes with

duplications on the genome. Sequencing analysis validated many of the previously reported HD overexpressed miRNA, including miR-19b, miR-92a, miR-151-3p, miR-219a-5p, among others (Martí et al., 2010). In addition, HD-sRNA-PT pool showed a strikingly overrepresentation of 5'-end tsRNA, which have been shown to accumulate by stress-induced cleavage of mature cytoplasmic tRNA in a wide variety of eukaryotes (Emara et al., 2010; Fu et al., 2009; Saikia et al., 2012; Thompson et al., 2008; Yamasaki et al., 2009). Notably, far from being random degradation products (Schimmel, 2017), produced tsRNA have been implicated in multiple relevant functions (Blaze & Akbarian, 2022; Krishna et al., 2021; B. Liu et al., 2021).

It is worth mentioning that since tRNA are key molecules canonically implicated in protein synthesis, full length tRNA destruction resulting in decreased rates of translation seems to be a feasible scenario. However, this hypothesis is overly simplistic since several studies have demonstrated that the steady state levels of tRNA is not significantly altered by tsRNA biogenesis (Saikia et al., 2012; Thompson et al., 2008; Yamasaki et al., 2009). Nevertheless, tsRNA are bioactive molecules that could eventually regulate gene expression at multiple levels, including via post-transcriptional regulation and/or inhibition of translation initiation (Guzzi et al., 2018; Haussecker et al., 2010; Ivanov et al., 2011; Lyons et al., 2017; Yeung et al., 2009) or, conversely, promoting translation though the interaction with ribosomal proteins, such as RPS21 (Z. Chen et al., 2019).

Oxidative stress has been proposed as a potential mechanism resulting in tRNA cleavage and, at the same time, it has been associated to multiple neurodevelopmental disorders, such as autism, Rett syndrome and Down syndrome (De Felice et al., 2012; Essa et al., 2013; Lintas et al., 2012), as well as to neurodegenerative diseases (reviewed in Gámez-Valero et al., 2020). Consistently with our observations, deep characterization of sRNA transcriptome of PD patients showed a significant dysregulation of tRNA-derived expression profiles, both in motor and pre-motor stages of the disease, reflecting early pathological perturbations (Pantano et al., 2016). Furthermore, alterations in tsRNA biogenesis have been associated with impaired neuronal functions and even with neurodegeneration (Anderson & Ivanov, 2014; Blanco et al., 2014; Hanada et al., 2013; Karaca et al., 2014).

In accordance with the differential vulnerability among HD brain regions, our data showed a major dysregulation in the tsRNA profile in the putamen compared to other brain areas. Taking this into account, we next focused on three top tsRNA candidates displaying an important overexpression in HD putamen, which was validated by RT-qPCR in an independent cohort of HD patients. Besides, they were also consistently upregulated in the cortex and cerebellum of HD patients. Hence,

DISCUSSION

we found that a specific 5'tRF-Ala derived from the tRNA-Ala-AGC-2 was able to compromise cell viability in striatal primary neurons, suggesting that at least this sRNA contributes to HD-sRNA-PT pathogenicity. Nonetheless, additional studies are needed to determine whether tsRNA are neurotoxic *in vivo*, in a model organism, and if their blockage could be further envisioned as a therapeutic strategy for HD. However, it is important to remark that our data provide the basis for further investigations linking aberrant expression of diverse types of tsRNA and HD neurodegeneration.

3. Importance of sRNA biogenesis in HD putamen

Role of endonucleases and RNA methyltransferases

It has been widely demonstrated that changes in cellular functional states are accompanied by finetuned modifications in sRNA expression patterns, which accommodate cell responses to environmental physiological and pathological stimuli. In fact, it has been recently described that different cellular stressors, such as oxidative stress, hypoxia or nutrition deprivation, result in highly dynamic changes in both cellular and extracellular tsRNA signatures (G. Li et al., 2022). Accordingly, multiple studies have demonstrated that tsRNA biogenesis is a highly regimented process implicating multiple ribonucleases, comprising the stressinduced endonucleases ANG and RNAse T2 (reviewed in Magee & Rigoutsos, 2020). Although we were not able to detect significant changes in the protein levels of these ribonucleases either in the putamen nor in the frontal cortex of HD patients, alterations in their activities could not be discarded. Likewise, recent research showing that only some tRNA halves rely on ANG, points to the existence of yet-tobe-identified cleavage mechanisms (Su et al., 2019). Moreover, it is worth mentioning that the rationale for the exploration of RNAse T2 levels, besides its implication in tRNA cleavage, was based on a study showing its pivotal role in generating RNA molecules that can be eventually recognized by TLR8 (Greulich et al., 2019).

Apart from the role of ribonucleases targeting tRNA, tsRNA biogenesis is tightly regulated through post-transcriptional modifications (M. Schaefer et al., 2010; Torres, Batlle, et al., 2014) critically impacting on tRNA stability (Blanco et al., 2014; Lyons et al., 2018; Tuorto et al., 2012). Hence, alterations in tRNA modification patterns shape tsRNA biogenesis determining their specific production (Schimmel, 2017) in addition to the fact that mutations in tRNA modification enzymes have been prominently associated with neurodevelopmental and neurodegenerative disorders (Boccaletto et al., 2022; Chujo & Tomizawa, 2021). Therefore, studying the expression of enzymes regulating tRNA post-transcriptional modifications is crucial to understand tsRNA biogenesis in HD putamen. Our results demonstrate that there is a reduction in the protein levels of the RNA methyltransferase NSun2, both in the putamen of HD patients and in the striatum of two different HD mouse

models, expressing either the N-terminal or the full length *mHTT* gene. Importantly, it has been described that NSun2 deficiency negatively impacts on learning and memory in NSun2-ablated *Drosophila* (Abbasi-Moheb et al., 2012) and mice models (Blaze et al., 2021; George et al., 2022) and appears as a cause for intellectual disability and neurological impairment in humans (Khan et al., 2012; Martinez et al., 2012). Besides, we show that the most significant alteration in NSun2 levels is observed in the putamen, indicating a specific deficiency in the most affected brain area in HD, whereas non-significant changes were detected in brain regions typically not considered to be primary sites of HD neuropathology. It is worth mentioning that our studies in HD mouse models allowed the exploration of this reduction in the striatum throughout disease progression, identifying NSun2 alterations even in pre-symptomatic stages. However, further studies will be important to uncover how these findings correlate with changes detected in humans.

In line with our results, it has been recently reported that AD patients present NSun2 reduced levels in the prefrontal cortex and hippocampus (Y. A. Kim et al., 2022), suggesting a plausible link between NSun2 deficiency and the stress conditions associated to neurodegeneration. For instance, there are alterations occurring along HD pathogenesis which are unrelated to HD-primary episodes but may be reactive events to secondary-common processes arising from neurodegeneration and eventually resulting in similar abnormalities across different neurodegenerative disorders. Consequently, more experiments in this field are required to shed light onto the relation between NSun2 and the mechanisms of neurodegeneration.

Additionally, we observed positive NSun2 staining in MSNs of the striatum with a reduction in its levels in R6/1 compared to WT mice. However, potential changes in NSun2 levels have not been evaluated in other neuronal and glial cells of this brain region. Hence, finding out whether it is an MSN-specific alteration contributing to their vulnerability appears of vital importance, which would be in accordance to previously published neuroprotective roles of NSun2 (Blanco et al., 2014) and would provide tentative evidence that targeting NSun2 could be of therapeutic value.

In agreement with the widely described function of NSun2 introducing cytosine-5 methylations, we explored m⁵C general levels in the brain of HD mice already displaying striatal NSun2 expression alterations. We observed that these animals also exhibited reduced m⁵C levels in the striatum, pointing to a mechanism that could be involved in the striatal enhanced sensitivity to different stressors, which is a process that has been already described in multiple paradigms (Begley et al., 2007; Jablonowski et al., 2006; M. Schaefer et al., 2010). Remarkably, there is some

DISCUSSION

direct evidence that natural RNAs are capable of activating immune cells and that the methylation status of these molecules can have a modulatory effect. In fact, a potent RNA-mediated immune stimulation is carried out by hypomodified RNAs through the activation of TLRs, identifying nucleoside modification as a mechanism that suppresses the immune-stimulatory effect of RNA (Durbin et al., 2016; Karikó et al., 2005; Tong et al., 2021). Therefore, we hypothesize that m⁵C reduction could be participating in the immune response activation exerted by HD-sRNA-PT. However, further experiments are required to demonstrate whether the m⁵C reduction observed is affecting DNA and/or RNA molecules and whether it has a specific impact on certain sRNA biotypes. Furthermore, it is important to note that an *in vivo* depletion of NSun2 leading to a decreased m⁵C RNA methylome, resulted in an enhanced recognition of the hypomethylated RNAs through the RNA sensor RIG-I triggering INF signaling (Y. Zhang et al., 2022), which is a mechanism that could potentially link NSun2 alterations found in HD putamen with the immune activation observed after HD-sRNA-PT injections.

Consistently with the hypothesis of an increased tsRNA biogenesis due to an hypomethylation of precursor tRNA as a consequence of a lack of NSun2 previously proposed (Blanco et al., 2014), we detected an overrepresentation of tsRNA in the HD putamen that resulted from the cleavage of NSun2 tRNA targets (Auxilien et al., 2012; Brzezicha et al., 2006; Khoddami & Cairns, 2013; Squires et al., 2012; Tuorto et al., 2012), suggesting that many tsRNA overexpressed in HD have been cleaved depending on the methylation status of the precursor tRNA. Therefore, accumulated evidence guided our efforts to study the modifications present in tRNA potentially providing an additional source of pathogenic alterations in HD.

Role of epitranscriptomic modifications

A deep characterization of several epitranscriptomic modifications in a purified fraction of tRNA from the putamen of HD patients and unaffected individuals was performed using LC-MS. Hence, we detected differential tRNA modification signatures between genotypes, including significant changes in ⁵fC, m⁶A, m¹I, acp³U, D and Y modifications. Unfortunately, we were not able to confirm the hypothesized reduction in m⁵C levels specifically in tRNA obtained from the putamen of HD patients. For instance, it is worth noting that NSun2 is not the only NSun family member responsible for m⁵C deposition in tRNA and thus NSun6 (Haag et al., 2015; Long et al., 2016) and Dnmt2 (Goll et al., 2006; M. Schaefer et al., 2010) could be compensating NSun2 deficiency as these two enzymes present common substrates (Tuorto et al., 2012). Accordingly, NSun2 KO studies using tRNA bisulfite sequencing have shown that not all NSun2-target methylation residues are equally affected by its ablation, as it is the case of the cytosine in the position 37 whose methylation remains unaltered independently of NSun2 activity (Blaze et al., 2021), pointing to an involvement of a combination of RNA methyltransferases in the final

tRNA m⁵C methylome. Furthermore, as NSun2 tRNA-targets are limited to a subset of tRNA isotypes, an exhaustive analysis discriminating between tRNA isotypes and cytosine residues positions would be interesting since our approach may have under covered specific alterations. However, it could not be discarded that although in the neurodevelopment NSun2 is essential for the inhibition of aberrant tsRNA production (Blanco et al., 2014), different processes might occur in the adult neurodegenerating brain consistently with the lack of tsRNA overproduction found in an adult NSun2 KO mouse model (Blaze et al., 2021).

Although tRNA are the most well-characterized targets of NSun2 methyltransferase activity, additional studies are required to explore the heterogeneous non-tRNA species potentially methylated by this enzyme in the HD brain. In fact, it has been described that NSun2 is also capable of targeting miRNA (Yuan et al., 2014), rRNA (Chow et al., 2007), snoRNA (Khoddami & Cairns, 2013), vault RNA (Hussain et al., 2013; Sajini et al., 2019) and even mRNA (Jian et al., 2021; X. Yang et al., 2017; X. Zhang et al., 2012). Moreover, deficiencies in NSun2 have also been associated to alterations in miRNA methylations leading to changes in tau phosphorylation levels and thus, modulating tau-induced toxicity in AD (Y. A. Kim et al., 2022). Given all this evidence, we consider that it would be really interesting to explore whether there is an m⁵C hypomethylation in certain sRNA biotypes contained in the HDsRNA-PT pool, besides tRNA, in order to correlate NSun2 striatal deficiency with HD pathogenic mechanisms. For instance, it is plausible to hypothesize that a general m⁵C hypomethylation in the HD-sRNA-PT, caused by the NSun2 reduction, could be triggering the aberrant INF signaling observed in the striatum of HD-sRNA-PTinjected animals, in accordance to the mechanism described by Zhang et al., 2022. In conclusion, future studies are needed to better untangle the complexity of NSun2 targets which may include other potential RNA subtypes already associated with HD pathogenesis.

There is increasing amount of evidence that has identified general tRNA hypomodification, as well as genetic mutations in the respective tRNA-modifying enzymes, as a process underlying several human pathological conditions, including neurological and metabolic disorders, cancer and mitochondrial-linked diseases (Pereira et al., 2018). Consistently, we detected different tRNA hypomethylations in HD putamen, namely m⁶A, m¹I and ⁵fC, which is a product of oxidation of m⁵C. However, the mechanisms leading to these altered epitranscriptome are still unclear as well as whether these alterations have direct consequences on the pathogenic mechanisms underlying HD. Therefore, an extensive characterization of several epitranscriptomic regulatory proteins in HD, that could explain the HD-associated dysregulated epitranscriptome, is becoming increasingly important (Figure 72).

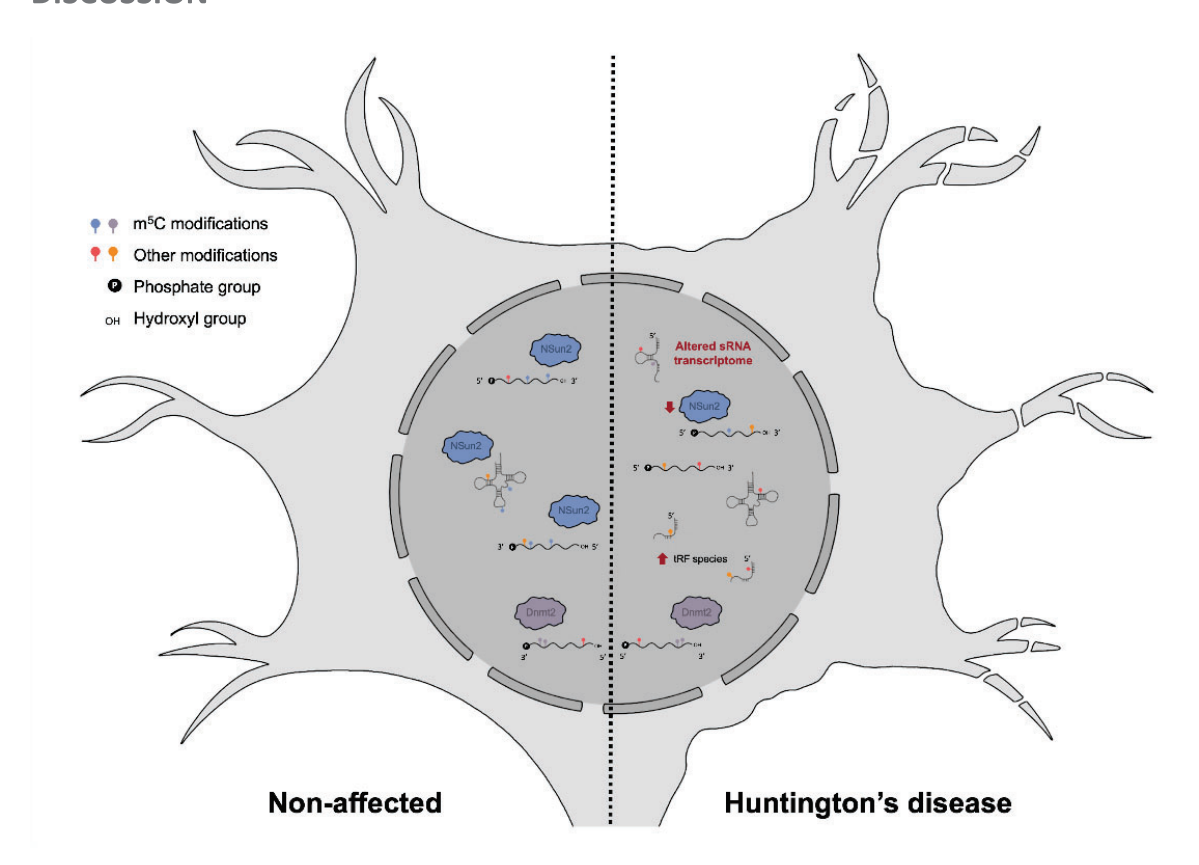


Figure 72. HD putamen exhibits a defective sRNA transcriptome, including an aberrant production of particular tsRNA species, together with specific alterations in post-transcriptional modification enzymes, potentially contributing to striatal vulnerability. Schematic representation of the proposed model showing alterations in post-transcriptional modification enzymes which may be involved in the dysregulated sRNA transcriptome found in HD putamen, with some species showing a potential neurotoxic role in HD pathogenic mechanisms.

Revealing modified species in HD putamen

Taken together, our results emphasized the importance of assessing tsRNA formation regulome as a layer of complexity previously disregarded in the HD context. However, there are important methodological concerns for the study of tRNA and tsRNA species that must be considered. First of all, it should be emphasized that the techniques used for RNA purification and library preparation have a significant impact on the high-throughput RNA-sequencing outcomes, potentially leading to unneglectable biases (Raabe et al., 2014). In fact, mapped read counts may under or overestimate real RNA abundances depending on the different library construction procedures, including the steps of reverse transcription, adaptor ligation or amplification (H. Shi et al., 2021; E. L. Van Dijk et al., 2014). As a consequence, RNAs bearing diverse modifications are often inefficiently and incompletely characterized limiting their discovery, which is a problem that particularly affects tsRNA species (Schimmel, 2017; X. Zhang et al., 2016). Therefore, most of the studies using conventional RNA sequencing techniques fail to capture a significant portion of the complex tsRNA pool.

Considering the main limitations in the study of these species, we can divide them into two major categories. On the one hand, tsRNA contain similar posttranscriptional modifications to those in mature tRNA, representing a challenge for the performance of a complete reverse transcription. An inefficient reverse transcription step results in the undercounting of bona fide tsRNA but also alters size estimations of these species due to premature reverse transcription abortion. On the other hand, sRNA metabolism involves enzymatic cleavage generating RNA products with diverse sequence endings depending on the ribonuclease, comprising -OH or -P groups in the 5' or the 3'-ends or even cyclic phosphate groups that result from a phosphate bridge between the 2'- and the 3'- positions of the pentose (2',3'-cP; Shigematsu et al., 2018). For instance, RNAse T2 is an example of enzyme that preferentially cleaves RNA molecules generating 5'-OH and 2',3'-cP ends (Greulich et al., 2019). Standard sRNA-sequencing methods rely on 5'-P and 3'-OH specific ends, which is the case of miRNA and some tsRNA, and alternative sRNA ends are not captured because of their incompatibility with adapter ligation protocols (Giraldez et al., 2019).

In order to tackle these limitations that could have been affecting our results, we performed a combinatorial pre-treatment resembling the PANDORAseq strategy (J. Shi et al., 2021). In this study, they used the dealkylating enzyme AlkB, which is a pre-treatment that has already been published to enhance tsRNA sequencing (Cozen et al., 2015) and whose substrates have been well-characterized, including m¹A, m³C and m¹G modifications (Aas et al., 2003; Delaney & Essigmann, 2004; Falnes, 2004). In our experiments, we employed a commercial kit containing a cocktail of demethylases and although we would expect similar results to those reported in the bibliography, LC-MS analysis of the modifications present in sRNA before and after demethylases pre-treatment should be further examined.

Regarding our results applying this methodology, we observed that T4PNK and T4PNK+D pre-treatments are able to unveil a more complex sRNA transcriptome, at the expense of a general drop in the coverage of sRNA presenting 5'-P and 3'-OH ends, mainly corresponding to miRNA. Hence, sRNA pre-treatments result in different biotype distributions adding novel species into the landscape but without losing information. Particularly, both pre-treatments resulted in an increased detection of certain underestimated biotypes in traditional sRNA-sequencing, with tsRNA being the most susceptible biotype and showing an enhanced discovery upon additional pre-treatments. This findings are in line with previous observations (Cozen et al., 2015; J. Shi et al., 2021) and provide an optimal scenario to highlight specific tsRNA species that have been previously underexplored.

Intriguingly, different sRNA biotypes presented divergent responses towards pretreatments. Contrasting with tsRNA enhanced uncovering, rRNA, snRNA and genes

DISCUSSION

showed a dramatic increased detection after T4PNK pre-treatment but no additional effect was observed upon the demethylation step. Remarkably, similar distribution patterns were observed across genotypes and consistent with previous reports (J. Shi et al., 2021). Strikingly, biotype distribution of non-treated individual ssRNA samples presented a slightly different signature to the one observed in sRNA pools, essentially regarding tsRNA. Although the increased detection of tsRNA is maintained in HD- compared to CTL-ssRNA-PT samples, the percentages of these species in individual samples is lower than the percentages observed in the pools. This can be explained by the fact that in the case of individual samples, we performed a pre-size-selection step during sRNA purification, which allowed the correction of false positive detection due to the removal of artificial tsRNA sources, namely precursor tRNA present in sRNA pools, and guaranteed a more reliable result (Cozen et al., 2015; J. Shi et al., 2021).

Focusing on specific tsRNA species, we detected a higher percentage of sequences annotating onto tRNA^{Asp} and tRNA^{Val} in HD putamen compared to the analogous region of non-affected individuals. In fact, differential expression analysis corroborates specific increases in tRNA^{Asp}-GTC and tRNA^{Val}-TAC clusters in HDversus CTL-ssRNA-PT samples, independently of the pre-treatment applied. Even at sequences level, 5'-end derived tsRNA from tRNA^{Asp}-GTC and tRNA^{Val}-TAC appear as top upregulated in HD putamen using different pre-treatments. Therefore, equivalent results in all sequencing conditions lead us to infer that these sequences display canonical 5'-P and 3'-OH termini configurations and almost no posttranscriptional methylations both in CTL- and HD-ssRNA-PT samples. Furthermore, the specific increase in 5'-derived tsRNA is in line with the widely described accumulation of these species in multiple stress conditions (Emara et al., 2010; Fu et al., 2009; Thompson et al., 2008; Yamasaki et al., 2009). Accordingly, it has been reported that tRNA^{Asp}-GTC is a direct NSun2 substrate and its stability decreases in the absence of NSun2 and Dnmt2 methyltransferases in mice (Hussain et al., 2013; Tuorto et al., 2012). Consequently, we can state that these tsRNA are differentially produced in HD putamen but also that NSun2 reduction may play a role on it.

Differential properties of sRNA are also stressed by the paired comparison of differently pre-treated samples when evaluating tsRNA species, suggesting HD-associated specific biochemical end-configurations and post-transcriptional modifications. Notably, we observed a reduction in the number of upregulated tsRNA clusters in HD samples after pre-treatments compared to non-treated conditions. This finding prompted us to assume that CTL-ssRNA-PT samples displayed a higher sensibility to pre-treatments than HD samples. This is based on the fact that pre-treating CTL-ssRNA-PT samples increases sRNA discovery, whereas HD-ssRNA-PT samples do not show the same sensibility and consequently, many significantly upregulated clusters observed in non-treated conditions lose their

significance after pre-treatments. Therefore, an increased sensibility indicates that CTL-ssRNA-PT samples contain tsRNA sequences presenting diverse non-canonical termini and more post-transcriptional modifications. Conversely, HD-ssRNA-PT samples bear a major prevalence of hypomodified and 5'-P- and 3'-OH-ended tsRNA sequences, which would be consistent with an increased tRNA cleavage caused by a general tRNA hypomodification status (Blanco et al., 2014; Lyons et al., 2018; Tuorto et al., 2012).

Regarding other sRNA biotypes, many studies have reported that vaultRNA1.1 presents an NSun2 target site along its sequence (Hussain et al., 2013; Khoddami & Cairns, 2013; Squires et al., 2012). Vault RNAs are components of macromolecular ribonucleoprotein complexes found in most species, but their functions are still under investigation (Hahne et al., 2020; Kedersha et al., 1990; Kedersha & Rome, 1986). However, it has been reported that they can be processed into small vault RNAs (svRNA) depending on their m⁵C methylation status (Hussain et al., 2013) and in turn regulate gene expression (Persson et al., 2009). For instance, an increased processing of the specific vaultRNA1.1 was shown in NSun2-depleted human fibroblasts, resulting in a higher detection of svRNA (Hussain et al., 2013). Accordingly, we have detected significantly increased levels of sRNA fragments annotating onto vaultRNA1.1 in HD-ssRNA-PT samples in line with reduced NSun2 levels. Therefore, the study of vaultRNA1.1 cleavage and its role in HD putamen appear as novel mechanisms that should be further investigated.

In summary, our results confirm that pre-treatment strategies prior sRNA-sequencing can provide a more comprehensive view of HD-associated sRNA transcriptome, highlighting novel species potentially implicated in HD pathogenesis. Furthermore, our data provides an initial mechanistic understanding of multiple alterations in sRNA post-transcriptional modifications in HD, which is a complementary and previously neglected information that may be useful not only for the study of the pathogenic mechanisms but also for the discovery of sRNA-based biomarkers.

4. Limitations of the study

Along with the insights here provided, a limitation of the present study is the failure to consider a possible functional interaction of HD-sRNA with other detrimental players, including the expanded CAG repeats adopting a hairpin structure and the expanded polyQ, which have been widely implicated in HD pathogenesis (reviewed in Bates et al., 2015; Heinz et al., 2021; Labbadia & Morimoto, 2013; Malik et al., 2021; Martí, 2016; Zuccato et al., 2010). Furthermore, the real scenario likely involves temporal sRNA expression dynamics that our design, analyzing the effect of sRNA accumulated at advanced stages of the disease, does not contemplate. In line with this idea, expression profiling and functional screening of sRNA along

DISCUSSION

disease evolution should help to elucidate if sRNA-mediated perturbations are an early phenomenon and whether sRNA transcriptome presents dynamic changes depending on the disease stage. Furthermore, although we have observed a substantial and acute decline of striatal function in mice injected with HD-sRNA-PT, additional studies to evaluate possible long-lasting detrimental effects of HD-sRNA-PT species should be performed.

It must not be forgotten that we have been dealing with a heterogeneous mixture of sRNA species derived from human tissues containing many different cell types. Moreover, despite the fact that sRNA injection into the brain of naïve mice results in obvious detrimental effects, it is important to remember that these outcomes are dependent on an exogenous injection. Hence, we cannot determine whether injected sRNA, although actually produced in the HD brain, would target the same cell types in the actual context of HD or if these sRNA accumulate and release in a similar manner to how we are providing them. Therefore, even though there is an evident effect, we have not been able to contextualize it within the disease due to the study design. Consequently, we cannot conclude whether the observed effects are cell-autonomous or non-autonomous, which is a concern that rise to prominence.

Remarkably, we used different sRNA fractions from the same human individuals for the epitranscriptomic experiment (tRNA fraction) and the sRNA-sequencing analyses (ssRNA fraction). Thus, we obtained paired information of the samples resulting in a complete view of tRNA methylation status and the associated sRNA transcriptomic signature for each individual. However, this strategy also presents some drawbacks with potential for further improvement, as it is the case of other RNA modifications that have not been addressed with the applied pre-treatments, including the remaining amino acids present in specific tsRNA ends interfering with adapter ligation (Honda et al., 2015; Raabe et al., 2014) or certain epitranscriptomic modifications untackled by demethylases (Wei et al., 2015). Additionally, specific techniques such as bisulfite sequencing (Blanco et al., 2014), 5-azacytidinemediated RNA immunoprecipitation (Khoddami & Cairns, 2013) and miCLIP associated to RNA methyltransferases immunoprecipitation (Hussain et al., 2013) represent valuable tools to identify specific modifications in the transcriptome at nucleotide resolution level. Hence, the identification of certain epitranscriptomic modifications within specific sRNA species using these strategies and the evaluation of their functional implications could be really valuable in the study of sRNA-associated HD pathogenic mechanisms, considering the obtained results in this thesis.

5. Potential and future perspectives

In summary, the present study indicates that human HD-sRNA derived from the putamen trigger motor coordination abnormalities in WT mice and recapitulate major HD pathological hallmarks, offering additional evidence supporting the idea that the intricate ncRNA world governs complex and fundamental processes although previously unexpected. Remarkably, the novel uncovered tsRNA species found dysregulated in HD may hold potential to provide insight into important biological and disease mechanisms. Furthermore, this extensive sRNA characterization represents a source of new potential targets not only for the development of therapeutics but also for the discovery of biomarkers for diagnosis and/or disease progression, as this sRNA-sequencing strategy can be applied in human biofluids, such as plasma.

Overall, the present results favor the idea that the orchestrated activity of sRNA, including sCAG, could be a causative factor in HD and further indicate that the blockage of sRNA biogenesis and/or toxic activity should be envisioned as a therapeutic strategy. For instance, although the relative contribution of these sRNA-associated mechanisms to overall HD pathogenesis is not yet clear, it has become obvious that they should be borne in mind because they might be evading the current approaches used for mHTT lowering in HD therapeutics.

CONCLUSIONS

- 1. HD-sRNA-PT are sufficient to induce HD-associated behavioral impairments and neuropathology, including selective transcriptional alterations underlying neurodegeneration and inflammation.
- 2. sCAG species contribute to motor impairment and neuronal dysfunction but do not have a major effect on transcriptional changes, cell death and neuroinflammation.
- 3. Immune activation triggered by both acute and sustained HD-sRNA-PT injections evidences a role of these species in the inflammatory processes occurring in HD putamen, eventually contributing to neurodegeneration.
- 4. HD-sRNA derived from the putamen exhibit specific properties at different levels, including types of sequences, biochemical configurations and/or post-transcriptional modifications, which underlie enhanced detrimental consequences compared to HD-sRNA produced in other HD brain areas.
- 5. tsRNA derived from the 5' ends are overrepresented in HD brain, especially in the putamen, with specific tsRNA species displaying a direct neurotoxic effect.
- 6. An early and specific reduction in NSun2 levels in the striatum together with an enrichment in tsRNA fragments derived from NSun2 substrates points to a contribution of this methyltransferase into HD pathogenic mechanisms.
- 7. Alternative sRNA sequencing strategies involving enzymatic pretreatments hold the potential to unravel an expanded sRNA transcriptome landscape, particularly unveiling additional tsRNA species, which may open new therapeutic opportunities for HD treatments.
- 8. The paired comparison of non-treated, T4PNK-treated and T4PNK+D-treated sRNA samples in differentiated biological conditions allowed us to infer HD-specific properties of sRNA. The obtained dataset sets the bases for future designs, such as bioinformatic tools, to identify alterations in sRNA biogenesis enzymes in HD pathogenesis.
- 9. HD-sRNA-PT transcriptome comprises a major proportion of sRNA species displaying 5'-P and 3'-OH configurations, which can be captured using standard sRNA-seq conditions, and represent potential candidates for striatal vulnerability.

- Aas, P. A., Otterlei, M., Falnes, P., Vågbø, C. B., Skorpen, F., Akbari, M., Sundheim, O., Bjørås, M., Slupphaug, G., Seeberg, E., & Krokan, H. E. (2003). Human and bacterial oxidative demethylases repair alkylation damage in both RNA and DNA. *Nature*, *421*(6925), 859–863. https://doi.org/10.1038/NATURE01363
- Abbasi-Moheb, L., Mertel, S., Gonsior, M., Nouri-Vahid, L., Kahrizi, K., Cirak, S., Wieczorek, D., Motazacker, M. M., Esmaeeli-Nieh, S., Cremer, K., Weißmann, R., Tzschach, A., Garshasbi, M., Abedini, S. S., Najmabadi, H., Ropers, H. H., Sigrist, S. J., & Kuss, A. W. (2012). Mutations in NSUN2 cause autosomal-recessive Intellectual Disability. *American Journal of Human Genetics*, 90(5), 847. https://doi.org/10.1016/J.AJHG.2012.03.021
- Alazami, A. M., Hijazi, H., Al-Dosari, M. S., Shaheen, R., Hashem, A., Aldahmesh, M. A., Mohamed, J. Y., Kentab, A., Salih, M. A., Awaji, A., Masoodi, T. A., & Alkuraya, F. S. (2013). Mutation in ADAT3, encoding adenosine deaminase acting on transfer RNA, causes intellectual disability and strabismus. *Journal of Medical Genetics*, *50*(7), 425–430. https://doi.org/10.1136/JMEDGENET-2012-101378
- Albin, R. L., Young, A. B., & Penney, J. B. (1989). The functional anatomy of basal ganglia disorders. *Trends in Neurosciences*, *12*(10), 366–375. https://doi.org/10.1016/0166-2236(89)90074-X
- Alcalá-Vida, R., Garcia-Forn, M., Castany-Pladevall, C., Creus-Muncunill, J., Ito, Y., Blanco, E., Golbano, A., Crespí-Vázquez, K., Parry, A., Slater, G., Samarajiwa, S., Peir, S., Croce, L. Di, Narita, M., & Pérez-Navarro, E. (2021). Neuron type-specific increase in lamin B1 contributes to nuclear dysfunction in Huntington's disease. *EMBO Molecular Medicine*, 13(2), e12105. https://doi.org/10.15252/EMMM.202012105
- Allaman, I., Bélanger, M., & Magistretti, P. J. (2011). Astrocyte-neuron metabolic relationships: For better and for worse. *Trends in Neurosciences*, *34*(2), 76–87. https://doi.org/10.1016/j.tins.2010.12.001
- Ament, S. A., Pearl, J. R., Cantle, J. P., Bragg, R. M., Skene, P. J., Coffey, S. R., Bergey, D. E., Wheeler, V. C., MacDonald, M. E., Baliga, N. S., Rosinski, J., Hood, L. E., Carroll, J. B., & Price, N. D. (2018). Transcriptional regulatory networks underlying gene expression changes in Huntington's disease. *Molecular Systems Biology*, 14(3), e7435. https://doi.org/10.15252/MSB.20167435
- Amor, S., Puentes, F., Baker, D., & Van Der Valk, P. (2010). Inflammation in neurodegenerative diseases. *Immunology*, 129(2), 154–169. https://doi.org/10.1111/J.1365-2567.2009.03225.X
- Anderson, P., & Ivanov, P. (2014). tRNA fragments in human health and disease. In *FEBS Letters* (Vol. 588, Issue 23, pp. 4297–4304). Elsevier. https://doi.org/10.1016/j.febslet.2014.09.001
- Anglada-Huguet, M., Xifró, X., Giralt, A., Zamora-Moratalla, A., Martín, E. D., & Alberch, J. (2014). Prostaglandin E2 EP1 receptor antagonist improves motor deficits and rescues memory decline in R6/1 mouse model of Huntington's disease. *Molecular Neurobiology*, 49(2), 784–795. https://doi.org/10.1007/s12035-013-8556-x
- Arlotta, P., Molyneaux, B. J., Jabaudon, D., Yoshida, Y., & Macklis, J. D. (2008). Ctip2 controls

- the differentiation of Medium Spiny Neurons and the establishment of the cellular architecture of the striatum. *Journal of Neuroscience*, *28*(3), 622–632. https://doi.org/10.1523/JNEUROSCI.2986-07.2008
- Ashrafizadeh, M., Zarrabi, A., Mostafavi, E., Aref, A. R., Sethi, G., Wang, L., & Tergaonkar, V. (2022). Non-coding RNA-based regulation of inflammation. *Seminars in Immunology*, 59(May), 101606. https://doi.org/10.1016/j.smim.2022.101606
- Auxilien, S., Guérineau, V., Szweykowska-Kuliñska, Z., & Golinelli-Pimpaneau, B. (2012). The human tRNA m5C methyltransferase Misu is multisite-specific. *RNA Biology*, *9*(11), 1331. https://doi.org/10.4161/RNA.22180
- Aznaourova, M., Schmerer, N., Schmeck, B., & Schulte, L. N. (2020). Disease-causing mutations and rearrangements in long non-coding RNA gene loci. *Frontiers in Genetics*, *11*, 1485. https://doi.org/10.3389/FGENE.2020.527484/BIBTEX
- Baleriola, J., Walker, C. A., Jean, Y. Y., Crary, J. F., Troy, C. M., Nagy, P. L., & Hengst, U. (2014). Axonally synthesized ATF4 transmits a neurodegenerative signal across brain regions. *Cell*, *158*(5), 1159. https://doi.org/10.1016/J.CELL.2014.07.001
- Banerjee, R., Chen, S., Dare, K., Gilreath, M., Praetorius-Ibba, M., Raina, M., Reynolds, N. M., Rogers, T., Roy, H., Yadavalli, S. S., & Ibba, M. (2010). tRNAs: cellular barcodes for amino acids. *FEBS Letters*, *584*(2), 387–395. https://doi.org/10.1016/J.FEBSLET.2009.11.013
- Bañez-Coronel, M., Ayhan, F., Tarabochia, A. D., Zu, T., Perez, B. A., Tusi, S. K., Pletnikova, O., Borchelt, D. R., Ross, C. A., Margolis, R. L., Yachnis, A. T., Troncoso, J. C., & Ranum, L. P. W. (2015). RAN translation in Huntington Disease. *Neuron*, *88*(4), 667–677. https://doi.org/10.1016/j.neuron.2015.10.038
- Bañez-Coronel, M., Porta, S., Kagerbauer, B., Mateu-Huertas, E., Pantano, L., Ferrer, I., Guzmán, M., Estivill, X., & Martí, E. (2012). A pathogenic mechanism in huntington's disease involves small CAG-repeated RNAs with neurotoxic activity. *PLoS Genetics*, 8(2). https://doi.org/10.1371/journal.pgen.1002481
- Bates, G. P., Dorsey, R., Gusella, J. F., Hayden, M. R., Kay, C., Leavitt, B. R., Nance, M., Ross, C. A., Scahill, R. I., Wetzel, R., Wild, E. J., & Tabrizi, S. J. (2015). Huntington disease. *Nature Reviews Disease Primers*, 1(April), 1–21. https://doi.org/10.1038/nrdp.2015.5
- Batista, P. J., Molinie, B., Wang, J., Qu, K., Zhang, J., Li, L., Bouley, D. M., Lujan, E., Haddad, B., Daneshvar, K., Carter, A. C., Flynn, R. A., Zhou, C., Lim, K. S., Dedon, P., Wernig, M., Mullen, A. C., Xing, Y., Giallourakis, C. C., & Chang, H. Y. (2014). m6A RNA modification controls cell fate transition in mammalian embryonic stem cells. *Cell Stem Cell*, *15*(6), 707. https://doi.org/10.1016/J.STEM.2014.09.019
- Baxa, M., Hruska-Plochan, M., Juhas, S., Vodicka, P., Pavlok, A., Juhasova, J., Miyanohara, A., Nejime, T., Klima, J., Macakova, M., Marsala, S., Weiss, A., Kubickova, S., Musilova, P., Vrtel, R., Sontag, E. M., Thompson, L. M., Schier, J., Hansikova, H., ... Motlik, J. (2013). A transgenic minipig model of Huntington's Disease. *Journal of Huntington's Disease*, 2(1), 47–68. https://doi.org/10.3233/JHD-130001
- Beal, M. F., Ferrante, R. J., Swartz, K. J., & Kowall, N. W. (1991). Chronic quinolinic acid

- lesions in rats closely resemble Huntington's disease. *The Journal of Neuroscience*, 11(6), 1649–1659. https://doi.org/10.1523/JNEUROSCI.11-06-01649.1991
- Becanovic, K., Pouladi, M. A., Lim, R. S., Kuhn, A., Pavlidis, P., Luthi-Carter, R., Hayden, M. R., & Leavitt, B. R. (2010). Transcriptional changes in Huntington disease identified using genome-wide expression profiling and cross-platform analysis. *Human Molecular Genetics*, 19(8), 1438–1452. https://doi.org/10.1093/HMG/DDQ018
- Begley, U., Dyavaiah, M., Patil, A., Rooney, J. P., DiRenzo, D., Young, C. M., Conklin, D. S., Zitomer, R. S., & Begley, T. J. (2007). Trm9-catalyzed tRNA modifications link translation to the DNA damage response. *Molecular Cell*, *28*(5), 860–870. https://doi.org/10.1016/J.MOLCEL.2007.09.021
- Bennett, C. F., & Swayze, E. E. (2010). RNA targeting therapeutics: molecular mechanisms of antisense oligonucleotides as a therapeutic platform. *Annual Review of Pharmacology and Toxicology*, 50, 259–293. https://doi.org/10.1146/ANNUREV.PHARMTOX.010909.105654
- Bergonzoni, G., Döring, J., & Biagioli, M. (2021). D1R- and D2R-Medium-Sized Spiny Neurons Diversity: Insights Into Striatal Vulnerability to Huntington's Disease Mutation. Frontiers in Cellular Neuroscience, 15, 16. https://doi.org/10.3389/FNCEL.2021.628010/BIBTEX
- Berrios, G. E., Wagle, A. C., Marková, I. S., Wagle, S. A., Rosser, A., & Hodges, J. R. (2002). Psychiatric symptoms in neurologically asymptomatic Huntington's disease gene carriers: a comparison with gene negative at risk subjects. *Acta Psychiatrica Scandinavica*, 105(3), 224–230. https://doi.org/10.1034/j.1600-0447.2002.00456.x
- Bertheloot, D., Naumovski, A. L., Langhoff, P., Horvath, G. L., Jin, T., Xiao, T. S., Garbi, N., Agrawal, S., Kolbeck, R., & Latz, E. (2016). RAGE enhances TLR responses through binding and internalization of RNA. *Journal of Immunology*, *197*(10), 4118. https://doi.org/10.4049/JIMMUNOL.1502169
- Bhatti, G. K., Khullar, N., Sidhu, I. S., Navik, U. S., Reddy, A. P., Reddy, P. H., & Bhatti, J. S. (2021). Emerging role of non-coding RNA in health and disease. *Metabolic Brain Disease*, *36*(6), 1119–1134. https://doi.org/10.1007/S11011-021-00739-Y
- Bibb, J. A., Yan, Z., Svenningsson, P., Snyder, G. L., Pieribone, V. A., Horiuchi, A., Nairn, A. C., Messer, A., & Greengard, P. (2000). Severe deficiencies in dopamine signaling in presymptomatic Huntington's disease mice. *Proceedings of the National Academy of Sciences of the United States of America*, 97(12), 6809–6814. https://doi.org/10.1073/PNAS.120166397/ASSET/73CA528D-BF1D-4531-86D8-9F337EA5F21D/ASSETS/GRAPHIC/PQ1201663005.JPEG
- Björk, G. R., Jacobsson, K., Nilsson, K., Johansson, M. J. O., Byström, A. S., & Persson, O. P. (2001). A primordial tRNA modification required for the evolution of life? *EMBO Journal*, 20(1–2), 231–239. https://doi.org/10.1093/emboj/20.1.231
- Blanchette, M., Labourier, E., Green, R. E., Brenner, S. E., & Rio, D. C. (2004). Genome-wide analysis reveals an unexpected function for the Drosophila splicing factor U2AF50 in the nuclear export of intronless mRNAs. *Molecular Cell*, *14*(6), 775–786. https://doi.org/10.1016/J.MOLCEL.2004.06.012

- Blanco, S., Dietmann, S., Flores, J. V, Hussain, S., Kutter, C., Humphreys, P., Lukk, M., Lombard, P., Treps, L., Popis, M., Kellner, S., Hölter, S. M., Garrett, L., Wurst, W., Becker, L., Klopstock, T., Fuchs, H., Gailus-Durner, V., Hrabě de Angelis, M., ... Frye, M. (2014). Aberrant methylation of tRNAs links cellular stress to neuro-developmental disorders. *The EMBO Journal*, *33*(18), 2020–2039. https://doi.org/10.15252/embj.201489282
- Blaze, J., & Akbarian, S. (2022). The tRNA regulome in neurodevelopmental and neuropsychiatric disease. *Molecular Psychiatry*, *January*. https://doi.org/10.1038/s41380-022-01585-9
- Blaze, J., Navickas, A., Phillips, H. L., Heissel, S., Plaza-Jennings, A., Miglani, S., Asgharian, H., Foo, M., Katanski, C. D., Watkins, C. P., Pennington, Z. T., Javidfar, B., Espeso-Gil, S., Rostandy, B., Alwaseem, H., Hahn, C. G., Molina, H., Cai, D. J., Pan, T., ... Akbarian, S. (2021). Neuronal NSun2 deficiency produces tRNA epitranscriptomic alterations and proteomic shifts impacting synaptic signaling and behavior. *Nature Communications*, 12(1), 1–16. https://doi.org/10.1038/s41467-021-24969-x
- Boccaletto, P., Stefaniak, F., Ray, A., Cappannini, A., Mukherjee, S., Purta, E., Kurkowska, M., Shirvanizadeh, N., Destefanis, E., Groza, P., Avşar, G., Romitelli, A., Pir, P., Dassi, E., Conticello, S. G., Aguilo, F., & Bujnicki, J. M. (2022). MODOMICS: a database of RNA modification pathways. 2021 update. *Nucleic Acids Research*, 50(D1), D231–D235. https://doi.org/10.1093/NAR/GKAB1083
- Bolam, J. P., Wainer, B. H., & Smith, A. D. (1984). Characterization of cholinergic neurons in the rat neostriatum. A combination of choline acetyltransferase immunocytochemistry, Golgi-impregnation and electron microscopy. *Neuroscience*, 12(3), 711–718. https://doi.org/10.1016/0306-4522(84)90165-9
- Borlongan, C. V., Koutouzis, T. K., Randall, T. S., Freeman, T. B., Cahill, D. W., & Sanberg, P. R. (1995). Systemic 3-nitropropionic acid: behavioral deficits and striatal damage in adult rats. *Brain Research Bulletin*, *36*(6), 549–556. https://doi.org/10.1016/0361-9230(94)00242-S
- Borrell-Pagès, M., Zala, D., Humbert, S., & Saudou, F. (2006). Huntington's disease: from huntingtin function and dysfunction to therapeutic strategies. *Cellular and Molecular Life Sciences*, 63(22), 2642–2660. https://doi.org/10.1007/S00018-006-6242-0/METRICS
- Bradshaw, W. J., Rehman, S., Pham, T. T. K., Thiyagarajan, N., Lee, R. L., Subramanian, V., & Acharya, K. R. (2017). Structural insights into human angiogenin variants implicated in Parkinson's disease and Amyotrophic Lateral Sclerosis. *Scientific Reports*, 7. https://doi.org/10.1038/SREP41996
- Brenner, S., Jacob, F., & Meselson, M. (1961). An unstable intermediate carrying information from genes to ribosomes for protein synthesis. *Nature*, *190*(4776), 576–581. https://doi.org/10.1038/190576A0
- Bridget, M., & Peplow, P. (2021). Altered microRNA expression in animal models of Huntington's disease and potential therapeutic strategies. *Neural Regeneration Research*, *16*(11), 2159. https://doi.org/10.4103/1673-5374.310673

- Brignull, H. R., Moore, F. E., Tang, S. J., & Morimoto, R. I. (2006). Polyglutamine proteins at the pathogenic threshold display neuron-specific aggregation in a pan-neuronal Caenorhabditis elegans model. *Journal of Neuroscience*, *26*(29), 7597–7606. https://doi.org/10.1523/JNEUROSCI.0990-06.2006
- Brochier, C., Gaillard, M. C., Diguet, E., Caudy, N., Dossat, C., Ségurens, B., Wincker, P., Roze, E., Caboche, J., Hantraye, P., Brouillet, E., Elalouf, J. M., & De Chaldée, M. (2008). Quantitative gene expression profiling of mouse brain regions reveals differential transcripts conserved in human and affected in disease models. *Physiological Genomics*, 33(2), 170–179. https://doi.org/10.1152/PHYSIOLGENOMICS.00125.2007/SUPPL_FILE/BROCHIER_TA BLES4 R2.XLS
- Bryant, C. D., & Yazdani, N. (2016). RNA-binding proteins, neural development and the addictions. *Genes, Brain, and Behavior,* 15(1), 169–186. https://doi.org/10.1111/GBB.12273
- Brzezicha, B., Schmidt, M., Makałowska, I., Jarmołowski, A., Pieńkowska, J., & Szweykowska-Kulińska, Z. (2006). Identification of human tRNA:m5C methyltransferase catalysing intron-dependent m5C formation in the first position of the anticodon of the pretRNA Leu (CAA). *Nucleic Acids Research*, 34(20), 6034–6043. https://doi.org/10.1093/NAR/GKL765
- Bsibsi, M., Ravid, R., Gveric, D., & Van Noort, J. M. (2002). Broad expression of Toll-Like receptors in the human central nervous system. *Journal of Neuropathology & Experimental Neurology, 61*(11), 1013–1021. https://doi.org/10.1093/JNEN/61.11.1013
- Burguete, A. S., Almeida, S., Gao, F. B., Kalb, R., Akins, M. R., & Bonini, N. M. (2015). GGGGCC microsatellite RNA is neuritically localized, induces branching defects, and perturbs transport granule function. *ELife*, *4*(DECEMBER2015). https://doi.org/10.7554/ELIFE.08881
- Carroll, J. B., Warby, S. C., Southwell, A. L., Doty, C. N., Greenlee, S., Skotte, N., Hung, G., Bennett, C. F., Freier, S. M., & Hayden, M. R. (2011). Potent and selective antisense oligonucleotides targeting single-nucleotide polymorphisms in the huntington disease gene / allele-specific silencing of mutant huntingtin. *Molecular Therapy*, 19(12), 2178–2185. https://doi.org/10.1038/mt.2011.201
- Cattaneo, E., & Conti, L. (1998). Generation and characterization of embryonic striatal conditionally immortalized ST14A cells. *Journal of Neuroscience Research*, *53*(2), 223–234. https://doi.org/10.1002/(SICI)1097-4547(19980715)53:2<223::AID-JNR11>3.0.CO;2-7
- Cech, T. R., & Steitz, J. A. (2014). The noncoding RNA revolution—Trashing old rules to forge new ones. *Cell*, *157*(1), 77–94. https://doi.org/10.1016/J.CELL.2014.03.008
- Chan, C. T. Y., Dyavaiah, M., DeMott, M. S., Taghizadeh, K., Dedon, P. C., & Begley, T. J. (2010). A quantitative systems approach reveals dynamic control of tRNA modifications during cellular stress. *PLoS Genetics*, *6*(12), 1–9. https://doi.org/10.1371/journal.pgen.1001247

- Chen, K.-P., Hua, K.-F., Tsai, F.-T., Lin, T.-Y., Cheng, C.-Y., Yang, D.-I., Hsu, H.-T., & Ju, T.-C. (2021). A selective inhibitor of the NLRP3 inflammasome as a potential therapeutic approach for neuroprotection in a transgenic mouse model of Huntington's disease. *Journal of Neuroinflammation*, 19, 56. https://doi.org/10.1186/s12974-022-02419-9
- Chen, Q., Yan, M., Cao, Z., Li, X., Zhang, Y., Shi, J., Feng, G.-H., Peng, H., Zhang, X., Zhang, Y., Qian, J., Duan, E., Zhai, Q., & Zhou, Q. (2016). Sperm tsRNAs contribute to intergenerational inheritance of an acquired metabolic disorder. *Science*, *351*(6271), 397–400. https://doi.org/10.1126/science.aad7977
- Chen, Z., Qi, M., Shen, B., Luo, G., Wu, Y., Li, J., Lu, Z., Zheng, Z., Dai, Q., & Wang, H. (2019). Transfer RNA demethylase ALKBH3 promotes cancer progression via induction of tRNA-derived small RNAs. *Nucleic Acids Research*, *47*(5), 2533–2545. https://doi.org/10.1093/NAR/GKY1250
- Cherubini, M., Lopez-Molina, L., & Gines, S. (2020). Mitochondrial fission in Huntington's disease mouse striatum disrupts ER-mitochondria contacts leading to disturbances in Ca2+ efflux and Reactive Oxygen Species (ROS) homeostasis. *Neurobiology of Disease*, 136. https://doi.org/10.1016/J.NBD.2020.104741
- Chiou, N. T., Kageyama, R., & Ansel, K. M. (2018). Selective export into extracellular vesicles and function of tRNA fragments during T cell activation. *Cell Reports*, *25*(12), 3356-3370.e4. https://doi.org/10.1016/J.CELREP.2018.11.073
- Chmielarz, P., Konovalova, J., Najam, S. S., Alter, H., Piepponen, T. P., Erfle, H., Sonntag, K. C., Schütz, G., Vinnikov, I. A., & Domanskyi, A. (2017). Dicer and microRNAs protect adult dopamine neurons. *Cell Death & Disease*, 8(5), e2813–e2813. https://doi.org/10.1038/cddis.2017.214
- Chow, C. S., Lamichhane, T. N., & Mahto, S. K. (2007). Expanding the nucleotide repertoire of the ribosome with post-transcriptional modifications. *ACS Chemical Biology*, *2*(9), 610. https://doi.org/10.1021/CB7001494
- Chujo, T., & Tomizawa, K. (2021). Human transfer RNA modopathies: diseases caused by aberrations in transfer RNA modifications. *The Febs Journal*, *288*(24), 7096. https://doi.org/10.1111/FEBS.15736
- Chung, H., Calis, J. J. A., Wu, X., Sun, T., Yu, Y., Sarbanes, S. L., Dao Thi, V. L., Shilvock, A. R., Hoffmann, H. H., Rosenberg, B. R., & Rice, C. M. (2018). Human ADAR1 prevents endogenous RNA from triggering translational shutdown. *Cell*, *172*(4), 811. https://doi.org/10.1016/J.CELL.2017.12.038
- Coleman, L. G., Zou, J., & Crews, F. T. (2017). Microglial-derived miRNA let-7 and HMGB1 contribute to ethanol-induced neurotoxicity via TLR7. *Journal of Neuroinflammation*, 14(1), 1–15. https://doi.org/10.1186/S12974-017-0799-4/FIGURES/8
- Cooper, J. K., Schilling, G., Peters, M. F., Herring, W. J., Sharp, A. H., Kaminsky, Z., Masone, J., Khan, F. A., Delanoy, M., Borchelt, D. R., Dawson, V. L., Dawson, T. M., & Ross, C. A. (1998). Truncated N-Terminal fragments of Huntingtin with expanded glutamine repeats form nuclear and cytoplasmic aggregates in cell culture. *Human Molecular Genetics*, 7(5), 783–790. https://doi.org/10.1093/HMG/7.5.783

- Cosentino, C., Toivonen, S., Villamil, E. D., Atta, M., Ravanat, J. L., Demine, S., Schiavo, A. A., Pachera, N., Deglasse, J. P., Jonas, J. C., Balboa, D., Otonkoski, T., Pearson, E. R., Marchetti, P., Eizirik, D. L., Cnop, M., & Igoillo-Esteve, M. (2018). Pancreatic β-cell tRNA hypomethylation and fragmentation link TRMT10A deficiency with diabetes. *Nucleic Acids Research*, *46*(19), 10302–10318. https://doi.org/10.1093/NAR/GKY839
- Cox, D. C., & Cooper, T. A. (2016). Non-canonical RAN translation of CGG repeats has canonical requirements. *Molecular Cell*, 62(2), 155–156. https://doi.org/10.1016/j.molcel.2016.04.004
- Cozen, A. E., Quartley, E., Holmes, A. D., Hrabeta-Robinson, E., Phizicky, E. M., & Lowe, T. M. (2015). ARM-seq: AlkB-facilitated RNA methylation sequencing reveals a complex landscape of modified tRNA fragments. *Nature Methods*, *12*(9), 879–884. https://doi.org/10.1038/NMETH.3508
- Creus-Muncunill, J., Badillos-Rodríguez, R., Garcia-Forn, M., Masana, M., Barriga, G. G. D., Guisado-Corcoll, A., Alberch, J., Malagelada, C., Delgado-García, J. M., Gruart, A., & Pérez-Navarro, E. (2019). Increased translation as a novel pathogenic mechanism in Huntington's disease. *Brain*, 142(10), 3158–3175. https://doi.org/10.1093/BRAIN/AWZ230
- Crotti, A., & Glass, C. K. (2015). The choreography of neuroinflammation in Huntington's disease. *Trends in Immunology*, *36*(6), 364–373. https://doi.org/10.1016/J.IT.2015.04.007
- Cummings, D. M., Milnerwood, A. J., Dallérac, G. M., Waights, V., Brown, J. Y., Vatsavayai, S. C., Hirst, M. C., & Murphy, K. P. S. J. (2006). Aberrant cortical synaptic plasticity and dopaminergic dysfunction in a mouse model of huntington's disease. *Human Molecular Genetics*, *15*(19), 2856–2868. https://doi.org/10.1093/HMG/DDL224
- D'anca, M., Buccellato, F. R., Fenoglio, C., & Galimberti, D. (2022). Circular RNAs: emblematic players of neurogenesis and neurodegeneration. *International Journal of Molecular Sciences*, *23*(8). https://doi.org/10.3390/IJMS23084134
- Dabrowska, M., Juzwa, W., Krzyzosiak, W. J., & Olejniczak, M. (2018). Precise Excision of the CAG Tract from the Huntingtin Gene by Cas9 Nickases. *Frontiers in Neuroscience*, 12. https://doi.org/10.3389/FNINS.2018.00075
- Das, K., & Rao, L. V. M. (2022). The role of microRNAs in inflammation. *International Journal of Molecular Sciences*, 23(24), 15479. https://doi.org/10.3390/IJMS232415479
- Davies, S. W., Beardsall, K., Turmaine, M., DiFiglia, M., Aronin, N., & Bates, G. P. (1998). Are neuronal intranuclear inclusions the common neuropathology of triplet-repeat disorders with polyglutamine-repeat expansions? *Lancet*, *351*(9096), 131–133. https://doi.org/10.1016/S0140-6736(97)08360-8
- de Brouwer, A. P. M., Abou Jamra, R., Körtel, N., Soyris, C., Polla, D. L., Safra, M., Zisso, A., Powell, C. A., Rebelo-Guiomar, P., Dinges, N., Morin, V., Stock, M., Hussain, M., Shahzad, M., Riazuddin, S., Ahmed, Z. M., Pfundt, R., Schwarz, F., de Boer, L., ... Schwartz, S. (2018). Variants in PUS7 cause Intellectual Disability with speech delay, microcephaly, short stature, and aggressive behavior. *American Journal of Human Genetics*, 103(6), 1045–1052. https://doi.org/10.1016/J.AJHG.2018.10.026

- De Felice, C., Signorini, C., Leoncini, S., Pecorelli, A., Durand, T., Valacchi, G., Ciccoli, L., & Hayek, J. (2012). The role of oxidative stress in Rett syndrome: an overview. *Annals of the New York Academy of Sciences*, 1259(1), 121–135. https://doi.org/10.1111/J.1749-6632.2012.06611.X
- de Mezer, M., Wojciechowska, M., Napierala, M., Sobczak, K., & Krzyzosiak, W. J. (2011). Mutant CAG repeats of Huntingtin transcript fold into hairpins, form nuclear foci and are targets for RNA interference. *Nucleic Acids Research*, *39*(9), 3852–3863. https://doi.org/10.1093/NAR/GKQ1323
- Delaney, J. C., & Essigmann, J. M. (2004). Mutagenesis, genotoxicity, and repair of 1-methyladenine, 3-alkylcytosines, 1-methylguanine, and 3-methylthymine in alkB Escherichia coli. *Proceedings of the National Academy of Sciences of the United States of America*, 101(39), 14051. https://doi.org/10.1073/PNAS.0403489101
- Deng, J., Ptashkin, R. N., Chen, Y., Cheng, Z., Liu, G., Phan, T., Deng, X., Zhou, J., Lee, I., Lee, Y. S., & Bao, X. (2015). Respiratory Syncytial Virus utilizes a tRNA fragment to suppress antiviral responses through a novel targeting mechanism. *Molecular Therapy*, 23(10), 1622–1629. https://doi.org/10.1038/mt.2015.124
- Deng, Y. P., Albin, R. L., Penney, J. B., Young, A. B., Anderson, K. D., & Reiner, A. (2004). Differential loss of striatal projection systems in Huntington's disease: A quantitative immunohistochemical study. *Journal of Chemical Neuroanatomy*, *27*(3), 143–164. https://doi.org/10.1016/j.jchemneu.2004.02.005
- Desplats, P. A., Kass, K. E., Gilmartin, T., Stanwood, G. D., Woodward, E. L., Head, S. R., Sutcliffe, J. G., & Thomas, E. A. (2006). Selective deficits in the expression of striatal-enriched mRNAs in Huntington's disease. *Journal of Neurochemistry*, *96*(3), 743–757. https://doi.org/10.1111/J.1471-4159.2005.03588.X
- Dhahbi, J. M., Spindler, S. R., Atamna, H., Boffelli, D., & Martin, D. I. K. (2014). Deep sequencing of serum small RNAs identifies patterns of 5' tRNA half and YRNA fragment expression associated with breast cancer. *Biomarkers in Cancer*, 6, BIC.S20764. https://doi.org/10.4137/BIC.S20764
- Dhahbi, J. M., Spindler, S. R., Atamna, H., Yamakawa, A., Boffelli, D., Mote, P., & Martin, D. I. K. (2013). 5' tRNA halves are present as abundant complexes in serum, concentrated in blood cells, and modulated by aging and calorie restriction. *BMC Genomics*, *14*(1), 1–14. https://doi.org/10.1186/1471-2164-14-298
- DiFiglia, M., Sena-Esteves, M., Chase, K., Sapp, E., Pfister, E., Sass, M., Yoder, J., Reeves, P., Pandey, R. K., Rajeev, K. G., Manoharan, M., Sah, D. W. Y., Zamore, P. D., & Aronin, N. (2007). Therapeutic silencing of mutant huntingtin with siRNA attenuates striatal and cortical neuropathology and behavioral deficits. *Proceedings of the National Academy of Sciences of the United States of America*, 104(43), 17204–17209. https://doi.org/10.1073/PNAS.0708285104
- Dobin, A., Davis, C. A., Schlesinger, F., Drenkow, J., Zaleski, C., Jha, S., Batut, P., Chaisson, M., & Gingeras, T. R. (2013). STAR: Ultrafast universal RNA-seq aligner. *Bioinformatics*, 29(1), 15–21. https://doi.org/10.1093/bioinformatics/bts635
- Dong, X., & Cong, S. (2021). The emerging roles of long non-coding RNAs in polyglutamine

- diseases. Journal of Cellular and Molecular Medicine, 25(17), 8095–8102. https://doi.org/10.1111/JCMM.16808
- Donovan, J., Rath, S., Kolet-Mandrikov, D., & Korennykh, A. (2017). Rapid RNase L-driven arrest of protein synthesis in the dsRNA response without degradation of translation machinery. *RNA*, 23(11), 1660–1671. https://doi.org/10.1261/RNA.062000.117/-/DC1
- Dozmorov, M. G., Giles, C. B., Koelsch, K. A., & Wren, J. D. (2013). Systematic classification of non-coding RNAs by epigenomic similarity. *BMC Bioinformatics*, *14 Suppl 14*(Suppl 14). https://doi.org/10.1186/1471-2105-14-S14-S2
- Duff, K., Paulsen, J. S., Beglinger, L. J., Langbehn, D. R., & Stout, J. C. (2007). Psychiatric symptoms in Huntington's Disease before diagnosis: the Predict-HD study. *Biological Psychiatry*, 62(12), 1341–1346. https://doi.org/10.1016/j.biopsych.2006.11.034
- Durbin, A. F., Wang, C., Marcotrigiano, J., & Gehrke, L. (2016). RNAs containing modified nucleotides fail to trigger RIG-I conformational changes for innate immune signaling. *MBio*, 7(5). https://doi.org/10.1128/MBIO.00833-16
- Durrenberger, P. F., Fernando, F. S., Kashefi, S. N., Bonnert, T. P., Seilhean, D., Nait-Oumesmar, B., Schmitt, A., Gebicke-Haerter, P. J., Falkai, P., Grünblatt, E., Palkovits, M., Arzberger, T., Kretzschmar, H., Dexter, D. T., & Reynolds, R. (2015). Common mechanisms in neurodegeneration and neuroinflammation: a BrainNet Europe gene expression microarray study. *Journal of Neural Transmission*, 122(7), 1055–1068. https://doi.org/10.1007/S00702-014-1293-0/FIGURES/6
- Duyao, M., Ambrose, C., Myers, R., Novelletto, A., Persichetti, F., Frontali, M., Folstein, S., Ross, C., Franz, M., Abbott, M., Gray, J., Conneally, P., Young, A., Penney, J., Hollingsworth, Z., Shoulson, I., Lazzarini, A., Falek, A., Koroshetz, W., ... Macdonald, M. (1993). Trinucleotide repeat length instability and age of onset in Huntington's disease. *Nature Genetics*, 4(4), 387–392. https://doi.org/10.1038/NG0893-387
- Duyao, M., Auerbach, A. B., Ryan, A., Persichetti, F., Barnes, G. T., McNeil, S. M., Ge, P., Vonsattel, J. P., Gusella, J. F., Joyner, A. L., & MacDonald, M. E. (1995). Inactivation of the mouse huntington's disease gene homolog Hdh. *Science*, *269*(5222), 407–410. https://doi.org/10.1126/science.7618107
- Eiring, A. M., Harb, J. G., Neviani, P., Garton, C., Oaks, J. J., Spizzo, R., Liu, S., Schwind, S., Santhanam, R., Hickey, C. J., Becker, H., Chandler, J. C., Andino, R., Cortes, J., Hokland, P., Huettner, C. S., Bhatia, R., Roy, D. C., Liebhaber, S. A., ... Perrotti, D. (2010). miR-328 Functions as an RNA Decoy to Modulate hnRNP E2 Regulation of mRNA Translation in Leukemic Blasts. *Cell*, 140(5), 652. https://doi.org/10.1016/J.CELL.2010.01.007
- El-Hattab, A. W., Saleh, M. A., Hashem, A., Al-Owain, M., Asmari, A. Al, Rabei, H., Abdelraouf, H., Hashem, M., Alazami, A. M., Patel, N., Shaheen, R., Faqeih, E. A., & Alkuraya, F. S. (2016). ADAT3-related intellectual disability: Further delineation of the phenotype. *American Journal of Medical Genetics. Part A, 170A*(5), 1142–1147. https://doi.org/10.1002/AJMG.A.37578
- Elbarbary, R. A., Takaku, H., Uchiumi, N., Tamiya, H., Abe, M., Nishida, H., & Nashimoto, M.

- (2009). Human cytosolic tRNase ZL can downregulate gene expression through miRNA. *FEBS Letters*, *583*(19), 3241–3246. https://doi.org/10.1016/J.FEBSLET.2009.09.015
- Elbarbary, R. A., Takaku, H., Uchiumi, N., Tamiya, H., Abe, M., Takahashi, M., Nishida, H., & Nashimoto, M. (2009). Modulation of gene expression by human cytosolic tRNase ZL through 5'-Half-tRNA. *PLOS ONE*, 4(6), e5908. https://doi.org/10.1371/JOURNAL.PONE.0005908
- Emara, M. M., Ivanov, P., Hickman, T., Dawra, N., Tisdale, S., Kedersha, N., Hu, G. F., & Anderson, P. (2010). Angiogenin-induced tRNA-derived stress-induced RNAs promote stress-induced stress granule assembly. *Journal of Biological Chemistry*, *285*(14), 10959–10968. https://doi.org/10.1074/jbc.M109.077560
- Essa, M. M., Braidy, N., Vijayan, K. R., Subash, S., & Guillemin, G. J. (2013). Excitotoxicity in the pathogenesis of autism. *Neurotoxicity Research*, 23(4), 393–400. https://doi.org/10.1007/S12640-012-9354-3/FIGURES/3
- Esteller, M. (2011). Non-coding RNAs in human disease. *Nature Reviews Genetics*, 12(12), 861–874. https://doi.org/10.1038/NRG3074
- Estrada-Sánchez, A. M., Montiel, T., Segovia, J., & Massieu, L. (2009). Glutamate toxicity in the striatum of the R6/2 Huntington's disease transgenic mice is age-dependent and correlates with decreased levels of glutamate transporters. *Neurobiology of Disease*, 34(1), 78–86. https://doi.org/10.1016/J.NBD.2008.12.017
- Estrada-Sánchez, A. M., & Rebec, G. V. (2012). Corticostriatal dysfunction and glutamate transporter 1 (GLT1) in Huntington's disease: interactions between neurons and astrocytes. *Basal Ganglia*, *2*(2), 57. https://doi.org/10.1016/J.BAGA.2012.04.029
- Ewels, P., Magnusson, M., Lundin, S., & Käller, M. (2016). MultiQC: Summarize analysis results for multiple tools and samples in a single report. *Bioinformatics*, *32*(19), 3047–3048. https://doi.org/10.1093/bioinformatics/btw354
- Faber, P. W., Alter, J. R., Macdonald, M. E., & Hart, A. C. (1999). Polyglutamine-mediated dysfunction and apoptotic death of a Caenorhabditis elegans sensory neuron. *Proceedings of the National Academy of Sciences of the United States of America*, 96(1), 179–184. https://doi.org/10.1073/PNAS.96.1.179/ASSET/E0414E04-0939-49A1-9EB7-2A779A0AC005/ASSETS/GRAPHIC/PQ0193197004.JPEG
- Falnes, P. (2004). Repair of 3-methylthymine and 1-methylguanine lesions by bacterial and human AlkB proteins. *Nucleic Acids Research*, *32*(21), 6260. https://doi.org/10.1093/NAR/GKH964
- Fan, M. M. Y., & Raymond, L. A. (2007). N-Methyl-d-aspartate (NMDA) receptor function and excitotoxicity in Huntington's disease. *Progress in Neurobiology*, *81*(5–6), 272–293. https://doi.org/10.1016/J.PNEUROBIO.2006.11.003
- Farina, K. L., Hüttelmaier, S., Musunuru, K., Darnell, R., & Singer, R. H. (2003). Two ZBP1 KH domains facilitate β -actin mRNA localization, granule formation, and cytoskeletal attachment. *Journal of Cell Biology*, 160(1), 77–87. https://doi.org/10.1083/JCB.200206003

- Feng, Y., Zou, L., Yan, D., Chen, H., Xu, G., Jian, W., Cui, P., & Chao, W. (2017). Extracellular miRNAs induce potent innate immune responses via TLR7/MyD88-dependent mechanisms. *Journal of Immunology*, 199(6), 2106. https://doi.org/10.4049/JIMMUNOL.1700730
- Fernandopulle, M. S., Lippincott-Schwartz, J., & Ward, M. E. (2021). RNA transport and local translation in neurodevelopmental and neurodegenerative disease. In *Nature Neuroscience* (Vol. 24, Issue 5, pp. 622–632). Nature Research. https://doi.org/10.1038/s41593-020-00785-2
- Ferrante, R. J. (2009). Mouse models of Huntington's Disease and methodological considerations for therapeutic trials. *Biochimica et Biophysica Acta*, *1792*(6), 506. https://doi.org/10.1016/J.BBADIS.2009.04.001
- Ferrante, R. J., Kowall, N. W., Beal, M. F., Martin, J. B., Bird, E. D., & Richardson, E. P. (1987). Morphologic and histochemical characteristics of a spared subset of striatal neurons in Huntington's disease. *Journal of Neuropathology and Experimental Neurology*, 46(1), 12–27. https://doi.org/10.1097/00005072-198701000-00002
- Fourie, C., Kim, E., Waldvogel, H., Wong, J. M., McGregor, A., Faull, R. L. M., & Montgomery, J. M. (2014). Differential changes in Postsynaptic Density Proteins in postmortem Huntington's Disease and Parkinson's Disease human brains. *Journal of Neurodegenerative Diseases*, 2014, 1–14. https://doi.org/10.1155/2014/938530
- Franciosi, S., Ryu, J. K., Shim, Y., Hill, A., Connolly, C., Hayden, M. R., McLarnon, J. G., & Leavitt, B. R. (2012). Age-dependent neurovascular abnormalities and altered microglial morphology in the YAC128 mouse model of Huntington disease. *Neurobiology of Disease*, *45*(1), 438–449. https://doi.org/10.1016/J.NBD.2011.09.003
- Franich, N. R., Hickey, M. A., Zhu, C., Osborne, G. F., Ali, N., Chu, T., Bove, N. H., Lemesre, V., Lerner, R. P., Zeitlin, S. O., Howland, D., Neueder, A., Landles, C., Bates, G. P., & Chesselet, M. F. (2019). Phenotype onset in Huntington's disease knock-in mice is correlated with the incomplete splicing of the mutant huntingtin gene. *Journal of Neuroscience Research*, *97*(12), 1590. https://doi.org/10.1002/JNR.24493
- Frye, M., Jaffrey, S. R., Pan, T., Rechavi, G., & Suzuki, T. (2016). RNA modifications: what have we learned and where are we headed? *Nature Reviews. Genetics*, *17*(6), 365–372. https://doi.org/10.1038/NRG.2016.47
- Frye, M., & Watt, F. M. (2006). The RNA methyltransferase Misu (NSun2) mediates Mycinduced proliferation and is upregulated in tumors. *Current Biology*, *16*(10), 971–981. https://doi.org/10.1016/J.CUB.2006.04.027
- Fu, H., Feng, J., Liu, Q., Sun, F., Tie, Y., Zhu, J., Xing, R., Sun, Z., & Zheng, X. (2009). Stress induces tRNA cleavage by angiogenin in mammalian cells. *FEBS Letters*, *583*(2), 437–442. https://doi.org/10.1016/J.FEBSLET.2008.12.043
- Gagliardi, S., Davin, A., Bini, P., Sinforiani, E., Poloni, T. E., Polito, L., Rivoiro, C., Binetti, G., Paterlini, A., Benussi, L., Ghidoni, R., Vanacore, N., & Cereda, C. (2019). A novel nonsense Angiogenin mutation is associated With Alzheimer Disease. *Alzheimer Disease and Associated Disorders*, 33(2), 163–165. https://doi.org/10.1097/WAD.0000000000000272

- Gagnon, K. T., Pendergraff, H. M., Deleavey, G. F., Swayze, E. E., Potier, P., Randolph, J., Roesch, E. B., Chattopadhyaya, J., Damha, M. J., Bennett, C. F., Montaillier, C., Lemaitre, M., & Corey, D. R. (2010). Allele-selective inhibition of Mutant Huntingtin expression with antisense oligonucleotides targeting the expanded CAG repeat. *Biochemistry*, 49(47), 10166. https://doi.org/10.1021/BI101208K
- Galka-Marciniak, P., Urbanek, M. O., & Krzyzosiak, W. J. (2012). Triplet repeats in transcripts: structural insights into RNA toxicity. *Biological Chemistry*, 393(11), 1299–1315. https://doi.org/10.1515/HSZ-2012-0218
- Gámez-Valero, A., Guisado-Corcoll, A., Herrero-Lorenzo, M., Solaguren-Beascoa, M., & Martí, E. (2020). Non-coding RNAs as sensors of oxidative stress in neurodegenerative diseases. *Antioxidants*, *9*(11), 1–30. https://doi.org/10.3390/antiox9111095
- García-Alcalde, F., Okonechnikov, K., Carbonell, J., Cruz, L. M., Götz, S., Tarazona, S., Dopazo, J., Meyer, T. F., & Conesa, A. (2012). Qualimap: Evaluating next-generation sequencing alignment data. *Bioinformatics*, 28(20), 2678–2679. https://doi.org/10.1093/bioinformatics/bts503
- García-Amado, M., & Prensa, L. (2012). Stereological analysis of neuron, glial and endothelial cell numbers in the human amygdaloid complex. *PLoS ONE*, *7*(6). https://doi.org/10.1371/journal.pone.0038692
- García-Cabezas, M., John, Y. J., Barbas, H., & Zikopoulos, B. (2016). Distinction of neurons, glia and endothelial cells in the cerebral cortex: An algorithm based on cytological features. *Frontiers in Neuroanatomy*, 10(NOV), 1–28. https://doi.org/10.3389/fnana.2016.00107
- Garcia-Silva, M. R., Cabrera-Cabrera, F., Güida, M. C., Cayota, A., Garcia-Silva, M. R., Cabrera-Cabrera, F., Güida, M. C., & Cayota, A. (2013). Novel aspects of tRNA-derived small RNAs with potential impact in infectious diseases. *Advances in Bioscience and Biotechnology*, 4(5), 17–25. https://doi.org/10.4236/ABB.2013.45A002
- Garcia-Silva, M. R., Frugier, M., Tosar, J. P., Correa-Dominguez, A., Ronalte-Alves, L., Parodi-Talice, A., Rovira, C., Robello, C., Goldenberg, S., & Cayota, A. (2010). A population of tRNA-derived small RNAs is actively produced in Trypanosoma cruzi and recruited to specific cytoplasmic granules. *Molecular and Biochemical Parasitology*, *171*(2), 64–73. https://doi.org/10.1016/J.MOLBIOPARA.2010.02.003
- Garriga-Canut, M., Agustín-Pavón, C., Herrmann, F., Sánchez, A., Dierssen, M., Fillat, C., & Isalan, M. (2012). Synthetic zinc finger repressors reduce mutant huntingtin expression in the brain of R6/2 mice. *Proceedings of the National Academy of Sciences of the United States of America*, 109(45). https://doi.org/10.1073/PNAS.1206506109/-/DCSUPPLEMENTAL/PNAS.201206506SI.PDF
- Gebauer, F., Schwarzl, T., Valcárcel, J., & Hentze, M. W. (2020). RNA-binding proteins in human genetic disease. *Nature Reviews Genetics*, *22*(3), 185–198. https://doi.org/10.1038/S41576-020-00302-Y
- Gebetsberger, J., Wyss, L., Mleczko, A. M., Reuther, J., & Polacek, N. (2017). A tRNA-derived fragment competes with mRNA for ribosome binding and regulates translation during

- stress. *RNA Biology*, *14*(10), 1364–1373. https://doi.org/10.1080/15476286.2016.1257470
- Geng, G., Wang, H., Xin, W., Liu, Z., Chen, J., Danting, Z., Han, F., & Ye, S. (2021). tRNA derived fragment (tRF)-3009 participates in modulation of IFN-α-induced CD4+ T cell oxidative phosphorylation in lupus patients. *Journal of Translational Medicine*, *19*(1), 1–13. https://doi.org/10.1186/S12967-021-02967-3/FIGURES/5
- George, H., Bashir, Z. I., & Hussain, S. (2022). Impaired hippocampal NMDAR-LTP in a transgenic model of NSUN2-deficiency. *Neurobiology of Disease*, *163*. https://doi.org/10.1016/J.NBD.2021.105597
- Gerfen, C. R. (1988). Synaptic organization of the striatum. *Journal of Electron Microscopy Technique*, *10*(3), 265–281. https://doi.org/10.1002/jemt.1060100305
- Gerfen, C. R., Engber, T. M., Mahan, L. C., Susel, Z., Chase, T. N., Monsma, F. J., & Sibley, D. R. (1990). D1 and D2 dopamine receptor-regulated gene expression of striatonigral and striatopallidal neurons. *Science*, *250*(1986), 1429–1432. http://dx.doi.org/10.1126/science.2147780
- Gipson, T. A., Neueder, A., Wexler, N. S., Bates, G. P., & Housman, D. (2013). Aberrantly spliced HTT, a new player in Huntington's disease pathogenesis. *RNA Biology*, *10*(11), 1647–1652. https://doi.org/10.4161/RNA.26706
- Giraldez, M. D., Spengler, R. M., Etheridge, A., Goicochea, A. J., Tuck, M., Choi, S. W., Galas, D. J., & Tewari, M. (2019). Phospho-RNA-seq: a modified small RNA-seq method that reveals circulating mRNA and lncRNA fragments as potential biomarkers in human plasma. *The EMBO Journal*, 38(11), 1–14. https://doi.org/10.15252/embj.2019101695
- Giralt, A., Saavedra, A., Alberch, J., & Pérez-Navarro, E. (2012). Cognitive dysfunction in Huntington's Disease: humans, mouse models and molecular mechanisms. *Journal of Huntington's Disease*, 1(2), 155–173. https://doi.org/10.3233/JHD-120023
- Gissi, C., Pesole, G., Cattaneo, E., & Tartari, M. (2006). Huntingtin gene evolution in Chordata and its peculiar features in the ascidian Ciona genus. *BMC Genomics*, *7*, 288. https://doi.org/10.1186/1471-2164-7-288
- Goll, M. G., Kirpekar, F., Maggert, K. A., Yoder, J. A., Hsieh, C. L., Zhang, X., Golic, K. G., Jacobsen, S. E., & Bestor, T. H. (2006). Methylation of tRNAAsp by the DNA methyltransferase homolog Dnmt2. *Science*, *311*(5759), 395–398. https://doi.org/10.1126/SCIENCE.1120976/SUPPL_FILE/GOLL.SOM.PDF
- Goodarzi, H., Liu, X., Nguyen, H. C. B., Zhang, S., Fish, L., & Tavazoie, S. F. (2015). Endogenous tRNA-derived fragments suppress breast cancer progression via YBX1 displacement. *Cell*, *161*(4), 790–802. https://doi.org/10.1016/J.CELL.2015.02.053
- Gordon, N. (2003). Huntington's disease of early onset or juvenile Huntington's disease. Hospital Medicine, 64(10), 576–580. https://doi.org/10.12968/HOSP.2003.64.10.2319
- Gray, M., Shirasaki, D. I., Cepeda, C., André, V. M., Wilburn, B., Lu, X. H., Tao, J., Yamazaki,

- I., Li, S. H., Sun, Y. E., Li, X. J., Levine, M. S., & Yang, X. W. (2008). Full-length human mutant huntingtin with a stable polyglutamine repeat can elicit progressive and selective neuropathogenesis in BACHD mice. *Journal of Neuroscience*, *28*(24), 6182–6195. https://doi.org/10.1523/JNEUROSCI.0857-08.2008
- Greenway, M. J., Alexander, M. D., Ennis, S., Traynor, B. J., Corr, B., Frost, E., Green, A., & Hardiman, O. (2004). A novel candidate region for ALS on chromosome 14q11.2. *Neurology*, 63(10), 1936–1938. https://doi.org/10.1212/01.WNL.0000144344.39103.F6
- Greenway, M. J., Andersen, P. M., Russ, G., Ennis, S., Cashman, S., Donaghy, C., Patterson, V., Swingler, R., Kieran, D., Prehn, J., Morrison, K. E., Green, A., Acharya, K. R., Brown, R. H., & Hardiman, O. (2006). ANG mutations segregate with familial and "sporadic" amyotrophic lateral sclerosis. *Nature Genetics*, 38(4), 411–413. https://doi.org/10.1038/NG1742
- Greulich, W., Wagner, M., Gaidt, M. M., Stafford, C., Cheng, Y., Linder, A., Carell, T., & Hornung, V. (2019). TLR8 is a sensor of RNase T2 degradation products. *Cell*, *179*(6), 1264. https://doi.org/10.1016/J.CELL.2019.11.001
- Griffioen, K., Mattson, M. P., & Okun, E. (2018). Deficiency of Toll-like receptors 2, 3 or 4 extends life expectancy in Huntington's disease mice. *Heliyon*, *4*(1), 508. https://doi.org/10.1016/J.HELIYON.2018.E00508
- Grosjean, H., Auxilien, S., Constantinesco, F., Simon, C., Corda, Y., Becker, H. F., Foiret, D., Morin, A., Jin, Y. X., Fournier, M., & Fourrey, J. L. (1996). Enzymatic conversion of adenosine to inosine and to N1-methylinosine in transfer RNAs: a review. *Biochimie*, 78(6), 488–501. https://doi.org/10.1016/0300-9084(96)84755-9
- Grosson, C. L. S., MacDonald, M. E., Duyao, M. P., Ambrose, C. M., Roffler-Tarlov, S., & Gusella, J. F. (1994). Synteny conservation of the Huntington's disease gene and surrounding loci on mouse Chromosome 5. *Mammalian Genome*, *5*(7), 424–428. https://doi.org/10.1007/BF00357002
- Gunawardena, S., Her, L. S., Brusch, R. G., Laymon, R. A., Niesman, I. R., Gordesky-Gold, B., Sintasath, L., Bonini, N. M., & Goldstein, L. S. B. (2003). Disruption of axonal transport by loss of huntingtin or expression of pathogenic polyQ proteins in Drosophila. *Neuron*, 40(1), 25–40. https://doi.org/10.1016/S0896-6273(03)00594-4
- Gusella, J. F., Wexler, N. S., Conneally, P. M., Naylor, S. L., Anderson, M. A., Tanzi, R. E., Watkins, P. C., Ottina, K., Wallace, M. R., Sakaguchi, A. Y., Young, A. B., Shoulson, I., Bonilla, E., & Martin, J. B. (1983). A polymorphic DNA marker genetically linked to Huntington's disease. *Nature*, 306(5940), 234–238. https://doi.org/10.1038/306234a0
- Guzzi, N., Cieśla, M., Ngoc, P. C. T., Lang, S., Arora, S., Dimitriou, M., Pimková, K., Sommarin, M. N. E., Munita, R., Lubas, M., Lim, Y., Okuyama, K., Soneji, S., Karlsson, G., Hansson, J., Jönsson, G., Lund, A. H., Sigvardsson, M., Hellström-Lindberg, E., ... Bellodi, C. (2018). Pseudouridylation of tRNA-derived fragments steers translational control in stem cells. Cell, 173(5), 1204-1216.e26. https://doi.org/10.1016/J.CELL.2018.03.008
- Haag, S., Sloan, K. E., Ranjan, N., Warda, A. S., Kretschmer, J., Blessing, C., Hübner, B.,

- Seikowski, J., Dennerlein, S., Rehling, P., Rodnina, M. V, Höbartner, C., & Bohnsack, M. T. (2016). NSUN3 and ABH1 modify the wobble position of mt-tRNAMet to expand codon recognition in mitochondrial translation. *The EMBO Journal*, *35*(19), 2104–2119. https://doi.org/10.15252/EMBJ.201694885
- Haag, S., Warda, A. S., Kretschmer, J., Günnigmann, M. A., Höbartner, C., & Bohnsack, M. T. (2015). NSUN6 is a human RNA methyltransferase that catalyzes formation of m5C72 in specific tRNAs. *RNA*, *21*(9), 1532–1543. https://doi.org/10.1261/RNA.051524.115
- Hahne, J. C., Lampis, A., & Valeri, N. (2020). Vault RNAs: hidden gems in RNA and protein regulation. *Cellular and Molecular Life Sciences*, 78(4), 1487–1499. https://doi.org/10.1007/S00018-020-03675-9
- Han, I., You, Y., Kordower, J. H., Brady, S. T., & Morfini, G. A. (2010). Differential vulnerability of neurons in Huntington's disease: the role of cell type-specific features. *Journal of Neurochemistry*, 113(5), 1073–1091. https://doi.org/10.1111/J.1471-4159.2010.06672.X
- Hanada, T., Weitzer, S., Mair, B., Bernreuther, C., Wainger, B. J., Ichida, J., Hanada, R., Orthofer, M., Cronin, S. J., Komnenovic, V., Minis, A., Sato, F., Mimata, H., Yoshimura, A., Tamir, I., Rainer, J., Kofler, R., Yaron, A., Eggan, K. C., ... Penninger, J. M. (2013). CLP1 links tRNA metabolism to progressive motor-neuron loss. *Nature*, 495(7442), 474–480. https://doi.org/10.1038/nature11923
- Harper, S. Q., Staber, P. D., He, X., Eliason, S. L., Martins, I. H., Mao, Q., Yang, L., Kotin, R. M., Paulson, H. L., & Davidson, B. L. (2005). RNA interference improves motor and neuropathological abnormalities in a Huntington's disease mouse model. *Proceedings of the National Academy of Sciences of the United States of America*, 102(16), 5820–5825. https://doi.org/10.1073/PNAS.0501507102/ASSET/D8CDF78E-56AC-4DB6-BD21-C4F2C3B6C916/ASSETS/GRAPHIC/ZPQ0150579450004.JPEG
- Haussecker, D., Huang, Y., Lau, A., Parameswaran, P., Fire, A. Z., & Kay, M. A. (2010). Human tRNA-derived small RNAs in the global regulation of RNA silencing. *RNA*, *16*(4), 673. https://doi.org/10.1261/RNA.2000810
- Hébert, S. S., Papadopoulou, A. S., Smith, P., Galas, M. C., Planel, E., Silahtaroglu, A. N., Sergeant, N., Buée, L., & de Strooper, B. (2010). Genetic ablation of Dicer in adult forebrain neurons results in abnormal tau hyperphosphorylation and neurodegeneration. *Human Molecular Genetics*, 19(20), 3959–3969. https://doi.org/10.1093/HMG/DDQ311
- Heinz, A., Nabariya, D. K., & Krauss, S. (2021). Huntingtin and its role in mechanisms of RNA-mediated toxicity. *Toxins*, *13*(7), 487. https://doi.org/10.3390/TOXINS13070487
- Heman-Ackah, S. M., Bassett, A. R., & Wood, M. J. A. (2016). Precision modulation of neurodegenerative disease-related gene expression in Human iPSC-derived neurons. *Scientific Reports*, *6*(1), 1–12. https://doi.org/10.1038/srep28420
- Hendreen, J. C., & Folstein, S. E. (1995). Early loss of neostriatal striosome neurons in Huntington's disease. *Journal of Neuropathology & Experimental Neurology*, *54*(1), 105–120.

- Hervás-Corpión, I., Guiretti, D., Alcaraz-Iborra, M., Olivares, R., Campos-Caro, A., Barco, Á., & Valor, L. M. (2018). Early alteration of epigenetic-related transcription in Huntington's disease mouse models. *Scientific Reports*, 8(1), 1–14. https://doi.org/10.1038/s41598-018-28185-4
- Ho, A. K., Sahakian, B. J., Brown, R. G., Barker, R. A., Hodges, J. R., Ané, M. N., Snowden, J., Thompson, J., Esmonde, T., Gentry, R., Moore, J. W., & Bodner, T. (2003). Profile of cognitive progression in early Huntington's disease. *Neurology*, *61*(12), 1702–1706. https://doi.org/10.1212/01.WNL.0000098878.47789.BD
- Ho, T. H., Charlet-B, N., Poulos, M. G., Singh, G., Swanson, M. S., & Cooper, T. A. (2004). Muscleblind proteins regulate alternative splicing. *The EMBO Journal*, *23*(15), 3103–3112. https://doi.org/10.1038/SJ.EMBOJ.7600300
- Hodges, A., Strand, A. D., Aragaki, A. K., Kuhn, A., Sengstag, T., Hughes, G., Elliston, L. A., Hartog, C., Goldstein, D. R., Thu, D., Hollingsworth, Z. R., Collin, F., Synek, B., Holmans, P. A., Young, A. B., Wexler, N. S., Delorenzi, M., Kooperberg, C., Augood, S. J., ... Luthi-Carter, R. (2006). Regional and cellular gene expression changes in human Huntington's disease brain. *Human Molecular Genetics*, 15(6), 965–977. https://doi.org/10.1093/HMG/DDL013
- Hodgson, J. G., Agopyan, N., Gutekunst, C. A., Leavitt, B. R., Lepiane, F., Singaraja, R., Smith, D. J., Bissada, N., McCutcheon, K., Nasir, J., Jamot, L., Xiao-Jiang, L., Stevens, M. E., Rosemond, E., Roder, J. C., Phillips, A. G., Rubin, E. M., Hersch, S. M., & Hayden, M. R. (1999). A YAC mouse model for Huntington's disease with full-length mutant huntingtin, cytoplasmic toxicity, and selective striatal neurodegeneration. *Neuron*, 23(1), 181–192. https://doi.org/10.1016/S0896-6273(00)80764-3
- Holt, C. E., Martin, K. C., & Schuman, E. M. (2019). Local translation in neurons: visualization and function. *Nature Structural & Molecular Biology*, *26*(7), 557–566. https://doi.org/10.1038/S41594-019-0263-5
- Honda, S., Loher, P., Shigematsu, M., Palazzo, J. P., Suzuki, R., Imoto, I., Rigoutsos, I., & Kirino, Y. (2015). Sex hormone-dependent tRNA halves enhance cell proliferation in breast and prostate cancers. *Proceedings of the National Academy of Sciences of the United States of America*, 112(29), E3816–E3825. https://doi.org/10.1073/PNAS.1510077112
- Hoss, A. G., Kartha, V. K., Dong, X., Latourelle, J. C., Dumitriu, A., Hadzi, T. C., MacDonald, M. E., Gusella, J. F., Akbarian, S., Chen, J. F., Weng, Z., & Myers, R. H. (2014). MicroRNAs located in the Hox gene clusters are implicated in Huntington's Disease pathogenesis. PLOS Genetics, 10(2), e1004188. https://doi.org/10.1371/JOURNAL.PGEN.1004188
- Hsu, R. J., Hsiao, K. M., Lin, M. J., Li, C. Y., Wang, L. C., Chen, L. K., & Pan, H. (2011). Long tract of untranslated CAG repeats is deleterious in transgenic mice. *PLOS ONE*, *6*(1), e16417. https://doi.org/10.1371/JOURNAL.PONE.0016417
- Huang, B., Yang, H., Cheng, X., Wang, D., Fu, S., Shen, W., Zhang, Q., Zhang, L., Xue, Z., Li, Y., Da, Y., Yang, Q., Li, Z., Liu, L., Qiao, L., Kong, Y., Yao, Z., Zhao, P., Li, M., & Zhang, R. (2017). tRF/miR-1280 suppresses stem cell-like cells and metastasis in colorectal

- cancer. *Cancer Research*, 77(12), 3194–3206. https://doi.org/10.1158/0008-5472.CAN-16-3146
- Huang, D. W., Sherman, B. T., & Lempicki, R. A. (2009a). Bioinformatics enrichment tools: paths toward the comprehensive functional analysis of large gene lists. *Nucleic Acids Research*, *37*(1), 1–13. https://doi.org/10.1093/nar/gkn923
- Huang, D. W., Sherman, B. T., & Lempicki, R. A. (2009b). Systematic and integrative analysis of large gene lists using DAVID bioinformatics resources. *Nature Protocols*, *4*(1), 44–57. https://doi.org/10.1038/nprot.2008.211
- Huang, Z., Du, Y. ping, Wen, J. tao, Lu, B. feng, & Zhao, Y. (2022). snoRNAs: functions and mechanisms in biological processes, and roles in tumor pathophysiology. *Cell Death Discovery*, 8(1), 1–10. https://doi.org/10.1038/s41420-022-01056-8
- Huntington, G. (2003). On chorea. *The Journal of Neuropsychiatry and Clinical Neurosciences*, *15*(1), 109–112. https://doi.org/10.1176/JNP.15.1.109
- Hussain, S., Sajini, A. A., Blanco, S., Dietmann, S., Lombard, P., Sugimoto, Y., Paramor, M., Gleeson, J. G., Odom, D. T., Ule, J., & Frye, M. (2013). NSun2-mediated cytosine-5 methylation of vault noncoding RNA determines its processing into regulatory small RNAs. *Cell Reports*, *4*(2), 255. https://doi.org/10.1016/J.CELREP.2013.06.029
- Itoh, K., Watanabe, A., Funami, K., Seya, T., & Matsumoto, M. (2008). The Clathrin-mediated endocytic pathway participates in dsRNA-induced IFN-β production. *The Journal of Immunology*, *181*(8), 5522–5529. https://doi.org/10.4049/JIMMUNOL.181.8.5522
- Ivanov, P., Emara, M. M., Villen, J., Gygi, S. P., & Anderson, P. (2011). Angiogenin-induced tRNA fragments inhibit translation initiation. *Molecular Cell*, *43*(4), 613–623. https://doi.org/10.1016/J.MOLCEL.2011.06.022
- Ivanov, P., O'Day, E., Emara, M. M., Wagner, G., Lieberman, J., & Anderson, P. (2014). G-quadruplex structures contribute to the neuroprotective effects of angiogenin-induced tRNA fragments. *Proceedings of the National Academy of Sciences of the United States of America*, 111(51), 18201–18206. https://doi.org/10.1073/PNAS.1407361111
- Jablonowski, D., Zink, S., Mehlgarten, C., Daum, G., & Schaffrath, R. (2006). tRNAGlu wobble uridine methylation by Trm9 identifies Elongator's key role for zymocin-induced cell death in yeast. *Molecular Microbiology*, *59*(2), 677–688. https://doi.org/10.1111/J.1365-2958.2005.04972.X
- Jackson, G. R., Salecker, I., Dong, X., Yao, X., Arnheim, N., Faber, P. W., MacDonald, M. E., & Zipursky, S. L. (1998). Polyglutamine-expanded human huntingtin transgenes induce degeneration of Drosophila photoreceptor neurons. *Neuron*, 21(3), 633–642. https://doi.org/10.1016/S0896-6273(00)80573-5
- Jacobsen, J. C., Bawden, C. S., Rudiger, S. R., McLaughlan, C. J., Reid, S. J., Waldvogel, H. J., MacDonald, M. E., Gusella, J. F., Walker, S. K., Kelly, J. M., Webb, G. C., Faull, R. L. M., Rees, M. I., & Snell, R. G. (2010). An ovine transgenic Huntington's disease model.

 Human Molecular Genetics, 19(10), 1873–1882.
 https://doi.org/10.1093/HMG/DDQ063

- Jehn, J., Treml, J., Wulsch, S., Ottum, B., Erb, V., Hewel, C., Kooijmans, R. N., Wester, L., Fast, I., & Rosenkranz, D. (2020). 5' tRNA halves are highly expressed in the primate hippocampus and might sequence-specifically regulate gene expression. *RNA*, *26*(6), 694–707. https://doi.org/10.1261/RNA.073395.119
- Jian, H., Zhang, C., Qi, Z. Y., Li, X., Lou, Y., Kang, Y., Deng, W., Lv, Y., Wang, C., Wang, W., Shang, S., Hou, M., Zhou, H., & Feng, S. (2021). Alteration of mRNA 5-methylcytosine modification in neurons after OGD/R and potential roles in cell stress response and apoptosis. Frontiers in Genetics, 12. https://doi.org/10.3389/FGENE.2021.633681/FULL
- Jin, J., Cheng, Y., Zhang, Y., Wood, W., Peng, Q., Hutchison, E., Mattson, M. P., Becker, K. G., & Duan, W. (2012). Interrogation of brain miRNA and mRNA expression profiles reveals a molecular regulatory network that is perturbed by mutant huntingtin. *Journal of Neurochemistry*, 123(4), 477–490. https://doi.org/10.1111/J.1471-4159.2012.07925.X
- Jöchl, C., Rederstorff, M., Hertel, J., Stadler, P. F., Hofacker, I. I., Schrettl, M., Haas, H., & Hüttenhofer, A. (2008). Small ncRNA transcriptome analysis from Aspergillus fumigatus suggests a novel mechanism for regulation of protein synthesis. *Nucleic Acids Research*, *36*(8), 2677–2689. https://doi.org/10.1093/NAR/GKN123
- Julien, C. L., Thompson, J. C., Wild, S., Yardumian, P., Snowden, J. S., Turner, G., & Craufurd, D. (2007). Psychiatric disorders in preclinical Huntington's disease. *Journal of Neurology, Neurosurgery, and Psychiatry*, 78(9), 939. https://doi.org/10.1136/JNNP.2006.103309
- Kalita, K., Makonchuk, D., Gomes, C., Zheng, J. J., & Hetman, M. (2008). Inhibition of nucleolar transcription as a trigger for neuronal apoptosis. *Journal of Neurochemistry*, 105(6), 2286. https://doi.org/10.1111/J.1471-4159.2008.05316.X
- Kapranov, P., Cheng, J., Dike, S., Nix, D. A., Duttagupta, R., Willingham, A. T., Stadler, P. F., Hertel, J., Hackermüller, J., Hofacker, I. L., Bell, I., Cheung, E., Drenkow, J., Dumais, E., Patel, S., Helt, G., Ganesh, M., Ghosh, S., Piccolboni, A., ... Gingeras, T. R. (2007). RNA maps reveal new RNA classes and a possible function for pervasive transcription. *Science*, 316(5830), 1484–1488. https://doi.org/10.1126/SCIENCE.1138341/SUPPL_FILE/KAPRANOV.SOM.PDF
- Kapur, M., Monaghan, C. E., & Ackerman, S. L. (2017). Regulation of mRNA translation in neurons–A Matter of life and death. *Neuron*, *96*(3), 616. https://doi.org/10.1016/J.NEURON.2017.09.057
- Karaca, E., Weitzer, S., Pehlivan, D., Shiraishi, H., Gogakos, T., Hanada, T., Jhangiani, S. N., Wiszniewski, W., Withers, M., Campbell, I. M., Erdin, S., Isikay, S., Franco, L. M., Gonzaga-Jauregui, C., Gambin, T., Gelowani, V., Hunter, J. V., Yesil, G., Koparir, E., ... Lupski, J. R. (2014). Human CLP1 mutations alter tRNA biogenesis, affecting both peripheral and central nervous system function. *Cell*, 157(3), 636–650. https://doi.org/10.1016/j.cell.2014.02.058
- Karikó, K., Buckstein, M., Ni, H., & Weissman, D. (2005). Suppression of RNA recognition by Toll-like receptors: the impact of nucleoside modification and the evolutionary origin

- of RNA. Immunity, 23(2), 165–175. https://doi.org/10.1016/j.immuni.2005.06.008
- Karlovich, C. A., John, R. M., Ramirez, L., Stainier, D. Y. R., & Myers, R. M. (1998). Characterization of the Huntington's disease (HD) gene homologue in the zebrafish Danio rerio. *Gene*, *217*(1–2), 117–125. https://doi.org/10.1016/S0378-1119(98)00342-4
- Kawaguchi, Y., Wilson, C. J., Augood, S. J., & Emson, P. C. (1995). Striatal interneurones: chemical, physiological and morphological characterization. *Trends in Neurosciences*, *18*(12), 527–535. https://doi.org/10.1016/0166-2236(95)98374-8
- Kedersha, N. L., Miquel, M. C., Bittner, D., & Rome, L. H. (1990). Vaults. II. Ribonucleoprotein structures are highly conserved among higher and lower eukaryotes. *The Journal of Cell Biology*, 110(4), 895. https://doi.org/10.1083/JCB.110.4.895
- Kedersha, N. L., & Rome, L. H. (1986). Isolation and characterization of a novel ribonucleoprotein particle: large structures contain a single species of small RNA. *The Journal of Cell Biology*, 103(3), 699. https://doi.org/10.1083/JCB.103.3.699
- Keegan, L. P., Gerber, A. P., Brindle, J., Leemans, R., Gallo, A., Keller, W., & O'Connell, M. A. (2000). The properties of a tRNA-specific Adenosine Deaminase from Drosophila melanogaster support an evolutionary link between pre-mRNA editing and tRNA modification. *Molecular and Cellular Biology*, 20(3), 825–833. https://doi.org/10.1128/mcb.20.3.825-833.2000
- Khan, M. A., Rafiq, M. A., Noor, A., Hussain, S., Flores, J. V., Rupp, V., Vincent, A. K., Malli, R., Ali, G., Khan, F. S., Ishak, G. E., Doherty, D., Weksberg, R., Ayub, M., Windpassinger, C., Ibrahim, S., Frye, M., Ansar, M., & Vincent, J. B. (2012). Mutation in NSUN2, which Encodes an RNA Methyltransferase, Causes Autosomal-Recessive Intellectual Disability. American Journal of Human Genetics, 90(5), 856. https://doi.org/10.1016/J.AJHG.2012.03.023
- Khoddami, V., & Cairns, B. R. (2013). Identification of direct targets and modified bases of RNA cytosine methyltransferases. *Nature Biotechnology*, *31*(5), 458–464. https://doi.org/10.1038/NBT.2566
- Kierdorf, K., & Fritz, G. (2013). RAGE regulation and signaling in inflammation and beyond. Journal of Leukocyte Biology, 94(1), 55–68. https://doi.org/10.1189/JLB.1012519
- Kim, A., Lalonde, K., Truesdell, A., Welter, P. G., Brocardo, P. S., Rosenstock, T. R., & Gilmohapel, J. (2021). New avenues for the treatment of huntington's disease. *International Journal of Molecular Sciences*, 22(16), 1–50. https://doi.org/10.3390/ijms22168363
- Kim, H. K., Fuchs, G., Wang, S., Wei, W., Zhang, Y., Park, H., Roy-Chaudhuri, B., Li, P., Xu, J., Chu, K., Zhang, F., Chua, M. S., So, S., Zhang, Q. C., Sarnow, P., & Kay, M. A. (2017). A transfer-RNA-derived small RNA regulates ribosome biogenesis. *Nature*, *552*(7683), 57–62. https://doi.org/10.1038/nature25005
- Kim, H. K., Xu, J., Chu, K., Park, H., Jang, H., Li, P., Valdmanis, P. N., Zhang, Q. C., & Kay, M. A. (2019). A tRNA-derived small RNA regulates ribosomal protein S28 protein levels after translation initiation in humans and mice. *Cell Reports*, 29(12), 3816.

- https://doi.org/10.1016/J.CELREP.2019.11.062
- Kim, J., Inoue, K., Ishii, J., Vanti, W. B., Voronov, S. V., Murchison, E., Hannon, G., & Abeliovich, A. (2007). A microRNA feedback circuit in midbrain dopamine neurons. *Science*, *317*(5842), 1220. https://doi.org/10.1126/SCIENCE.1140481
- Kim, Y. A., Siddiqui, T., Blaze, J., Cosacak, M. I., Winters, T., Kumar, A., Tein, E., Sproul, A. A., Teich, A. F., Bartolini, F., Akbarian, S., Kizil, C., Hargus, G., & Santa-Maria, I. (2022). RNA methyltransferase NSun2 deficiency promotes neurodegeneration through epitranscriptomic regulation of tau phosphorylation. *Acta Neuropathologica*, 145(1), 29–48. https://doi.org/10.1007/S00401-022-02511-7
- Kimura, H., McGeer, P. L., Peng, F., & McGeer, E. G. (1980). Choline acetyltransferase-containing neurons in rodent brain demonstrated by immunohistochemistry. *Science*, 208(4447), 1057–1059. https://doi.org/10.1126/science.6990490
- Komara, M., Al-Shamsi, A. M., Ben-Salem, S., Ali, B. R., & Al-Gazali, L. (2015). A novel Single-Nucleotide Deletion (c.1020delA) in NSUN2 causes Intellectual Disability in an Emirati child. *Journal of Molecular Neuroscience*, 57(3), 393–399. https://doi.org/10.1007/S12031-015-0592-8/TABLES/2
- Konieczny, P., Stepniak-Konieczna, E., & Sobczak, K. (2018). MBNL expression in autoregulatory feedback loops. *RNA Biology*, *15*(1), 1. https://doi.org/10.1080/15476286.2017.1384119
- Kordasiewicz, H. B., Stanek, L. M., Wancewicz, E. V., Mazur, C., McAlonis, M. M., Pytel, K. A., Artates, J. W., Weiss, A., Cheng, S. H., Shihabuddin, L. S., Hung, G., Bennett, C. F., & Cleveland, D. W. (2012). Sustained Therapeutic Reversal of Huntington's Disease by Transient Repression of Huntingtin Synthesis. *Neuron*, *74*(6), 1031–1044. https://doi.org/10.1016/j.neuron.2012.05.009
- Kozlowski, P., de Mezer, M., & Krzyzosiak, W. J. (2010). Trinucleotide repeats in human genome and exome. *Nucleic Acids Research*, *38*(12), 4027. https://doi.org/10.1093/NAR/GKQ127
- Kremer, B., Goldberg, P., Andrew, S. E., Theilmann, J., Telenius, H., Zeisler, J., Squitieri, F., Lin, B., Bassett, A., Almqvist, E., Bird, T. D., & Hayden, M. R. (1994). A worldwide study of the Huntington's disease mutation. The sensitivity and specificity of measuring CAG repeats. *The New England Journal of Medicine*, 330(20), 1401–1406. https://doi.org/10.1056/NEJM199405193302001
- Krishna, S., Raghavan, S., DasGupta, R., & Palakodeti, D. (2021). tRNA-derived fragments (tRFs): establishing their turf in post-transcriptional gene regulation. *Cellular and Molecular Life Sciences*, 78(6), 2607–2619. https://doi.org/10.1007/s00018-020-03720-7
- Krol, J., Fiszer, A., Mykowska, A., Sobczak, K., de Mezer, M., & Krzyzosiak, W. J. (2007). Ribonuclease Dicer cleaves triplet repeat hairpins into shorter repeats that silence specific targets. *Molecular Cell*, 25(4), 575–586. https://doi.org/10.1016/j.molcel.2007.01.031
- Krzyzosiak, W. J., Sobczak, K., Wojciechowska, M., Fiszer, A., Mykowska, A., & Kozlowski, P.

- (2012). Triplet repeat RNA structure and its role as pathogenic agent and therapeutic target. *Nucleic Acids Research*, 40(1), 11. https://doi.org/10.1093/NAR/GKR729
- Kumar, A., Vaish, M., & Ratan, R. R. (2014). Transcriptional dysregulation in Huntington's disease: a failure of adaptive transcriptional homeostasis. *Drug Discovery Today*, 19(7), 956–962. https://doi.org/10.1016/j.drudis.2014.03.016
- Labadorf, A., Hoss, A. G., Lagomarsino, V., Latourelle, J. C., Hadzi, T. C., Bregu, J., MacDonald, M. E., Gusella, J. F., Chen, J. F., Akbarian, S., Weng, Z., & Myers, R. H. (2015). RNA sequence analysis of human Huntington Disease brain reveals an extensive increase in inflammatory and developmental gene expression. *PLOS ONE*, *10*(12), e0143563. https://doi.org/10.1371/JOURNAL.PONE.0143563
- Labbadia, J., & Morimoto, R. I. (2013). Huntington's disease: underlying molecular mechanisms and emerging concepts. *Trends in Biochemical Sciences*, *38*(8), 378–385. https://doi.org/10.1016/j.tibs.2013.05.003
- Langfelder, P., Cantle, J. P., Chatzopoulou, D., Wang, N., Gao, F., Al-Ramahi, I., Lu, X. H., Ramos, E. M., El-Zein, K., Zhao, Y., Deverasetty, S., Tebbe, A., Schaab, C., Lavery, D. J., Howland, D., Kwak, S., Botas, J., Aaronson, J. S., Rosinski, J., ... Yang, X. W. (2016). Integrated genomics and proteomics define huntingtin CAG length—dependent networks in mice. *Nature Neuroscience*, *19*(4), 623–633. https://doi.org/10.1038/NN.4256
- Langfelder, P., Gao, F., Wang, N., Howland, D., Kwak, S., Vogt, T. F., Aaronson, J. S., Rosinski, J., Coppola, G., Horvath, S., & Yang, X. W. (2018). MicroRNA signatures of endogenous Huntingtin CAG repeat expansion in mice. *PloS One*, *13*(1). https://doi.org/10.1371/JOURNAL.PONE.0190550
- Lawlor, K. T., O'Keefe, L. V., Samaraweera, S. E., van Eyk, C. L., McLeod, C. J., Maloney, C. A., Dang, T. H. Y., Suter, C. M., & Richards, R. I. (2011). Double-stranded RNA is pathogenic in Drosophila models of expanded repeat neurodegenerative diseases. *Human Molecular Genetics*, 20(19), 3757–3768. https://doi.org/10.1093/HMG/DDR292
- Le Gras, S., Keime, C., Anthony, A., Lotz, C., De Longprez, L., Brouillet, E., Cassel, J. C., Boutillier, A. L., & Merienne, K. (2017). Altered enhancer transcription underlies Huntington's disease striatal transcriptional signature. *Scientific Reports*, 7(1), 1–11. https://doi.org/10.1038/srep42875
- Lee, E., Hwang, I., Park, S., Hong, S., Hwang, B., Cho, Y., Son, J., & Yu, J. W. (2018). MPTP-driven NLRP3 inflammasome activation in microglia plays a central role in dopaminergic neurodegeneration. *Cell Death & Differentiation*, *26*(2), 213–228. https://doi.org/10.1038/s41418-018-0124-5
- Lee, H., Fenster, R. J., Pineda, S. S., Gibbs, W. S., Mohammadi, S., Davila-Velderrain, J., Garcia, F. J., Therrien, M., Novis, H. S., Gao, F., Wilkinson, H., Vogt, T., Kellis, M., LaVoie, M. J., & Heiman, M. (2020). Cell Type-Specific Transcriptomics Reveals that Mutant Huntingtin Leads to Mitochondrial RNA Release and Neuronal Innate Immune Activation.

 Neuron, 107(5), 891-908.e8. https://doi.org/10.1016/j.neuron.2020.06.021
- Lee, R., Feinbaum, R., & Ambros, V. (1993). The C. elegans heterochronic gene lin-4 encodes

- small RNAs with antisense complementarity to lin-14. Cell, 116(116), 843–854.
- Lee, S. T., Chu, K., Im, W. S., Yoon, H. J., Im, J. Y., Park, J. E., Park, K. H., Jung, K. H., Lee, S. K., Kim, M., & Roh, J. K. (2011). Altered microRNA regulation in Huntington's disease models. *Experimental Neurology*, 227(1), 172–179. https://doi.org/10.1016/J.EXPNEUROL.2010.10.012
- Lee, W. C. M., Yoshihara, M., & Littleton, J. T. (2004). Cytoplasmic aggregates trap polyglutamine-containing proteins and block axonal transport in a Drosophila model of Huntington's disease. *Proceedings of the National Academy of Sciences of the United States of America*, 101(9), 3224–3229. https://doi.org/10.1073/PNAS.0400243101
- Lehmann, S. M., Krüger, C., Park, B., Derkow, K., Rosenberger, K., Baumgart, J., Trimbuch, T., Eom, G., Hinz, M., Kaul, D., Habbel, P., Kälin, R., Franzoni, E., Rybak, A., Nguyen, D., Veh, R., Ninnemann, O., Peters, O., Nitsch, R., ... Lehnardt, S. (2012). An unconventional role for miRNA: let-7 activates Toll-like receptor 7 and causes neurodegeneration. *Nature Neuroscience*, *15*(6), 827–835. https://doi.org/10.1038/NN.3113
- Lence, T., Akhtar, J., Bayer, M., Schmid, K., Spindler, L., Ho, C. H., Kreim, N., Andrade-Navarro, M. A., Poeck, B., Helm, M., & Roignant, J. Y. (2016). m6A modulates neuronal functions and sex determination in Drosophila. *Nature*, *540*(7632), 242–247. https://doi.org/10.1038/NATURE20568
- Letiembre, M., Liu, Y., Walter, S., Hao, W., Pfander, T., Wrede, A., Schulz-Schaeffer, W., & Fassbender, K. (2009). Screening of innate immune receptors in neurodegenerative diseases: A similar pattern. *Neurobiology of Aging*, *30*, 759–768. https://doi.org/10.1016/j.neurobiologing.2007.08.018
- Li, G., Manning, A. C., Bagi, A., Yang, X., Gokulnath, P., Spanos, M., Howard, J., Chan, P. P., Sweeney, T., Kitchen, R., Li, H., Laurent, B. D., Aranki, S. F., Kontaridis, M. I., Laurent, L. C., Van Keuren-Jensen, K., Muehlschlegel, J., Lowe, T. M., & Das, S. (2022). Distinct stress-dependent signatures of cellular and extracellular tRNA-derived small RNAs. *Advanced Science*, e2200829. https://doi.org/10.1002/ADVS.202200829
- Li, L. B., Yu, Z., Teng, X., & Bonini, N. M. (2008). RNA toxicity is a component of ataxin-3 degeneration in Drosophila. *Nature*, *453*(7198), 1107–1111. https://doi.org/10.1038/NATURE06909
- Li, M., Kao, E., Malone, D., Gao, X., Wang, J. Y. J., & David, M. (2018). DNA damage-induced cell death relies on SLFN11-dependent cleavage of distinct type II tRNAs. *Nature Structural & Molecular Biology*, 25(11), 1047–1058. https://doi.org/10.1038/S41594-018-0142-5
- Li, S., & Hu, G. F. (2012). Emerging role of angiogenin in stress response and cell survival under adverse conditions. *Journal of Cellular Physiology*, 227(7), 2822. https://doi.org/10.1002/JCP.23051
- Li, S., Xu, Z., & Sheng, J. (2018). tRNA-derived small RNA: a novel regulatory small non-coding RNA. In *Genes* (Vol. 9, Issue 5). MDPI AG. https://doi.org/10.3390/genes9050246

- Li, Y., Luo, J., Zhou, H., Liao, J. Y., Ma, L. M., Chen, Y. Q., & Qu, L. H. (2008). Stress-induced tRNA-derived RNAs: a novel class of small RNAs in the primitive eukaryote Giardia lamblia. *Nucleic Acids Research*, *36*(19), 6048. https://doi.org/10.1093/NAR/GKN596
- Lin, B., Rommens, J. M., Graham, R. K., Kalchman, M., Macdonald, H., Nasir, J., Delaney, A., Goldberg, Y. P., & Hayden, M. R. (1993). Differential 3' polyadenylation of the Huntington disease gene results in two mRNA species with variable tissue expression.

 Human Molecular Genetics, 2(10), 1541–1545.
 https://doi.org/10.1093/HMG/2.10.1541
- Lin, L., Park, J. W., Ramachandran, S., Zhang, Y., Tseng, Y. T., Shen, S., Waldvogel, H. J., Curtis, M. A., Richard, R. L., Troncoso, J. C., Pletnikova, O., Ross, C. A., Davidson, B. L., & Xing, Y. (2016). Transcriptome sequencing reveals aberrant alternative splicing in Huntington's disease. *Human Molecular Genetics*, 25(16), 3454. https://doi.org/10.1093/HMG/DDW187
- Lintas, C., Sacco, R., & Persico, A. M. (2012). Genome-wide expression studies in Autism spectrum disorder, Rett syndrome, and Down syndrome. *Neurobiology of Disease*, *45*, 57–68. https://doi.org/10.1016/j.nbd.2010.11.010
- Liu, B., Cao, J., Wang, X., Guo, C., Liu, Y., & Wang, T. (2021). Deciphering the tRNA-derived small RNAs: origin, development, and future. *Cell Death & Disease*, 13(1), 1–13. https://doi.org/10.1038/s41419-021-04472-3
- Liu, G. Q., & Gack, M. U. (2020). Distinct and orchestrated functions of RNA sensors in innate immunity. *Immunity*, *53*(1), 26. https://doi.org/10.1016/J.IMMUNI.2020.03.017
- Liu, T., Xu, Z. Z., Park, C. K., Berta, T., & Ji, R. R. (2010). Toll-like Receptor-7 mediates Pruritus. Nature Neuroscience, 13(12), 1460. https://doi.org/10.1038/NN.2683
- Livak, K. J., & Schmittgen, T. D. (2001). Analysis of relative gene expression data using real-time quantitative PCR and the 2-ΔΔCT method. *Methods*, *25*(4), 402–408. https://doi.org/10.1006/meth.2001.1262
- Lloret, A., Dragileva, E., Teed, A., Espinola, J., Fossale, E., Gillis, T., Lopez, E., Myers, R. H., MacDonald, M. E., & Wheeler, V. C. (2006). Genetic background modifies nuclear mutant huntingtin accumulation and HD CAG repeat instability in Huntington's disease knock-in mice. *Human Molecular Genetics*, 15(12), 2015–2024. https://doi.org/10.1093/hmg/ddl125
- Long, T., Li, J., Li, H., Zhou, M., Zhou, X. L., Liu, R. J., & Wang, E. D. (2016). Sequence-specific and Shape-selective RNA Recognition by the Human RNA 5-Methylcytosine Methyltransferase NSun6. *The Journal of Biological Chemistry*, *291*(46), 24293–24303. https://doi.org/10.1074/JBC.M116.742569
- Love, M. I., Huber, W., & Anders, S. (2014). Moderated estimation of fold change and dispersion for RNA-seq data with DESeq2. *Genome Biology*, *15*(12), 1–21. https://doi.org/10.1186/s13059-014-0550-8
- Luthi-Carter, R., Strand, A., Peters, N. L., Solano, S. M., Hollingsworth, Z. R., Menon, A. S., Frey, A. S., Spektor, B. S., Penney, E. B., Schilling, G., Ross, C. A., Borchelt, D. R., Tapscott, S. J., Young, A. B., Cha, J. H. J., & Olson, J. M. (2000). Decreased expression

- of striatal signaling genes in a mouse model of Huntington's disease. *Human Molecular Genetics*, *9*(9), 1259–1271. https://doi.org/10.1093/HMG/9.9.1259
- Lyons, S. M., Fay, M. M., & Ivanov, P. (2018). The role of RNA modifications in the regulation of tRNA cleavage. *FEBS Letters*, *592*(17), 2828–2844. https://doi.org/10.1002/1873-3468.13205
- Lyons, S. M., Gudanis, D., Coyne, S. M., Gdaniec, Z., & Ivanov, P. (2017). Identification of functional tetramolecular RNA G-quadruplexes derived from transfer RNAs. *Nature Communications*, 8(1). https://doi.org/10.1038/s41467-017-01278-w
- Magee, R. G., Telonis, A. G., Loher, P., Londin, E., & Rigoutsos, I. (2018). Profiles of miRNA isoforms and tRNA fragments in prostate cancer. *Scientific Reports*, 8(1), 5314. https://doi.org/10.1038/S41598-018-22488-2
- Magee, R., Londin, E., & Rigoutsos, I. (2019). TRNA-derived fragments as sex-dependent circulating candidate biomarkers for Parkinson's disease. *Parkinsonism and Related Disorders*, 65(December 2018), 203–209. https://doi.org/10.1016/j.parkreldis.2019.05.035
- Magee, R., & Rigoutsos, I. (2020). On the expanding roles of tRNA fragments in modulating cell behavior. *Nucleic Acids Research*, 48(17), 9433–9448. https://doi.org/10.1093/nar/gkaa657
- Malik, I., Kelley, C. P., Wang, E. T., & Todd, P. K. (2021). Molecular mechanisms underlying nucleotide repeat expansion disorders. *Nature Reviews Molecular Cell Biology*, 22(9), 589–607. https://doi.org/10.1038/S41580-021-00382-6
- Mangiarini, L., Sathasivam, K., Seller, M., Cozens, B., Harper, A., Hetherington, C., Lawton, M., Trottier, Y., Lehrach, H., Davies, S. W., & Bates, G. P. (1996). Exon I of the HD gene with an expanded CAG repeat is sufficient to cause a progressive neurological phenotype in transgenic mice. *Cell*, *87*(3), 493–506. https://doi.org/10.1016/S0092-8674(00)81369-0
- Marsh, J. L., Pallos, J., & Thompson, L. M. (2003). Fly models of Huntington's disease. *Human Molecular Genetics*, *12*(suppl_2), R187–R193. https://doi.org/10.1093/HMG/DDG271
- Martí, E. (2016). RNA toxicity induced by expanded CAG repeats in Huntington's disease. *Brain Pathology*, 26(6), 779–786. https://doi.org/10.1111/bpa.12427
- Martí, E., Pantano, L., Bañez-Coronel, M., Llorens, F., Miñones-Moyano, E., Porta, S., Sumoy, L., Ferrer, I., & Estivill, X. (2010). A myriad of miRNA variants in control and Huntington's disease brain regions detected by massively parallel sequencing. *Nucleic Acids Research*, 38(20), 7219–7235. https://doi.org/10.1093/NAR/GKQ575
- Martin, I., Kim, J. W., Lee, B. D., Kang, H. C., Xu, J. C., Jia, H., Stankowski, J., Kim, M. S., Zhong, J., Kumar, M., Andrabi, S. A., Xiong, Y., Dickson, D. W., Wszolek, Z. K., Pandey, A., Dawson, T. M., & Dawson, V. L. (2014). Ribosomal protein s15 phosphorylation mediates LRRK2 neurodegeneration in Parkinson's disease. *Cell*, 157(2), 472. https://doi.org/10.1016/J.CELL.2014.01.064
- Martin, M. (2011). Cutadapt removes adapter sequences from high-throughput sequencing

- reads. EMBnet. Journal, 17(1), 10-12. https://doi.org/10.14806/EJ.17.1.200
- Martinez, F. J., Lee, J. H., Lee, J. E., Blanco, S., Nickerson, E., Gabrie, S., Frye, M., Al-Gazali, L., & Gleeson, J. G. (2012). Whole Exome Sequencing identifies a splicing mutation in NSUN2 as a cause of a Dubowitz-like syndrome. *Journal of Medical Genetics*, *49*(6), 380. https://doi.org/10.1136/JMEDGENET-2011-100686
- Masuda, A., Andersen, H. S., Doktor, T. K., Okamoto, T., Ito, M., Andresen, B. S., & Ohno, K. (2012). CUGBP1 and MBNL1 preferentially bind to 3'UTRs and facilitate mRNA decay. *Scientific Reports*, 2(1), 1–10. https://doi.org/10.1038/srep00209
- McColgan, P., & Tabrizi, S. J. (2018). Huntington's disease: a clinical review. *European Journal of Neurology*, 25(1), 24–34. https://doi.org/10.1111/ene.13413
- Menalled, L. B. (2005). Knock-in mouse models of Huntington's disease. *NeuroRx*, 2(3), 465–470. https://doi.org/10.1602/NEURORX.2.3.465/METRICS
- Menalled, L. B., Kudwa, A. E., Miller, S., Fitzpatrick, J., Watson-Johnson, J., Keating, N., Ruiz, M., Mushlin, R., Alosio, W., McConnell, K., Connor, D., Murphy, C., Oakeshott, S., Kwan, M., Beltran, J., Ghavami, A., Brunner, D., Park, L. C., Ramboz, S., & Howland, D. (2012). Comprehensive behavioral and molecular characterization of a new knock-in mouse model of Huntington's Disease: zQ175. *PLOS ONE*, 7(12), e49838. https://doi.org/10.1371/JOURNAL.PONE.0049838
- Mercer, T. R., Dinger, M. E., & Mattick, J. S. (2009). Long non-coding RNAs: insights into functions. *Nature Reviews Genetics*, 10(3), 155–159. https://doi.org/10.1038/NRG2521
- Merienne, N., Meunier, C., Schneider, A., Seguin, J., Nair, S. S., Rocher, A. B., Le Gras, S., Keime, C., Faull, R., Pellerin, L., Chatton, J. Y., Neri, C., Merienne, K., & Déglon, N. (2019). Cell-Type-Specific Gene Expression Profiling in Adult Mouse Brain Reveals Normal and Disease-State Signatures. *Cell Reports*, 26(9), 2477-2493.e9. https://doi.org/10.1016/j.celrep.2019.02.003
- Michlewski, G., & Krzyzosiak, W. J. (2004). Molecular architecture of CAG repeats in human disease related transcripts. *Journal of Molecular Biology*, *340*(4), 665–679. https://doi.org/10.1016/J.JMB.2004.05.021
- Miller, J. W., Urbinati, C. R., Teng-Umnuay, P., Stenberg, M. G., Byrne, B. J., Thornton, C. A., & Swanson, M. S. (2000). Recruitment of human muscleblind proteins to (CUG)n expansions associated with myotonic dystrophy. *The EMBO Journal*, 19(17), 4439–4448. https://doi.org/10.1093/EMBOJ/19.17.4439
- Monteys, A. M., Ebanks, S. A., Keiser, M. S., & Davidson, B. L. (2017). CRISPR/Cas9 editing of the Mutant Huntingtin allele in vitro and in vivo. *Molecular Therapy*, 25(1), 12–23. https://doi.org/10.1016/J.YMTHE.2016.11.010
- Motorin, Y., & Helm, M. (2010). tRNA stabilization by modified nucleotides. *Biochemistry*, 49(24), 4934–4944. https://doi.org/10.1021/bi100408z
- Motorin, Y., Lyko, F., & Helm, M. (2010). 5-methylcytosine in RNA: detection, enzymatic formation and biological functions. *Nucleic Acids Research*, *38*(5), 1415–1430.

- https://doi.org/10.1093/NAR/GKP1117
- Müller, M., Legrand, C., Tuorto, F., Kelly, V. P., Atlasi, Y., Lyko, F., & Ehrenhofer-Murray, A. E. (2019). Queuine links translational control in eukaryotes to a micronutrient from bacteria. *Nucleic Acids Research*, *47*(7), 3711. https://doi.org/10.1093/NAR/GKZ063
- Murmann, A. E., Gao, Q. Q., Putzbach, W. E., Patel, M., Bartom, E. T., Law, C. Y., Bridgeman, B., Chen, S., McMahon, K. M., Thaxton, C. S., & Peter, M. E. (2018). Small interfering RNAs based on huntingtin trinucleotide repeats are highly toxic to cancer cells. *EMBO Reports*, 19(3), e45336. https://doi.org/10.15252/EMBR.201745336
- Mykowska, A., Sobczak, K., Wojciechowska, M., Kozlowski, P., & Krzyzosiak, W. J. (2011). CAG repeats mimic CUG repeats in the misregulation of alternative splicing. *Nucleic Acids Research*, *39*(20), 8938. https://doi.org/10.1093/NAR/GKR608
- Nabariya, D. K., Heinz, A., Derksen, S., & Krauß, S. (2022). Intracellular and intercellular transport of RNA organelles in CXG repeat disorders: the strength of weak ties. *Frontiers in Molecular Biosciences*, *9*. https://doi.org/10.3389/FMOLB.2022.1000932
- Nakanishi, A., Kaneko, N., Takeda, H., Sawasaki, T., Morikawa, S., Zhou, W., Kurata, M., Yamamoto, T., Akbar, S. M. F., Zako, T., & Masumoto, J. (2018). Amyloid β directly interacts with NLRP3 to initiate inflammasome activation: identification of an intrinsic NLRP3 ligand in a cell-free system. *Inflammation and Regeneration*, *38*(1). https://doi.org/10.1186/S41232-018-0085-6
- Nalavade, R., Griesche, N., Ryan, D. P., Hildebrand, S., & Krauß, S. (2013). Mechanisms of RNA-induced toxicity in CAG repeat disorders. *Cell Death & Disease*, *4*(8), e752–e752. https://doi.org/10.1038/cddis.2013.276
- Napierala, M., & Krzyzosiak, W. J. (1997). CUG repeats present in myotonin kinase RNA form metastable "slippery" hairpins. *The Journal of Biological Chemistry*, *272*(49), 31079–31085. https://doi.org/10.1074/JBC.272.49.31079
- Napierala, M., Michalowski, D., de Mezer, M., & Krzyzosiak, W. J. (2005). Facile FMR1 mRNA structure regulation by interruptions in CGG repeats. *Nucleic Acids Research*, *33*(2), 451. https://doi.org/10.1093/NAR/GKI186
- Nasir, J., Lin, B., Bucan, M., Koizumi, T., Nadeau, J. H., & Hayden, M. R. (1994). The murine homologues of the Huntington disease gene (Hdh) and the alpha-adducin gene (Add1) map to mouse chromosome 5 within a region of conserved synteny with human chromosome 4p16.3. *Genomics*, 22(1), 198–201. https://doi.org/10.1006/GENO.1994.1361
- Naver, B., Stub, C., Møller, M., Fenger, K., Hansen, A. K., Hasholt, L., & Sørensen, S. A. (2003). Molecular and behavioral analysis of the R6/1 Huntington's disease transgenic mouse. *Neuroscience*, 122(4), 1049–1057. https://doi.org/10.1016/j.neuroscience.2003.08.053
- Neueder, A., Dumas, A. A., Benjamin, A. C., & Bates, G. P. (2018). Regulatory mechanisms of incomplete huntingtin mRNA splicing. *Nature Communications*, *9*(1). https://doi.org/10.1038/S41467-018-06281-3

- Neueder, A., Landles, C., Ghosh, R., Howland, D., Myers, R. H., Faull, R. L. M., Tabrizi, S. J., & Bates, G. P. (2017). The pathogenic exon 1 HTT protein is produced by incomplete splicing in Huntington's disease patients. *Scientific Reports*, 7(1). https://doi.org/10.1038/S41598-017-01510-Z
- Nithianantharajah, J., Barkus, C., Murphy, M., & Hannan, A. J. (2008). Gene–environment interactions modulating cognitive function and molecular correlates of synaptic plasticity in Huntington's disease transgenic mice. *Neurobiology of Disease*, *29*(3), 490–504. https://doi.org/10.1016/J.NBD.2007.11.006
- Norden, D. M., Trojanowski, P. J., Villanueva, E., Navarro, E., & Godbout, J. P. (2016). Sequential activation of microglia and astrocyte cytokine expression precedes increased iba-1 or GFAP immunoreactivity following systemic immune challenge. *Glia*, 64(2), 300–316. https://doi.org/10.1002/GLIA.22930
- Nøstvik, M., Kateta, S. M., Schönewolf-Greulich, B., Afenjar, A., Barth, M., Boschann, F., Doummar, D., Haack, T. B., Keren, B., Livshits, L. A., Mei, D., Park, J., Pisano, T., Prouteau, C., Umair, M., Waqas, A., Ziegler, A., Guerrini, R., Møller, R. S., & Tümer, Z. (2021). Clinical and molecular delineation of PUS3-associated neurodevelopmental disorders. *Clinical Genetics*, 100(5), 628–633. https://doi.org/10.1111/CGE.14051
- Novak, M. J. U., & Tabrizi, S. J. (2010). Huntington's disease. *BMJ*, *340*(7762), 34–40. https://doi.org/10.1136/bmj.c3109
- Novati, A., Hentrich, T., Wassouf, Z., Weber, J. J., Yu-Taeger, L., Déglon, N., Nguyen, H. P., & Schulze-Hentrich, J. M. (2018). Environment-dependent striatal gene expression in the BACHD rat model for Huntington disease. *Scientific Reports*, 8(1), 1–15. https://doi.org/10.1038/s41598-018-24243-z
- Ochoa, E., Ramirez, P., Gonzalez, E., De Mange, J., Ray, W. J., Bieniek, K. F., & Frost, B. (2023). Pathogenic tau-induced transposable element-derived dsRNA drives neuroinflammation. *Science Advances*, *9*(1), eabq5423. https://doi.org/10.1126/SCIADV.ABQ5423
- Olmo, I. G., Olmo, R. P., Gonçalves, A. N. A., Pires, R. G. W., Marques, J. T., & Ribeiro, F. M. (2021). High-throughput sequencing of BACHD mice reveals upregulation of neuroprotective miRNAs at the pre-symptomatic stage of Huntington's Disease. *ASN NEURO*, 13. https://doi.org/10.1177/17590914211009857
- Osterweil, E. K., Krueger, D. D., Reinhold, K., & Bear, M. F. (2010). Hypersensitivity to mGluR5 and ERK1/2 leads to excessive protein synthesis in the hippocampus of a mouse model of Fragile X Syndrome. *The Journal of Neuroscience*, *30*(46), 15616. https://doi.org/10.1523/JNEUROSCI.3888-10.2010
- Packer, A. N., Xing, Y., Harper, S. Q., Jones, L., & Davidson, B. L. (2008). The bifunctional microRNA miR-9/miR-9* regulates REST and CoREST and is downregulated in Huntington's disease. *The Journal of Neuroscience*, *28*(53), 14341–14346. https://doi.org/10.1523/JNEUROSCI.2390-08.2008
- Padhi, A. K., Jayaram, B., & Gomes, J. (2013). Prediction of functional loss of human Angiogenin mutants associated with ALS by molecular dynamics simulations. *Scientific Reports*, *3*(1), 1–9. https://doi.org/10.1038/srep01225

- Pantano, L., Estivill, X., & Martí, E. (2011). A non-biased framework for the annotation and classification of the non-miRNA small RNA transcriptome. *Bioinformatics*, *27*(22), 3202–3203. https://doi.org/10.1093/BIOINFORMATICS/BTR527
- Pantano, L., Friedländer, M. R., Escaramís, G., Lizano, E., Pallarès-Albanell, J., Ferrer, I., Estivill, X., & Martí, E. (2016). Specific small-RNA signatures in the amygdala at premotor and motor stages of Parkinson's disease revealed by deep sequencing analysis. *Bioinformatics*, 32(5), 673–681. https://doi.org/10.1093/BIOINFORMATICS/BTV632
- Paramasivam, A., Meena, A. K., Venkatapathi, C., Pitceathly, R. D. S., & Thangaraj, K. (2020). Novel biallelic NSUN3 variants cause early-onset mitochondrial Encephalomyopathy and Seizures. *Journal of Molecular Neuroscience: MN, 70*(12), 1962–1965. https://doi.org/10.1007/S12031-020-01595-8
- Park, J. W., Parisky, K., Celotto, A. M., Reenan, R. A., & Graveley, B. R. (2004). Identification of alternative splicing regulators by RNA interference in Drosophila. *Proceedings of the National Academy of Sciences of the United States of America*, 101(45), 15974–15979. https://doi.org/10.1073/PNAS.0407004101/SUPPL_FILE/07004TABLE2.PDF
- Park, S. H., Kukushkin, Y., Gupta, R., Chen, T., Konagai, A., Hipp, M. S., Hayer-Hartl, M., & Hartl, F. U. (2013). PolyQ proteins interfere with nuclear degradation of cytosolic proteins by sequestering the Sis1p chaperone. *Cell*, 154(1), 134–145. https://doi.org/10.1016/J.CELL.2013.06.003
- Parlato, R., Kreiner, G., Erdmann, G., Rieker, C., Stotz, S., Savenkova, E., Berger, S., Grummt, I., & Schútz, G. (2008). Activation of an endogenous suicide response after perturbation of rRNA synthesis leads to neurodegeneration in mice. *Journal of Neuroscience*, 28(48), 12759–12764. https://doi.org/10.1523/JNEUROSCI.2439-08.2008
- Patro, R., Mount, S. M., & Kingsford, C. (2014). Sailfish enables alignment-free isoform quantification from RNA-seq reads using lightweight algorithms. *Nature Biotechnology*, 32(5), 462–464. https://doi.org/10.1038/nbt.2862
- Pattison, L. R., Kotter, M. R., Fraga, D., & Bonelli, R. M. (2006). Apoptotic cascades as possible targets for inhibiting cell death in Huntington's disease. *Journal of Neurology*, 253(9), 1137–1142. https://doi.org/10.1007/S00415-006-0198-8/FIGURES/1
- Paulsen, J. S., Nehl, C., Hoth, K. F., Kanz, J. E., Benjamin, M., Conybeare, R., McDowell, B., & Turner, B. (2005). Depression and stages of Huntington's disease. *Journal of Neuropsychiatry and Clinical Neurosciences*, 17(4), 496–502. https://doi.org/10.1176/JNP.17.4.496/ASSET/IMAGES/LARGE/RL0016T2.JPEG
- Paulsen, J. S., Ready, R. E., Hamilton, J. M., Mega, M. S., & Cummings, J. L. (2001). Neuropsychiatric aspects of Huntington's disease. *J Neurol Neurosurg Psychiatry*, 5(71), 310–314.
- Pavese, N., Gerhard, A., Tai, Y. F., Ho, A. K., Turkheimer, F., Barker, R. A., Brooks, D. J., & Piccini, P. (2006). Microglial activation correlates with severity in Huntington disease: a clinical and PET study. *Neurology*, *66*(11), 1638–1643. https://doi.org/10.1212/01.WNL.0000222734.56412.17

- Pawar, K., Shigematsu, M., Sharbati, S., & Kirino, Y. (2020). Infection-induced 5'-half molecules of tRNAHisGUG activate Toll-like receptor 7. *PLoS Biology*, *18*(12 December), 1–28. https://doi.org/10.1371/journal.pbio.3000982
- Pereira, M., Francisco, S., Varanda, A. S., Santos, M., Santos, M. A. S., & Soares, A. R. (2018). Impact of tRNA Modifications and tRNA-Modifying Enzymes on Proteostasis and Human Disease. *International Journal of Molecular Sciences*, 19(12). https://doi.org/10.3390/IJMS19123738
- Pereira, M., Soares, A. R., Ribeiro, D. R., Pinheiro, M. M., Ferreira, M., & Kellner, S. (2021). m5U54 tRNA hypomodification by lack of TRMT2A drives the generation of tRNA-derived small RNAs. *International Journal of Molecular Sciences*, 22(6), 1–19. https://doi.org/10.3390/IJMS22062941
- Persson, H., Kvist, A., Vallon-Christersson, J., Medstrand, P., Borg, Å., & Rovira, C. (2009). The non-coding RNA of the multidrug resistance-linked vault particle encodes multiple regulatory small RNAs. *Nature Cell Biology*, *11*(10), 1268–1271. https://doi.org/10.1038/NCB1972
- Petry, S., Keraudren, R., Nateghi, B., Loiselle, A., Pircs, K., Jakobsson, J., Sephton, C., Langlois, M., Amour, I. S., & Hébert, S. S. (2022). Widespread alterations in microRNA biogenesis in human Huntington's disease putamen. *Acta Neuropathologica Communications*, 10(1), 1–11. https://doi.org/10.1186/s40478-022-01407-7
- Pietrzak, M., Rempala, G., Nelson, P. T., Zheng, J. J., & Hetman, M. (2011). Epigenetic silencing of nucleolar rRNA genes in Alzheimer's Disease. *PLoS ONE*, *6*(7). https://doi.org/10.1371/JOURNAL.PONE.0022585
- Pircs, K., Petri, R., Madsen, S., Brattås, P. L., Vuono, R., Ottosson, D. R., St-Amour, I., Hersbach, B. A., Matusiak-Brückner, M., Lundh, S. H., Petersén, Å., Déglon, N., Hébert, S. S., Parmar, M., Barker, R. A., & Jakobsson, J. (2018). Huntingtin aggregation impairs autophagy, leading to Argonaute-2 accumulation and global microRNA dysregulation. *Cell Reports*, 24(6), 1397–1406. https://doi.org/10.1016/J.CELREP.2018.07.017
- Pliatsika, V., Loher, P., Magee, R., Telonis, A. G., Londin, E., Shigematsu, M., Kirino, Y., & Rigoutsos, I. (2018). MINTbase v2.0: a comprehensive database for tRNA-derived fragments that includes nuclear and mitochondrial fragments from all The Cancer Genome Atlas projects. *Nucleic Acids Research*, 46(D1), D152–D159. https://doi.org/10.1093/NAR/GKX1075
- Pong, S. K., & Gullerova, M. (2018). Noncanonical functions of microRNA pathway enzymes Drosha, DGCR8, Dicer and Ago proteins. *FEBS Letters*, *592*(17), 2973–2986. https://doi.org/10.1002/1873-3468.13196
- Préhaud, C., Mégret, F., Lafage, M., & Lafon, M. (2005). Virus infection switches TLR-3-Positive human neurons to become strong producers of Beta Interferon. *Journal of Virology*, 79(20), 12893. https://doi.org/10.1128/JVI.79.20.12893-12904.2005
- Pringsheim, T., Wiltshire, K., Day, L., Dykeman, J., Steeves, T., & Jette, N. (2012). The incidence and prevalence of Huntington's disease: A systematic review and meta-analysis. *Movement Disorders*, *27*(9), 1083–1091. https://doi.org/10.1002/mds.25075

- Prinz, M., Garbe, F., Schmidt, H., Mildner, A., Gutcher, I., Wolter, K., Piesche, M., Schroers, R., Weiss, E., Kirschning, C. J., Rochford, C. D. P., Brück, W., & Becher, B. (2006). Innate immunity mediated by TLR9 modulates pathogenicity in an animal model of multiple sclerosis. *Journal of Clinical Investigation*, 116(2), 456. https://doi.org/10.1172/JCI26078
- Prud'homme, G. J., Glinka, Y., Lichner, Z., & Yousef, G. M. (2016). Neuropilin-1 is a receptor for extracellular miRNA and AGO2/miRNA complexes and mediates the internalization of miRNAs that modulate cell function. *Oncotarget*, 7(42), 68057. https://doi.org/10.18632/ONCOTARGET.10929
- Puigdellívol, M., Saavedra, A., & Pérez-Navarro, E. (2016). Cognitive dysfunction in Huntington's disease: mechanisms and therapeutic strategies beyond BDNF. *Brain Pathology*, 26(6), 752–771. https://doi.org/10.1111/BPA.12432
- Quan, Z., Zheng, D., & Qing, H. (2017). Regulatory roles of long non-coding rnas in the central nervous system and associated neurodegenerative diseases. *Frontiers in Cellular Neuroscience*, 11, 175. https://doi.org/10.3389/FNCEL.2017.00175/BIBTEX
- Qureshi, I. A., & Mehler, M. F. (2012). Emerging roles of non-coding RNAs in brain evolution, development, plasticity and disease. *Nature Reviews Neuroscience*, *13*(8), 528–541. https://doi.org/10.1038/NRN3234
- Raabe, C. A., Tang, T. H., Brosius, J., & Rozhdestvensky, T. S. (2014). Biases in small RNA deep sequencing data. *Nucleic Acids Research*, 42(3), 1414. https://doi.org/10.1093/NAR/GKT1021
- Raina, M., & Ibba, M. (2014). tRNAs as regulators of biological processes. *Frontiers in Genetics*, *5*(JUN), 171. https://doi.org/10.3389/FGENE.2014.00171/BIBTEX
- Rajman, M., & Schratt, G. (2017). MicroRNAs in neural development: from master regulators to fine-tuners. *Development*, *144*(13), 2310–2322. https://doi.org/10.1242/DEV.144337
- Ramos, J., Han, L., Li, Y., Hagelskamp, F., Kellner, S. M., Alkuraya, F. S., Phizicky, E. M., & Fu, D. (2019). Formation of tRNA wobble inosine in humans is disrupted by a millennia-old mutation causing Intellectual Disability. *Molecular and Cellular Biology*, *39*(19). https://doi.org/10.1128/MCB.00203-19
- Rau, F., Freyermuth, F., Fugier, C., Villemin, J. P., Fischer, M. C., Jost, B., Dembele, D., Gourdon, G., Nicole, A., Duboc, D., Wahbi, K., Day, J. W., Fujimura, H., Takahashi, M. P., Auboeuf, D., Dreumont, N., Furling, D., & Charlet-Berguerand, N. (2011). Misregulation of miR-1 processing is associated with heart defects in myotonic dystrophy. *Nature Structural & Molecular Biology*, 18(7), 840–845. https://doi.org/10.1038/NSMB.2067
- Rawlins, M. D., Wexler, N. S., Wexler, A. R., Tabrizi, S. J., Douglas, I., Evans, S. J. W., & Smeeth, L. (2016). The prevalence of Huntington's Disease. *Neuroepidemiology*, 46(2), 144–153. https://doi.org/10.1159/000443738
- Reddy, P. H., & Shirendeb, U. P. (2012). Mutant huntingtin, abnormal mitochondrial dynamics, defective axonal transport of mitochondria, and selective synaptic

- degeneration in Huntington's disease. *Biochimica et Biophysica Acta, 1822*(2), 101–110. https://doi.org/10.1016/J.BBADIS.2011.10.016
- Reddy, P. H., Williams, M., Charles, V., Garrett, L., Pike-Buchanan, L., Whetsell, W. O., Miller, G., & Tagle, D. A. (1998). Behavioural abnormalities and selective neuronal loss in HD transgenic mice expressing mutated full-length HD cDNA. *Nature Genetics*, 20(2), 198–202. https://doi.org/10.1038/2510
- Reiner, A., Albin, R. L., Anderson, K. D., D'Amato, C. J., Penney, J. B., & Young, A. B. (1988). Differential loss of striatal projection neurons in Huntington disease. *Proceedings of the National Academy of Sciences of the United States of America*, 85(15), 5733–5737. https://doi.org/10.1073/pnas.85.15.5733
- Reiner, A., Dragatsis, I., & Dietrich, P. (2011). Genetics and neuropathology of Huntington's disease. *International Review of Neurobiology*, *98*, 325. https://doi.org/10.1016/B978-0-12-381328-2.00014-6
- Richfield, E. K., Maguire-Zeiss, K. A., Vonkeman, H. E., & Voorn, P. (1995). Preferential loss of preproenkephalin versus preprotachykinin neurons from the striatum of Huntington's disease patients. *Annals of Neurology*, *38*(6), 852–861. https://doi.org/10.1002/ANA.410380605
- Rieker, C., Engblom, D., Kreiner, G., Domanskyi, A., Schober, A., Stotz, S., Neumann, M., Yuan, X., Grummt, I., Schütz, G., & Parlato, R. (2011). Nucleolar disruption in dopaminergic neurons leads to oxidative damage and Parkinsonism through repression of Mammalian Target of Rapamycin Signaling. *The Journal of Neuroscience*, 31(2), 453. https://doi.org/10.1523/JNEUROSCI.0590-10.2011
- Rikani, A. A., Choudhry, Z., Choudhry, A. M., Rizvi, N., Ikram, H., Mobassarah, N. J., & Tulli, S. (2014). The mechanism of degeneration of striatal neuronal subtypes in Huntington disease. *Annals of Neurosciences*, 21(3), 112. https://doi.org/10.5214/ANS.0972.7531.210308
- Romo, L., Ashar-Patel, A., Pfister, E., & Aronin, N. (2017). Alterations in mRNA 3'UTR isoform abundance accompany gene expression changes in human Huntington's Disease brains. *Cell Reports*, *20*(13), 3057–3070. https://doi.org/10.1016/J.CELREP.2017.09.009
- Romo, L., Mohn, E. S., & Aronin, N. (2018). A fresh look at Huntingtin mRNA processing in Huntington's Disease. *Journal of Huntington's Disease*, 7(2), 101–108. https://doi.org/10.3233/JHD-180292
- Rosas, H. D., Koroshetz, W. J., Chen, Y. I., Skeuse, C., Vangel, M., Cudkowicz, M. E., Caplan, K., Marek, K., Seidman, L. J., Makris, N., Jenkins, B. G., & Goldstein, J. M. (2003). Evidence for more widespread cerebral pathology in early HD: an MRI-based morphometric analysis. *Neurology*, 60(10), 1615–1620. https://doi.org/10.1212/01.WNL.0000065888.88988.6E
- Rosenblatt, A., Liang, K. Y., Zhou, H., Abbott, M. H., Gourley, L. M., Margolis, R. L., Brandt, J., & Ross, C. A. (2006). The association of CAG repeat length with clinical progression in Huntington disease. *Neurology*, *66*(7), 1016–1020. https://doi.org/10.1212/01.wnl.0000204230.16619.d9

- Ross, C. A., Aylward, E. H., Wild, E. J., Langbehn, D. R., Long, J. D., Warner, J. H., Scahill, R. I., Leavitt, B. R., Stout, J. C., Paulsen, J. S., Reilmann, R., Unschuld, P. G., Wexler, A., Margolis, R. L., & Tabrizi, S. J. (2014). Huntington disease: natural history, biomarkers and prospects for therapeutics. *Nature Reviews Neurology*, *10*(4), 204–216. https://doi.org/10.1038/NRNEUROL.2014.24
- Ross, C. A., & Tabrizi, S. J. (2011). Huntington's disease: from molecular pathogenesis to clinical treatment. *The Lancet Neurology*, *10*(1), 83–98. https://doi.org/10.1016/S1474-4422(10)70245-3
- Rozowsky, J., Kitchen, R. R., Park, J. J., Galeev, T. R., Diao, J., Warrell, J., Thistlethwaite, W., Subramanian, S. L., Milosavljevic, A., & Gerstein, M. (2019). exceRpt: a comprehensive analytic platform for extracellular RNA profiling. *Cell Systems*, 8(4), 352-357.e3. https://doi.org/10.1016/J.CELS.2019.03.004
- Rué, L., Bañez-Coronel, M., Creus-Muncunill, J., Giralt, A., Alcalá-Vida, R., Mentxaka, G., Kagerbauer, B., Zomeño-Abellán, M. T., Aranda, Z., Venturi, V., Pérez-Navarro, E., Estivill, X., & Martí, E. (2016). Targeting CAG repeat RNAs reduces Huntington's disease phenotype independently of huntingtin levels. *Journal of Clinical Investigation*. https://doi.org/10.1172/JCI83185
- Rué, L., López-Soop, G., Gelpi, E., Martínez-Vicente, M., Alberch, J., & Pérez-Navarro, E. (2013). Brain region- and age-dependent dysregulation of p62 and NBR1 in a mouse model of Huntington's disease. *Neurobiology of Disease*, 52, 219–228. https://doi.org/10.1016/J.NBD.2012.12.008
- Ruggero, K., Guffanti, A., Corradin, A., Sharma, V. K., De Bellis, G., Corti, G., Grassi, A., Zanovello, P., Bronte, V., Ciminale, V., & D'Agostino, D. M. (2014). Small noncoding RNAs in cells transformed by Human T-Cell Leukemia Virus Type 1: a role for a tRNA fragment as a primer for reverse transcriptase. *Journal of Virology*, 88(7), 3612–3622. https://doi.org/10.1128/JVI.02823-13/SUPPL_FILE/ZJV999098792SO1.PDF
- Saavedra, A., García-Martínez, J. M., Xifró, X., Giralt, A., Torres-Peraza, J. F., Canals, J. M., Díaz-Hernández, M., Lucas, J. J., Alberch, J., & Pérez-Navarro, E. (2010). PH domain leucine-rich repeat protein phosphatase 1 contributes to maintain the activation of the PI3K/Akt pro-survival pathway in Huntington's disease striatum. *Cell Death and Differentiation*, 17(2), 324–335. https://doi.org/10.1038/CDD.2009.127
- Saavedra, A., Giralt, A., Rué, L., Xifró, X., Xu, J., Ortega, Z., Lucas, J. J., Lombroso, P. J., Alberch, J., & Pérez-Navarro, E. (2011). Striatal-Enriched Protein Tyrosine Phosphatase expression and activity in Huntington's Disease: a STEP in the resistance to excitotoxicity. *The Journal of Neuroscience*, *31*(22), 8150. https://doi.org/10.1523/JNEUROSCI.3446-10.2011
- Saikia, M., Jobava, R., Parisien, M., Putnam, A., Krokowski, D., Gao, X.-H., Guan, B.-J., Yuan, Y., Jankowsky, E., Feng, Z., Hu, G., Pusztai-Carey, M., Gorla, M., Sepuri, N. B. V., Pan, T., & Hatzoglou, M. (2014). Angiogenin-cleaved tRNA halves interact with Cytochrome c, protecting cells from apoptosis during osmotic stress. *Molecular and Cellular Biology*, 34(13), 2450. https://doi.org/10.1128/MCB.00136-14
- Saikia, M., Krokowski, D., Guan, B. J., Ivanov, P., Parisien, M., Hu, G. F., Anderson, P., Pan,

- T., & Hatzoglou, M. (2012). Genome-wide identification and quantitative analysis of cleaved tRNA fragments induced by cellular stress. *Journal of Biological Chemistry*, 287(51), 42708–42725. https://doi.org/10.1074/jbc.M112.371799
- Sajini, A. A., Choudhury, N. R., Wagner, R. E., Bornelöv, S., Selmi, T., Spanos, C., Dietmann, S., Rappsilber, J., Michlewski, G., & Frye, M. (2019). Loss of 5-methylcytosine alters the biogenesis of vault-derived small RNAs to coordinate epidermal differentiation. *Nature Communications*, 10(1), 1–13. https://doi.org/10.1038/s41467-019-10020-7
- Saletore, Y., Meyer, K., Korlach, J., Vilfan, I. D., Jaffrey, S., & Mason, C. E. (2012). The birth of the Epitranscriptome: deciphering the function of RNA modifications. *Genome Biology*, *13*(10), 175. https://doi.org/10.1186/GB-2012-13-10-175/FIGURES/5
- Salta, E., & De Strooper, B. (2012). Non-coding RNAs with essential roles in neurodegenerative disorders. *The Lancet Neurology*, *11*(2), 189–200. https://doi.org/10.1016/S1474-4422(11)70286-1
- Santini, E., Huynh, T. N., MacAskill, A. F., Carter, A. G., Pierre, P., Ruggero, D., Kaphzan, H., & Klann, E. (2013). Exaggerated translation causes synaptic and behavioral aberrations associated with autism. *Nature*, *493*(7432), 411. https://doi.org/10.1038/NATURE11782
- Sapp, E., Ge, P., Aizawa, H., Bird, E., Penney, J., Young, A. B., Vonsattel, J. P., & Difiglia, M. (1995). Evidence for a preferential loss of enkephalin immunoreactivity in the external globus pallidus in low grade Huntington's disease using high resolution image analysis. *Neuroscience*, *64*(2), 397–404. https://doi.org/10.1016/0306-4522(94)00427-7
- Sapp, E., Kegel, K. B., Aronin, N., Hashikawa, T., Uchiyama, Y., Tohyama, K., Bhide, P. G., Vonsattel, J. P., & Difiglia, M. (2001). Early and progressive accumulation of reactive microglia in the Huntington Disease brain. *Journal of Neuropathology & Experimental Neurology*, 60(2), 161–172. https://doi.org/10.1093/JNEN/60.2.161
- Sarker, G., Sun, W., Rosenkranz, D., Pelczar, P., Opitz, L., Efthymiou, V., Wolfrum, C., & Peleg-Raibstein, D. (2019). Maternal overnutrition programs hedonic and metabolic phenotypes across generations through sperm tsRNAs. *Proceedings of the National Academy of Sciences of the United States of America*, 116(21), 10547–10556. https://doi.org/10.1073/PNAS.1820810116/SUPPL_FILE/PNAS.1820810116.SAPP.PD
- Sathasivam, K., Neueder, A., Gipson, T. A., Landles, C., Benjamin, A. C., Bondulich, M. K., Smith, D. L., Faull, R. L. M., Roos, R. A. C., Howland, D., Detloff, P. J., Housman, D. E., & Bates, G. P. (2013). Aberrant splicing of HTT generates the pathogenic exon 1 protein in Huntington disease. *Proceedings of the National Academy of Sciences of the United States of America*, 110(6), 2366–2370. https://doi.org/10.1073/PNAS.1221891110/-/DCSUPPLEMENTAL/PNAS.201221891SI.PDF
- Saudou, F., & Humbert, S. (2016). The biology of Huntingtin. *Neuron*, *89*(5), 910–926. https://doi.org/10.1016/J.NEURON.2016.02.003
- Savas, J. N., Ma, B., Deinhardt, K., Culver, B. P., Restituito, S., Wu, L., Belasco, J. G., Chao, M. V., & Tanese, N. (2010). A role for Huntington disease protein in dendritic RNA

- granules. *Journal of Biological Chemistry*, *285*(17), 13142–13153. https://doi.org/10.1074/jbc.M110.114561
- Savas, J. N., Makusky, A., Ottosen, S., Baillat, D., Then, F., Krainc, D., Shiekhattar, R., Markey, S. P., & Tanese, N. (2008). Huntington's disease protein contributes to RNA-mediated gene silencing through association with Argonaute and P bodies. *Proceedings of the National Academy of Sciences of the United States of America*, 105(31), 10820–10825. https://doi.org/10.1073/PNAS.0800658105
- Schaefer, A., O'Carroll, D., Chan, L. T., Hillman, D., Sugimori, M., Llinas, R., & Greengard, P. (2007). Cerebellar neurodegeneration in the absence of microRNAs. *The Journal of Experimental Medicine*, 204(7), 1553. https://doi.org/10.1084/JEM.20070823
- Schaefer, M., Pollex, T., Hanna, K., Tuorto, F., Meusburger, M., Helm, M., & Lyko, F. (2010). RNA methylation by Dnmt2 protects transfer RNAs against stress-induced cleavage. *Genes & Development*, *24*(15), 1590–1595. https://doi.org/10.1101/GAD.586710
- Schaffer, A. E., Eggens, V. R. C., Caglayan, A. O., Reuter, M. S., Scott, E., Coufal, N. G., Silhavy, J. L., Xue, Y., Kayserili, H., Yasuno, K., Rosti, R. O., Abdellateef, M., Caglar, C., Kasher, P. R., Cazemier, J. L., Weterman, M. A., Cantagrel, V., Cai, N., Zweier, C., ... Gleeson, J. G. (2014). CLP1 founder mutation links tRNA splicing and maturation to cerebellar development and neurodegeneration. *Cell*, *157*(3), 651–663. https://doi.org/10.1016/j.cell.2014.03.049
- Schiffer, N. W., Broadley, S. A., Hirschberger, T., Tavan, P., Kretzschmar, H. A., Giese, A., Haass, C., Hartl, F. U., & Schmid, B. (2007). Identification of anti-prion compounds as efficient inhibitors of polyglutamine protein aggregation in a zebrafish model. *The Journal of Biological Chemistry*, 282(12), 9195–9203. https://doi.org/10.1074/JBC.M607865200
- Schilling, G., Becher, M. W., Sharp, A. H., Jinnah, H. A., Duan, K., Kotzuk, J. A., Slunt, H. H., Ratovitski, T., Cooper, J. K., Jenkins, N. A., Copeland, N. G., Price, D. L., Ross, C. A., & Borchelt, D. R. (1999). Intranuclear inclusions and neuritic aggregates in transgenic mice expressing a mutant N-terminal fragment of huntingtin. *Human Molecular Genetics*, 8(3), 397–407. https://doi.org/10.1093/HMG/8.3.397
- Schilling, J., Broemer, M., Atanassov, I., Duernberger, Y., Vorberg, I., Dieterich, C., Dagane, A., Dittmar, G., Wanker, E., van Roon-Mom, W., Winter, J., & Krauß, S. (2019). Deregulated splicing is a major mechanism of RNA-induced toxicity in Huntington's Disease. *Journal of Molecular Biology*, 431(9), 1869–1877. https://doi.org/10.1016/J.JMB.2019.01.034
- Schimmel, P. (2017). The emerging complexity of the tRNA world: mammalian tRNAs beyond protein synthesis. *Nature Reviews Molecular Cell Biology*, *19*(1), 45–58. https://doi.org/10.1038/NRM.2017.77
- Schmieder, R., Lim, Y. W., & Edwards, R. (2012). Identification and removal of ribosomal RNA sequences from metatranscriptomes. *Bioinformatics*, *28*(3), 433–435. https://doi.org/10.1093/bioinformatics/btr669
- Sellier, C., Freyermuth, F., Tabet, R., Tran, T., He, F., Ruffenach, F., Alunni, V., Moine, H., Thibault, C., Page, A., Tassone, F., Willemsen, R., Disney, M. D., Hagerman, P. J., Todd,

- P. K., & Charlet-Berguerand, N. (2013). Sequestration of DROSHA and DGCR8 by expanded CGG RNA repeats alters microRNA processing in fragile X-associated tremor/ataxia syndrome. *Cell Reports*, *3*(3), 869–880. https://doi.org/10.1016/J.CELREP.2013.02.004
- Shaheen, R., Han, L., Faqeih, E., Ewida, N., Alobeid, E., Phizicky, E. M., & Alkuraya, F. S. (2016). A homozygous truncating mutation in PUS3 expands the role of tRNA modification in normal cognition. *Human Genetics*, 135(7), 707. https://doi.org/10.1007/S00439-016-1665-7
- Shao, Y., Sun, Q., Liu, X., Wang, P., Wu, R., & Ma, Z. (2017). tRF-Leu-CAG promotes cell proliferation and cell cycle in non-small cell lung cancer. *Chemical Biology & Drug Design*, *90*(5), 730–738. https://doi.org/10.1111/CBDD.12994
- Sharma, A., Hoeffer, C. A., Takayasu, Y., Miyawaki, T., McBride, S. M., Klann, E., & Suzanne Zukin, R. (2010). Dysregulation of mTOR signaling in Fragile X Syndrome. *The Journal of Neuroscience*, *30*(2), 694. https://doi.org/10.1523/JNEUROSCI.3696-09.2010
- Sharma, U., Conine, C. C., Shea, J. M., Boskovic, A., Derr, A. G., Bing, X. Y., Belleannee, C., Kucukural, A., Serra, R. W., Sun, F., Song, L., Carone, B. R., Ricci, E. P., Li, X. Z., Fauquier, L., Moore, M. J., Sullivan, R., Mello, C. C., Garber, M., & Rando, O. J. (2016). Biogenesis and function of tRNA fragments during sperm maturation and fertilization in mammals.

 Science, 351(6271), 391–396. https://doi.org/10.1126/SCIENCE.AAD6780/SUPPL FILE/SHARMA.SM.PDF
- Shen, Y., Yu, X., Zhu, L., Li, T., Yan, Z., & Guo, J. (2018). Transfer RNA-derived fragments and tRNA halves: biogenesis, biological functions and their roles in diseases. In *Journal of Molecular Medicine* (Vol. 96, Issue 11, pp. 1167–1176). Springer Verlag. https://doi.org/10.1007/s00109-018-1693-y
- Sheng, J., & Xu, Z. (2016). Three decades of research on angiogenin: a review and perspective. *Acta Biochimica et Biophysica Sinica*, 48(5), 399. https://doi.org/10.1093/ABBS/GMV131
- Shi, H., Zhou, Y., Jia, E., Pan, M., Bai, Y., & Ge, Q. (2021). Bias in RNA-seq library preparation: current challenges and solutions. *BioMed Research International*, 2021. https://doi.org/10.1155/2021/6647597
- Shi, J., Zhang, Y., Tan, D., Zhang, X., Yan, M., Zhang, Y., Franklin, R., Shahbazi, M., Mackinlay, K., Liu, S., Kuhle, B., James, E. R., Zhang, L., Qu, Y., Zhai, Q., Zhao, W., Zhao, L., Zhou, C., Gu, W., ... Chen, Q. (2021). PANDORA-seq expands the repertoire of regulatory small RNAs by overcoming RNA modifications. *Nature Cell Biology*, *23*(4), 424–436. https://doi.org/10.1038/s41556-021-00652-7
- Shigematsu, M., Kawamura, T., & Kirino, Y. (2018). Generation of 2',3'-cyclic phosphate-containing RNAs as a hidden layer of the transcriptome. *Frontiers in Genetics*, *9*, 562. https://doi.org/10.3389/FGENE.2018.00562/BIBTEX
- Shin, D., Shin, J. Y., McManus, M. T., Ptáček, L. J., & Fu, Y. H. (2009). Dicer ablation in oligodendrocytes provokes neuronal impairment in mice. *Annals of Neurology*, 66(6), 843. https://doi.org/10.1002/ANA.21927

- Simmons, D. A., Casale, M., Alcon, B., Pham, N., Narayan, N., & Lynch, G. (2007). Ferritin accumulation in dystrophic microglia is an early event in the development of Huntington's disease. *Glia*, *55*(10), 1074–1084. https://doi.org/10.1002/GLIA.20526
- Skotte, N. H., Southwell, A. L., Østergaard, M. E., Carroll, J. B., Warby, S. C., Doty, C. N., Petoukhov, E., Vaid, K., Kordasiewicz, H., Watt, A. T., Freier, S. M., Hung, G., Seth, P. P., Bennett, C. F., Swayze, E. E., & Hayden, M. R. (2014). Allele-specific suppression of mutant huntingtin using antisense oligonucleotides: providing a therapeutic option for all Huntington disease patients. *PloS One*, *9*(9). https://doi.org/10.1371/JOURNAL.PONE.0107434
- Slota, J. A., & Booth, S. A. (2019). MicroRNAs in neuroinflammation: Implications in disease pathogenesis, biomarker discovery and therapeutic applications. *Non-Coding RNA*, 5(2), 35. https://doi.org/10.3390/NCRNA5020035
- Slow, E. J., van Raamsdonk, J., Rogers, D., Coleman, S. H., Graham, R. K., Deng, Y., Oh, R., Bissada, N., Hossain, S. M., Yang, Y. Z., Li, X. J., Simpson, E. M., Gutekunst, C. A., Leavitt, B. R., & Hayden, M. R. (2003). Selective striatal neuronal loss in a YAC128 mouse model of Huntington disease. *Human Molecular Genetics*, 12(13), 1555–1567. https://doi.org/10.1093/HMG/DDG169
- Sobala, A., & Hutvagner, G. (2013). Small RNAs derived from the 5' end of tRNA can inhibit protein translation in human cells. *RNA Biology*, *10*(4), 553–563. https://doi.org/10.4161/RNA.24285
- Sobczak, K., de Mezer, M., Michlewski, G., Krol, J., & Krzyzosiak, W. J. (2003). RNA structure of trinucleotide repeats associated with human neurological diseases. *Nucleic Acids Research*, *31*(19), 5469–5482. https://doi.org/10.1093/NAR/GKG766
- Sobczak, K., & Krzyzosiak, W. J. (2004). Imperfect CAG repeats form diverse structures in SCA1 transcripts. *Journal of Biological Chemistry*, *279*(40), 41563–41572. https://doi.org/10.1074/jbc.M405130200
- Sobczak, K., & Krzyzosiak, W. J. (2005). CAG repeats containing CAA interruptions form branched hairpin structures in spinocerebellar ataxia type 2 transcripts. *Journal of Biological Chemistry*, 280(5), 3898–3910. https://doi.org/10.1074/jbc.M409984200
- Song, C., Perides, G., & Liu, Y. F. (2002). Expression of full-length polyglutamine-expanded Huntingtin disrupts growth factor receptor signaling in rat pheochromocytoma (PC12) cells. *Journal of Biological Chemistry*, *277*(8), 6703–6707. https://doi.org/10.1074/jbc.M110338200
- Sørensen, S. A., & Fenger, K. (1992). Causes of death in patients with Huntington's disease and in unaffected first degree relatives. *Journal of Medical Genetics*, *29*(12), 911–914. https://doi.org/10.1136/jmg.29.12.911
- Speer, J., Gehrke, C. W., Kuo, K. C., Waalkes, ? T Phillip, & Borek, E. (1979). tRNA breakdown products as markers for cancer. *Cancer*, *44*, 2120–2123. https://doi.org/10.1002/1097-0142
- Spenkuch, F., Motorin, Y., & Helm, M. (2014). Pseudouridine: still mysterious, but never a fake (uridine)! *RNA Biology*, 11(12), 1540–1554.

- https://doi.org/10.4161/15476286.2014.992278
- Squires, J. E., Patel, H. R., Nousch, M., Sibbritt, T., Humphreys, D. T., Parker, B. J., Suter, C. M., & Preiss, T. (2012). Widespread occurrence of 5-methylcytosine in human coding and non-coding RNA. *Nucleic Acids Research*, *40*(11), 5023–5033. https://doi.org/10.1093/NAR/GKS144
- Stancu, I. C., Cremers, N., Vanrusselt, H., Couturier, J., Vanoosthuyse, A., Kessels, S., Lodder, C., Brône, B., Huaux, F., Octave, J. N., Terwel, D., & Dewachter, I. (2019). Aggregated Tau activates NLRP3–ASC inflammasome exacerbating exogenously seeded and non-exogenously seeded Tau pathology in vivo. *Acta Neuropathologica*, *137*(4), 599. https://doi.org/10.1007/S00401-018-01957-Y
- Stanek, L. M., Sardi, S. P., Mastis, B., Richards, A. R., Treleaven, C. M., Taksir, T., Misra, K., Cheng, S. H., & Shihabuddin, L. S. (2014). Silencing mutant Huntingtin by adenoassociated virus-mediated RNA interference ameliorates disease manifestations in the YAC128 mouse model of Huntington's Disease. *Human Gene Therapy*, 25(5), 461. https://doi.org/10.1089/HUM.2013.200
- Statello, L., Guo, C. J., Chen, L. L., & Huarte, M. (2020). Gene regulation by long non-coding RNAs and its biological functions. *Nature Reviews Molecular Cell Biology*, *22*(2), 96–118. https://doi.org/10.1038/s41580-020-00315-9
- Steibel, J. P., Poletto, R., Coussens, P. M., & Rosa, G. J. M. (2009). A powerful and flexible linear mixed model framework for the analysis of relative quantification RT-PCR data. *Genomics*, 94(2), 146–152. https://doi.org/10.1016/j.ygeno.2009.04.008
- Stepanov, G. A., Filippova, J. A., Komissarov, A. B., Kuligina, E. V., Richter, V. A., Semenov, D. V., & Tang, T. H. (2015). Regulatory role of small nucleolar RNAs in human diseases. *BioMed Research International*, 2015. https://doi.org/10.1155/2015/206849
- Su, Z., Kuscu, C., Malik, A., Shibata, E., & Dutta, A. (2019). Angiogenin generates specific stress-induced tRNA halves and is not involved in tRF-3-mediated gene silencing. *The Journal of Biological Chemistry*, *294*(45), 16930–16941. https://doi.org/10.1074/JBC.RA119.009272
- Sun, X., Li, P. P., Zhu, S., Cohen, R., Marque, L. O., Ross, C. A., Pulst, S. M., Chan, H. Y. E., Margolis, R. L., & Rudnicki, D. D. (2015). Nuclear retention of full-length HTT RNA is mediated by splicing factors MBNL1 and U2AF65. *Scientific Reports*, *5*. https://doi.org/10.1038/SREP12521
- Sun, X., Marque, L. O., Cordner, Z., Pruitt, J. L., Bhat, M., Li, P. P., Kannan, G., Ladenheim, E. E., Moran, T. H., Margolis, R. L., & Rudnicki, D. D. (2014). Phosphorodiamidate morpholino oligomers suppress mutant huntingtin expression and attenuate neurotoxicity. Human Molecular Genetics, 23(23), 6302. https://doi.org/10.1093/HMG/DDU349
- Tabrizi, S. J., Estevez-Fraga, C., van Roon-Mom, W. M. C., Flower, M. D., Scahill, R. I., Wild, E. J., Muñoz-Sanjuan, I., Sampaio, C., Rosser, A. E., & Leavitt, B. R. (2022). Potential disease modifying therapies for Huntington's disease, lessons learned and future opportunities. *The Lancet. Neurology*, 21(7), 645. https://doi.org/10.1016/S1474-4422(22)00121-1

- Tabrizi, S. J., Flower, M. D., Ross, C. A., & Wild, E. J. (2020). Huntington disease: new insights into molecular pathogenesis and therapeutic opportunities. *Nature Reviews Neurology*, *16*(10), 529–546. https://doi.org/10.1038/S41582-020-0389-4
- Tabrizi, S. J., Ghosh, R., & Leavitt, B. R. (2019). Huntingtin lowering strategies for disease modification in Huntington's Disease. *Neuron*, *101*(5), 801–819. https://doi.org/10.1016/J.NEURON.2019.01.039
- Tabrizi, S. J., Schobel, S., Gantman, E. C., Mansbach, A., Borowsky, B., Konstantinova, P., Mestre, T. A., Panagoulias, J., Ross, C. A., Zauderer, M., Mullin, A. P., Romero, K., Sivakumaran, S., Turner, E. C., Long, J. D., & Sampaio, C. (2022). A biological classification of Huntington's disease: the Integrated Staging System. *The Lancet. Neurology*, 21(7), 632–644. https://doi.org/10.1016/S1474-4422(22)00120-X
- Tai, Y. F., Pavese, N., Gerhard, A., Tabrizi, S. J., Barker, R. A., Brooks, D. J., & Piccini, P. (2007). Microglial activation in presymptomatic Huntington's disease gene carriers. *Brain*, 130(7), 1759–1766. https://doi.org/10.1093/BRAIN/AWM044
- Taliaferro, J. M., Vidaki, M., Oliveira, R., Olson, S., Zhan, L., Saxena, T., Wang, E. T., Graveley, B. R., Gertler, F. B., Swanson, M. S., & Burge, C. B. (2016). Distal alternative last exons localize mRNAs to neural projections. *Molecular Cell*, *61*(6), 821–833. https://doi.org/10.1016/j.molcel.2016.01.020
- Talimur Reza, A. M. M., & Yuan, Y. G. (2021). microRNAs mediated regulation of the ribosomal proteins and its consequences on the global translation of proteins. *Cells*, 10(1), 1–27. https://doi.org/10.3390/CELLS10010110
- Tang, S. C., Lathia, J. D., Selvaraj, P. K., Jo, D. G., Mughal, M. R., Cheng, A., Siler, D. A., Markesbery, W. R., Arumugam, T. V., & Mattson, M. P. (2008). Toll-Like Receptor-4 mediates neuronal apoptosis induced by Amyloid β-Peptide and the Membrane Lipid Peroxidation Product 4-Hydroxynonenal. *Experimental Neurology*, *213*(1), 114. https://doi.org/10.1016/J.EXPNEUROL.2008.05.014
- Tang, X., Ren, H., Guo, M., Qian, J., Yang, Y., & Gu, C. (2021). Review on circular RNAs and new insights into their roles in cancer. *Computational and Structural Biotechnology Journal*, 19, 910–928. https://doi.org/10.1016/J.CSBJ.2021.01.018
- Tao, J., Wu, H., Lin, Q., Wei, W., Lu, X. H., Cantle, J. P., Ao, Y., Olsen, R. W., Yang, X. W., Mody, I., Sofroniew, M. V., & Sun, Y. E. (2011). Deletion of astroglial Dicer causes non-cell autonomous neuronal dysfunction and degeneration. *The Journal of Neuroscience*, 31(22), 8306. https://doi.org/10.1523/JNEUROSCI.0567-11.2011
- Tartari, M., Gissi, C., Lo Sardo, V., Zuccato, C., Picardi, E., Pesole, G., & Cattaneo, E. (2008). Phylogenetic comparison of huntingtin homologues reveals the appearance of a primitive polyQ in sea urchin. *Molecular Biology and Evolution*, *25*(2), 330–338. https://doi.org/10.1093/MOLBEV/MSM258
- Telenius, H., Kremer, B., Goldberg, Y. P., Theilmann, J., Andrew, S. E., Zeisler, J., Adam, S., Greenberg, C., Ives, E. J., Clarke, L. A., & Hayden, M. R. (1994). Somatic and gonadal mosaicism of the Huntington disease gene CAG repeat in brain and sperm. *Nature Genetics*, 6(4), 409–414. https://doi.org/10.1038/NG0494-409

- Tepper, J. M., & Bolam, J. P. (2004). Functional diversity and specificity of neostriatal interneurons. *Current Opinion in Neurobiology*, *14*(6), 685–692. https://doi.org/10.1016/J.CONB.2004.10.003
- Tepper, J. M., Tecuapetla, F., Koós, T., & Ibáñez-Sandoval, O. (2010). Heterogeneity and diversity of striatal GABAergic interneurons. *Frontiers in Neuroanatomy*, *4*(DEC), 1–18. https://doi.org/10.3389/fnana.2010.00150
- The Huntington's Disease Collaborative Research Group. (1993). A novel gene containing a trinucleotide repeat that is expanded and unstable on Huntington's disease chromosomes. *Cell*, 72(6), 971–983. https://doi.org/10.1016/0092-8674(93)90585-E
- Thelen, M. P., & Kye, M. J. (2020). The role of RNA binding proteins for local mRNA translation: implications in neurological disorders. *Frontiers in Molecular Biosciences*, 6, 161. https://doi.org/10.3389/FMOLB.2019.00161/BIBTEX
- Thomou, T., Mori, M. A., Dreyfuss, J. M., Konishi, M., Sakaguchi, M., Wolfrum, C., Rao, T. N., Winnay, J. N., Garcia-Martin, R., Grinspoon, S. K., Gorden, P., & Kahn, C. R. (2017). Adipose-derived circulating miRNAs regulate gene expression in other tissues. *Nature*, 542(7642), 450. https://doi.org/10.1038/NATURE21365
- Thompson, D. M., Lu, C., Green, P. J., & Parker, R. (2008). tRNA cleavage is a conserved response to oxidative stress in eukaryotes. *RNA*, *14*(10), 2095–2103. https://doi.org/10.1261/RNA.1232808
- Tian, B., White, R. J., Xia, T., Welle, S., Turner, D. H., Mathews, M. B., & Thornton, C. A. (2000). Expanded CUG repeat RNAs form hairpins that activate the double-stranded RNA-dependent protein kinase PKR. *RNA*, *6*(1), 79. https://doi.org/10.1017/S1355838200991544
- Tomita, K., Ogawa, T., Uozumi, T., Watanabe, K., & Masaki, H. (2000). A cytotoxic ribonuclease which specifically cleaves four isoaccepting arginine tRNAs at their anticodon loops. *Proceedings of the National Academy of Sciences*, *97*(15), 8278–8283. https://doi.org/10.1073/PNAS.140213797
- Tong, J., Wang, X., Liu, Y., Ren, X., Wang, A., Chen, Z., Yao, J., Mao, K., Liu, T., Meng, F. L., Pan, W., Zou, Q., Liu, J., Zhou, Y., Xia, Q., Flavell, R. A., Zhu, S., & Li, H. B. (2021). Pooled CRISPR screening identifies m6A as a positive regulator of macrophage activation. *Science Advances*, 7(18), 4742–4770. https://doi.org/10.1126/SCIADV.ABD4742
- Topol, A., English, J. A., Flaherty, E., Rajarajan, P., Hartley, B. J., Gupta, S., Desland, F., Zhu, S., Goff, T., Friedman, L., Rapoport, J., Felsenfeld, D., Cagney, G., Mackay-Sim, A., Savas, J. N., Aronow, B., Fang, G., Zhang, B., Cotter, D., & Brennand, K. J. (2015). Increased abundance of translation machinery in stem cell–derived neural progenitor cells from four schizophrenia patients. *Translational Psychiatry*, *5*(10), e662. https://doi.org/10.1038/TP.2015.118
- Torres-Peraza, J. F., Giralt, A., García-Martínez, J. M., Pedrosa, E., Canals, J. M., & Alberch, J. (2008). Disruption of striatal glutamatergic transmission induced by mutant huntingtin involves remodeling of both postsynaptic density and NMDA receptor signaling. *Neurobiology of Disease*, 29(3), 409–421. https://doi.org/10.1016/J.NBD.2007.10.003

- Torres, A. G., Batlle, E., & Ribas De Pouplana, L. (2014). Role of tRNA modifications in human diseases. *Trends in Molecular Medicine*, 20(6), 306–314. https://doi.org/10.1016/j.molmed.2014.01.008
- Torres, A. G., & Martí, E. (2021). Toward an Understanding of Extracellular tRNA Biology. *Frontiers in Molecular Biosciences*, 8, 233. https://doi.org/10.3389/FMOLB.2021.662620/BIBTEX
- Torres, A. G., Piñeyro, D., Filonava, L., Stracker, T. H., Batlle, E., & Ribas De Pouplana, L. (2014). A-to-I editing on tRNAs: biochemical, biological and evolutionary implications. *FEBS Letters*, *588*(23), 4279–4286. https://doi.org/10.1016/J.FEBSLET.2014.09.025
- Tosar, J. P., & Cayota, A. (2020). Extracellular tRNAs and tRNA-derived fragments. *RNA Biology*, *17*(8), 1149–1167. https://doi.org/10.1080/15476286.2020.1729584
- Trettel, F., Rigamonti, D., Hilditch-Maguire, P., Wheeler, V. C., Sharp, A. H., Persichetti, F., Cattaneo, E., & MacDonald, M. E. (2000). Dominant phenotypes produced by the HD mutation in STHdh(Q111) striatal cells. *Human Molecular Genetics*, *9*(19), 2799–2809. https://doi.org/10.1093/hmg/9.19.2799
- Trottier, Y., Lutz, Y., Stevanin, G., Imbert, G., Devys, D., Cancel, G., Saudou, F., Weber, C., David, G., Tora, L., Agid, Y., Brice, A., & Mandel, J. L. (1995). Polyglutamine expansion as a pathological epitope in Huntington's disease and four dominant cerebellar ataxias. *Nature*, *378*(6555), 403–406. https://doi.org/10.1038/378403A0
- Tsoi, H., & Chan, H. Y. E. (2013). Expression of expanded CAG transcripts triggers nucleolar stress in huntington's disease. *Cerebellum*, 12(3), 310–312. https://doi.org/10.1007/S12311-012-0447-6/FIGURES/1
- Tsoi, H., & Chan, H. Y. E. (2014). Roles of the nucleolus in the CAG RNA-mediated toxicity. *Biochimica et Biophysica Acta (BBA) - Molecular Basis of Disease*, 1842(6), 779–784. https://doi.org/10.1016/J.BBADIS.2013.11.015
- Tsoi, H., Lau, C. K., Lau, K. F., & Chan, H. Y. E. (2011). Perturbation of U2AF65/NXF1-mediated RNA nuclear export enhances RNA toxicity in polyQ diseases. *Human Molecular Genetics*, 20(19), 3787–3797. https://doi.org/10.1093/HMG/DDR297
- Tsoi, H., Lau, T. C. K., Tsang, S. Y., Lau, K. F., & Chan, H. Y. E. (2012). CAG expansion induces nucleolar stress in polyglutamine diseases. *Proceedings of the National Academy of Sciences of the United States of America*, 109(33), 13428–13433. https://doi.org/10.1073/PNAS.1204089109/SUPPL_FILE/PNAS.201204089SI.PDF
- Tuorto, F., Legrand, C., Cirzi, C., Federico, G., Liebers, R., Müller, M., Ehrenhofer-Murray, A. E., Dittmar, G., Gröne, H., & Lyko, F. (2018). Queuosine-modified tRNAs confer nutritional control of protein translation. *The EMBO Journal*, *37*(18). https://doi.org/10.15252/EMBJ.201899777
- Tuorto, F., Liebers, R., Musch, T., Schaefer, M., Hofmann, S., Kellner, S., Frye, M., Helm, M., Stoecklin, G., & Lyko, F. (2012). RNA cytosine methylation by Dnmt2 and NSun2 promotes tRNA stability and protein synthesis. *Nature Publishing Group*. https://doi.org/10.1038/nsmb.2357

- Turmaine, M., Raza, A., Mahal, A., Mangiarini, L., Bates, G. P., & Davies, S. W. (2000).

 Nonapoptotic neurodegeneration in a transgenic mouse model of Huntington's disease. *Proceedings of the National Academy of Sciences of the United States of America*, 97(14), 8093–8097.

 https://doi.org/10.1073/PNAS.110078997/ASSET/F2C3C203-C8B5-46F0-96E1-25C638766981/ASSETS/GRAPHIC/PQ1100789004.JPEG
- Valadão, P. A. C., Santos, K. B. S., Ferreira e Vieira, T. H., Macedo e Cordeiro, T., Teixeira, A. L., Guatimosim, C., & de Miranda, A. S. (2020). Inflammation in Huntington's disease: a few new twists on an old tale. *Journal of Neuroimmunology*, *348*. https://doi.org/10.1016/J.JNEUROIM.2020.577380
- van Dellen, A., Welch, J., Dixon, R. M., Cordery, P., York, D., Styles, P., Blakemore, C., & Hannan, A. J. (2000). N-Acetylaspartate and DARPP-32 levels decrease in the corpus striatum of Huntington's disease mice. *Neuroreport*, *11*(17), 3751–3757. https://doi.org/10.1097/00001756-200011270-00032
- van der Burg, J. M., Björkqvist, M., & Brundin, P. (2009). Beyond the brain: widespread pathology in Huntington's disease. *The Lancet Neurology*, 8(8), 765–774. https://doi.org/10.1016/S1474-4422(09)70178-4
- Van Dijk, E. L., Jaszczyszyn, Y., & Thermes, C. (2014). Library preparation methods for next-generation sequencing: Tone down the bias. *Experimental Cell Research*, *322*, 12–20. https://doi.org/10.1016/j.yexcr.2014.01.008
- van Dijk, J. G., van der Velde, E. A., Roos, R. A. C., & Bruyn, G. W. (1986). Juvenile Huntington disease. *Human Genetics*, 73(3), 235–239. https://doi.org/10.1007/BF00401235
- van Duijn, E., Craufurd, D., Hubers, A. A. M., Giltay, E. J., Bonelli, R., Rickards, H., Anderson, K. E., Van Walsem, M. R., Van Der Mast, R. C., Orth, M., & Landwehrmeyer, G. B. (2014). Neuropsychiatric symptoms in a European Huntington's disease cohort (REGISTRY). *Journal of Neurology, Neurosurgery and Psychiatry*, 85(12), 1411–1418. https://doi.org/10.1136/jnnp-2013-307343
- van Es, M. A., Schelhaas, H. J., Van Vught, P. W. J., Ticozzi, N., Andersen, P. M., Groen, E. J. N., Schulte, C., Blauw, H. M., Koppers, M., Diekstra, F. P., Fumoto, K., Leclerc, A. L., Keagle, P., Bloem, B. R., Scheffer, H., Van Nuenen, B. F. L., Van Blitterswijk, M., Van Rheenen, W., Wills, A. M., ... Van Den Berg, L. H. (2011). Angiogenin variants in Parkinson Disease and Amyotrophic Lateral Sclerosis. *Annals of Neurology*, *70*(6), 964. https://doi.org/10.1002/ANA.22611
- Van Haute, L., Dietmann, S., Kremer, L., Hussain, S., Pearce, S. F., Powell, C. A., Rorbach, J., Lantaff, R., Blanco, S., Sauer, S., Kotzaeridou, U., Hoffmann, G. F., Memari, Y., Kolb-Kokocinski, A., Durbin, R., Mayr, J. A., Frye, M., Prokisch, H., & Minczuk, M. (2016). Deficient methylation and formylation of mt-tRNA(Met) wobble cytosine in a patient carrying mutations in NSUN3. *Nature Communications*, 7. https://doi.org/10.1038/NCOMMS12039
- van Raamsdonk, J. M., Warby, S. C., & Hayden, M. R. (2007). Selective degeneration in YAC mouse models of Huntington disease. *Brain Research Bulletin*, 72(2–3), 124–131. https://doi.org/10.1016/J.BRAINRESBULL.2006.10.018

- Vickers, K. C., Palmisano, B. T., Shoucri, B. M., Shamburek, R. D., & Remaley, A. T. (2011). MicroRNAs are transported in plasma and delivered to recipient cells by high-density lipoproteins. *Nature Cell Biology*, *13*(4), 423. https://doi.org/10.1038/NCB2210
- Vonsattel, J. P. (2008). Huntington disease models and human neuropathology: Similarities and differences. *Acta Neuropathologica*, *115*(1), 55–69. https://doi.org/10.1007/S00401-007-0306-6/FIGURES/3
- Vonsattel, J. P., & DiFiglia, M. (1998). Huntington Disease. *Journal of Neuropathology & Experimental Neurology*, *57*(5), 369–384. https://doi.org/10.1097/00005072-199805000-00001
- Vonsattel, J. P., Myers, R. H., Stevens, T. J., Ferrante, R. J., Bird, E. D., & Richardson, E. P. (1985). Neuropathological classification of Huntington's Disease. *Journal of Neuropathology & Experimental Neurology*, 44(6), 559–577. https://doi.org/10.1097/00005072-198511000-00003
- Walker, F. O. (2007). Huntington's disease. *Lancet*, *369*(9557), 218–228. https://doi.org/10.1016/S0140-6736(07)60111-1
- Walter, S., Letiembre, M., Liu, Y., Heine, H., Penke, B., Hao, W., Bode, B., Manietta, N., Walter, J., Schulz-Schüffer, W., & Faßbender, K. (2007). Role of the toll-like receptor 4 in neuroinflammation in Alzheimer's disease. *Cellular Physiology and Biochemistry: International Journal of Experimental Cellular Physiology, Biochemistry, and Pharmacology*, 20(6), 947–956. https://doi.org/10.1159/000110455
- Wang, E. T., Cody, N. A. L., Jog, S., Biancolella, M., Wang, T. T., Treacy, D. J., Luo, S., Schroth, G. P., Housman, D. E., Reddy, S., Lécuyer, E., & Burge, C. B. (2012). Transcriptomewide regulation of pre-mRNA splicing and mRNA localization by muscleblind proteins. *Cell*, 150(4), 710–724. https://doi.org/10.1016/j.cell.2012.06.041
- Wang, J., Czech, B., Crunk, A., Wallace, A., Mitreva, M., Hannon, G. J., & Davis, R. E. (2011). Deep small RNA sequencing from the nematode Ascaris reveals conservation, functional diversification, and novel developmental profiles. *Genome Research*, 21(9), 1462. https://doi.org/10.1101/GR.121426.111
- Wang, L. C., Chen, K. Y., Pan, H., Wu, C. C., Chen, P. H., Liao, Y. T., Li, C., Huang, M. L., & Hsiao, K. M. (2011). Muscleblind participates in RNA toxicity of expanded CAG and CUG repeats in Caenorhabditis elegans. *Cellular and Molecular Life Sciences*, *68*(7), 1255–1267. https://doi.org/10.1007/S00018-010-0522-4/FIGURES/7
- Wang, Q., Lee, I., Ren, J., Ajay, S. S., Lee, Y. S., & Bao, X. (2013). Identification and functional characterization of tRNA-derived RNA fragments (tRFs) in respiratory syncytial virus infection. *Molecular Therapy*, 21(2), 368–379. https://doi.org/10.1038/MT.2012.237
- Wang, T., Cao, L., He, S., Long, K., Wang, X., Yu, H., Ma, B., Xu, X., & Li, W. (2020). Small RNA sequencing reveals a novel tsRNA-06018 playing an important role during adipogenic differentiation of hMSCs. *Journal of Cellular and Molecular Medicine*, *24*(21), 12736. https://doi.org/10.1111/JCMM.15858
- Wang, X., Matuszek, Z., Huang, Y., Parisien, M., Dai, Q., Clark, W., Schwartz, M. H., & Pan, T. (2018). Queuosine modification protects cognate tRNAs against ribonuclease

- cleavage. RNA, 24(10), 1305-1313. https://doi.org/10.1261/RNA.067033.118/-/DC1
- Wang, X., & Proud, C. G. (2006). The mTOR pathway in the control of protein synthesis. *Physiology*, 21(5), 362–369. https://doi.org/10.1152/PHYSIOL.00024.2006/ASSET/IMAGES/LARGE/Y0024-6-04.JPEG
- Wang, Z., Xiang, L., Shao, J., & Yuan, Z. (2006). The 3' CCACCA sequence of tRNAAla(UGC) is the motif that is important in inducing Th1-like immune response, and this motif can be recognized by Toll-like receptor 3. *Clinical and Vaccine Immunology*, *13*(7), 733–739. https://doi.org/10.1128/CVI.00019-06
- Warby, S. C., Visscher, H., Collins, J. A., Doty, C. N., Carter, C., Butland, S. L., Hayden, A. R., Kanazawa, I., Ross, C. J., & Hayden, M. R. (2011). HTT haplotypes contribute to differences in Huntington disease prevalence between Europe and East Asia. *European Journal of Human Genetics*, 19(5), 561–566. https://doi.org/10.1038/ejhg.2010.229
- Watanabe, A., Tatematsu, M., Saeki, K., Shibata, S., Shime, H., Yoshimura, A., Obuse, C., Seya, T., & Matsumoto, M. (2011). Raftlin is involved in the nucleocapture complex to induce Poly(I:C)-mediated TLR3 activation. *The Journal of Biological Chemistry*, 286(12), 10702. https://doi.org/10.1074/JBC.M110.185793
- Waters, C. W., Varuzhanyan, G., Talmadge, R. J., & Voss, A. A. (2013). Huntington disease skeletal muscle is hyperexcitable owing to chloride and potassium channel dysfunction. *Proceedings of the National Academy of Sciences of the United States of America*, 110(22), 9160–9165. https://doi.org/10.1073/PNAS.1220068110/SUPPL_FILE/PNAS.201220068SI.PDF
- Wei, F. Y., Zhou, B., Suzuki, T., Miyata, K., Ujihara, Y., Horiguchi, H., Takahashi, N., Xie, P., Michiue, H., Fujimura, A., Kaitsuka, T., Matsui, H., Koga, Y., Mohri, S., Suzuki, T., Oike, Y., & Tomizawa, K. (2015). Cdk5rap1-mediated 2-methylthio modification of mitochondrial tRNAs governs protein translation and contributes to myopathy in mice and humans. *Cell Metabolism*, 21(3), 428–442. https://doi.org/10.1016/J.CMET.2015.01.019
- Wexler, A. (2013). A brief prehistory of Huntington's Disease. *Journal of Huntington's Disease*, 2(3), 231–237. https://doi.org/10.3233/JHD-139006
- White, J. K., Auerbach, W., Duyao, M. P., Vonsattel, J. P., Gusella, J. F., Joyner, A. L., & MacDonald, M. E. (1997). Huntingtin is required for neurogenesis and is not impaired by the Huntington's disease CAG expansion. *Nature Genetics*, *17*(4), 404–410. https://doi.org/10.1038/NG1297-404
- Wilson, R. C., & Doudna, J. A. (2013). Molecular mechanisms of RNA interference. *Annual Review of Biophysics*, *42*(1), 217–239. https://doi.org/10.1146/ANNUREV-BIOPHYS-083012-130404
- Wiseman, S. L., Shimizu, Y., Palfrey, C., & Nairn, A. C. (2013). Proteasomal degradation of Eukaryotic Elongation Factor-2 Kinase (EF2K) is regulated by cAMP-PKA signaling and the SCFβTRCP Ubiquitin E3 Ligase. *The Journal of Biological Chemistry*, *288*(24), 17803. https://doi.org/10.1074/JBC.M113.477182

- Wojciechowska, M., & Krzyzosiak, W. J. (2011). Cellular toxicity of expanded RNA repeats: focus on RNA foci. *Human Molecular Genetics*, *20*(19), 3811–3821. https://doi.org/10.1093/HMG/DDR299
- Woolnough, J. L., Atwood, B. L., & Giles, K. E. (2015). Argonaute 2 binds directly to tRNA genes and promotes gene repression in cis. *Molecular and Cellular Biology*, 35(13), 2278. https://doi.org/10.1128/MCB.00076-15
- Wu, W., Lee, I., Spratt, H., Fang, X., & Bao, X. (2021). tRNA-Derived fragments in Alzheimer's Disease: implications for new disease biomarkers and neuropathological mechanisms. *Journal of Alzheimer's Disease: JAD, 79*(2), 793–806. https://doi.org/10.3233/JAD-200917
- Xu, H., Chen, W., Zheng, F., Tang, D., Dai, W., Huang, S., Zhang, C., Zeng, J., Wang, G., & Dai, Y. (2020). The potential role of tRNAs and small RNAs derived from tRNAs in the occurrence and development of systemic lupus erythematosus. *Biochemical and Biophysical Research Communications*, 527(2), 561–567. https://doi.org/10.1016/J.BBRC.2020.04.114
- Yamasaki, S., Ivanov, P., Hu, G. F., & Anderson, P. (2009). Angiogenin cleaves tRNA and promotes stress-induced translational repression. *The Journal of Cell Biology*, *185*(1), 35–42. https://doi.org/10.1083/JCB.200811106
- Yang, J. Y., Deng, X. Y., Li, Y. S., Ma, X. C., Feng, J. X., Yu, B., Chen, Y., Luo, Y. L., Wang, X., Chen, M. L., Fang, Z. X., Zheng, F. X., Li, Y. P., Zhong, Q., Kang, T. B., Song, L. B., Xu, R. H., Zeng, M. S., Chen, W., ... Gao, S. (2018). Structure of Schlafen13 reveals a new class of tRNA/rRNA- targeting RNase engaged in translational control. *Nature Communications*, 9(1), 1–13. https://doi.org/10.1038/s41467-018-03544-x
- Yang, S., Chang, R., Yang, H., Zhao, T., Hong, Y., Kong, H. E., Sun, X., Qin, Z., Jin, P., Li, S., & Li, X. J. (2017). CRISPR/Cas9-mediated gene editing ameliorates neurotoxicity in mouse model of Huntington's disease. *The Journal of Clinical Investigation*, 127(7), 2719. https://doi.org/10.1172/JCI92087
- Yang, S. H., Cheng, P. H., Banta, H., Piotrowska-Nitsche, K., Yang, J. J., Cheng, E. C. H., Snyder, B., Larkin, K., Liu, J., Orkin, J., Fang, Z. H., Smith, Y., Bachevalier, J., Zola, S. M., Li, S. H., Li, X. J., & Chan, A. W. S. (2008). Towards a transgenic model of Huntington's disease in a non-human primate. *Nature*, *453*(7197), 921–924. https://doi.org/10.1038/NATURE06975
- Yang, S., Yang, H., Huang, L., Chen, L., Qin, Z., Li, S., & Li, X. J. (2020). Lack of RAN-mediated toxicity in Huntington's disease knock-in mice. *Proceedings of the National Academy of Sciences of the United States of America*, 117(8), 4411–4417. https://doi.org/10.1073/PNAS.1919197117/SUPPL_FILE/PNAS.1919197117.SAPP.PD F
- Yang, X., Yang, Y., Sun, B. F., Chen, Y. S., Xu, J. W., Lai, W. Y., Li, A., Wang, X., Bhattarai, D. P., Xiao, W., Sun, H. Y., Zhu, Q., Ma, H. L., Adhikari, S., Sun, M., Hao, Y. J., Zhang, B., Huang, C. M., Huang, N., ... Yang, Y. G. (2017). 5-methylcytosine promotes mRNA export NSUN2 as the methyltransferase and ALYREF as an m5C reader. *Cell Research*, *27*(5), 606. https://doi.org/10.1038/CR.2017.55

- Yeri, A., Courtright, A., Reiman, R., Carlson, E., Beecroft, T., Janss, A., Siniard, A., Richholt, R., Balak, C., Rozowsky, J., Kitchen, R., Hutchins, E., Winarta, J., McCoy, R., Anastasi, M., Kim, S., Huentelman, M., & Van Keuren-Jensen, K. (2017). Total extracellular small RNA profiles from plasma, saliva, and urine of healthy subjects. *Scientific Reports*, 7. https://doi.org/10.1038/SREP44061
- Yeung, M. L., Bennasser, Y., Watashi, K., Le, S. Y., Houzet, L., & Jeang, K. T. (2009). Pyrosequencing of small non-coding RNAs in HIV-1 infected cells: evidence for the processing of a viral-cellular double-stranded RNA hybrid. *Nucleic Acids Research*, 37(19), 6575. https://doi.org/10.1093/NAR/GKP707
- Young, A. B., Shoulson, I., Penney, J. B., Starosta-Rubinstein, S., Gomez, F., Travers, H., Ramos-Arroyo, M. A., Snodgrass, S. R., Bonilla, E., Moreno, H., & Wexler, N. S. (1986). Huntington's disease in Venezuela: neurologic features and functional decline. *Neurology*, *36*(2), 244–249. https://doi.org/10.1212/WNL.36.2.244
- Yu, Z., Teng, X., & Bonini, N. M. (2011). Triplet repeat-derived siRNAs enhance RNA-mediated toxicity in a Drosophila model for myotonic dystrophy. *PLoS Genetics*, 7(3). https://doi.org/10.1371/JOURNAL.PGEN.1001340
- Yu, Z. X., Li, S. H., Evans, J., Pillarisetti, A., Li, H., & Li, X. J. (2003). Mutant Huntingtin causes context-dependent neurodegeneration in mice with Huntington's Disease. *Journal of Neuroscience*, 23(6), 2193–2202. https://doi.org/10.1523/JNEUROSCI.23-06-02193.2003
- Yuan, S., Tang, H., Xing, J., Fan, X., Cai, X., Li, Q., Han, P., Luo, Y., Zhang, Z., Jiang, B., Dou, Y., Gorospe, M., & Wang, W. (2014). Methylation by NSun2 represses the levels and function of microRNA 125b. *Molecular and Cellular Biology*, 34(19), 3630. https://doi.org/10.1128/MCB.00243-14
- Zaborske, J. M., Bauer DuMont, V. L., Wallace, E. W. J., Pan, T., Aquadro, C. F., & Drummond, D. A. (2014). A nutrient-driven tRNA modification alters translational fidelity and genome-wide protein coding across an animal Genus. *PLoS Biology*, *12*(12), 1002015. https://doi.org/10.1371/JOURNAL.PBIO.1002015
- Zeitler, B., Froelich, S., Marlen, K., Shivak, D. A., Yu, Q., Li, D., Pearl, J. R., Miller, J. C., Zhang, L., Paschon, D. E., Hinkley, S. J., Ankoudinova, I., Lam, S., Guschin, D., Kopan, L., Cherone, J. M., Nguyen, H. O. B., Qiao, G., Ataei, Y., ... Zhang, H. S. (2019). Alleleselective transcriptional repression of mutant HTT for the treatment of Huntington's disease. *Nature Medicine*, *25*(7), 1131–1142. https://doi.org/10.1038/S41591-019-0478-3
- Zhang, S., Li, H., Zheng, L., Li, H., Feng, C., & Zhang, W. (2019). Identification of functional tRNA-derived fragments in senescence-accelerated mouse prone 8 brain. *Aging*, 11(22), 10485–10498. https://doi.org/10.18632/AGING.102471
- Zhang, X., Cozen, A. E., Liu, Y., Chen, Q., & Lowe, T. M. (2016). Small RNA modifications: integral to function and disease. *Trends in Molecular Medicine*, *22*(12), 1025. https://doi.org/10.1016/J.MOLMED.2016.10.009
- Zhang, X., Liu, Z., Yi, J., Tang, H., Xing, J., Yu, M., Tong, T., Shang, Y., Gorospe, M., & Wang, W. (2012). The tRNA methyltransferase NSun2 stabilizes p16INK4 mRNA by

- methylating the 3'-untranslated region of p16. *Nature Communications*, 3(1), 1–12. https://doi.org/10.1038/ncomms1692
- Zhang, Y., Zhang, L. S., Dai, Q., Chen, P., Lu, M., Kairis, E. L., Murugaiah, V., Xu, J., Shukla, R. K., Liang, X., Zou, Z., Cormet-Boyaka, E., Qiu, J., Peeples, M. E., Sharma, A., He, C., & Li, J. (2022). 5-methylcytosine (m5C) RNA modification controls the innate immune response to virus infection by regulating type I interferons. *Proceedings of the National Academy of Sciences of the United States of America*, 119(42). https://doi.org/10.1073/PNAS.2123338119/-/DCSUPPLEMENTAL
- Zhang, Y., Zhang, X., Shi, J., Tuorto, F., Li, X., Liu, Y., Liebers, R., Zhang, L., Qu, Y., Qian, J., Pahima, M., Liu, Y., Yan, M., Cao, Z., Lei, X., Cao, Y., Peng, H., Liu, S., Wang, Y., ... Chen, Q. (2018). Dnmt2 mediates intergenerational transmission of paternally acquired metabolic disorders through sperm small non-coding RNAs. *Nature Cell Biology*, *20*(5), 535. https://doi.org/10.1038/S41556-018-0087-2
- Zhang, Y., Zhang, Y., Shi, J., Zhang, H., Cao, Z., Gao, X., Ren, W., Ning, Y., Ning, L., Cao, Y., Chen, Y., Ji, W., Chen, Z. J., Chen, Q., & Duan, E. (2014). Identification and characterization of an ancient class of small RNAs enriched in serum associating with active infection. *Journal of Molecular Cell Biology*, 6(2), 172–174. https://doi.org/10.1093/JMCB/MJT052
- Zheng, G., Qin, Y., Clark, W. C., Dai, Q., Yi, C., He, C., Lambowitz, A. M., & Pan, T. (2015). Efficient and quantitative high-throughput tRNA sequencing. *Nature Methods*, *12*(9), 835–837. https://doi.org/10.1038/NMETH.3478
- Zheng, L. L., Xu, W. L., Liu, S., Sun, W. J., Li, J. H., Wu, J., Yang, J. H., & Qu, L. H. (2016). tRF2Cancer: A web server to detect tRNA-derived small RNA fragments (tRFs) and their expression in multiple cancers. *Nucleic Acids Research*, *44*(W1), W185–W193. https://doi.org/10.1093/NAR/GKW414
- Zhou, J., Liu, S., Chen, Y., Fu, Y., Silver, A. J., Hill, M. S., Lee, I., Lee, Y. S., & Bao, X. (2017). Identification of two novel functional tRNA-derived fragments induced in response to respiratory syncytial virus infection. *The Journal of General Virology*, *98*(7), 1600. https://doi.org/10.1099/JGV.0.000852
- Zu, T., Gibbens, B., Doty, N. S., Gomes-Pereira, M., Huguet, A., Stone, M. D., Margolis, J., Peterson, M., Markowski, T. W., Ingram, M. A. C., Nan, Z., Forster, C., Low, W. C., Schoser, B., Somia, N. V., Clark, H. B., Schmechel, S., Bitterman, P. B., Gourdon, G., ... Ranum, L. P. W. (2011). Non-ATG-initiated translation directed by microsatellite expansions. *Proceedings of the National Academy of Sciences of the United States of America*, 108(1), 260–265. https://doi.org/10.1073/PNAS.1013343108
- Zuccato, C., Valenza, M., & Cattaneo, E. (2010). Molecular mechanisms and potential therapeutical targets in Huntington's disease. *Physiological Reviews*, *90*(3), 905–981. https://doi.org/10.1152/PHYSREV.00041.2009
- Zuo, Y., Zhu, L., Guo, Z., Liu, W., Zhang, J., Zeng, Z., Wu, Q., Cheng, J., Fu, X., Jin, Y., Zhao, Y., & Peng, Y. (2021). tsRBase: a comprehensive database for expression and function of tsRNAs in multiple species. *Nucleic Acids Research*, *49*(D1), D1038. https://doi.org/10.1093/NAR/GKAA888

Supplementary Table 1. According to EnrichR tool, top downregulated terms in HD-sRNA-PT- versus vehicle-injected mice and not significantly altered in CTL-sRNA-PT- versus vehicle-injected animals. Table shows the top ten terms enriched in multiple databases.

Database: KEGG 2019 mouse

Name	P value	Adj P value	Z score	Combined score
Cholinergic synapse	0.000008128	0.002203	3.30	38.66
Cocaine addiction	0.0003408	0.02309	4.04	32.22
Synaptic vesicle cycle	0.0002150	0.02309	3.29	27.78
Mannose type O-glycan biosynthesis	0.003886	0.1170	4.78	26.52
Axon guidance	0.0002723	0.02309	2.30	18.90
Adrenergic signaling in cardiomyocytes	0.0005232	0.02835	2.38	17.97
Amphetamine addiction	0.002193	0.08429	2.91	17.80
Taurine and hypotaurine metabolism	0.03559	0.4384	5.07	16.91
Cardiac muscle contraction	0.002488	0.08429	2.71	16.28
Calcium signaling pathway	0.001307	0.05902	2.08	13.79

Database: Wikipathways 2019 mouse

Name	P value	Adj P value	Z score	Combined score
Monoamine GPCRs WP570	0.001475	0.06195	4.34	28.27
G-Protein Signaling Pathways WP232	0.0005175	0.03260	2.86	21.66
Calcium Regulation in the Cardiac Cell WP553	0.0004757	0.03260	2.40	18.34
Alanine and aspartate metabolism WP240	0.08001	0.8993	3.38	8.53
GPCRs, Class C Metabotropic glutamate, pheromone WP327	0.08001	0.8993	3.38	8.53
Notch Signaling Pathway WP29	0.03697	0.8993	2.43	8.01
Hypothetical Network for Drug Addiction WP1246	0.05905	0.8993	2.60	7.36
Myometrial Relaxation and Contraction Pathways WP385	0.01846	0.5814	1.81	7.22
Splicing factor NOVA regulated synaptic proteins WP1983	0.06670	0.8993	2.25	6.10
Glycolysis and Gluconeogenesis WP157	0.05961	0.8993	2.15	6.07

Database: Reactome 2016 pathways

Name	P value	Adj P value	Z score	Combined score
LGI-ADAM interactions Homo sapiens R- HSA-5682910	0.00001635	0.002766	13.56	149.41
Neuronal System Homo sapiens R-HSA- 112316	4.75E-12	4.818E-09	3.62	119.32

Acetylcholine Neurotransmitter Release Cycle Homo sapiens R-HSA-264642	0.00007705	0.006016	9.49	89.86
Ras activation upon Ca ²⁺ influx through NMDA receptor Homo sapiens R-HSA-442982	0.00007705	0.006016	9.49	89.86
Serotonin Neurotransmitter Release Cycle Homo sapiens R-HSA-181429	0.0001186	0.007522	8.62	77.97
Transmission across Chemical Synapses Homo sapiens R-HSA-112315	3.76E-07	0.000191	3.43	74.37
CREB phosphorylation through the activation of CaMKII Homo sapiens R-HSA-442729	0.0003105	0.01854	9.03	72.94
Trafficking of AMPA receptors Homo sapiens R-HSA-399719	0.00002746	0.003325	6.46	67.90
Glutamate Binding, Activation of AMPA Receptors and Synaptic Plasticity Homo sapiens R-HSA-399721	0.00002746	0.003325	6.46	67.90
Phase 1 - inactivation of fast Na ⁺ channels Homo sapiens R-HSA-5576894	0.00005185	0.005263	6.78	66.94

Database: GO Biological Process 2018

				-
Name	P value	Adj P value	Z score	Combined score
Long-term synaptic potentiation (GO:0060291)	3.00E-05	0.00002299	14.95	259.01
Neurotransmitter receptor diffusion trapping (GO:0099628)	0.00007290	0.008932	22.57	214.97
Post-synaptic neurotransmitter receptor diffusion trapping (GO:0098970)	0.00007290	0.008932	22.57	214.97
Positive regulation of synaptic transmission (GO:0050806)	6.06E-09	0.00001856	7.65	197.50
Regulation of AMPA receptor activity (GO:2000311)	1.75E-04	0.00007663	11.50	178.92
Regulation of cation channel activity (GO:2001257)	2.52E-08	0.00003866	6.99	170.68
Regulation of glutamate receptor signaling pathway (GO:1900449)	7.64E-05	0.00004679	9.31	152.57
Regulation of synaptic vesicle exocytosis (GO:2000300)	0.000006968	0.001255	12.06	143.17
Regulation of neurotransmitter receptor activity (GO:0099601)	1.18E-04	0.00006028	8.84	141.08
Post-synaptic density assembly (GO:0097107)	0.0006670	0.04594	18.04	131.92

Database: GO Molecular Function 2018

Name	P value	Adj P value	Z score	Combined score
Tau-protein kinase activity (GO:0050321)	0.00001760	0.004143	20.32	222.48
Phosphatidylinositol transporter activity (GO:0008526)	0.001261	0.08903	13.53	90.32
Syntaxin-1 binding (GO:0017075)	0.0003105	0.02986	9.03	72.94
Clathrin light chain binding (GO:0032051)	0.005596	0.1975	13.52	70.11
Histone-arginine N-methyltransferase activity (GO:0008469)	0.002146	0.1210	10.82	66.50

NMDA glutamate receptor activity (GO:0004972)	0.009292	0.2734	10.14	47.44
Syntaxin binding (GO:0019905)	0.00001536	0.004143	3.86	42.76
Voltage-gated cation channel activity (GO:0022843)	0.00001364	0.004143	3.41	38.18
Protein-arginine omega-N asymmetric methyltransferase activity (GO:0035242)	0.01411	0.3435	8.11	34.56
Protein-arginine N-methyltransferase activity (GO:0016274)	0.007132	0.2398	6.76	33.4

Database: Disease Perturbation from GEO Down

Name	P value	Adj P value	Z score	Combined score
Huntington's disease DOID-12858 mouse GSE3621 sample 703	7.95E-33	6.652E-30	-1.69	125.21
Huntington's disease DOID-12858 mouse GSE3621 sample 702	7.10E-28	1.486E-25	-1.74	108.82
Huntington's disease DOID-12858 mouse GSE3621 sample 704	5.07E-28	1.414E-25	-1.7	107.16
Cerebral Infarction C0007785 mouse GSE63 sample 262	3.46E-29	1.448E-26	-1.59	104.42
Gamma-hydroxybutyric acidemia C0268631 mouse GSE2866 sample 205	7.37E-26	1.234E-23	-1.69	97.58
Bipolar Disorder 3312 human GSE12654 sample 461	2.25E-25	3.139E-23	-1.62	91.72
Amyotrophic lateral sclerosis DOID-332 mouse GSE3343 sample 685	2.27E-22	2.713E-20	-1.61	80.2
Depression 1596 human GSE12654 sample 462	1.03E-21	1.081E-19	-1.63	78.53
Alexander Disease C0270726 mouse GSE977 sample 87	9.08E-19	8.442E-17	-1.71	70.97
Huntington's disease DOID-12858 mouse GSE3248 sample 722	8.32E-18	6.967E-16	-1.67	65.78

Database: Single Gene Perturbations from GEO down

Name	P value	Adj P value	Z score	Combined score
Psap hypomorphic prosaposin deficiency mouse GSE8307 sample 2498	1.30E-55	3.171E-52	-1.88	237.51
Htt Knock-in mouse GSE19780 sample 768	1.36E-47	1.663E-44	-1.85	199.24
Htt Huntington's Disease mutation mouse GSE857 sample 2514	6.22E-39	5.067E-36	-1.73	152.53
Htt Mutation mouse GSE3621 sample 2926	7.95E-33	4.86E-30	-1.92	141.69
Nfe2l2 KO mouse GSE18344 sample 1258	7.54E-28	2.305E-25	-2.16	134.69
Htt Mutation mouse GSE3621 sample 2928	5.07E-28	2.066E-25	-1.89	118.59
Psap hypomorphic prosaposin deficiency mouse GSE8307 sample 2509	1.71E-28	8.35E-26	-1.78	113.93
Acvrl1 mouse GSE3621 sample 2925	7.10E-28	2.305E-25	-1.8	112.34
Psap KO mouse GSE8307 sample 2491	1.44E-27	3.921E-25	-1.75	107.95
Nfe2l2 KO mouse GSE18344 sample 1259	2.24E-23	4.573E-21	-2.07	107.74

Supplementary Table 2. According to DAVID Server tool, top downregulated terms in HD-sRNA-PT- versus vehicle-injected mice and not significantly altered in CTL-sRNA-PT- versus vehicle-injected animals. Table shows the top ten terms enriched in multiple databases.

Functional annotation

Category	Term	Count	%	P value	Benjamini
UP_KEYWORDS	Synapse	83	7.1	1.7E-28	7.6E-26
UP_KEYWORDS	Membrane	580	49.4	3.5E-22	7.7E-20
UP_KEYWORDS	Cell junction	105	8.9	3.4E-21	5.1E-19
GOTERM_CC_DIRECT	Cell junction	85	7.2	2.3E-20	1.3E-17
GOTERM_CC_DIRECT	Post-synaptic density	50	4.3	3.0E-19	8.4E-17
UP_KEYWORDS	Methylation	123	10.5	4.8E-16	5.3E-14
GOTERM_CC_DIRECT	Post-synaptic membrane	48	4.1	3.7E-15	6.9E-13
UP_KEYWORDS	Phosphoprotein	593	50.5	1.2E-14	1.0E-12
UP_KEYWORDS	Post-synaptic cell membrane	41	3.5	4.6E-14	3.4E-12
GOTERM_CC_DIRECT	Dendrite	60	5.1	8.8E-14	1.2E-11

Supplementary Table 3. According to EnrichR tool, top upregulated terms in HD-sRNA-PT- versus vehicle-injected mice and not significantly altered in CTL-sRNA-PT- versus vehicle-injected animals. Table shows the top ten terms enriched in multiple databases.

Database: KEGG 2019 mouse

Name	P value	Adj P value	Z score	Combined score
Legionellosis	9.832E-07	0.0000449	6.62	137.37
Toll-like receptor signaling pathway	4.53E-09	5.234E-07	5.07	132.31
TNF signaling pathway	5.73E-09	5.234E-07	4.86	125.79
NF-kappa B signaling pathway	3.61E-08	0.000002473	5.07	121.80
IL-17 signaling pathway	9.87E-08	0.000005409	4.98	114.83
Malaria	2.50E-05	0.00076	6.28	109.98
Cytokine-cytokine receptor interaction	7.27E-12	1.991E-09	3.28	106.73
Pertussis	1.90E-04	0.000004510	4.31	66.68
Measles	6.54E-06	0.0002238	3.52	66.34
Amoebiasis	9.25E-05	0.000002534	3.89	63.01

Database: Wikipathways 2019 mouse

Name	P value	Adj P value	Z score	Combined score
TYROBP Causal Network WP3625	1.67E-12	2.424E-10	9.98	339.41
Apoptosis Modulation by HSP70 WP166	4.64E-04	0.00001346	14.12	205.91
Apoptosis WP1254	3.02E-07	0.00002188	5.26	115.31
Type II interferon signaling (IFNG) WP1253	7.30E-04	0.00001512	6.93	97.91
Osteoclast WP454	0.0001080	0.001044	9.87	90.13
Lung fibrosis WP3632	5.38E-05	0.00001948	5.21	87.22
Spinal Cord Injury WP2432	2.64E-06	0.0001276	4.33	85.52
Matrix Metalloproteinases WP441	0.00002892	0.0003226	6.04	63.12
Toll Like Receptor signaling WP88	0.00002069	0.0002500	5.65	60.94
Microglia Pathogen Phagocytosis Pathway WP3626	0.000009942	0.0001311	5.13	59.10

Database: Reactome 2016 pathways

Name	P value	Adj P value	Z score	Combined score
MyD88 deficiency (TLR2/4) Homo sapiens R-HSA-5602498	4.42E-07	0.00005446	98.87	2129.60
IRAK4 deficiency (TLR2/4) Homo sapiens R-HSA-5603041	4.42E-07	0.00005446	98.87	2129.60
TRIF-mediated programmed cell death Homo sapiens R-HSA-2562578	0.000005271	0.0002246	23.03	279.89
Diseases associated with the TLR signaling cascade Homo sapiens R-HSA-5602358	2.50E-06	0.0002131	13.87	274.63
Diseases of Immune System Homo sapiens R-HSA-5260271	2.50E-06	0.0002131	13.87	274.63
Activation of NIMA Kinases NEK9, NEK6, NEK7 Homo sapiens R-HSA-2980767	0.0001193	0.002939	24.65	222.67
Chemokine receptors bind chemokines Homo sapiens R-HSA-380108	2.98E-08	0.000006592	7.46	180.81
Extracellular matrix organization Homo sapiens R-HSA-1474244	4.97E-15	2.753E-12	3.72	148.33
Phosphorylation of Emi1 Homo sapiens R-HSA-176417	0.0009316	0.01613	19.71	137.54
CLEC7A/inflammasome pathway Homo sapiens R-HSA-5660668	0.0009316	0.01613	19.71	137.5

Database: GO Molecular Function 2018

Name	P value	Adj P value	Z score	Combined score
Toll-like receptor binding (GO:0035325)	0.000001719	0.0001869	34.55	458.56
C-C chemokine binding (GO:0019957)	0.00001458	0.001110	29.60	329.57
Chemokine receptor activity (GO:0004950)	4.91E-05	0.00001246	13.19	222.00
Chemokine binding (GO:0019956)	4.64E-04	0.00008833	14.12	205.91

G-protein coupled chemoattractant receptor activity (GO:0001637)	0.000001426	0.0001808	14.82	199.47
Collagen binding (GO:0005518)	3.49E-08	0.00001327	7.89	189.87
Cytokine receptor activity (GO:0004896)	2.67E-09	0.000002031	6.57	175.06
Cysteine-type endopeptidase activity involved in execution phase of apoptosis (GO:0097200)	0.000009368	0.0008911	13.17	152.43
Cysteine-type endopeptidase activity involved in apoptotic process (GO:0097153)	0.00003390	0.002150	9.87	101.61
CXCR chemokine receptor binding (GO:0045236)	0.00005884	0.003054	8.78	85.4

Supplementary Table 4. According to DAVID Server tool, top upregulated terms in HD-sRNA-PT- versus vehicle-injected mice and not significantly altered in CTL-sRNA-PT- versus vehicle-injected animals. Table shows the top ten terms enriched in multiple databases.

Functional annotation

Category	Term	Count	%	P value	Benjamini
GOTERM_BP_DIRECT	Inflammatory response	128	9.9	2.5E-53	1.1E-49
UP_KEYWORDS	Immunity	124	9.6	1.8E-41	8.4E-39
UP_KEYWORDS	Polymorphism	968	74.6	3.6E-40	8.2E-38
UP_KEYWORDS	Disulfide bond	387	29.8	1.4E-35	2.1E-33
UP_SEQ_FEATURE	Glycosylation site:N-linked (GlcNAc)	451	34.8	6.3E-35	2.0E-31
UP_SEQ_FEATURE	Sequence variant	983	75.8	1.2E-34	2.0E-31
UP_KEYWORDS	Glycoprotein	469	36.2	1.5E-34	1.7E-32
UP_KEYWORDS	Innate immunity	81	6.2	1.9E-34	1.7E-32
UP_SEQ_FEATURE	Disulfide bond	342	26.4	5.5E-33	6.1E-30
UP_SEQ_FEATURE	Signal peptide	375	28.9	1.9E-32	1.6E-29

Supplementary Table 5. According to EnrichR tool, top upregulated terms in HD-sRNA-PT- versus CTL-sRNA-PT-injected mice. Table shows the top ten terms enriched in multiple databases.

Database: KEGG 2019 mouse

Name	P value	Adj P value	Z score	Combined score
Salmonella infection	0.000199	0.000007563	28.06	432.88
Malaria	0.00001928	0.0002017	28.98	314.65
Prion diseases	0.0001824	0.0009903	31.07	267.47
Rheumatoid arthritis	0.000007852	0.0001989	20.95	246.21
Cytosolic DNA-sensing pathway	0.00004613	0.0003506	22.87	228.32

IL-17 signaling pathway	0.00001162	0.0002017	19.23	218.54
Cytokine-cytokine receptor interaction	3.33E-05	0.000002528	12.67	218.18
Toll-like receptor signaling pathway	0.00001752	0.0002017	17.59	192.64
Chagas disease (American trypanosomiasis)	0.00002123	0.0002017	16.87	181.50
Pertussis	0.0001093	0.0006925	18.09	165.00

Database: Wikipathways 2019 mouse

Name	P value	Adj P value	Z score	Combined score
Lung fibrosis WP3632	0.000001602	0.00004807	29.58	394.74
Cytokines and Inflammatory Response WP222	0.00009063	0.0006797	40.14	373.68
Iron Homeostasis WP1596	0.001063	0.005313	48.65	333.10
IL-1 Signaling Pathway WP37	0.0002352	0.001411	28.32	236.63
Spinal Cord Injury WP2432	0.00001752	0.0002628	17.59	192.64
Chemokine signaling pathway WP2292	0.00003522	0.0003522	10.92	111.93
Type II interferon signaling (IFNG) WP1253	0.005456	0.02338	19.75	102.89
Biogenic Amine Synthesis WP522	0.04767	0.1589	22.23	67.66
Hypertrophy Model WP202	0.06306	0.1892	16.38	45.26
Matrix Metalloproteinases WP441	0.09014	0.1995	11.11	26.73

Database: Reactome 2016 pathways

Name	P value	Adj P value	Z score	Combined score
Interleukin-1 processing Homo sapiens R-HSA-448706	0.0002161	0.003890	126.54	1067.95
Chemokine receptors bind chemokines Homo sapiens R-HSA-380108	2.66E-05	0.000002394	40.44	705.44
Interferon alpha/beta signaling Homo sapiens R-HSA-909733	0.000002759	0.0001242	26.29	336.47
CLEC7A/inflammasome pathway Homo sapiens R-HSA-5660668	0.01934	0.1216	62.28	245.72
Transport of nucleosides and free purine and pyrimidine bases across the plasma membrane Homo sapiens R-HSA-83936	0.02253	0.1216	51.90	196.84
Histidine catabolism Homo sapiens R- HSA-70921	0.02253	0.1216	51.90	196.84
Interleukin-1 signaling Homo sapiens R- HSA-446652	0.0003945	0.005663	23.48	184.02
MAPK1 (ERK2) activation Homo sapiens R-HSA-112411	0.02888	0.1254	38.92	137.96
Regulation of gene expression by Hypoxia-inducible Factor Homo sapiens R-HSA-1234158	0.03204	0.1254	34.59	119.03
MAPK3 (ERK1) activation Homo sapiens R-HSA-110056	0.03204	0.1254	34.59	119.03

Database: GO Biological Process 2018

Name	P value	Adj P value	Z score	Combined score
Regulation of natural killer cell chemotaxis (GO:2000501)	3.53E-06	0.0007328	435.67	8479.17
Negative regulation of bone mineralization (GO:0030502)	0.000005306	0.0002204	120.53	1463.99
Response to type I interferon (GO:0034340)	0.0002161	0.004024	126.54	1067.95
Negative regulation of biomineral tissue development (GO:0070168)	0.00001162	0.0004526	87.64	995.83
Positive regulation of leukocyte chemotaxis (GO:0002690)	1.04E-06	0.0004053	44.43	918.93
Eosinophil migration (GO:0072677)	0.000001028	0.00006404	65.30	900.29
Eosinophil chemotaxis (GO:0048245)	0.000001028	0.00006404	65.30	900.29
Positive regulation of interleukin-2 biosynthetic process (GO:0045086)	0.0002876	0.004745	105.44	859.80
Regulation of T-helper 2 cell cytokine production (GO:2000551)	0.0002876	0.004745	105.44	859.80
Lipopolysaccharide-mediated signaling pathway (GO:0031663)	0.00001780	0.0006161	74.15	810.94

Database: GO Molecular Function 2018

Name	P value	Adj P value	Z score	Combined score
Chemokine activity (GO:0008009)	3.83E-04	0.00001376	40.43	597.40
Chemokine receptor binding (GO:0042379)	5.29E-04	0.00001376	37.67	544.43
CCR chemokine receptor binding (GO:0048020)	0.000006901	0.0001346	38.38	456.12
Interleukin-1 receptor binding (GO:0005149)	0.001063	0.01658	48.65	333.10
Cytokine activity (GO:0005125)	3.77E-05	0.000002939	18.89	322.96
Bile acid:sodium symporter activity (GO:0008508)	0.01934	0.1114	62.28	245.72
Phospholipase activator activity (GO:0016004)	0.01934	0.1114	62.28	245.72
Interleukin-6 receptor binding (GO:0005138)	0.02253	0.1114	51.90	196.84
Lipase activator activity (GO:0060229)	0.02253	0.1114	51.90	196.84
RNA-directed DNA polymerase activity (GO:0003964)	0.02571	0.1114	44.48	162.84

Supplementary Table 6. According to DAVID Server tool, top upregulated terms in HD-sRNA-PT- versus CTL-sRNA-PT-injected mice. Table shows the top ten pathways enriched in multiple databases.

Functional annotation

Category	Term	Count	%	P value	Benjamini
GOTERM_BP_DIRECT	Immune response	11	33.3	2.4E-9	1.1E-6
KEGG_PATHWAY	Cytokine-cytokine receptor interaction	10	30.3	5.0E-9	3.1E-7
UP_KEYWORDS	Cytokine	8	24.2	1.4E-8	1.6E-6
GOTERM_BP_DIRECT	Inflammatory response	10	30.3	1.8E-8	4.1E-6
GOTERM_BP_DIRECT	Response to virus	7	21.2	4.4E-8	6.8E-6
UP_KEYWORDS	Inflammatory response	7	21.2	1.1E-7	6.5E-6
GOTERM_BP_DIRECT	Neutrophil chemotaxis	6	18.2	1.3E-7	1.4E-5
GOTERM_BP_DIRECT	Chemokine-mediated signaling pathway	6	18.2	1.8E-7	1.7E-5
GOTERM_CC_DIRECT	Extracellular region	14	42.4	8.6E-7	5.3E-5
INTERPRO	Chemokine interleukin-8-like domain	5	15.2	9.9E-7	1.2E-4

Supplementary Table 7. Differentially expressed tsRNA sequences in HD-ssRNA-PT versus CTL-ssRNA-PT samples in non-treated conditions. Significantly DE tsRNA sequences are shown (Adjusted P < 0.05).

Туре	Isoacceptor	tsRNA sequence	log2FoldChange	P value	Adjusted P
5'-half	ProCGG	GGCTCGTTGGTCTAGGGGTATGATTCTCGCTT	5.757384928	7.23E-13	6.62E-11
5'-half	ValTAC	GGTTCCATAGTGTAGCGGTTATCACGTCTGCTTT	5.201117801	3.26E-13	3.98E-11
5'-half	ValTAC	GGTTCCATAGTGTAGTGGTTATCACGTCTGCTTT	4.570807936	3.37E-10	2.47E-08
i-tRF	GlyCCC	CATTCTTGCGACCCGGGTT	4.009309159	9.67E-06	0.000153019
5'-half	ValTAC	GGTTCCATAGTGTAGTGGTTATCACATCTGCTTT	4.007644759	6.28E-09	2.55E-07
5'-half	AspGTC	TCCTCGTTAGTATAGTGGTTAGTATCCCCGCCTGT	4.000207577	1.01E-14	1.85E-12
5'-half	ValTAC	GGTTCCATAGTGTAGCGGTTATCACGTCTGCTT	3.903881155	3.53E-07	9.30E-06
3'-tRF	AspGTC	CGGGAGACCGGGGTTCGATTCCCCGACGGGGAGC	3.810646964	2.21E-15	8.08E-13
5'-half	AspGTC	TCCTCGTTAGTATAGTGGTGAGTATCCCCGCCTGT	3.526687256	1.81E-09	1.10E-07
5'-half	GlyCCC	GCGCCGCTGGTGTAGTGGTATCATGCAAGATT	3.363874186	3.67E-09	1.92E-07
5'-half	GluCTC	TCCCTGGTGGTCTAGTGGTTAGGATTCGGCGCT	3.217425225	2.12E-06	3.88E-05
5'-tRF	LeuAAG	GGTAGCGTGGCCGAGCGGTCT	3.095161372	0.001756288	0.010395306
5'-half	ValTAC	GGTTCCATAGTGTAGCGGTTATCACGTCTGCT	3.085355213	4.54E-05	0.000592876
5'-half	LysCTT	GCCCGGCTAGCTCAGTCGGTAGAGCATGAGACT	2.977268243	2.04E-07	6.22E-06
5'-tRF	AlaAGC	GGGGGATTAGCTCAAATGG	2.961968922	0.00191128	0.010901018
5'-half	ValTAC	GGTTCCATAGTGTAGTGGTTATCACGTCTGCT	2.950029323	5.59E-05	0.000682248
5'-half	LysCTT	GCCCGGCTAGCTCAGTCGGTAGAGCATGAGACC	2.776304549	1.24E-06	2.53E-05
5'-tRF	AsnGTT	GTCTCTGTGGCGCAATCGG	2.733926465	0.001257933	0.008370975
5'-half	ValTAC	GGTTCCATAGTGTAGTGGTTATCACGTCTGCTT	2.717426755	0.000196687	0.001999651
5'-half	GluTTC	TCCCACATGGTCTAGCGGTTAGGATTCCTGGTTTT	2.526834142	8.51E-05	0.000916474
5'-half	GluTTC	TCCCACATGGTCTAGCGGTTAGGATTCCTGGTT	2.405499253	0.002336978	0.012396142
5'-half	GlyGCC	GCATTGGTGGTTCAGTGGTAGAATTCTCGCCT	2.395699068	0.000232614	0.00218299
3'-tRF	AspGTC	GCGGGAGACCGGGGTTCGATTCCCCGACGGGGAGC	2.38462194	3.56E-07	9.30E-06
5'-half	ValTAC	GGTTCCATAGTGTAGTGGTTATCACATCTGCT	2.364958897	0.000972675	0.006846139
5'-tRF	AspGTC	TCCTCGTTAGTATAGTGGTTAGTATCCCCGCCTGTC	2.362483452	4.52E-06	7.53E-05
i-tRF	GlyCCC	CATTCTTGCGACCCGGGT	2.356273883	0.008192782	0.033172561

5'-half	ValTAC	GGTTCCATAGTGTAGTGGTTATCACATCTGCTT	2.189801485	0.001227658	0.008320794
5'-tRF	ValCAC	GTTTCCGTAGTGTAGCGGTTATCACATT	2.03295774	5.20E-05	0.000656091
3'-tRF	AspGTC	CGGGAGACCGGGGTTCGATTCCCCGACGGGGAGCC	1.993318209	7.89E-05	0.000874627
5'-half	GlyGCC	GCATTGGTGGTTCAGTGGTAGAATTCTCGCCTGC	1.9752392	0.002188357	0.011954306
5'-tRF	GluTTC	TCCCACATGGTCTAGCGGTTAGGATT	1.950398782	0.000439596	0.003581701
5'-half	GluTTC	TCCCATATGGTCTAGCGGTTAGGATTCCTGGTT	1.922420011	0.011192679	0.039772043
5'-half	GluTTC	TCCCACATGGTCTAGCGGTTAGGATTCCTGGTTT	1.89849904	0.004436555	0.020297238
5'-half	LysCTT	GCCCGGCTAGCTCAGTCGGTAGAGCATGGGACT	1.890392145	0.006579856	0.028002642
5'-half	GluTTC	TCCCACATGGTCTAGCGGTTAGGATTCCTGGT	1.850650595	0.008829132	0.033999309
5'-tRF	ArgTCT	GGCTCCGTGGCGCAATGG	1.801283711	0.001806444	0.01049458
5'-tRF	AspGTC	TCCTCGTTAGTATAGTGGTGAGTATCCCCGCCTGTC	1.797092269	0.003094493	0.015305195
3'-tRF	GluTTC	CAGGCGGCCCGGGTTCGACTCCCGGTGTGGGAAC	1.790450874	0.005094143	0.02301798
5'-half	ValCAC	GCTTCTGTAGTGTAGTGGTTATCACGTTCGCCT	1.75397465	0.006676499	0.028087341
3'-tRF	AspGTC	GGGAGACCGGGGTTCGATTCCCCGACGGGGAGC	1.746617631	0.001395657	0.008807075
i-tRF	GInTTG	GTAATGGTTAGCACTCTGGACT	1.684219827	0.008750637	0.033999309
5'-tRF	TrpCCA	GACCTCGTGGCGCAACGG	1.566909543	0.009859919	0.037190604
3'-tRF	GluTTC	GCCGCGGCCCGGGTTCGATTCCCGGTCAGGGAACC	1.429600789	0.008368305	0.033291299
5'-half	LysTTT	GCCCGGATAGCTCAGTCGGTAGAGCATCAGACT	1.424705164	0.012584905	0.04345354
5'-tRF	GlyCCC	GCGCCGCTGGTGTAGTGGTATCATGCA	1.302433892	0.010782732	0.039464798
3'-tRF	PheGAA	TCGATCCCGGGTTTCGGCACCA	-1.444247918	0.013995079	0.047427766
5'-tRF	ArgTCT	GGCTCTGTGGCGCAATGGA	-1.509043804	0.014880234	0.049964821
3'-tRF	LeuTAA	AACCCCACTCCTGGTACCA	-1.554359846	0.012195134	0.042508752
5'-tRF	ValTAC	GGTTCCATAGTGTAGCGGTTATCACGTCTGCTTTAC	-1.58747015	0.00165543	0.010098123
5'-half	ValCAC	GTTTCCGTAGTGTAGCGGTTATCACATTCGCC	-1.76522728	0.002491998	0.013029589
i-tRF	GInCTG	TAGCACTCTGGACTCTGAATCC	-1.789538383	0.001935973	0.010901018
5'-half	ValTAC	GGTTCCATAGTGTAGTGGTTATCACGTCTGCTTTA	-1.822719814	0.003913721	0.018722897
3'-tRF	ArgACG	TCGACTCCTGGCTGGCTCGCCA	-1.82410336	0.01325576	0.045342132
i-tRF	HisGTG	TGGTTAGTACTCTGCGTTGTG	-1.891548595	0.00995814	0.037190604
5'-half	GlyGCC	GCATGGGTGGTTCAGTGGTAGAATTCTCGCC	-1.899818054	0.002905087	0.014565232
5'-half	LysCTT	GCCCGGCTAGCTCAGTCGGTAGAGCATGGGACTC	-1.939577247	0.008727425	0.033999309
i-tRF	HisGTG	GGTTAGTACTCTGCGTTG	-1.98045021	0.00774422	0.032208917
3'-tRF	HisGTG	TCGAATCCGAGTCACGGCACCA	-1.985155648	0.001760953	0.010395306
5'-tRF	ValAAC	GTTTCCGTAGTGTAGTGGT	-2.029214468	0.001322879	0.008494275
5'-tRF	ValCAC	GTTTCCGTAGTGTAGTGGTTATCACGTTCGC	-2.095764547	1.18E-05	0.000173274
i-tRF	GInCTG	TAGCACTCTGGACTCTGAATCCA	-2.122778391		0.012349906
3'-tRF	AlaCGC	CGATCCCCGGCATCTCCACC	-2.128828893	0.011785672	0.041476498
5'-half	ValAAC	GTTTCCGTAGTGTAGTGGTCATCACGTTCGCC	-2.129756229	0.004028424	0.018902604
5'-half	AspGTC	TCCTCGTTAGTATAGTGGTTAGTATCCCCGCCTG	-2.183862063	0.000884108	0.006603742
3'-tRF	GlyCCC	ATTCTTGCGACCCGGGTTCGATTCCCGGGCGCGCACC	-2.196931869	0.00393897	0.018722897
5'-half	GlyCCC	GCGCCGCTGGTGTAGTGGTATCATGCAAGATTCC	-2.206626711	0.001580932	0.009807137
5'-half	ValAAC	GTTTCCGTAGTGTAGTGGTTATCACGTTCGCC	-2.215878704		0.005783414
3'-tRF	lleGAT	AAACCCCCTTATTTCTACC	-2.22116065		0.033999309
5'-half	ValAAC	GTTTCCGTAGTGTAGTGGTTATCACGTTCGCCTA	-2.240030569		0.039772043
3'-tRF	LeuCAA	TCGAATCCCACTTCTGACACCA	-2.248718179		0.018913308
i-tRF	GluCTC	AGTGGTTAGGATTCGGCGC	-2.261877481		0.039464798
5'-tRF	GlyCCC	GCGCCGCTGGTGTAGTGGTATCATGCAAGATTCCC	-2.280441879		0.003581701
3'-tRF	ValTAC	ACGCAGAAGGTCCTGGGTTCGAGCCCCAGTGGAACCACC	-2.353071778		0.024102375
i-tRF	GluCTC	CTAGTGGTTAGGATTCGGCGCTCT	-2.401920167		0.008184669
i-tRF	GInCTG	TAGCACTCTGGACTCTGAATC	-2.41061746		0.011756724
3'-tRF	AlaTGC	CCCGGGTTCGATCCCCGGCATCTCCACCA	-2.523112038		0.033036443
3'-tRF	GlyCCC	ATTCTTGCGACCCGGGTTCGATTCCCGGGCGCGCAC	-2.528614921	0.00095608	
3'-tRF	ArgACG	CGACTCCTGGCTGGCTCGCCA	-2.53160267		0.033172561
3'-tRF	GlnCTG	CAAATCTCGGTGGAACCTCCA	-2.580125172		0.016801017
i-tRF	GINTTG	TTAGCACTCTGGACTTTG	-2.593864812		0.010301017
i-tRF	GINTTG	TGGTTAGCACTCTGGACTC	-2.593004612		0.003381701
5'-tRF	ArgACG	GGGCCAGTGGCGCAATGGA	-2.594004591		0.013227538
3'-half					
	MetCAT	TAATCTGAAGGTCCTGAGTTCGAACCTCAGAGGGGGCACC	-2.632056039		0.024102375
i-tRF	HisGTG	AGTGGTTAGTACTCAGCGAGGA	-2.6980729		0.039772043
3'-tRF	HisGTG	CGAATCCGCGTCGAACCACCA	-2.727828583		0.008468282
3'-tRF	TyrGTA	CGATTCCGGCTCGAAGGACCA	-2.742862944	0.005021298	0.024204647

i-tRF	HisGTG	AGTGGTTAGTACTCTGCGTTGTG	-2.779826773	0.000954528	0.006846139
3'-tRF	ArgACG	TTCGACTCCTGGCTGGCTCGCCA	-2.797862652	6.51E-05	0.000744957
i-tRF	GlyGCC	GTAGAATTCTCGCCTGCC	-2.803770905	0.005317205	0.023732889
3'-tRF	MetCAT	ATACCCTTCCCGTACTACC	-2.937454103	0.000850211	0.006482861
i-tRF	GInCTG	TTAGCACTCTGGACTCTG	-2.940034365	0.000510086	0.00405851
3'-tRF	PheGAA	GTTCGATCCCGGGTTTCGGCACCA	-2.945741159	2.34E-06	4.08E-05
5'-tRF	ArgCCG	GACCCAGTGGCCTAATGGA	-2.995180756	0.000225201	0.00216904
i-tRF	HisGTG	ATAGTGGTTAGTACTCTGCGTTG	-3.011503175	0.002661197	0.013527752
3'-tRF	SerTGA	GAATCCTGCCGACTACGCCA	-3.065958559	0.000278885	0.002551795
5'-tRF	ValCAC	GTTTCCGTAGTGTAGCGGTTATCACATTCGCCTCAC	-3.136083774	2.86E-05	0.000402005
5'-half	LysCTT	GCCCGGCTAGCTCAGTCGGTAGAGCATGAGACTC	-3.195211305	4.25E-08	1.56E-06
5'-half	LysCTT	GCCCGGCTAGCTCAGTCGGTAGAGCATGAGAC	-3.215633766	6.20E-07	1.51E-05
i-tRF	HisGTG	TATAGTGGTTAGTACTCTGCGTTGTG	-3.220368549	9.68E-05	0.001012311
i-tRF	LysTTT	AGTCGGTAGAGCATCAGAC	-3.295793127	1.98E-06	3.81E-05
3'-tRF	AlaTGC	GATCCCCGGCATCTCCACCA	-3.413877135	0.000202717	0.002005251
3'-tRF	PheGAA	TTCGATCCCGGGTTTCGGCACCA	-3.424361656	5.00E-09	2.29E-07
i-tRF	GlyGCC	ATTGGTGGTTCAGTGGTAGAATTCTCGCC	-3.442979232	6.09E-05	0.000718937
5'-tRF	ArgTCG	GACCACGTGGCCTAATGGA	-3.457942684	4.14E-05	0.000561249
3'-tRF	PheGAA	CGATCCCGGGTTTCGGCACCA	-3.491080371	6.96E-08	2.32E-06
5'-tRF	ValCAC	GTTTCCGTAGTGTAGTGGTTATCACGTTCGCCTCAC	-3.509729453	1.14E-06	2.44E-05
3'-half	MetCAT	TAATCTGAAGGTCGTGAGTTCGAGCCTCACACGGGGCACC	-3.543405066	0.000414186	0.003581701
3'-tRF	LeuCAG	CGAATCCCACTTCTGACACCA	-3.573772961	1.00E-05	0.000153019
5'-half	ValCAC	GTTTCCGTAGTGTAGCGGTTATCACATTCGCCTCA	-4.034194655	7.46E-07	1.71E-05

Supplementary Table 8. Differentially expressed tsRNA sequences in HD-ssRNA-PT versus CTL-ssRNA-PT samples in T4PNK-treated conditions. Significantly DE tsRNA sequences are shown (Adjusted P < 0.05).

Туре	Isoacceptor	tsRNA sequence	log2FoldChange	P value	Adjusted P
i-tRF	GInTTG	AATCCAGCGATCCGAGTTC	3.627629246	1.46E-08	2.72E-06
3'-tRF	SerTGA	GAATCCTGCCGACTACGC	2.466487928	3.94E-06	0.000183382
5'-half	ProCGG	GGCTCGTTGGTCTAGGGGTATGATTCTCGCTT	2.463406961	1.90E-05	0.000508281
5'-tRF	ArgTCT	GGCTCCGTGGCGCAATGG	2.428853167	5.02E-05	0.000982611
i-tRF	CysGCA	ATAGCTCAGTGGTAGAGCATTTGACT	2.345885944	0.00014732	0.002107809
i-tRF	GInCTG	CTGAATCCAGCGATCCGAGTTC	2.288489649	3.51E-06	0.000183382
3'-tRF	SerAGA	CGAATCCTGCCGACTACGC	2.257927818	1.20E-06	0.00014839
5'-tRF	ArgTCT	GGCTCCGTGGCGCAATGGA	2.199060238	0.000827822	0.008322966
5'-half	ValTAC	GGTTCCATAGTGTAGCGGTTATCACGTCTGCT	2.184419281	2.37E-06	0.000183382
i-tRF	HisGTG	TGGTTAGTACTCTGCGTTGT	2.146995233	0.008369713	0.047369381
3'-tRF	GlyTCC	CGATTCCCGGCCAACGCACC	2.119782337	3.88E-06	0.000183382
5'-half	ValTAC	GGTTCCATAGTGTAGTGGTTATCACGTCTGCT	2.042082109	2.86E-06	0.000183382
5'-tRF	IleTAT	GCTCCAGTGGCGCAATCGG	2.027499588	2.82E-05	0.000617682
5'-half	ValTAC	GGTTCCATAGTGTAGTGGTTATCACGTCTGCTTT	1.960791471	1.91E-05	0.000508281
i-tRF	HisGTG	AGTGGTTAGTACTCTGCGTTGT	1.941818165	6.24E-05	0.001104528
i-tRF	GInTTG	GGTGTAATGGTTAGCACTCTGGACT	1.923221736	0.000912256	0.008701523
5'-tRF	AspGTC	TCCTCGTTAGTATAGTGGTTAGTATCCCCGCCTGTC	1.92004399	0.000330344	0.003732896
5'-half	ValTAC	GGTTCCATAGTGTAGCGGTTATCACGTCTGCTT	1.851362543	0.00028907	0.003468839
5'-tRF	AspGTC	TCCTCGTTAGTATAGTGGTGAGTATCCCCGCCTGTC	1.80735186	5.97E-05	0.001104528
5'-half	ValTAC	GGTTCCATAGTGTAGCGGTTATCACGTCTGCTTT	1.77385652	0.000722525	0.007679413
3'-tRF	AspGTC	ACGCGGGAGACCGGGGTTCGATTCCCCGACGGGGAGC	1.771658178	1.91E-05	0.000508281
i-tRF	HisGTG	GGTTAGTACTCTGCGTTGT	1.769155212	0.004071006	0.028044705
5'-half	AspGTC	TCCTCGTTAGTATAGTGGTGAGTATCCCCGCCTGT	1.76875278	7.19E-05	0.001214967
i-tRF	GInTTG	GGTTAGCACTCTGGACTT	1.738153627	0.000196179	0.002606375
5'-tRF	AsnGTT	GTCTCTGTGGCGCAATCGG	1.626723649	0.004223057	0.028563222
3'-tRF	AlaTGC	CGATCCCCGGCATCTCCACCA	1.577204494	0.00435245	0.028912706
5'-half	ValTAC	GGTTCCATAGTGTAGTGGTTATCACGTCTGCTT	1.476453388	0.000331144	0.003732896
3'-tRF	AspGTC	ACGCGGGAGACCGGGGTTCAATTCCCCGACGGGGAGC	1.448207264	0.000240853	0.002986573
5'-half	GluCTC	TCCCTGGTGGTCTAGTGGTTAGGATTCGGCGCT	1.42219469	0.001845332	0.014923124

5'-tRF	ValTAC	GGTTCCATAGTGTAGCGGTTATCACGTCTGC	1.341731193	0.006532404	0.041045745
3'-tRF	GlyGCC	CGATTCCCGGCCAATGCACC	1.321500635	0.003157071	0.023028044
5'-half	ValTAC	GGTTCCATAGTGTAGTGGTTATCACATCTGCTTT	1.294409759	0.003259057	0.023314792
3'-tRF	AlaCGC	CGATCCCCGGCATCTCCACC	1.285908357	0.00673062	0.041045745
i-tRF	GInCTG	GGTTAGCACTCTGGACTC	1.275516864	0.002570967	0.019127997
5'-tRF	ValTAC	GGTTCCATAGTGTAGTGGTTATCACGTCTGC	1.270683242	0.006645713	0.041045745
i-tRF	GInTTG	TGGTTAGCACTCTGGACT	1.175143859	0.007776399	0.04520032
i-tRF	GluCTC	AGTGGTTAGGATTCGGCGCTC	-1.157337117	0.00401066	0.028044705
i-tRF	GInCTG	GTTAGCACTCTGGACTCTGAATCC	-1.297945744	0.008404245	0.047369381
5'-tRF	ValTAC	GGTTCCATAGTGTAGTGGTTATCACGTCT	-1.396038103	0.00209741	0.01660078
5'-tRF	TrpCCA	GGCCTCGTGGCGCAACGG	-1.492884895	0.000765612	0.007911329
i-tRF	GluCTC	CTAGTGGTTAGGATTCGGCGCTCT	-1.501722257	0.004488476	0.029293209
3'-tRF	HisGTG	TCGAATCCGAGTCACGGCACC	-1.541357532	0.001219277	0.011062707
5'-tRF	ValCAC	GTTTCCGTAGTGTAGTGGTTATCACGTTC	-1.626619246	0.001113633	0.010356788
5'-tRF	MetCAT	GCCTCCTTAGCGCAGTAGG	-1.63889298	0.001262401	0.011181263
5'-tRF	GlyGCC	GCATGGGTGGTTCAGTGGTAGAATT	-1.765430301	0.002206892	0.017103416
3'-tRF	AspGTC	AAATCCTATATATCTTACCA	-1.801844179	0.00018197	0.002507137
i-tRF	HisGTG	TTAGTACTCTGCGTTGTG	-1.812528399	0.001425745	0.011786155
5'-tRF	SerAGA	GTAGTCGTGGCCGAGTGGTTAAG	-1.856822683	0.007572759	0.044715336
5'-tRF	ArgTCG	GACCACGTGGCCTAATGGA	-1.893627535	0.001354851	0.01145465
5'-tRF	ValCAC	GTTTCCGTAGTGTAGCGGTTATCACATTC	-1.908158536	0.002254843	0.017118402
3'-tRF	SerTGA	CGATTCCTTTTTTGCC	-1.924559279	0.001328661	0.01145465
3'-tRF	AlaTGC	CCCGGGTTCGATCCCCGGCATCTCCACCA	-1.937926775	0.000686735	0.007513693
i-tRF	GInCTG	GGTTAGCACTCTGGACTCTG	-1.972912015	0.007529283	0.044715336
i-tRF	GluCTC	AGTGGTTAGGATTCGGCGCTCT	-2.036357676	3.54E-05	0.000730788
5'-tRF	GInTTG	GGTCCCATGGTGTAATGGTTAGCACTCTG	-2.054831353	0.000855048	0.008370466
3'-tRF	AspGTC	AAATCCTATATATCTTACC	-2.099489443	8.84E-05	0.001370226
i-tRF	GInCTG	ATGGTTAGCACTCTGGACTCTGAATCC	-2.209226455	7.72E-05	0.001248182
5'-half	AspGTC	TCCTCGTTAGTATAGTGGTTAGTATCCCCGCCTG	-2.272530751	5.43E-06	0.000224539
3'-tRF	IleGAT	AAACCCCCTTATTTCTACC	-2.279924775	2.20E-05	0.000544481
3'-tRF	HisGTG	TCGAATCCGAGTCACGGCACCA	-2.300177651	8.42E-06	0.000313133
3'-tRF	GluTTC	GCCGCGGCCCGGGTTCGATTCCCGGTCAGGGAACC	-2.311659957	0.005110025	0.032774641
5'-tRF	LysCTT	GCCCGGCTAGCTCAGTCGGTAGAGCATGGGACTCTT	-2.328044179	0.00014293	0.002107809
i-tRF	MetCAT	ATAATCTGAAGGTCCTGAGT	-2.497896047	2.36E-05	0.000548541
3'-tRF	AlaTGC	GGGTTCGATCCCCGGCATCTCCACCA	-2.810912823	1.40E-05	0.000473269
3'-tRF	AspGTC	GCTAAATCCTATATCTTACCA	-2.965676581	0.000217083	0.002784645
3'-tRF	AspGTC	AGGCTAAATCCTATATATCTTACCA	-3.233928009	2.09E-09	7.77E-07

Supplementary Table 9. Differentially expressed tsRNA sequences in HD-ssRNA-PT versus CTL-ssRNA-PT samples in T4PNK+D-treated conditions. Significantly DE tsRNA sequences are shown (Adjusted P < 0.05).

Туре	Isoacceptor	tsRNA sequence	log2FoldChange	P value	Adjusted P
5'-half	ProCGG	GGCTCGTTGGTCTAGGGGTATGATTCTCGCTT	3.459374063	1.75E-08	3.18E-06
i-tRF	GInTTG	AATCCAGCGATCCGAGTTC	2.929931139	2.94E-07	2.68E-05
5'-tRF	ArgTCT	GGCTCCGTGGCGCAATGG	2.755635132	2.50E-07	2.68E-05
5'-half	ValTAC	GGTTCCATAGTGTAGCGGTTATCACGTCTGCT	2.18980057	1.03E-06	7.48E-05
3'-tRF	AspGTC	GGGAGACCGGGGTTCGATTCCCCGACGGGGAGC	2.178544297	9.17E-05	0.002086049
i-tRF	GInCTG	CTGAATCCAGCGATCCGAGTTC	2.153559703	0.00015993	0.00323414
3'-tRF	AspGTC	GAGACCGGGGTTCGATTCCCCGACGGGGAGC	2.125937167	1.38E-05	0.000556211
5'-half	ValTAC	GGTTCCATAGTGTAGTGGTTATCACGTCTGCT	2.124697922	4.49E-06	0.00027255
i-tRF	CysGCA	ATAGCTCAGTGGTAGAGCATTTGACT	2.052000779	0.00361929	0.030637708
5'-tRF	ArgTCT	GGCTCCGTGGCGCAATGGA	2.038972498	0.000277855	0.005056962
i-tRF	GlyCCC	CATTCTTGCGACCCGGGT	2.00015443	0.003847611	0.031122896
3'-tRF	SerTGA	GAATCCTGCCGACTACGC	1.995083772	0.001529764	0.014653525
5'-half	AspGTC	TCCTCGTTAGTATAGTGGTGAGTATCCCCGCCTGT	1.962261002	4.69E-05	0.001555324
3'-tRF	SerAGA	CGAATCCTGCCGACTACGC	1.858440616	0.000458354	0.006282035
3'-tRF	AspGTC	AGACCGGGGTTCGATTCCCCGACGGGGAGC	1.839001062	0.000698403	0.008140962

5'-tRF	AspGTC	TCCTCGTTAGTATAGTGGTGAGTATCCCCGCCTGTC	1.824433452	1.24E-05	0.000556211
i-tRF	HisGTG	TGGTTAGTACTCTGCGTTGT	1.718426271	0.000480585	0.006282035
5'-tRF	AspGTC	TCCTCGTTAGTATAGTGGTTAGTATCCCCGCCTGTC	1.716153237	0.000461963	0.006282035
i-tRF	GInTTG	GGTGTAATGGTTAGCACTCTGGACT	1.703097377	0.000483233	0.006282035
3'-tRF	AspGTC	ACGCGGGAGACCGGGGTTCGATTCCCCGACGGGGAGC	1.657918554	0.00257322	0.022845169
5'-half	ValTAC	GGTTCCATAGTGTAGCGGTTATCACGTCTGCTT	1.653419237	0.000715689	0.008140962
5'-half	ValTAC	GGTTCCATAGTGTAGCGGTTATCACGTCTGCTTT	1.64086758	0.001085967	0.01162624
5'-half	ValTAC	GGTTCCATAGTGTAGTGGTTATCACGTCTGCTT	1.601292485	0.000470468	0.006282035
i-tRF	HisGTG	AGTGGTTAGTACTCTGCGTTGT	1.60118835	0.001274131	0.013065305
5'-half	ValTAC	GGTTCCATAGTGTAGTGGTTATCACGTCTGCTTT	1.559735128	0.000664548	0.008063181
5'-half	AspGTC	TCCTCGTTAGTATAGTGGTTAGTATCCCCGCCTGT	1.54195951	0.003174078	0.027508672
5'-tRF	ValTAC	GGTTCCATAGTGTAGTGGTTATCACGTCTGC	1.194531525	0.006483656	0.049646265
i-tRF	GInCTG	TTAGCACTCTGGACTCTGAATCC	-1.301017274	0.00596932	0.047235487
5'-tRF	ArgTCG	GACCACGTGGCCTAATGGA	-1.373506191	0.00370983	0.030690409
i-tRF	GluCTC	AGTGGTTAGGATTCGGCGCTCT	-1.423098538	0.001328067	0.013065305
3'-half	GluCTC	CACCGCCGCGGCCCGGGTTCGATTCCCGGTCAGGGAACCA	-1.589362739	0.002319101	0.021644941
5'-tRF	MetCAT	GCCTCCTTAGCGCAGTAGG	-1.59126592	0.00250945	0.022835998
5'-tRF	ArgCCG	GACCCAGTGGCCTAATGGA	-1.640490592	0.001325231	0.013065305
i-tRF	GInCTG	GTTAGCACTCTGGACTCTGAATCC	-1.692660028	0.000431572	0.006282035
5'-tRF	ArgACG	GGGCCAGTGGCGCAATGGA	-1.703387509	0.00654676	0.049646265
3'-tRF	AspGTC	AAATCCTATATATCTTACCA	-1.806492554	0.000646477	0.008063181
3'-tRF	AlaTGC	CCCGGGTTCGATCCCCGGCATCTCCACCA	-1.90169675	8.90E-05	0.002086049
3'-tRF	ValTAC	AGAAGGTCCTGGGTTCGAGCCCCAGTGGAACCACC	-1.90845042	0.000471035	0.006282035
3'-tRF	AlaTGC	GGGTTCGATCCCCGGCATCTCCACCA	-1.925882191	5.99E-05	0.001678484
5'-tRF	GInTTG	GGTCCCATGGTGTAATGGTTAGCACTCTG	-1.990741367	0.000238547	0.004570065
i-tRF	GInCTG	ATGGTTAGCACTCTGGACTCTGAATCC	-2.081021837	4.70E-05	0.001555324
i-tRF	GlyGCC	AGAATTCTCGCCTGCCACG	-2.115327846	0.001036414	0.011431957
3'-tRF	IleGAT	AAACCCCCTTATTTCTACC	-2.144089325	7.84E-05	0.002037169
3'-tRF	AspGTC	AAATCCTATATATCTTACC	-2.166366235	5.16E-05	0.001565754
i-tRF	MetCAT	ATAATCTGAAGGTCCTGAGT	-2.198440097	0.000308789	0.005352336
3'-tRF	SerTGA	CGATTCCTTTTTTGCC	-2.233003987	0.000133938	0.002867853
3'-tRF	AspGTC	GCTAAATCCTATATCTTACCA	-2.969107387	6.38E-06	0.000331611
3'-tRF	AspGTC	AGGCTAAATCCTATATCTTACCA	-3.105191476	6.23E-09	2.27E-06

Acta Neuropathologica (2021) 141:565–584 https://doi.org/10.1007/s00401-021-02272-9

ORIGINAL PAPER



Huntington's disease brain-derived small RNAs recapitulate associated neuropathology in mice

Jordi Creus-Muncunill^{1,2,3,9} · Anna Guisado-Corcoll^{1,2,3} · Veronica Venturi⁴ · Lorena Pantano⁵ · Georgia Escaramís^{1,6} · Marta García de Herreros^{1,2,3} · Maria Solaguren-Beascoa¹ · Ana Gámez-Valero¹ · Cristina Navarrete⁴ · Mercè Masana^{1,2,3} · Franc Llorens^{3,7,8} · Daniela Diaz-Lucena^{3,7} · Esther Pérez-Navarro^{1,2,3} · Eulàlia Martí^{1,4,6}

Received: 12 January 2021 / Revised: 19 January 2021 / Accepted: 20 January 2021 / Published online: 6 February 2021 © The Author(s), under exclusive licence to Springer-Verlag GmbH, DE part of Springer Nature 2021

Abstract

Progressive motor alterations and selective death of striatal medium spiny neurons (MSNs) are key pathological hallmarks of Huntington's disease (HD), a neurodegenerative condition caused by a CAG trinucleotide repeat expansion in the coding region of the huntingtin (HTT) gene. Most research has focused on the pathogenic effects of the resultant protein product(s); however, growing evidence indicates that expanded CAG repeats within mutant HTT mRNA and derived small CAG repeat RNAs (sCAG) participate in HD pathophysiology. The individual contribution of protein versus RNA toxicity to HD pathophysiology remains largely uncharacterized and the role of other classes of small RNAs (sRNA) that are strongly perturbed in HD is uncertain. Here, we demonstrate that sRNA produced in the putamen of HD patients (HD-sRNA-PT) are sufficient to induce HD pathology in vivo. Mice injected with HD-sRNA-PT show motor abnormalities, decreased levels of striatal HD-related proteins, disruption of the indirect pathway, and strong transcriptional abnormalities, paralleling human HD pathology. Importantly, we show that the specific blockage of sCAG mitigates HD-sRNA-PT neurotoxicity only to a limited extent. This observation prompted us to identify other sRNA species enriched in HD putamen with neurotoxic potential. We detected high levels of tRNA fragments (tRFs) in HD putamen, and we validated the neurotoxic potential of an Alanine derived tRF in vitro. These results highlight that HD-sRNA-PT are neurotoxic, and suggest that multiple sRNA species contribute to striatal dysfunction and general transcriptomic changes, favoring therapeutic strategies based on the blockage of sRNA-mediated toxicity.

Keywords RNA toxicity · Striatum · Striatopallidal · CAG repeat · tRFs · Polyglutamine disorders

Jordi Creus-Muncunill and Anna Guisado-Corcoll have contributed equally to this work.

- Esther Pérez-Navarro estherperez@ub.edu
- Departament de Biomedicina, Facultat de Medicina i Ciències de la Salut, Institut de Neurociències, Universitat de Barcelona, Casanova 143, Barcelona, Catalonia, Spain
- Institut d'Investigacions Biomèdiques August Pi i Sunyer (IDIBAPS), Barcelona, Catalonia, Spain
- ³ Centro de Investigación Biomédica en Red sobre Enfermedades Neurodegenerativas (CIBERNED), Barcelona, Catalonia, Spain
- ⁴ Centre for Genomic Regulation (CRG), The Barcelona Institute for Science and Technology, Dr. Aiguader 88, Barcelona, Catalonia, Spain

- Department of Biostatistics, Harvard T.H. Chan School of Public Health, Boston, MA, USA
- ⁶ Centro de Investigación Biomédica en Red sobre Epidemiología y Salud Pública (CIBERESP), Barcelona, Catalonia, Spain
- Bellvitge Biomedical Research Institute (IDIBELL), L'Hospitalet de Llobregat, Barcelona, Catalonia, Spain
- Bepartment of Neurology, National Reference Center for CJD Surveillance, University Medical Center Göttingen, Göttingen, Germany
- Present Address: Department of Neurology, Icahn School of Medicine at Mount Sinai, New York, NY 10029, USA

